# Electrophysiological and pharmacological *in vivo* characterization of EEG fingerprints / biomarkers in AD mouse models

**Dissertation**

**zur**

**Erlangung des Doktorgrades (Dr. rer. nat.)**
**der**
**Mathematisch-Naturwissenschaftlichen Fakultät**
**der**
**Rheinischen Friedrich-Wilhelms-Universität Bonn**

vorgelegt von

**Muhammad Imran Arshaad**

aus

**Hafizabad, Pakistan**

Bonn 2020

Angefertigt mit Genehmigung der Mathematisch-Naturwissenschaftlichen Fakultät der Rheinischen Friedrich-Wilhelms-Universität Bonn

1. **Gutachter: Prof. Dr. Dr. Marco Weiergräber**
2. **Gutachter: Prof. Dr. Christa E. Müller**

Tag der Promotion: 23.12.2020
Erscheinungsjahr: 2021

# Acknowledgements

First, I would like to express my heartiest gratitude to Almighty God for giving me strength to fulfill all the requirements of my study.

I would like to express my deepest gratitude to Prof. Dr. Dr. Marco Weiergräber for his kindness and continuous support to pursue my PhD study. His guidance, motivation, enthusiasm and immense knowledge helped me a lot to fulfil my goals. I am extremely impressed by his foresightedness, critical realization of the matters and his discipline.

I am grateful to Prof. Dr. Christa E. Müller for being my co-supervisor and her kind support and suggestions to be a member of BIGS DrugS family.

I am very thankful to Prof. Dr. Günther Weindl and PD. Dr. Dan Ehninger as reviewers of my thesis and being the part of my examination committee.

I wish to express my special thanks to Dr. Anna Papazoglou for her continuous support, kindness, motivation and encouragement throughout my PhD study and stay at Bonn.

My sincere thanks to Ms. Christina Henseler for her constant support and assistance in my lab work and administrative matters.

A special thanks to Dr. Anna Papazoglou and Ms. Christina Henseler for their nice company and for being always available to help me.

I am thankful to Dr. Matthias Vogel for his cooperation and suggestions in my research project.

I would like to thanks my lab colleagues for their support and nice company specially Dr. Julien Soós, Johanna Daubner, Jenni Teipelke, Moritz Liebmann, Andreas Lundt, Carola Wormuth and Abdul Karim.

I would also like to acknowledge the funding source, Higher Education Commission (HEC) of Pakistan and the German Academic Exchange Service (DAAD) scholarship program, University of Bonn and BfArM to support throughout my PhD study, specially our DAAD representative Ms. Elke Burbach for her kind support and help.

Last but not the least, I would like to thank my beloved family who have despite all their sufferings supported and encouraged me to pursue my education and allow me to study abroad.

I would like to pay special thanks to my parents, sister, brothers and my wife for the support and encouragement.

# Dedication

**“Dedicated to my beloved family and respected teachers”**

# List of Contents

# List of Tables

# List of Figures

# Abbreviations

| | |
|---|---|
| [m/z] | mass-to-charge ratio |
| ° C | temperature in degrees Celsius |
| Aβ | amyloid-β |
| ACH | amyloid-cascade-hypotheses |
| AD | Alzheimer’s disease |
| ADAM | a disintegrin and metalloproteinase |
| ApoE | apolipoprotein E |
| APP | Amyloid precursor protein |
| AS | active state |
| aMCI | amnestic mild cognitive impairment |
| BACE | β-site of APP cleaving enzyme (beta secretase) |
| CA | cornu ammonis |
| CA1 | hippocampal CA1-region |
| CE | collision energy |
| CFC | cross-frequency-coupling |
| CNRQ | calibrated normalized relative quality |
| CNS | central nervous System |
| DAG | diacylglycerole |
| DC | dark cycle |
| DHP | dihydropyridine |
| DMSO | dimethyl sulfoxide |
| DNA | deoxyribonucleic acid (deoxyribonucleic acid) |
| EC | entorhinal cortex |
| EEG | electroencephalogram |
| EOAD | early onset Alzheimer’s disease |
| ESI | electron spray ionization |
| eV | electron volts |
| FAD | familial Alzheimer’s disease |
| FCS | fetal calf serum |
| FDA | food and drug administration (US food and drug administration) |
| GABA | gamma-aminobutyric acid (γ-aminobutyric acid) |

| | |
|---|---|
| GPCR | G-protein coupled receptors |
| GT | genotype |
| h | hour |
| hAPP | human amyloid precursor protein |
| hPa | Pascal (kg × $m^{-1}$ × $s^{-2}$) |
| HPLC | high performance liquid chromatography |
| HVA | high voltage-activated |
| Hz | Hertz ($s^{-1}$) |
| i.p. | intraperitoneal |
| i.v. | intravenous |
| IS | internal standard |
| KO | knockout |
| LC | light cycle |
| LC-MS/MS | liquid chromatography-tandem-mass spectrometry (liquid chromatography with mass spectrometry coupling) |
| LTP | long-term potentiation |
| LVA | low voltage-activated |
| M | molar (mol×$l^{-1}$) |
| mAChR | muscarinic acetylcholine receptor |
| MC | motor cortex |
| min | minutes |
| MRI | magnetic resonance imaging |
| MRM | multiple reaction monitoring |
| MS / DBB | medial septum / diagonal band of Broca |
| MVA | mid voltage-activated |
| NAS | nonactive state |
| NDs | neurodegenerative diseases |
| NFT | neurofibrillary tangles |
| NPY | neuropeptide Y |
| NREM | non-rapid eye movement (sleep) |
| PBS | phosphate buffered saline |
| PET | positron emission tomography |
| PFA | para-formaldehyde |
| PKC | protein kinase C |

| | |
|---|---|
| PPIs | Proton Pump Inhibitors |
| PSD | power spectrum density |
| PSEN1 | presenilin-1 |
| PSEN2 | presenilin-2 |
| PS | paradoxical sleep |
| qPCR | quantitative polymerase chain reaction |
| REM | rapid-eye movement |
| rpm | rotation per minute |
| Rt | retention time |
| R-type | “resistant” type $Ca^{2+}$ channels |
| s | second |
| SD | standard deviation |
| SEM | standard error of the mean |
| SK | small-conductance potassium channel |
| SNP | single nucleotide polymorphism |
| SWS | slow-wave sleep |
| TG | transgenic |
| TGN | trigeminal ganglion neuron |
| TM | transmitter |
| T-type | “transient” type $Ca^{2+}$ channels |
| VGCC | voltage-gated $Ca^{2+}$ channels |
| WT | wild type |

# Summary

Alzheimer’s disease (AD) is a major leading cause of deaths worldwide with underlying conditions of dementia and cognitive decline mostly in older age patients (≥ 65 years). Currently, there are approximately 50 million people worldwide suffering from dementia, and the prevalence is likely to increase up to 130 million in 2050 with 60-70% of cases due to AD. There is no medication available for AD, which can cure the disease or stop its progression. Electrophysiological biomarkers, most importantly the electroencephalographic (EEG) fingerprints, are very important tools to detect not only the incidence of dementia but also characterize the progression of the disease in later life, better than other diagnostic markers. The present study was designed to investigate the hippocampal (CA1) and cortical (M1) seizures activity and EEG frequency characteristics by a Fast Fourier Transform (FFT) based approach using implantable video EEG radiotelemetry in $Ca_v3.2^{-/-}$ and APPswePS1dE9 mice under unrestrained conditions. In the first part of my studies, I investigated the role of $Ca_v3.2$ $Ca^{2+}$ channels in CA1 oscillatory patterns, particularly in theta genesis. FFT based analysis of long-term baseline recordings revealed an enhanced relative hippocampal type II theta (4.1-12 Hz) and relative alpha power (8-12 Hz) in $Ca_v3.2^{-/-}$ mice, predominately in the inactive phase of dark cycles. These findings correlated with our post-urethane analysis, which demonstrated the increased type theta II upon $Ca_v3.2$ ablation. RT-qPCR of $Ca_v3.2^{+/+}$ and $Ca_v3.2^{-/-}$ mice was carried out to evaluate the potential role of highly expressed hippocampal genes in molecular mechanisms of theta genesis and memory formation. This analysis identified a reduced dynein light chain Tctex-Type 1 (dynlt1b) expression in $Ca_v3.2$ deficient mice. Furthermore, RT-qPCR analysis of the septohippocampal GABAergic system revealed a decrease in GABA A δ subunit (Gabrd) and GABA B1 (Gabbr1) receptor subunits. These finding strongly support the hypothesis that the $Ca_v3.2$ T-type VGCC ablation activates the tonic mode of action in septal GABAergic interneurons that leads to tonic inhibition of hippocampal GABAergic interneurons and disinhibition of pyramidal neurons with increased type II theta oscillatory activity. Moreover, these results suggest a significant role of T-type $Ca_v3.2$ $Ca^{2+}$ channels in hippocampal theta related cognitive functions and memory formation. Thus, $Ca_v3.2$ T-type channels could serve as potential therapeutic drug target for different neuropsychiatric conditions.

In the second part of my study, FFT based frequency and seizure analysis was performed in 3-6 months old APPswePS1dE9 AD mice after chronic administration of pantoprazole. Initially, the analysis was carried out in younger mice of both genders (age: 12-16 weeks) and later in older male mice (age: 17-21 weeks). FFT based frequency analysis in younger mice revealed a decrease in hippocampal and cortical theta ($\theta_1$: 4-8 Hz) relative power in APPswePS1dE9 male mice compared to controls during the dark cycle while no significant changes in theta frequency relative powers ($\theta_1$: 4-8 Hz, $\theta_2$: 4.1-12 Hz) were observed in both female genotypes. However, enhanced relative theta powers ($\theta_1$: 4-8 Hz, $\theta_2$: 4.1-12 Hz) were also detected in pantoprazole treated controls compared to untreated controls recorded during the dark cycle from the hippocampus and motor cortex. No significant changes in relative theta powers ($\theta_1$: 4-8 Hz, $\theta_2$: 4.1-12 Hz) were detected between pantoprazole treated and untreated APPswePS1dE9 mice. A significant higher hippocampal and cortical beta frequency relative powers ($\beta_1$12.1-30 Hz, $\beta_2$: 16-24 Hz, $\beta_3$: 16-30 Hz) were found in APPswePS1dE9 male mice during both dark and light cycles. Relative cortical beta powers were also higher in APPswePS1dE9 female mice during the light cycle. Furthermore, a significant increase in cortical relative gamma low power ($\gamma_{low}$: 30-50 Hz) was identified in APPswePS1dE9 mice of both genders during dark and light cycles while cortical gamma high power ($\gamma_{mid}$: 50-70 Hz) was elevated in APPswePS1dE9 male mice during the dark cycle. Moreover, electroencephalographic seizure analysis revealed significantly increased cortical seizure parameters in APPswePS1dE9 mice of both genders compared to controls during dark and light cycles. Interestingly, reduced cortical seizures parameters were found in pantoprazole treated APPswePS1dE9 mice as compared to untreated APPswePS1dE9 mice of both genders at light cycle. Additionally, pantoprazole was detected by LC-MS/MS analysis of plasma and liver tissues from both genders. Later, the FFT based analysis of older male mice also revealed consistent findings of reduced hippocampal theta ($\theta_1$: 4-8 Hz) and enhanced cortical gamma mid ($\gamma_{mid}$: 50-70 Hz) relative powers in APPswePS1dE9 mice. Furthermore, urethane administration resulted in enhanced relative hippocampal theta powers in APPswePS1dE9 mice that were subsequently reduced following atropine administration. Similarly, enhanced seizures parameters were also detected in APPswePS1dE9 mice compared to controls but reduced seizure markers were observed in pantoprazole treated APPswePS1dE9 mice compared to untreated APPswePS1dE9 mice. Age and gender EEG oscillatory activity specific alterations in APPswePS1dE9 mice suggest a functional and diagnostic role of EEG. In the future, EEG could be recognized as diagnostic biomarker for AD. An increased theta activity in pantoprazole treated controls might be associated with enhanced theta related cognitive ability in healthy male controls. No positive or negative effects of chronic pantoprazole administration were observed in theta and gamma frequency parameters in APPswePS1dE9 mice. These findings suggest a neutral role of pantoprazole long-term administration in AD progression.

In future studies, a gender and age specific pharmacokinetics, pharmacodynamics and pharmacogenetics approaches will be necessary to analyze the efficacy and safety profile of pantoprazole/PPIs in normal healthy controls, MCI and AD patients on individualized basis.

# 1. Introduction

## 1.1. Neurodegenerative diseases

Neurodegenerative diseases are one of the major health concerns around the world that are characterized by progressive structural and functional loss of neurons in the central and peripheral nervous system (CNS and PNS), with prevalence of almost 50 million people worldwide. Neurodegeneration processes start from a specific area of the nervous system with susceptibility to specific nerve cells and with the passage of time, it spreads to the other areas and cells of the nervous system with continuous and anticipated pattern (Ehrenberg et al., 2020; Fu, Hardy, & Duff, 2018). According to World Health Organization (WHO) (World Health, 2019) neurodegenerative diseases are one of the leading threats to people's health. One of the greatest risk factors for the development of the majority of neurodegenerative disorders, is aging and the prevalence of these neurological diseases is dramatically increasing as the number of elderly people has been continuously rising (Heemels, 2016; Hou et al., 2019). In addition, environmental and genetic factors also play a significant role in the development of these diseases (Chin-Chan, Navarro-Yepes, & Quintanilla-Vega, 2015).

Numerous misfolded proteins accumulate extracellularly and intracellularly in the CNS to form insoluble aggregates (inclusions) and their transfer among the cells and amplification leads to the gradual loss of nerve cells in various neurological disorders. The progressive loss of nerve cells occurs due to various cellular toxicity processes caused by protein accumulation (Fu et al., 2018; Peng, Trojanowski, & Lee, 2020). Currently, there is no treatment available, which can cure or stop the progression of these neurodegenerative diseases.

Different types of neurodegenerative diseases express specific clinical symptoms and outcomes depending on the CNS area involved and the degeneration of specific nerve cells in it. These different neurological disease including, i.e., Alzheimer's disease (AD), Parkinson's disease (PD), amyotrophic lateral sclerosis (ALS), frontotemporal lobar degeneration (FTLD) and Huntington's disease (HD).

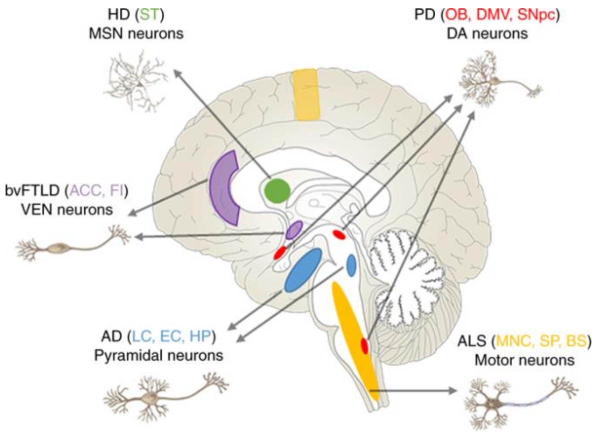

**Figure 1.1: Different regions and types of neurons those are vulnerable in neurodegenerative diseases.** Early effected regions in different neurodegenerative diseases are highlighted in different colors. LC, locus coeruleus; HP, hippocampus; OB, olfactory bulb; DMW, dorsal motor nucleus of the vagus; MNC, motor neocortex; SP, spinal cord; BS, brain stem; FI, frontal insula; DG, fascia dentata of the dentate gyrus; ST, striatum (Fu et al., 2018).

## 1.2. Alzheimer’s disease

Alzheimer’s disease is one the major forms of neurodegenerative diseases and a leading cause of deaths worldwide linked with underlying conditions of dementia, memory deficit and cognitive decline mostly in aging populations (DeTure & Dickson, 2019; N. Ma, Tie, Yu, Zhang, & Wan, 2020). Dementia is characterized by a number of symptoms including decline in memory, problem solving, language and mental skills, which effect everyday life activities (ALZ.ORG, 2020).

### 1.2.1. Historical background of Alzheimer’s disease

A German psychiatrist, Dr. Alois Alzheimer, first identified the histopathological hallmarks of a neurodegenerative disease in 1906, currently known as AD. He described symptomatic and anatomical characteristics of the disease in a clinical report of his 51 years old dementiac female patient Auguste D. who suffered from severe memory problems and disorientation in time and place. The patient died after four and half years due to severe mental illness and related somatic implications. The post mortem examination revealed an atrophic brain with neurofibrillary bundles, which were visualized using Bielschowsky’s silver staining. He also described the deposition of a special “substance” in the cortex, currently known as amyloid plaques (Alzheimer, Stelzmann, Schnitzlein, & Murtagh, 1995).

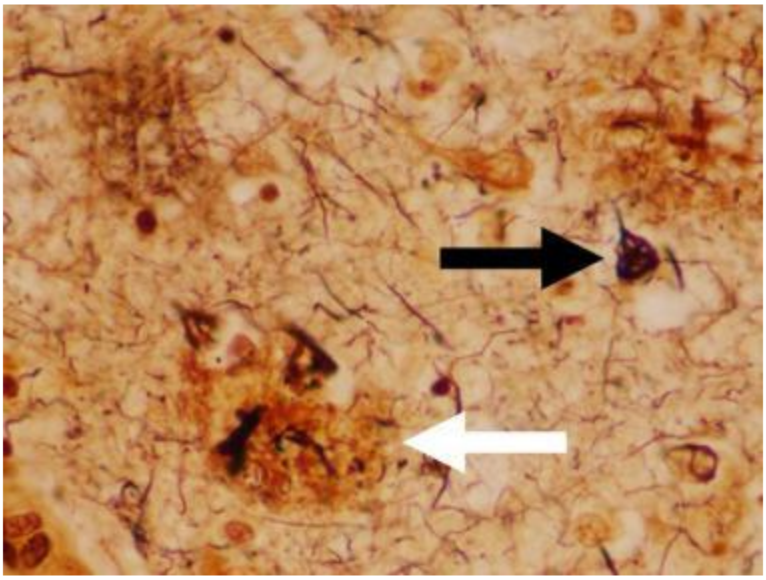

**Figure 1.2: The histopathology of dementia. Neurofibrillary tangles (black arrow) and senile plaques (white arrow) observed after Bielschowsky's silver staining of the cortex** ("Dementia Pathology," 2019).

### 1.2.2. Epidemiology

According to the WHO latest report, there are 50 million people with dementia worldwide. This prevalence is likely to increase up to 82 million in 2030 and 152 million in 2050, respectively. The incidence is expected to reach 10 million new cases each year. Almost 60% of people suffering from dementia are residents of low- and middle-income countries. AD is one of the major form of dementia which contributes to almost 60-70% of all cases of dementia (WHO). Approximately, more than 1.5 million inhabitants are affected by AD in Germany ("Alzheimer's and Dementia in Germany," 2020). This neurological illness also has serious psychological and socioeconomic effect on families, caregivers and on society itself. The approximated rise in economic burden for the care of demented patients could be 2 trillion US$ per annum by 2030 (El-Hayek et al., 2019).

### 1.2.3. Pathophysiology

#### Etiology

There are number of risk factors associated with the AD. Ageing is the greatest risk factor for the AD resulting in the late-onset type of AD (LOAD). The incidence of all forms of dementia doubles every 6.3 year with approximately 3.9 per 1000 for ages 60-90 and 104.8 per 1000 for age above 90. The prevalence of dementia is approximately 10% for people above age 65 and

40% for age above 80 (DeTure & Dickson, 2019). It is very important to understand that age is not the only factor responsible for the Alzheimer’s dementia and not every normal ageing population become demented (Nelson et al., 2011).

### Genetics and family history

It is not obligatory that an individual with a family history of AD will suffer from the same disease although they are at greater risk if they have parents or first degree relatives with AD compared to others with no Alzheimer’s family background (Green, Billings, Roozendaal, McGaugh, & LaFerla, 2006; Loy, Schofield, Turner, & Kwok, 2014). It has been reported that various genes are associated with a higher risk for AD. For example, Ryman et al. (2014) reported that mutant forms of presenilin-1 (PSEN1), presenilin-2 (PSEN2) genes, and amyloid precursor protein (APP) could be causative factors for the dominant inherited form of familial AD (FAD) which can be observed at younger age around 20, with an average onset of 46.2 years. It has been reported that AD like pathology observed around the age of 40 in patients with Down’s syndrome having partial or full chromosome 21 trisomy includes the APP resident area on chromosome 21. Larger group of people with Down’s syndrome after the age of 50 represents the symptoms of dementia (Ballard, Mobley, Hardy, Williams, & Corbett, 2016; DeTure & Dickson, 2019; Kang et al., 1987). One of the most common genetic risk factors for the sporadic LOAD is the apolipoprotein E gene (APOE) (Lane, Hardy, & Schott, 2018). The apolipoprotein-e4 (APOE-e4) gene is one of the important risk factor for the LOAD. Every individual inherits pair of APO alleles from three types of APO gene (e2, e3, e4) from both parents (ALZ.ORG, 2020; Rajan et al., 2017; M. X. Tang et al., 1998). There is three-fold increase in the risk of suffering from AD by inheritance of one copy of the e4 form of the APO compared to others with pairs of e3 alleles. Furthermore, the risk of AD is increased by eight- to twelvefold if someone inherit two copies of e4 form of APO (Holtzman, Herz, & Bu, 2012; Loy et al., 2014). Jansen et al. (2019) and Karch et al. (2018) were also reported other genes, such as PLD3, TREM2 and ADAM10 to serve as risk factors for LOAD, involved in tau and APP pathogenesis (Jansen et al., 2019; Karch et al., 2018).

In addition to age and genetic risk factors, gender also plays a significant role in the development of AD. Altmann et al. (2014) reported that females with positive e4 allele of the APOE-e4 gene exhibited a higher risk of developing AD compared to positive e4 males. Almost 11% of males and 17% of females at the age of 71 and older suffer from AD in United States (Altmann, Tian, Henderson, & Greicius, 2014; Mazure & Swendsen, 2016; Plassman et al., 2011; Vegeto et al., 2020). It has been revealed by pathological studies that females suffer more from AD dementia. In addition, more senile plaques and higher tau levels were observed in the female hippocampus and cortex compared to male study groups (Barnes et al., 2005; Corder et al., 2004).

The WHO has defined further aspects that might positively influence AD, i.e., giving up smoking habits, regular physical activity, proper management of hypertension and diabetes to decrease the chance of developing dementia and cognitive decline (WHO).

### Areas of the central nervous system and nerve cells involved in Alzheimer's disease etiopathogenesis

Nerve cells susceptible to the Alzheimer's neuropathology lost early in the disease include the cholinergic nerve cells of the basal forebrain (Davies & Maloney, 1976) and the pyramidal nerve cells of the CA1 area, the subiculum and the entorhinal cortex (EC) layer II of the hippocampal formation (Hyman, Van Hoesen, Damasio, & Barnes, 1984; Morrison & Hof, 2002; Stranahan & Mattson, 2010). Further, noradrenergic innervation to the locus coeruleus of the brain stem (Bondareff, Mountjoy, & Roth, 1982), and forebrain rostral neurons (Muratore et al., 2017) are also lost in early AD. The inhibitory neurons involved in expression of calcium binding proteins are less effected (Iwamoto, Thangnipon, Crawford, & Emson, 1991). However, Sarter and Bruno. (2002), Mattson and Magnus. (2006), and Muratore et al. (2017) reported that the caudal nerve cells expressed in the spinal cord and hind brain, interneurons in the cortex, granular cells present at dentate gyrus and different parts of layer III, V and VI of EC are comparatively less harmed in early onset of AD (Mattson & Magnus, 2006; Muratore et al., 2017; Sarter & Bruno, 2002).

### 1.2.4. Pathogenesis of Alzheimer's disease

There are a number of neuropathological factors relevant for AD. However, the extracellular amyloid beta (Aβ) plaques and intracellular hyperphosphorylated tau deposits are the most important pathological hallmarks of AD.

### Amyloid beta

Aβ are the 39-43 amino acid protein segments, which are the cleavage product of transmembrane amyloid beta precursor protein (APP). The cleavage of the APP is processed by different membrane bound enzymes (α, β and γ secretases) which results into the formation of various soluble parts of proteins and peptides (Penke, Bogár, Paragi, Gera, & Fülöp, 2019). The α-secretase mediates the non-amyloidogenic pathway of APP cleavage into the soluble fragment of APPα (sAPPα) and the C terminal fragment (α-CTF or 83A). α-CTF is further processed by γ-secretase into the APP intracellular domain (AICD) and a 3-kDa peptide (P3), while the other pathway of amyloidogenic APP cleavage is processed first by β-secretase into soluble APPβ fragments and a C terminal fragment (β –CTF or C99) having complete Aβ domain which is further processed by γ-secretase into amyloid beta peptides of 37-43 amino acids fragments and APP intracellular domain (AICD) (Graham, Bonito-Oliva, & Sakmar, 2017; Zhou, Sun, Ma, & Liu, 2018). Among the cleaved peptide fragments, $A\beta_{1\text{-}40}$ and $A\beta\text{-}_{42}$ are the predominant fragments (McGowan et al., 2005; Wildburger et al., 2017). The catalytic subunits of γ-secretase are presenilin-1 (PSEN1) and presenilin-2 (PSEN2). Mutation in PSEN1 and PSEN2 enhance the production and toxicity of the Aβ peptides (Blennow, de Leon, & Zetterberg, 2006). During normal physiological homeostatic conditions, Aβ monomers plays very important roles in synaptic activity and consolidation of memory ((Brothers, Gosztyla, & Robinson, 2018; Hillen, 2019). Aβ (40-42 amino acids) monomers assemble to form Aβ aggregates and later develop into the protofibrils, which are transitory prefibril structure. The protofibrils structures construct the filamentous fibrils that lead to the formation of plaques. These plaques ultimately accumulate extracellularly in different regions of the brain and form a pathological hallmark of AD (Graham et al., 2017).

### Tau and Alzheimer’s disease pathophysiology

Tau is an intracellular, straight, microtubule linked protein found in nerve cells within the brain. It consists of six monomeric isoforms with 352 to 451 amino acids observed after splicing that perform key function in formation of aggregates in tau pathomechanisms (Caillet-Boudin, Buée, Sergeant, & Lefebvre, 2015; Penke, Szűcs, & Bogár, 2020). Physiologically, tau stabilizes the microtubular structure, sustains the cellular homeostatic condition of the brain and hinders the process of neurodegeneration (Mroczko, Groblewska, & Litman-Zawadzka, 2019). Tau monomers can go through various post-translational modifying processes such as ubiquitination, acetylation, phosphorylation and glycosylation. The hyperphosphorylation process of tau is mediated by kinases in the cells. This hyperphopsphorylated tau forms the soluble aggregates, which further develop into the filaments of double helical structure. These filaments lead to the formation of neurofibrillary tangles (NFTs) inside the cells. The process of intracellular formation and accumulation of NFTs disrupts the cytoskeleton stabilization and axonal transportation and ultimately causes neurodegenerative processes and cell death (Almansoub et al., 2019; Graham et al., 2017).

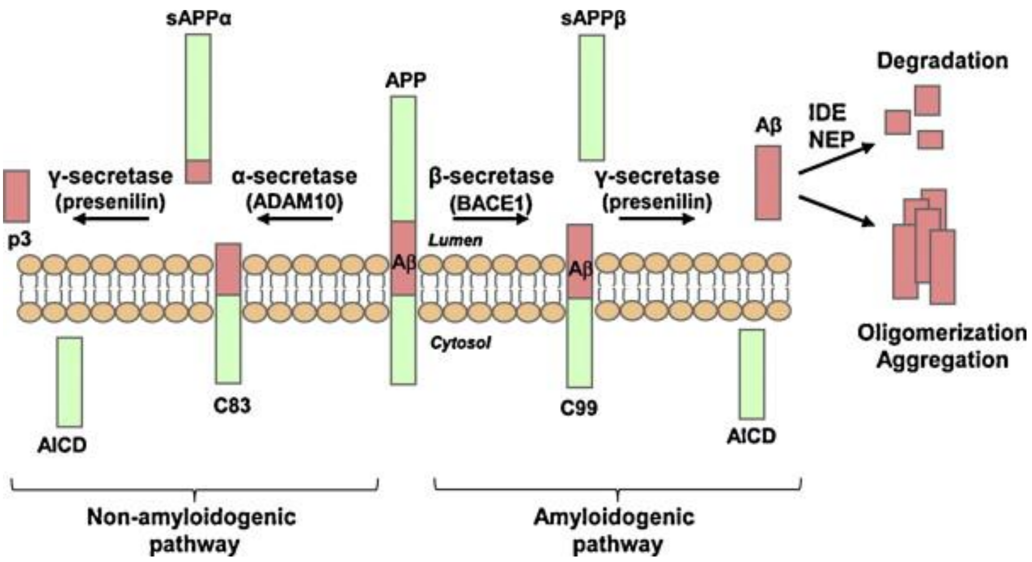

**Figure 1.3: Amyloid precursor protein (APP) processing amyloidogenic and non-amyloidogenic pathways** (Salminen et al., 2013).

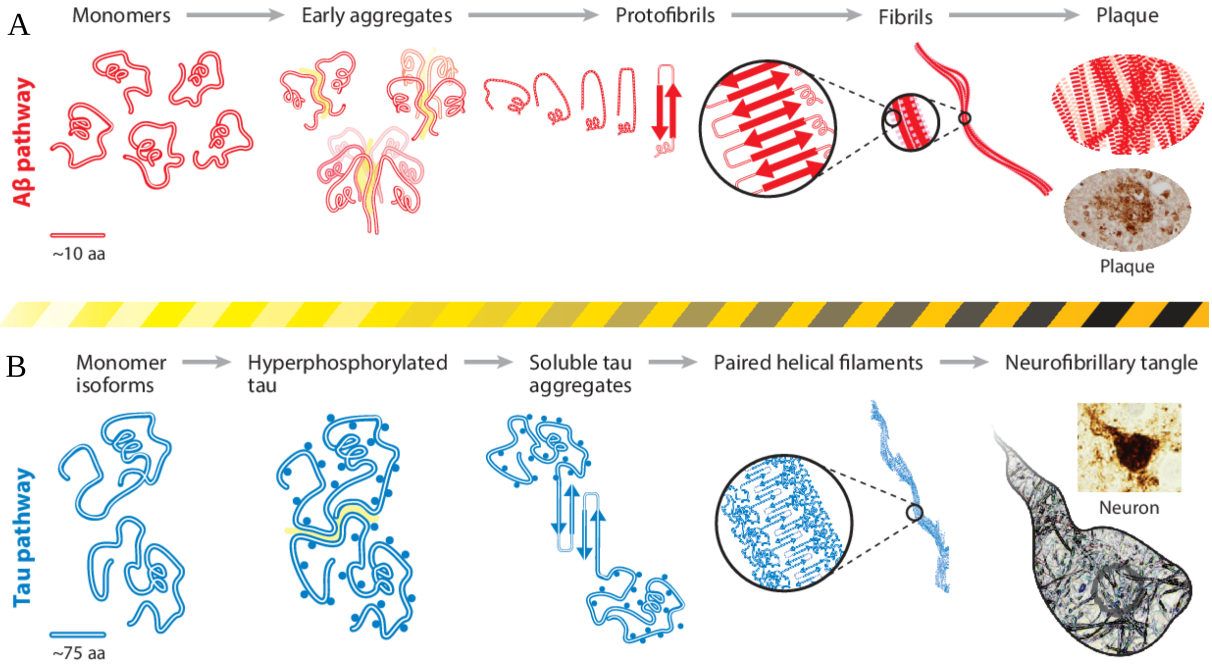

**Figure 1.4: Pathological hallmarks of AD.** Aβ plaques (A) and neurofibrillary (B) tangle formation pathways (Graham et al., 2017).

### 1.2.5. Different phases of Alzheimer's disease

Different phases are involved in the development of AD starting from an asymptomatic form to a severe form of AD termed "continuum" or continuity of AD (ALZ.ORG, 2020). There are three major phases of the "continuum" of AD: an asymptomatic preclinical phase, an early mild symptomatic phase of AD with mild cognition decline (mild cognitive impairment, MCI), and the mild to severe form of the Alzheimer's dementia (Albert et al., 2011; McKhann et al., 2011; Sperling et al., 2011). The total time span of each phase of preclinical to severe Alzheimer's dementia depends on the number of risk factors, such as gender, age, genetic history and some other modifiable/variable factors (Vermunt et al., 2019). Different phases of the Alzheimer's "continuum" are depicted in figure 1.5 and describe below:

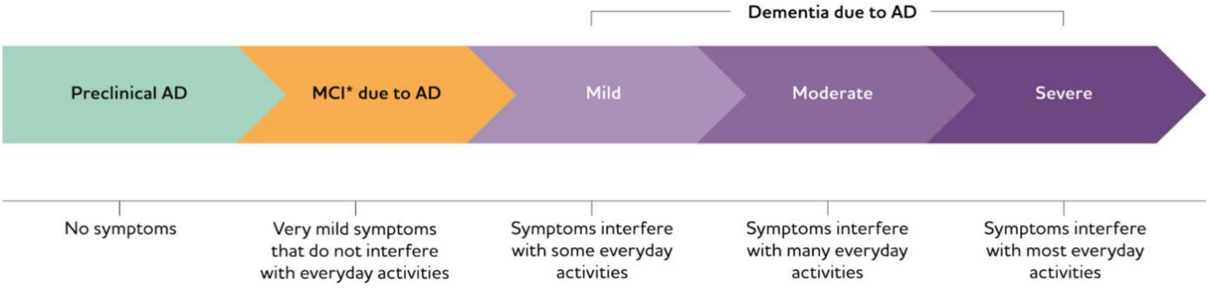

**Figure 1.5: Continuity (continuum) of Alzheimer's disease** (ALZ.ORG, 2020).

#### Preclinical phase

During the preclinical phase, people have detectable brain changes as early signs of AD but without symptoms such as memory decline. These early detectable brain changes including the abnormal Aβ level displayed on positron emission tomography (PET) scan and in cerebrospinal fluid (CSF) analysis, and reduction of glucose metabolism appeared on PET scan. However, these changes can be managed by the brain and enable the persons to perform normal functions (ALZ.ORG, 2020).

#### Mild cognitive impairment phase of Alzheimer's disease

In this phase, symptoms of memory problems and thinking ability issues appear along with the detection of biomarkers of brain alterations including the Aβ abnormality. Friends and family can observe mild cognitive and behavioral changes, but everyday life activities are not impaired. These mild brain changes appear because brain cannot compensate them at this stage (ALZ.ORG, 2020). It has been reported that 15% of people with MCI with age above 65 had suffered from Alzheimer’s dementia after a 2 years follow-up (Petersen, 2018). In addition, Ward et al. (2013) reported that 38 % of patients with MCI had suffered from Alzheimer’s dementia after a 5 years follow-up (Ward, Tardiff, Dye, & Arrighi, 2013).

### Alzheimer’s dementia

Alzheimer’s dementia is the third phase of AD in which everyday life activities are disturbed including a decline in memory function, behavioral alterations and thinking disabilities. These changes were accompanied by pathophysiological CNS alterations. These pathological changes in the brain and related symptoms progress over years to develop mild, moderate and severe forms of Alzheimer’s dementia depending on the severity of neurodegeneration (ALZ.ORG, 2020).

### Mild form of Alzheimer’s dementia

During this phase, some of the everyday life activities are disturbed but individuals in this stage still can perform many daily important activities independently. However, they need support from others to perform these problematic daily activities for adequate performance (ALZ.ORG, 2020).

### Moderate form of Alzheimer’s dementia

In this phase of Alzheimer’s dementia, people may have problems with proper communication and performance of everyday life activities (dressing, bathing etc.). There is also development behavioral changes (ALZ.ORG, 2020).

### Severe forms of Alzheimer’s dementia

In the severe stage of Alzheimer’s dementia, patients need proper help all the time to perform every activity of daily life. At this phase of Alzheimer’s dementia, severe neurodegeneration in most areas of the CNS affects almost every physical activity of the body including proper movement, eating etc. The individual becomes bed restrained, which can lead to severe skin and body infections. Degeneration of nerves involved in swallowing might cause difficulties in eating and drinking which may affect the food to be swallowed in the trachea with potential aspiration pneumonia. These severe conditions in this phase can result in organ failure and death (ALZ.ORG, 2020).

### 1.2.6. Diagnosis of Alzheimer’s dementia

There are number of psychiatric and neurological diagnostic tests, which can help to diagnose Alzheimer’s dementia.

**Social and psychological evaluation**

- Social and psychological evaluation can be performed by taking family, medical and psychiatric history of an individual and then evaluation of collected history about behavioral and memory issues.
- Collecting the views of friends and family about behavioral changes and thinking abilities of an individual.
- Performing psychological and physical evaluation to assess memory, cognitive and thinking abilities.

**Neurological examination**

- Evaluation of blood biomarkers and CNS examination of an individual by imaging techniques to find out other factors involved in dementia like stroke, Parkinson’s disease, deficiencies of some vitamins, tumors, disturbed sleep habits, vascular dementia etc. ("Dementia," 2020).
- PET scan is used to evaluate the rise in Aβ levels in the brain, which is a hallmark of Alzheimer’s dementia (Johnson et al., 2013).
- Evaluation of CSF for the abnormal level of tau and Aβ by lumbar puncture. Normal levels of tau and Aβ could be a sign of non-Alzheimer’s dementia (Shaw et al., 2018).

There is hope that the diagnosis of AD could be possible by analysis of simple examination of blood biomarkers in the future but it requires a huge number of multiscale clinical studies (Olsson et al., 2016; Weller & Budson, 2018).

## 1.3. Electroencephalography and neurological diseases

Electroencephalography (EEG) is a fundamental technique used to measure the electrical activity of the brain in the form of electrophysiological signals generated by the postsynaptic potentials of a number of structurally related neurons. Different brain states can be analyzed with the help of this technique by analyzing various electrophysiological signals recorded. EEG is a dynamic technique used for the diagnoses of various disorders of the CNS (Alturki, AlSharabi, Abdurraqeeb, & Aljalal, 2020; Cassani, Estarellas, San-Martin, Fraga, & Falk, 2018;

Jurcak, Tsuzuki, & Dan, 2007; Seeck et al., 2017), such as epilepsies, and AD identification (Tsolaki, Kazis, Kompatsiaris, Kosmidou, & Tsolaki, 2014; Yu, Zhu, Cai, Wang, Liu, Shi, et al., 2020). A German psychiatrist Hans Berger analyzed the first EEG in 1929. Berger used a galvanometer along with suitable electrodes to record bio potential changes from the head of individuals under resting state conditions (Berger, 1929). There are different types of EEG signal frequencies including delta (δ) 0.1-4 Hz, theta (θ) 4-8 Hz, alpha (α) 8-12 Hz, beta (β) 12-30 Hz and gamma (γ) >30 Hz and additionally other subtypes of some of these signals as well. These different EEG frequencies provides specific information individually related to neuronal coordination and function of the distinct brain regions (Cassani et al., 2018; Cohen & Gulbinaite, 2014; Nunez & Srinivasan, 2014).

EEG is a neurophysiological biomarker for AD, as EEG signaling patterns have been reported to be useful for the analysis of different states of the brain in AD (Pineda, Ramos, Betting, & Campanharo, 2020). EEG is a technique which can differentiate the AD individuals from the healthy controls that’s why it is suggested by the clinicians to perform EEG of Alzheimer’s patients as well (Hegerl & Möller, 1997; Jonkman, 1997). Moretti et al. (2004) found and reported the role of alpha, delta and theta EEG power bands in normal individuals, patients with vascular dementia and mild AD (Moretti et al., 2004). Benwell et al. (2019) reported a decrease in alpha (α) and beta (β) and rise in delta (δ) and theta (θ) EEG power bands analyzed from the brain of the AD patients as compared to normal healthy subjects, indicating the role of different EEG oscillations pattern in cognitive decline in AD subjects (Benwell et al., 2020). Farina et al. (2020) reported the role of resting stage EEG by analyzing oscillatory power bands and by structural MRI to differentiate between normal control older people, individuals with MCI and AD patients (F. R. Farina et al., 2020). Moreover, the EEG has been used for the differential diagnosis among the Alzheimer’s dementia, vascular dementia and Lewis bodies dementia (Colloby et al., 2016; Garn, Coronel, Waser, Caravias, & Ransmayr, 2017; Neto, Allen, Aurlien, Nordby, & Eichele, 2015; Neto, Biessmann, Aurlien, Nordby, & Eichele, 2016). Yu et al. (2019) investigated that the analyses of cross frequency coupling between different EEG oscillatory power bands could be helpful to identify the variation in different brain structures before the display of seizure symptoms (Yu, Zhu, Cai, Wang, Liu, Wang, et al., 2020).

### 1.3.1. Theta oscillations

Hippocampal theta oscillations (4.1-12 Hz) are highly organized neuronal waves with large amplitude which are present throughout the awake behavioral state and consistently present throughout paradoxical sleep (Muller et al., 2012). These neuronal waves reflect the subthreshold membrane potential and intensely modulate the spiking at hippocampus (Lubenov & Siapas, 2009). Theta are also involved in neurological and behavioral functions such as learning and memory consolidation (Vertes, 2005). Moreover, theta rhythm play important roles in encoding the “When” in addition to coding of “Where” of episodic memory (Kraus et al., 2015; MacDonald, Carrow, Place, & Eichenbaum, 2013). The hippocampus and medial septum-diagonal band of Broca (MS-DBB) are thought to be involved in the induction and maintenance of theta oscillations (Borhegyi, Varga, Szilagyi, Fabo, & Freund, 2004; Lubenov & Siapas, 2009; S. Ma et al., 2009; Simon, Poindessous-Jazat, Dutar, Epelbaum, & Bassant, 2006; Takano & Hanada, 2009; Varga et al., 2008). The exact intra- and extrahippocampal location of theta generator is still under debate (Goutagny, Manseau, Jackson, Danik, & Williams, 2008). However, the GABAergic neurons in the medial septum were reported to serve as a pacemaker and to project rhythmic activity to hippocampal interneurons and pyramidal cells (Hangya, Borhegyi, Szilágyi, Freund, & Varga, 2009). Based on the dualistic theory, two types of hippocampal theta oscillations are distinguished: type I (atropine-resistant) and type II (atropine-sensitive). Atropine-resistant (type I) theta oscillations appear during awakening, voluntary behavior and movement because the frequency and amplitude of these oscillations are unaffected by the muscarinic blocker atropine, and are thought to be linked to metabotropic glutamate group 1 receptors, NMDA and AMPA receptors (Buzsáki, 2002; Chuang, Bianchi, Kim, Shin, & Wong, 2001; Gillies et al., 2002). In contrast, atropine-sensitive type II theta oscillations appear during alert immobile and urethane induced anesthesia. They are eradicated by anticholinergic drug, i.e., atropine (Buzsáki, 1986, 2002; Buzsáki et al., 2003; Kramis, Vanderwolf, & Bland, 1975; Vanderwolf, Buzsaki, Cain, Cooley, & Robertson, 1988). Stimulation of muscarinic receptors ($M_1$/$M_3$/$M_5$) can generate type II atropine sensitive theta rhythms by activation of the G-protein-coupled receptors (GPCRs) ($G\alpha_{q/11}$) signaling pathway through phospholipase $\beta_{1/4}$ (PLC $\beta_{1/4}$), inositol triphosphate ($InsP_3$), diacylglycerole (DAG), $Ca^{2+}$ and protein kinase C (PKC) (Muller et al., 2012; J. Shin et al., 2009). Various downstream effects of this pathway related to generation of atropine sensitive type II theta oscillations have been proposed. Further, stimulation of muscarinic cholinergic receptors leads to inhibition of the calcium dependent $K^+$ channel that are stimulated by $Ca^{2+}$ influx through action potentials (Brown, 2010). The inactivation of hippocampal PLC$\beta_1$ and septal PLC$\beta_4$ leads to the complete loss or attenuation of synchronized cholinergic theta power (J. Shin et al., 2009; J. Shin, Kim, Bianchi, Wong, & Shin, 2005).

## 1.4. Voltage gated calcium channels and theta oscillation

Based on the cellular and subcellular expression and functional input to the dendrites, voltage gated calcium channels (VGCCs) serve as an essential element in theta generation although the exact mechanisms are still not fully known (Magee & Carruth, 1999; Magee & Johnston, 1995). Calcium channel $Ca_V2.3$ R-type VGCCs are reported to be expressed in hippocampal pyramidal neurons and considered to be involved in theta genesis (Bloodgood & Sabatini, 2007; Catterall, 2011; Catterall, Leal, & Nanou, 2013; Giessel & Sabatini, 2010; Nanou & Catterall, 2018; Yasuda, Sabatini, & Svoboda, 2003). It has been reported that divalent heavy metal ions like nickel ($Ni^{2+}$) inhibit the high and low voltage-activated calcium channels (Kuzmiski, Barr, Zamponi, & MacVicar, 2005; C. Tai, Kuzmiski, & MacVicar, 2006). The LVA (T-type) voltage gated calcium channels consist of three subtypes $\alpha_1$G ($Ca_v3.1$), $\alpha_1$H ($Ca_v3.2$) and $\alpha_1$I ($Ca_v3.3$) encoded by different $\alpha_1$ subunit genes, CACNA1G, CACNA1H, CACNA1I and Cacna1g, Cacna1h, Cacna1i in humans and mouse respectively (Bosch, Hou, Fang, Kelly, & Rønnekleiv, 2009; Lory, Nicole, & Monteil, 2020; Perez-Reyes, 1998). Each isoform of T-type channels exhibits specific pharmacological and biophysical characteristics as well as physiologically diverse cellular and subcellular distribution in the CNS and PNS (Chemin et al., 2002; Molineux et al., 2006). Mostly, all three T-type voltage gated calcium channel isoforms are highly expressed in different areas of the CNS, i.e., cerebellum, thalamus, hippocampus, cortex and the spinal cord (Leresche & Lambert, 2017; Talley et al., 1999). T-type voltage gated calcium channels are involved in the rhythmic burst firing mode of various neurons (Schampel & Kuerten, 2017), associated with the generation of specific oscillatory patterns during the circadian rhythm (Powell, Cain, Snutch, & O'Brien, 2014). These low voltage-activated calcium channels play essential physiological and pathological roles mostly in the CNS such as in sleep, neuropathic pain, and absence epilepsy (Y. Zhang, Jiang, Snutch, & Tao, 2013). These findings are primarily based on studies in genetically modified mouse strains of these T-type channels isoforms (Anderson et al., 2005; Kim et al., 2001). However, the knockout of T-type calcium channel genes may also result in compensatory reactions that mask the particular implications T-type channel functions (Choi et al., 2007). Moreover, within the T-type calcium channel family, the $Ca_v3.2$ ($\alpha_1$H) subtype is most specifically expressed in the dentate gyrus neurons of the hippocampus (Talley et al., 1999) and plays an important role in various pathophysiological states of the CNS (Y. Zhang et al., 2013).

Gangadharan et al. (2016) reported enhanced object exploration and open field exploration behavior and an increase in type II theta oscillations in $Ca_v3.1^{-/-}$ knockout mice. This effect was associated with tonic firing of septohippocampal GABAergic neurons (Gangadharan et al., 2016). $Ca_v3.2$ calcium channels are highly expressed in septohippocampal system sometimes even higher than the $Ca_v3.1$ in the structure involved in theta genesis (Aguado, Garcia-Madrona, Gil-Minguez, & Lujan, 2016). $Ca_v3.2$ was identified in all subfields of dendrites in the hippocampal CA1 region, in extrasynaptic membranes of spine and shafts of dendrites and in intracellular membranes. Besides pyramidal cells, $Ca_v3.2$ was also identified in dendritic shafts of interneurons. Furthermore, $Ca_v$ 3.2 was also found presynaptically in axon terminals to form synapsis with dendritic spines (Aguado et al., 2016). Expression studies clearly indicated a role of $Ca_v3.2$ in the generation of theta oscillation. It has been reported in earlier studies that $Ca_v3.2$ plays a very important role in hippocampal long term potentiation (LTP), passive avoidance tasks and cued context fear conditioning (C. C. Chen et al., 2012). It has also been observed that anxiety levels are significantly increased, memory is impaired and sensitivity to psychostimulant reduced in $Ca_v3.2$ ($\alpha_1$H) knockout mice (Gangarossa, Laffray, Bourinet, & Valjent, 2014). The first project of the present study was designed to evaluate the role of $Ca_v3.2$ T-type calcium channels in the initiation, maintenance and modulation of hippocampal theta oscillations and the underlying electrophysiological and molecular mechanisms.

## 1.5. Therapeutic approaches for Alzheimer’s disease

Currently, there is no medication available, which can stop or significantly slow the process of neurodegeneration and progression of AD. The U.S. Food and Drug Administration (FDA) has not approved yet any specific drug for the treatment of moderate to severe form of Alzheimer’s dementia (ALZ.ORG, 2020). It has been reported that active management of AD and other forms of dementia could effectively improve the quality of life of the patients and their caretakers (ALZ.ORG, 2020; Grossberg et al., 2010; Vickrey et al., 2006).

### 1.5.1. Non-pharmacological approaches

There are various non-pharmacological approaches used to improve the symptoms of Alzheimer’s dementia without use of medication, which can improve cognitive abilities, overall everyday life activities and number of behavioral problems such as discomfort, disturbed normal sleep habits, depression and aggressive behaviors. It has been reported that the non-pharmacological approaches can be more helpful compared to current pharmacological therapy in the improvement of symptoms like aggressive and agitated behavior associated with dementia (ALZ.ORG, 2020; Watt et al., 2019). Groot et al. (2016) and Farina et al. (2014) reported that physical exercise showed improvement in the cognitive functions of individuals with Alzheimer’s dementia (N. Farina, Rusted, & Tabet, 2014; Groot et al., 2016). It has been reported that various types of cognitive therapies and psychological intervention improved cognitive performance, anxiety and depression in individuals suffering from Alzheimer's dementia (Bahar-Fuchs, Martyr, Goh, Sabates, & Clare, 2019; Fukushima et al., 2016).

### 1.5.2. Pharmacological approaches

Currently, there are very few drugs available to improve the cognitive symptoms but there is no current pharmacological therapy, which can significantly slow or even stop disease progression. The FDA has recommended two classes of medications for the symptomatic treatment or improvement of Alzheimer's dementia. The medications include acetylcholinesterase inhibitors (AChEIs) such as galantamine, rivastigmine, donepezil, and NMDA (*N*-methyl-D-aspartate) receptor blocker, such as memantine (Atri, 2019).

AChEIs increase the amount acetylcholine (ACh) by blocking the acetylcholinesterase enzyme which degrades ACh at synapses (Yiannopoulou & Papageorgiou, 2013). The resultant increased amount of acetylcholine neurotransmitter in the CNS of AD patients can enhance cognitive performance for a short period of time (Howard et al., 2015). The FDA has approved rivastigmine and donepezil for the symptomatic management of mild, moderate and sever forms of the Alzheimer's dementia, however, galantamine for the management of mild to moderate form of the Alzheimer's dementia (Rountree, Atri, Lopez, & Doody, 2013). Another medicine used for the symptomatic management of mild to moderate forms of the Alzheimer's dementia is memantine. Memantine non-competitively blocks the NMDA mediated neuronal excitotoxicity (Cummings, Tong, & Ballard, 2019; Matsunaga, Kishi, & Iwata, 2015; Yiannopoulou & Papageorgiou, 2013, 2020).

Moreover, other pathophysiological conditions that serve as potential risk factors for AD and cognitive decline such as, vitamins (D, folic acid, $B_{12}$) deficiencies, thyroid dysfunctioning, infections, cardiovascular diseases and diabetes, need to be included in the AD management (Blokh, Stambler, Lubart, & Mizrahi, 2017; Yiannopoulou & Papageorgiou, 2020).

### 1.5.3. Future aspects of Alzheimer's disease therapeutics

Currently, a number of clinical trials are going on for the management of disease progression by targeting the neuropathological hallmarks of AD: Aβ plaques and neurofibrillary tangles of tau protein (Braak & Del Tredici, 2020; Mann & Hardy, 2013; Weller & Budson, 2018). Still these trials are unsuccessful for the treatment of pathological hallmark of AD. Additionally, number of other therapies are also in pipeline for the management of AD including anti-inflammatory agents, neuro enhancers to increase the neuronal communication for the improvement of cognition, various neuroprotective agents, various growth factor stimulating agents and also various therapeutic approaches based on stem cells (Huang, Chao, & Hu, 2020; Yiannopoulou & Papageorgiou, 2020). It has been found from number of studies that the evaluation of population at early stage, using a number of novel diagnostic markers and subsequent therapy at pre-phase could be effective in the management of progression of AD (Aisen et al., 2017; Yiannopoulou & Papageorgiou, 2020). However, it is very important to analyze in detail the complex pathological mechanism of AD to identify the novel biomarkers for the effective therapeutic strategy to slow or stop the progression of disease (Huang et al., 2020).

### 1.6. Proton pump inhibitors

Proton pump inhibitors (PPIs) chemically belong to the benzimidazole family that consists of two important structural parts, the benzimidazole and a pyridine ring. The pyridine part accumulates in the canniculus of the gastric parietal cells because of its $pk_a$ 4.0. However, the benzimidazole part with $pk_a$ 1.0 participates in the activation process of PPIs by gastric acid. PPIs are week basis prodrugs converted into the sulfenamides or sulfenic acids by the acid activation process. These activated forms covalently inhibit the $H^+/K^+$-ATPase by interaction with cysteine residues. The $H^+/K^+$-ATPase is an enzyme responsible for gastric acid secretion (Sachs et al., 1976; J. M. Shin & Kim, 2013; J. M. Shin & Sachs, 2008). The first benzimidazole derivative and $H^+/K^+$-ATPase pump inhibitor was omeprazole reported to be used for clinical purposes, followed by a number of other $H^+/K^+$-ATPase pump inhibitors synthesized and marketed such as lansoprazole, pantoprazole, rabeprazole, esomeprazole and dexlansoprazole (Sachs, Shin, & Howden, 2006; J. M. Shin & Kim, 2013; Wallmark, Larsson, & Humble, 1985). PPIs are a first line therapy effectively used in all age groups for the treatment of gastroesophageal reflux disease (GERD), peptic ulcer, Zollinger-Ellison syndrome, Barret's esophagus, dyspepsia, and also as a preventive measure for drug induced ulcers (Cheng et al., 2020; Sachs et al., 2006; J. M. Shin & Sachs, 2008; Strand, Kim, & Peura, 2017).

#### 1.6.1. Pharmacodynamic aspects of proton pump inhibitors

The process of gastric acid secretion is activated by the rise in intracellular calcium ($Ca^+$) mediated by acetylcholine and gastrin, and also by activation of histamine mediated adenylate cyclase and formation of cyclic adenosine monophosphate (cAMP). Intracellular calcium and cAMP mediate the movement of $H^+/K^+$-ATPase from the cytosol to the canaliculus by stimulating kinases and phosphorylation pathways (Helgadottir & Bjornsson, 2019; Lindberg et al., 1990). The $H^+/K^+$-ATPase proton pump appears at the canaliculus of the gastric parietal cells stimulated by ACh, gastrin and histamine. It exchanges extracellular $K^+$-ions with intracellular $H^+$-ions by an ATP dependent mechanism. This mechanism promotes the secretion of gastric acid into the lumen of the stomach (Sachs et al., 1976; J. M. Shin & Kim, 2013; J. M. Shin & Sachs, 2008). PPIs block the last step process of gastric acid secretion by inhibiting the $H^+/K^+$-ATPase proton pump (Morschel, Mafra, & Eduardo, 2018; Strand et al., 2017). This covalent inhibition of $H^+/K^+$-ATPase mediates longer action of PPIs that last for 24 to 48 hours in relation to their half-lives (J. M. Shin & Sachs, 2008; Strand et al., 2017).

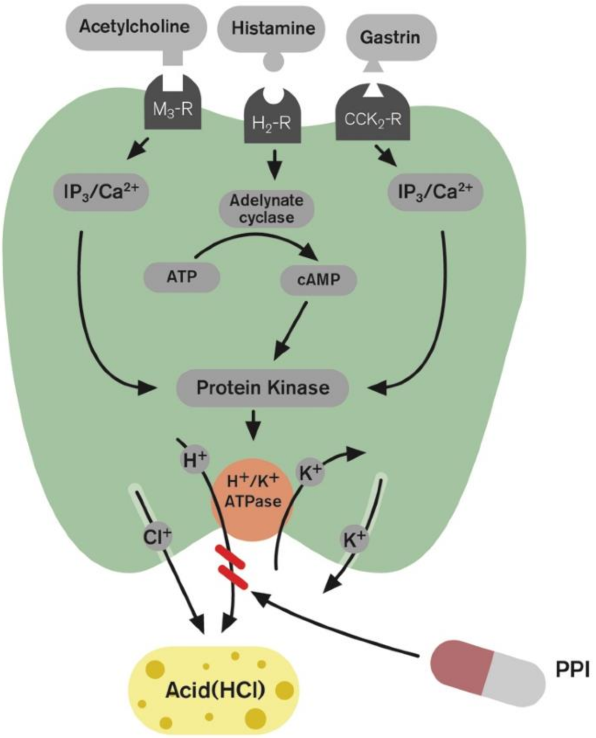

**Figure 1.6: The $H^+/K^+$-ATPase (proton pump) placed at the canaliculus of the parietal cell mediates the exchange of extracellular $K^+$ with intracellular the $H^+$ and involved in the secretion of acid ($H^+$) ion into the lumen of the stomach.** The major stimulating agents for the secretion of gastric acid at the gastric parietal cells are acetylcholine, histamine and also less extensive agent, gastrin. Adenosine triphosphate (ATP), adenosine monophosphate (cAMP), Cholecystokinin type 2 receptor ($CCK_2$-R), histamine type 2 receptors ($H_2$-R), inositol triphosphate ($IP_3$), muscarinic type 3 receptors ($M_3$-R), proton pump inhibitor (PPI) (Helgadottir & Bjornsson, 2019).

### 1.6.2. Pantoprazole

Pantoprazole is one of the most effective PPIs used worldwide for the treatment of gastroesophageal reflux disease (GERD) and gastric and duodenal ulcers (Poole, 2001). Like other PPIs, pantoprazole also belongs to substituted benzimidazoles and irreversible blocker of $H^+/K^+$-ATPase (Fitton & Wiseman, 1996; Hartmann et al., 1996). After the clinical approval of omeprazole for the treatment of reflux esophagitis in 1989, pantoprazole was the fourth proton pump inhibitor approved by FDA in 2000 for the treatment of reflux esophagitis (Cheer, Prakash, Faulds, & Lamb, 2003; Mathews, Reid, Tian, & Cai, 2010). Dabrowsky et al. (2018) reported that 40 mg single oral daily dose of pantoprazole proved effective in the alleviation of GERD symptoms for 8 weeks (Dabrowski, Štabuc, & Lazebnik, 2018). The absolute bioavailability of pantoprazole is 77% after single oral dose, which remains the same after multiple dosing, with elimination half-life of 1.1 h, $T_{max}$ of 2-3 h, with a $C_{max}$ of 2.5 mg/l, and an apparent distribution volume of about 0.15 l/kg (Hartmann et al., 1996). Liver enzymes extensively metabolize Pantoprazole, starting with a first phase of O-demethylation by CYP2C19 and CYP3A4 and followed by a second phase of sulfate conjugation. Furthermore, sulfide and sulfone metabolites are formed by reduction or oxidation of the sulfoxide group (Huber et al., 1995; Kromer, 1995; Meyer, 1996). Pantoprazole metabolites are mainly 80% excreted via urine and about 20 % via bile (Hartmann et al., 1996).

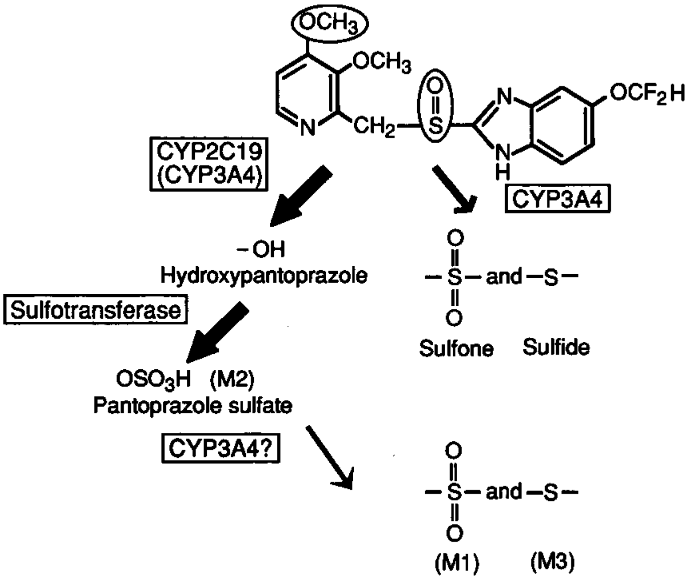

**Figure 1.7: Pantoprazole metabolic pathways in liver** (Meyer, 1996).

### 1.6.3. Proton pump inhibitors and neurological diseases

PPIs are the first line therapy for the management of gastric ulcer and GERD (Helgadottir & Bjornsson, 2019) which considered safe and effective for both short and the long-term use. However, there has been issue emerged in recent studies about the improper and long-term use of PPIs (Novotny, Klimova, & Valis, 2018; Strand et al., 2017). Number on adverse drug reactions (ADRs) are associated with long-term use of PPIs including CNS side effects (Makunts, Alpatty, Lee, Atayee, & Abagyan, 2019). It has been reported that expression of various isoforms of $H^+/K^+$-ATPase indicated its role in the CNS (Modyanov et al., 1991) including the process of endocytosis and exocytosis at nerve endings (Tabares & Betz, 2010; D. Wang & Hiesinger, 2013). This illustrated the role of $H^+/K^+$-ATPase not only confined to the gastric parietal cells (Novotny et al., 2018; J. Shin et al., 2009; J. M. Shin & Sachs, 2008). Various ADRs have been reported with broad use of PPIs including diarrhea, headache, abdominal pain, upper respiratory tract infection (Bernshteyn & Masood, 2020), cardiovascular problems (Shiraev & Bullen, 2018), severe kidney damage (Li, Xie, & Al-Aly, 2018) and infections (Hafiz, Wong, Paynter, David, & Peeters, 2018). Additionally, PPIs also have CNS adverse effects, such as decline in memory, impaired auditory and visual senses, migraine and peripheral neuropathies (Makunts et al., 2019).

### 1.6.4. Proton pump inhibitors and Alzheimer's dementia

Various studies reported a correlation between the use of PPIs and dementia. Gomm et al. (2016) revealed a link between the use of PPIs and the development of dementia in elderly patients (Gomm et al., 2016). Tai et al. (2017) also reported the correlation between the use PPIs and a rise in dementia problems in an Asian population (S. Y. Tai et al., 2017). PPIs have also been reported to increase Aβ37, Aβ40 and Aβ42 production by modulating the APP cleavage activity of β and γ secretases. This was analyzed during in vitro cellular studies and in vivo mouse models of AD (Badiola et al., 2013). Zhang et al. (2020) revealed by meta-analysis that PPIs enhance the possibility of dementia (Y. Zhang et al., 2020). Another study has elucidated the role of PPIs in inhibition of the choline acetyltransferase (ChAT). ChAT is an enzyme responsible for the synthesis of acetylcholine. Thus, PPIs inhibitory effects on the cholinergic system could be a potential cause of dementia (Kumar, Kumar, Nordberg, Långström, & Darreh-Shori, 2020). Akter et al. (2015) analyzed that long-term use of PPIs in elderly could be the cause of progression of AD (Akter et al., 2015). Haenisch et al. (2015) also found a correlation between the use of PPIs and the risk of dementia in an epidemiological cohort study conducted in elderly people in Germany (Haenisch et al., 2015). However, another case control study from Germany revealed a decline in risk of dementia after use of PPIs (Booker, Jacob, Rapp, Bohlken, & Kostev, 2016). Hashioka et al. (2009) and Hashioka et al. (2011) reported that the PPIs significantly attenuate the interferon-gamma (IFN-γ) activated neurotoxicity of human astrocytes by inhibition of the signal transducer and activator of transcription (STAT) 3 signaling pathway. Antineurotoxic properties of PPIs are useful option for the treatment of AD and other neuroinflammatory disorders linked with activates astrocytes (Hashioka, Klegeris, & McGeer, 2009, 2011). Goldstein et al. (2017) also reported that there is no link observed between the use of PPIs and the risk of dementia (Goldstein et al., 2017).

## 1.7. Transgenic mouse models

The mouse (Mus musculus) has been used as a model organism for the evaluation of human diseases because these two species are anticipated to be similar physiologically and genetically. In addition, it is easy to produce inbred murine strains in laboratory to make them available for experiments (Morse, 2007; Perlman, 2016; Rosenthal & Brown, 2007). Additionally, various advanced methodological approaches have been used to produce different transgenic knockin and knockout mouse models of human disease, which further enhanced the use of mice as a human disease research model (Fox, 2007; Perlman, 2016).

### 1.7.1. Calcium channel mutated mouse models

VGCCs play very important roles in the release of neurotransmitters in synapses for neuronal cells communication. However, various CNS disorders have been associated with abnormality and mutations in VGCCs subunits. Mouse models with ion channels defects have given the linkage between channels mutations and modification of cellular functions (Ball & Gregg, 2002). The first part of the present study was to evaluate the role $Ca_v3.2$ T-type calcium channel knockout mice in memory formation. $Ca_v3.2$ deficient mice have been reported to exhibit coronary artery dysfunction and cardiac fibrosis (C. C. Chen et al., 2003), sensory neuronal hyperexcitability (Jacus, Uebele, Renger, & Todorovic, 2012; Voisin, Bourinet, & Lory, 2016), altered pain response (Choi et al., 2007; Tsubota et al., 2018), age-induced endothelial dysfunction (Thuesen et al., 2018), epilepsy (Becker et al., 2008; Zamponi, Lory, & Perez-Reyes, 2010), elevated anxiety, impaired memory and reduced sensitivity to psychostimulants (Gangarossa et al., 2014) and altered mechanoreception (R. Wang & Lewin, 2011).

### 1.7.2. Mouse models of Alzheimer's disease

Various transgenic mouse models are currently under research that present different pathological features of AD, particularly increase in A$\beta_{1-42}$ load produced by over expression of one or more APPs mutants. These mutations induce various features of AD related pathologies like plaque formation, deterioration of synaptic and neuronal functions, decline in memory formation and learning (Games et al., 1995; Götz et al., 2004; Myers & McGonigle, 2019; Papazoglou, Soos, et al., 2016). The second part of my study was performed in APPswePS1dE9 transgenic mice. These APPswePS1dE9 with a C57BL/6J background carries a human APP with Swedish double mutation (APPswe) co-integrated with human PS1 with exon 9 deletion (PS1dE) (Jankowsky et al., 2004). Generally, enhanced A$\beta_{1-42}$ levels can be linked with an increase in mortality in different transgenic AD mice (Chin et al., 2004; Hsiao, 1994; Leissring et al., 2003). However, 10-15% mortality has been reported in APPswePS1dE9 transgenic mice regardless of the pathophysiological features (Minkeviciene et al., 2009) Aβ plaque formation starts about 4 month of age in the cortex and hippocampus (Garcia-Alloza et al., 2006; Shemer et al., 2006) while decline in memory is observed around 6 months in radial arm water maze (Xiong, Hongmei, Lu, & Yu, 2011). A decline in cognitive and behavioral parameters is observed at 12 months of age respectively using Morris water maze testing. It has been considered that an increase in Aβ load in the cerebral cortex is correlated with seizure-induced deaths (Paesler et al., 2015; Palop et al., 2007). Moreover, neurodegeneration processes disrupt the central rhythmicity, specifically theta and gamma architecture (Papazoglou, Soos, et al., 2016; Siwek et al., 2015).

Earlier studies have investigated the APPswePS1dE9 mouse models to evaluate the specific EEG oscillation patterns, brain rhythmicity and sleep analysis (Gurevicius, Lipponen, & Tanila, 2013; Jyoti, Plano, Riedel, & Platt, 2010; Minkeviciene et al., 2009; Palop et al., 2007; Wisor & Kilduff, 2005; Xiong et al., 2011). As compared to previous studies, we have analyzed the relative EEG frequencies by using FFT based approach and seizures analysis from the motor cortex (M1) and hippocampal (CA1) regions of the brain. My study was carried out in both male and female APPswePS1dE9 mice in different age dependent subgroups to investigate the relative EEG oscillation pattern of each frequency range for the characterization and detailed understanding of the pathophysiology of the AD. Additionally, we have also analyzed the role of chronic pantoprazole administration in the APPswePS1dE9 mice groups for the pharmacological evaluation of AD.

# 2. Aims of study

Currently, there is no medication available, which can stop or significantly slow the process of neurodegeneration and progression of Alzheimer's disease (AD) to improve the patient's quality of life. The fundamental objectives of Alzheimer's research are the prevention and the evaluation of population for early stage detection of disease before it progresses and induces neuronal damage. Electroencephalography (EEG) is used to measure the electrical activity of the brain via electrophysiological signals, which are differentiated into frequency bands such as alpha, beta, theta, sigma and gamma. These EEG frequencies provide specific information individually linked to nerve cell coordination and function of distinct brain regions. However, the question arises whether the EEG can be a diagnostic biomarker for early detection and monitoring of AD. It is thus mandatory to investigate characteristic changes in oscillatory EEG patterns and to unravel whether these alterations can be detected prior to disease onset. To address these questions, this study was designed as follows:

## 2.1. Hippocampal EEG alterations in $Ca_v3.2$ deficient mice and the involvement of the GABAergic system

The first part of the present study was performed to evaluate the role of low voltage-activated T-type $Ca_v3.2$ ($\alpha_1$H) VGCCs in initiation, maintenance and modulation of hippocampal theta oscillatory architecture and the underlying electrophysiological and molecular mechanisms. Previous studies have revealed that ablation of $Ca_v3.2$ $Ca^{2+}$ channels is associated with anxiety related behavior and impairment of long-term potentiation (LTP), learning and memory formation.

Therefore, the aim of this study was to investigate the following hypothesis:

1) $Ca_v3.2$ deficient mice exhibit alterations in hippocampal (CA1) type II theta oscillatory behavior. Fast Fourier Transform (FFT) based EEG frequency analysis of CA1 recordings using implantable video EEG radiotelemetry under unrestrained conditions was used to investigate this phenomenon.
2) Expression of gene candidates relevant for type II theta genesis in septohippocampal system are altered upon $Ca_v3.2$ ablation. RT-qPCR was used to reveal and validate these candidate genes.

## 2.2. Analysis of the alteration of central rhythmicity in 3-6 months old APPswePS1dE9 Alzheimer mice following chronic administration of pantoprazole

The second part of my study was carried out initially in younger male and female (age: 12-16 weeks) and later in male (age: 17-21 weeks) controls and APPswePS1dE9 Alzheimer’s mice. Pantoprazole was continuously administered to younger groups for 6 weeks and older groups for ~13 weeks. Previous studies have reported a potential negative impact of proton pump inhibitors (PPIs) on AD incidence and progression, while, on the other hand, some recent studies also reported positive effect of PPIs on AD. Thus, the present study was designed to perform FFT based frequency and seizure analysis in controls and APPswePS1dE9 mice following chronic pantoprazole administration.

The present study was aimed to investigate the following objectives:

1) Analysis of hippocampal theta and cortical gamma oscillatory relative powers in APPswePS1dE9 mice compared to controls of both adolescent and adult mouse groups.
2) Investigation of chronic pantoprazole administration on central rhythmicity, particularly the hippocampal theta and cortical gamma activity associated with cognition as analyzed in APPswePS1dE9 mice compared to controls of both genders.
3) Analysis of seizures activity in both genders and genotypes, and its association with alterations in central rhythmicity and symptoms of AD progression.
4) Influence of chronic pantoprazole administration on seizures activity in both adolescent and adult mouse groups.

# 3. Materials and Methods

## 3.1. Materials

**Table 3.1**: **Chemicals.**

| **Chemicals** | **Company** |
|---|---|
| 0.9% NaCl | B. Braun Melsungen AG, Germany |
| 2-Propanol - Purity: ≥ 99.5 % (HPLC grade) | Sigma-Aldrich Chemie GmbH, Germany |
| Acetic acid - Purity: ≥ 99.8 % | Merck KGaA, Germany |
| Acetonitrile (CAN)<br>LC-MS Chromasolv® - Purity: ≥ 99.9 % | Sigma-Aldrich Chemie GmbH, Germany |
| Agarose | Sigma-Aldrich Chemie GmbH, Germany |
| Ammonium acetate<br>Purity: LC-MS grade | Sigma-Aldrich Chemie GmbH, Germany |
| Boric Acid $H_3BO_3$ | Sigma-Aldrich Chemie GmbH, Germany |
| dd$H_2O$ (double-distill water) – analysis grade<br>Sartorius arium® | Sartorius AG, Germany |
| D-Glucose 5% (w/v) - for injection | B. Braun Melsungen AG, Germany |
| Dichloromethane<br>Purity: ≥ 99.8 % (HPLC grade) | Sigma-Aldrich Chemie GmbH, Germany |
| Dimethyl sulfoxide<br>Purity: ≥ 99.8 % (HPLC grade) | Sigma-Aldrich Chemie GmbH, Germany |
| Disodium EDTA | Sigma-Aldrich Chemie GmbH, Germany |
| Eosin Y (Solvent red 43)<br>Storage: light sensitive | Sigma/Aldrich Chemie GmbH, Germany |
| Ethanol | Merck, Germany |
| Fetal calf serum (FCS), Gibco® | Thermo scientific, Germany |
| Hematoxylin (Natural Black 1) | Sigma-Aldrich Chemie GmbH, Germany |
| Human liver microsomes, Gibco® | Thermo scientific, Germany |
| Isoflurane Baxter® 100% (v/v) | Baxter International, Germany |
| Ketamine HCl Ketavet®<br>Injectable 100 mg/ml Ketamine | Pfizer, USA |
| Methanol - Purity: ≥ 99.9 % | Sigma-Aldrich Chemie GmbH, Germany |

| | |
|---|---|
| NADPH, tetrasodium salt | Biomol GmbH, Germany |
| Pantoprazole sodium hydrates<br>Purity: ≥ 98 %  (HPLC grade) | Sigma-Aldrich Chemie GmbH, Germany |
| Pantoprazole-D7 sodium salt (D6-Major)<br>Purity: ≥ 97 % (HPLC grade) | Santa Cruz Biotechnology Inc, USA |
| Paraformaldehyde (PFA) | Merck, Germany |
| Rimadyl®, Injectable 50 mg/ml Carprofen | Pfizer, Germany |
| Ringer’s solution for injection | B. Braun Melsungen AG, Germany |
| Rompun® - Injectable 100 mg/ml xylazine | Bayer, Germany |
| Trizma Base | Sigma-Aldrich Chemie GmbH, Germany |

**Table 3.2: Laboratory equipment.**

| Equipment | Company |
|---|---|
| Aesculap Exacta Wireless shaver ‘small’ | Aesculap, Germany |
| Auto sampler | Shimadzu Corporation, Japan |
| Binocular surgical magnification<br>Microscope Zeiss Stemi 2000 | Zeiss, Germany |
| Centrifuges:<br>Eppendorf Centrifuge 524R (21130 × g)<br>Avanti J-26 XP Centrifuge (82,000 × g) | <br>Eppendorf AG, Germany<br>Beckman Coulter Inc, USA |
| Chemidoc Touch (Gel documentation) | Bio-Rad, Germany |
| Cold light source KL2500 LCD | Schott, Germany |
| Column<br>Accucore® C8 LC column<br>(50 mm× 3 mm × 2.7 µm) | Thermo Scientific, Germany |
| Degasser | Shimadzu Corporation, Japan |
| Electric blanket<br>AEG® HK5510 100W | AEG AG, Germany |
| Incubator:<br>Stuart® Orbital Incubator S1500 | Stuart Equipment, UK |
| LightCycler® 480 System (qPCR) | Roche, Germany |
| MS / MS System<br>QTRAP® 6500 | AB Sciex GmbH, Germany |

| | |
|---|---|
| Nitrogen evaporator<br>(evaporator system EVA-EC1-S) | VLM, Germany |
| Pump A | Shimadzu Corporation, Japan |
| Pump B | Shimadzu Corporation, Japan |
| Spectrophotometer - Nano Drop ND-1000 | PeqLab Biotechnology GmbH, Germany |
| Stereotactic framework - Neurostar 51730M | Stoelting Europe, Ireland |
| Surgical Drill 141<br>Industrial drill grinder IBS / E | Proxxon GmbH, Germany<br>Lange-Zahnbohrfabrik e.K, Germany |
| Thermocycler (C1000) | BioRad, Germany |
| Tissue homogenizer:<br>TissueLyzer II®<br>TissueRuptor II® | Qiagen GmbH, Germany |
| Ultrapure water system<br>Sartorius arium® pro UV | Sartorius AG, Germany |
| Vacuum Centrifuge<br>S-Concentrator, SA-VC-300H | Helmut Saur, Germany |
| Vibratome<br>Vibroslice Tissue Cutter EMS 5000mz | Campden Instruments Limited, UK |
| Vortex Mixer: VWR VV3 S40 | VWR International, USA |
| Weighing balance - AX205 Delta Range® | Mettler-Toledo GmbH, Germany |

**Table 3.3: Consumables.**

| Consumables | Company |
|---|---|
| ALZET®2002 osmotic pump | Charles River, Germany |
| Bepanthen® dexpanthenol | Bayer, Germany |
| Betaisodonna® - Povidone-Iodine | Mundipharma, Germany |
| Cement: Dental glassionomercement | Kent Dental, UK |
| Cotton swab | Hartmann, Germany |
| Electrode extension<br>UEWLGESEANND<br>Tungsten Microelectrode | FHC, USA |
| Drape sheet | Hartmann, Germany |
| Gauze swabs | Hartmann, Germany |

| | |
|---|---|
| Gloves | Unigloves, Germany |
| HPLC Vials<br>100 vials, with 200 µl insert | Macherey-Nagel GmbH, Germany |
| Omnican® 50 (insulin syringe) | Braun, Germany |
| Omnican® fine dosage 1ml | Braun, Germany |
| Pipette Tips:<br>epT.I.P.S Reloads® 50-1000 µl<br>epT.I.P.S Reloads® 2-200 µl<br>epT.I.P.S Reloads® 0.1-10 µl | Eppendorf AG, Germany |
| Pipettes:<br>Eppendorf Research Plus 0.5-5 ml<br>Eppendorf Research 100-1.000 µl<br>Eppendorf Research 20-200 µl<br>Eppendorf Research 10-100 µl<br>Eppendorf Research 2-20 µl<br>Eppendorf Research 0.5-10 µl<br>Eppendorf Research 0.1-2.5 µl | Eppendorf AG, Germany |
| Reaction Vessels:<br>DNA LoBind Tubes® 1.5 ml<br>DNA LoBind Tubes® 2.0 ml<br>Safe-Lock-Tubes® 1.5 ml<br>Safe-Lock-Tubes® 2.0 ml | Eppendorf AG, Germany |
| Scalpel | Braun, Germany |
| Sugi® Eye spear pointed tip | Kettenbach, Germany |
| Sutures:<br>Sabafil® Nylon USP 6/0, thread length 45 cm | SABANA Medical Supplies, Germany |

**Table 3.4: Surgical instruments.**

| Surgical instruments | Company |
|---|---|
| Bulldog clamps | Aesculap, Germany |
| Graefe forceps-curved with teeth | |
| Graefe forceps-curved, serrated | |
| Halsey micro needle holder (15.5 cm) | |

| | |
|---|---|
| Iris scissors extra thin (15.5 cm) | OR<br>Fine Science Tools, Germany |
| Lexar baby scissors (10 cm) | |
| Olsen-Hegar Needle Holder extra delicate | |
| Standard tweezers (12 cm / 14.5 cm length) | |
| Tissue forceps 1x2 teeth (12 cm length) | |
| Tungsten carbide iris scissors (11.5 cm) | |

**Table 3.5: EEG Recording system.**

| Equipment | Company |
|---|---|
| Data exchange matrix | Data Science International, USA |
| RPC-1 Receiver | |
| Transmitters:<br>TA10ETA-F20<br>TL11M2-F20-EET | |

**Table 3.6: Software.**

| Software | Company name |
|---|---|
| Analyst 1.6.2 | AB SciexPte. Ltd., Singapore |
| ChemDrawProfessional 16.0 | PerkinElmer Inc., USA |
| DataQuest ART 4.36 | Data Sciences International, USA |
| GraphPad Prism 6 | GraphPad Software Inc., USA |
| LightCycler 480 software | Roche, Germany |
| Mass Spectrum Interpreter 2 | NIST Mass Spectrometry Data, National Institute of Standards and Technology, USA |
| Microsoft Excel 2016 | Microsoft Corp., USA |
| MultiQuant 3.0.1 | AB SciexPte. Ltd., Singapore |
| NeuroScore 3.1.6 | Data Sciences International, USA |
| Neurostar 2.6.0 | Neurostar, Germany |
| qBase+ - qPCR analysis | Biogazelle, Belgium |

## 3.2. Methods

### 3.2.1. Ethics statement

All experimental procedures were performed according to the guidelines of the German Council on Animal Care and every experimental protocol was approved by the local Institutional and National Committee on Animal Care (Landesamt fur Natur, Umwelt und Verbraucherschutz, LANUV, Germany). All animal experimentation was conducted according to the European Communities Council Directive November 24, 1986 (86/609/EEC) and of September 22, 2010 (2010/63/EU). Special considerations were done to reduce the animal size and their sufferings to follow the 3R (Replacement, Reduction, Refinement) strategy.

### 3.2.2. Experimental animal housing

Mice were transferred from the main animal facility to the experimental lab animal room one week before the transmitter implantation took place in order to acclimatize. Mice were housed in groups of 3-4 in clear type II polycarbonate cages (26.7cm x 20.7 cm x 14.0 cm, area: 410 $cm^2$) with *ad libitum* access to drinking water and standard food pellets. Animal cages were kept in ventilated cabinets (Techniplast, Germany and Bioscape, Germany) at a temperature of 21 ± 2°C, 50–60% relative humidity, and a conventional 12 h/12 h dark/light cycle beginning at 5:00 pm.

**Figure 3.1**: **Ventilated cabinets for standard housing conditions for pre- and post-surgery placement and EEG recordings** (Lundt, Wormuth, Siwek, Muller, et al., 2016; Papazoglou, Soos, et al., 2016).

### 3.2.3. Experimental animals - $Ca_v3.2$ deficient mice

$Ca_v3.2^{+/-}$ embryos (kindly provided by Kevin Campbell via MMRCC – Mutant Mouse Resource & Research Centers) were re-derived with C57BL/6J mice and maintained with random intra-strain mating obtaining all genotypes wild type (WT), heterozygous (HT), knockout (KO).

### Genotyping $Ca_v3.2$ mice

All mice were genotyped by PCR twice, at the start and at the end of the experiment for genotype verification. DNA preparation from an ear punch and genotyping PCR was performed by the KAPA Mouse genotyping kit (Sigma Aldrich, Germany) (Tab. 3.7). The following set of primers was used: WT-fwd/KO-fwd: 5'-ATT CAA GGG CTT CCA CAG GGT A-3',WT-rev: 5'-CAT CTC AGG GCC TCT GGA CCA C-3', KO-rev: 5'-GCT AAA GCG CAT GCT CCA GAC TG -3'. The PCR was carried out by the C1000 thermal cycler (BioRad, Germany). Subsequently, PCR products were separated via 1.5% agarose gel electrophoresis and visualized by ChemiDoc Touch (BioRad, Germany) (Fig. 3.2).

**Table 3.7: Ca$_v$3.2 mice PCR cycling parameters.**

| Steps | Temp. (°C) | Duration | Cycles |
|---|---|---|---|
| 1.Denaturation | 94 | 3 min | 1 |
| 2.Denaturation | 94 | 30 sec | 34 x |
| Annealing | 60 | 30 sec | |
| Elongation | 72 | 60 sec | |
| Final elongation | 72 | 10 min | 1 |

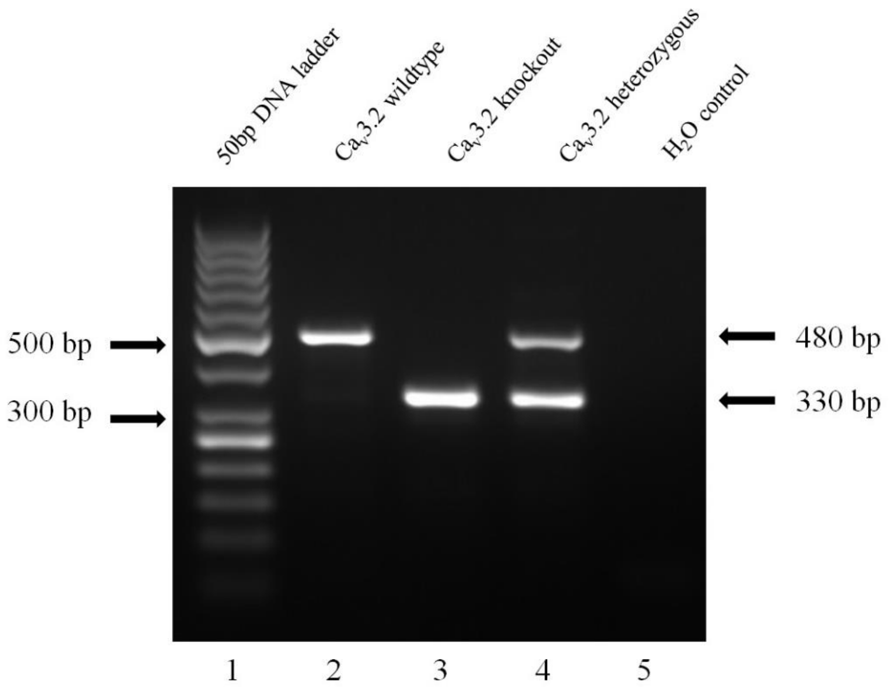

**Figure 3.2: Ca$_v$3.2 mice genotyping PCR**. DNA ladder (lane 1); WT animal (lane 2); KO animal (lane 3); HT animal (lane 4); water control (no DNA) (lane 5).

### 3.2.4. Experimental animals - APPswePS1dE9 transgenic mice

APPswePS1dE9 transgenic (TG) mice were kindly provided by Priv.-Doz. Dr. Dan Ehninger, Translational Biogerontology, German Centre for Neurodegenerative diseases (DZNE), Bonn, Germany (B6.Cg-TG(APPswe,PSEN1dE9)85Dbo/Mmjax, Jackson Laboratory, USA). The APPswePS1dE9 mice have Black 6 background and carry a chimeric mouse/human APP gene with the Swedish mutation (APPswe) as well as the human presenilin-1 gene lacking exon 9 (Jankowsky et al., 2004).

### Genotyping of APPswePS1dE9 mice

All mice were genotyped twice, once at the start and once at the end of the experiment for genotype verification. DNA from an ear punch was isolated by peqGOLD DNA tissue Mini Kit, (PEQLAB, Germany). PCR primers are presented on Table. 3.8. The PCR was performed with Red Taq Master Mix (Sigma Aldrich, Germany) (Tab. 3.9) on C1000 thermal cycler (BioRad). The amplified PCR products were separated by agarose 1.5% gel electrophoresis and visualized by ChemiDoc Touch (BioRad, Germany) (Fig. 3.3).

**Table 3.8: Primers used for mice genotyping.**

| Primer | Sequence (5´-3´) | Gene Size |
|---|---|---|
| Primer oIMR3610 (*APP-forward) | AGGACTGACCACTCGACCAG | 377 bp |
| Primer oIMR3611 (*APP-reverse) | CGGGGGTCTAGTTCTGC | |
| Primer oIMR1644 (*PSEN1-forward) | AATAGAGACACGGAGCA | 608 bp |
| Primer oIMR1645 (*PSEN1-reverse) | GCCATGAGGGACACATATCAT | |
| *Chrm5 Forward (internal control) | ACCTTGGACCAAATCTGAGTGTA | 257 bp |
| *Chrm5 Reverse (internal control) | GGCCAAGCTGAGCAGGTAAT | |

*APP primers amplify the mouse generic APP gene (377 bp).

*PSEN1 primers amplify the mouse generic PSEN1 gene (608 bp).

*Chrm5 primers amplify the mouse muscarinic 5-receptor gene (257 bp) – used as internal control.

**Table 3.9: PCR steps.**

| Steps | Temp. (ºC) | Duration | Cycles |
|---|---|---|---|
| 1.Denaturation | 94 | 3 min | 1 |
| 2.Denaturation | 94 | 30 sec | 34 x |
| Annealing | 48 | 30 sec | |
| Elongation | 72 | 60 sec | |
| Final elongation (optional) | 72 | 10 min | 1 |

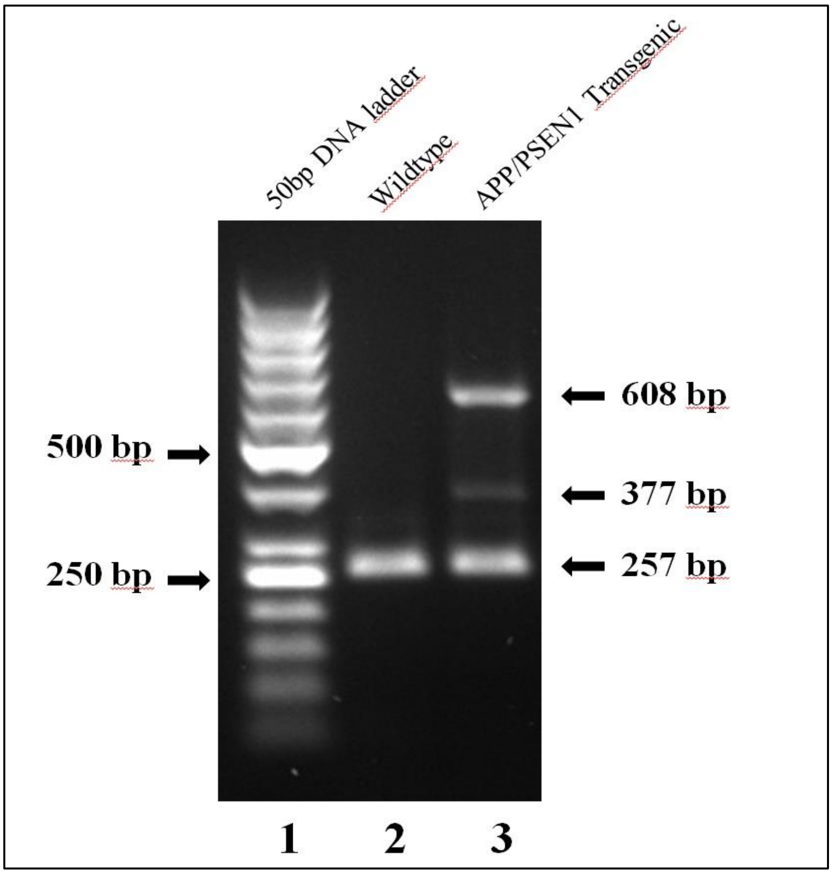

**Figure 3.3: APPswePS1dE9 mice genotyping PCR**. DNA ladder (lane 1); WT animal (lane 2); TG animal (lane 3).

### 3.2.5. Radiotelemetry system and transmitters

Implantable EEG radiotelemetry is an in vivo methodological approach used to measure physiological and behavioral parameters from conscious and unrestrained animals (Lundt, Wormuth, Siwek, Muller, et al., 2016; Papazoglou, Soos, et al., 2016). The telemetry system used in my study is from Data Science International (DSI, USA) (Fig. 3.4).

The Cav3.2 mice were implanted with the one channel Physio Tel TA10ETA-F20 transmitter with the following technical specifications: 3.9 g, 1.9 cc, input voltage range ±2.5 mV, channel bandwidth 1-200Hz (B), nominal sampling rate (f) 1000 Hz (f = 5B), temperature operating range 34-41$^{o}$C, warranted battery life 4 months, on/off mechanism magnetically actuated (DSI, USA).

The APPswePS1dE9 mice were implanted with the two channel TL11M2-F20EET transmitter with the following technical specifications: 3.9 g, 1.9 cc, input voltage range ±1.25 mV, channel bandwidth 1-50 Hz (B), nominal sampling rate (f) 250 Hz (f = 5B), temperature operating range 34-41$^{o}$C, warranted battery life 1.5 months, on/off mechanism magnetically actuated, (DSI, USA). The minimum animal weight for subcutaneous implantation of TA10ETA-F20 and TL11M2-F20EET is 20 g. Therefore, the weight of all implanted animals included in this work was higher than 20 g at the day of implantation (Lundt, Wormuth, Siwek, Muller, et al., 2016; Papazoglou, Lundt, et al., 2016; Weiergraber, Henry, Hescheler, Smyth, & Schneider, 2005).

Both transmitters that were used could also measure the mouse temperature and activity. In our experiments, the transmitters were implanted subcutaneously. Although temperature measured from subcutaneous pouch do not represent the body core temperature, data were shown that subcutaneous body temperature could be correlate with body core temperature under environmentally controlled conditions. Thus subcutaneous temperature measured by the transmitter could be used as a physiological parameter (Lundt, Wormuth, Siwek, Muller, et al., 2016; McCafferty, Gallon, & Nord, 2015; Moons, Hermans, Remie, Duchateau, & Odberg, 2007; Müller et al., 2017; Papazoglou, Lundt, et al., 2016). The activity data provided by the transmitter was measured as mean relative activity units. The units were calculated by the binary system, where, activity = 0 - inactive state and activity > 0 - active state. These units represent the activity in horizontal plane and integrate both trip distance, velocity and acceleration (Lundt, Wormuth, Siwek, Muller, et al., 2016).

**Figure 3.4: Each cage with an implanted mouse was placed on a receiver plate that was connected to a data exchange matrix**. The EEG recording data was transferred through the receiver to the data exchange matrix and stored to the connected a computer.

### 3.2.6. Radiotelemtric transmitter placement and electrode implantation

#### 3.2.6.1. Anesthesia

Mice were placed in a chamber with continuous supply of isoflurane (Baxter, 100 % v/v) (3-5%) and carbogen (5% $CO_2$ and 95% $O_2$, 0.5-1 l/min) to induce anesthesia (Fig. 3.5A). The anesthetized mice were placed on heating blanket to avoid surgical hypothermia and they were continuously supplied with isoflurane (1.5-3%) and carbogen (5% $CO_2$ and 95% $O_2$, 0.5-1 l/min) through a silicon facemask to maintain the depth of anesthesia (Fig. 3.5A).

**Note:** Appropriate anesthetic concentration of isoflurane depends on the age, sex, body weight and genotype of the animal. Therefore, it was necessary to check the depth of anesthesia by reflexes using foot pinch and tail pinch. A scavenger system was used during the isoflurane application to avoid exposure of anesthetic gas (Lundt, Wormuth, Siwek, Muller, et al., 2016; Papazoglou, Lundt, et al., 2016).

#### 3.2.6.2. Transmitter placement

Following anesthesia, dexpanthenol (Bepanthen, Bayer Vital GmbH, Germany) was applied in the eyes of the animal to avoid corneal desiccation during the surgery. The animal hair from the upper head region were shaved and the area was disinfected (Betaisodona®Solution, Mundipharma GmbH, Germany). A midline incision was made by scalpel from forehead region and the craniometric landmarks bregma and lambda were visualized (Fig. 3.6B). Furthermore, a subcutaneous pouch was formed by blunt dissection using surgical scissors starting from nuchal site to lower side abdominal region. Physiological normal saline (1 ml, 0.9%, NaCl) was flushed into the pouch and the transmitter was placed inside the pouch at the back of the animal with sensing leads oriented cranially.

#### 3.2.6.3. Electrode implantation

Following transmitter placement, the experimental animals were placed in the mouse 3D stereotaxic frame (Neurostar, Germany) (Fig. 3.5) under constant anesthesia supply. The mouse head was fixed by using the ear bar and the nose clamp so that the craniometric landmarks bregma and lambda were positioned at the same level (Fig. 3.5B). Holes on the mouse skull were made pressure free with a neurosurgical drill at a full speed (90000 RPM). Holes were made at specific coordinates according to the brain area of interest (Fig. 3.6C1). All stereotaxic coordinates presented on Table 3.10 were based on Paxinos and Watson Mouse Brain Atlas (Paxinos, 1998).

**Table 3.10: Electrode positioning coordinates.**

| | **Transmitters** | |
|---|---|---|
| **Hippocampus (CA1)** | **TA10ETA-F20** | **TL11M2-F20EET** |
| Anterior-Posterior | -2.0 mm | -2.0 mm |
| Lateral | 1.5 mm (right hemisphere) | 1.5 mm (right hemisphere) |
| Dorsal-Ventral | 1.5 mm | 1.5 mm |

| | **Transmitters** | |
|---|---|---|
| **Motor Cortex (M1)** | **TA10ETA-F20** | **TL11M2-F20EET** |
| Anterior-Posterior | N/A | 1.42 mm |
| Lateral | N/A | -2.0 mm (left hemisphere) |
| Dorsal-Ventral | N/A | 0.0 mm |

Epidural reference electrodes for both channels were positioned on the cerebellar cortex as follows: AP 5.5 mm, L + 1.5 mm (right hemisphere) and -1.5 mm (left hemisphere) (Fig. 3.6D). The sensing lead of the transmitter that was placed at CA1 region was mechanically attached to a tungsten electrode (FHC, USA), bent at a 90° angle and cut at 1.5 mm (Fig. 3.6C3). The tungsten electrode had a shank diameter of 250 $\mu$m, a tip impedance of 50–100 kΩ and was insulated with epoxylite/parylene coated (Fig. 3.6C3).

Motor cortex and reference electrodes were placed directly on the dura mater. The stainless steel helix of the transmitter sensing lead was exposed by removing the silicon coating and bent at the tip. The bending tip was inserted in the skull hole as shown in Fig. 3.6D.

Surface and deep electrodes were fixed using glass ionomer cement (Kent Dental, Kent Express Ltd., UK). Then scalp was closed using over-and-over sutures (Ethilon, 6-0) and antiseptic (Betaisodona®Solution, Mundipharma GmbH, Germany) was applied on closed scalp (Lundt, Wormuth, Siwek, Muller, et al., 2016; Papazoglou, Lundt, et al., 2016; Weiergraber, Henry, Hescheler, et al., 2005).

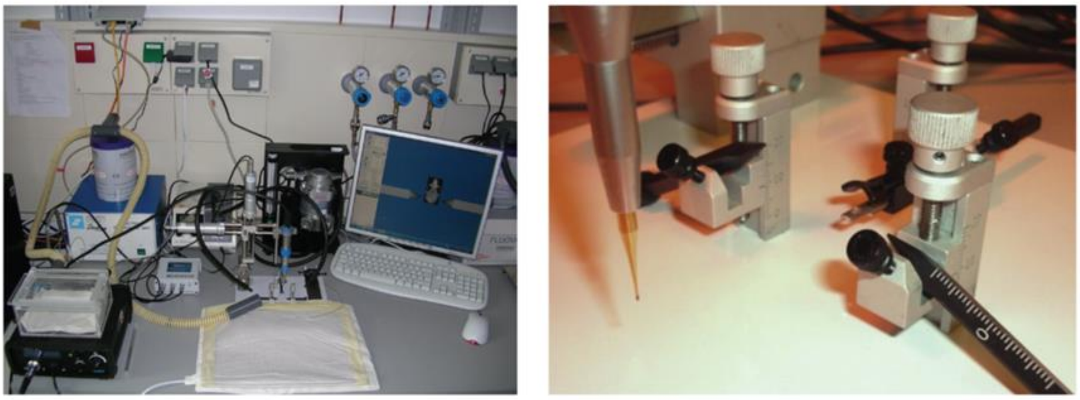

(A) (B)

**Figure 3.5: (A) Isoflurane chamber, isoflurane evaporator, isoflurane scavenger module, 3D computerized stereotaxic frame, heating blanket (B) High precision drill and stereotaxic frame including the ear bar and the nose clamp** (Lundt, Wormuth, Siwek, Muller, et al., 2016; Papazoglou, Lundt, et al., 2016; Weiergraber, Henry, Hescheler, et al., 2005).

#### 3.2.6.4. Postoperative pain management and care

For postoperative pain management, Carprofen (5mg/kg, Rimadyl, Parke-Davis/Pfizer, Germany) was administered subcutaneously 10-15 minutes before the end of the surgery. Due to body surface/body volume ratio, mice are highly susceptible to hypothermia. Thus, freshly implanted animals were positioned on a heating pad for 3-4 days to avoid post-surgical hypothermia and to maintain physiologically body core temperature. The animals were fed with moisten pellets in order to facilitate the food uptake. Mice were given 10 additional days after surgery to fully recover, prior to EEG recording. This recovery period was based on the observation that no differences in basic physiological/behavioral parameters such as food/water uptake, motor activity, and body core temperature were detected between radiotransmitter implanted, non-implanted, and sham-operated mice 10 days after surgery (Kramer & Kinter, 2003; Lundt, Wormuth, Siwek, Muller, et al., 2016; Papazoglou, Lundt, et al., 2016) (Fig. 3.6F).

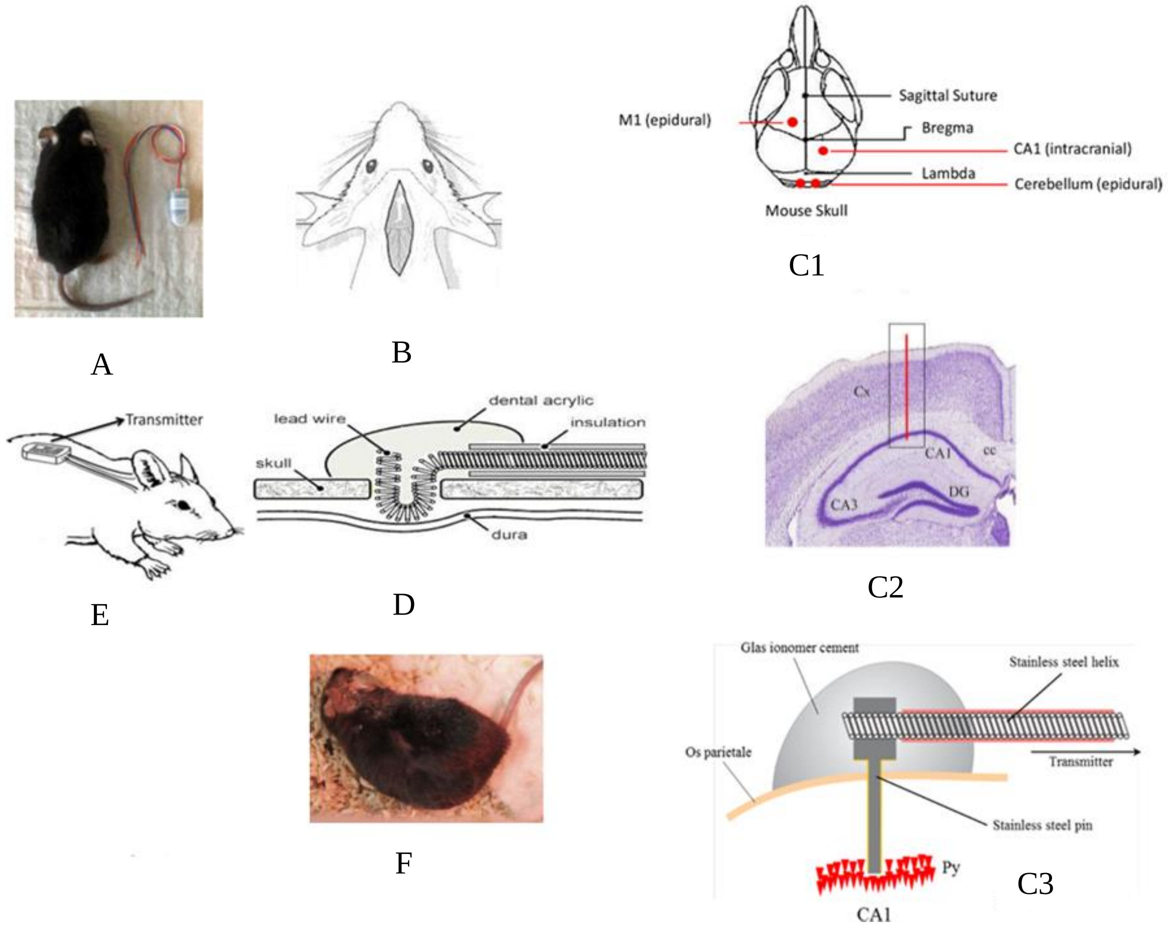

**Figure 3.6: Transmitter, stereotaxic surface and deep electrode implantation**: (A) C57BL/6 mouse and 2 channel radiotransmitter (TL11M2-F20EET) (B) mouse midline incision on the forehead region (C1) epidural differential electrode is placed on the motor cortex (M1), and an additional intrahippocampal differential electrode is placed in the CA1 region of the hippocampus. Both epidural reference electrodes are localized on the cerebellum (C2) coronal section (scheme) illustrating the localization of the deep, intracranial electrode for CA1 EEG (C3) deep electrode attached with sensing lead of radiotransmitter and their placement at mouse skull (D) scheme of an epidural electrode placement in mice (E) scheme of a radiotransmitter subcutaneously placed at the back of a mouse (F) mouse after transmitter/electrode implantation (Lundt, Wormuth, Siwek, Muller, et al., 2016; Papazoglou, Lundt, et al., 2016; Weiergraber, Henry, Hescheler, et al., 2005).

#### 3.2.6.5. Confirmation of EEG electrode placement

To confirm whether electrodes were positioned in the CA1 target area, brains were extirpated postmortem and fixed in 4% PFA. Then, brains were cut to 60 $\mu$m slices using a Vibroslice Tissue Cutter EMS 5000-MZ (Campden Instruments Limited, UK). Slices were stained with hematoxylin/eosin or with Nissl staining to visualize the branch canal (Fig. 3.6C2). Animals, in which electrodes were not placed in the target region, were excluded from frequency analysis.

### 3.2.7. Ca$_v$3.2 project

#### 3.2.7.1. Study animals

In total, eight Ca$_v$3.2$^{+/+}$ (male♂, mean age: 124±1 days or 17.73 ± 0.196 weeks) and eight Ca$_v$3.2$^{-/-}$ (male♂, mean age: 129 ± 4 days or 18.39 ± 0.594 weeks) were analyzed in this study.

#### 3.2.7.2. Experimental design and EEG recording

Ca$_v$3.2 animals were implanted with a TA10ETA-F20 transmitter and recorded from the hippocampal CA1 region.

The first 24 h baseline recording (R1) was performed at day 10 post implantation from the CA1 hippocampal region. The second 24 h baseline recording (R2) was performed at day 17 post implantation.

Additionally, at day 18 and 25 after implantation (U1 and U2 respectively) the animals were injected with urethane (800 mg/kg freshly dissolved in 0.9% NaCl Sigma-Aldrich, Germany,) and an EEG was recorded (U1, U2 respectively) (Fig. 3.7).

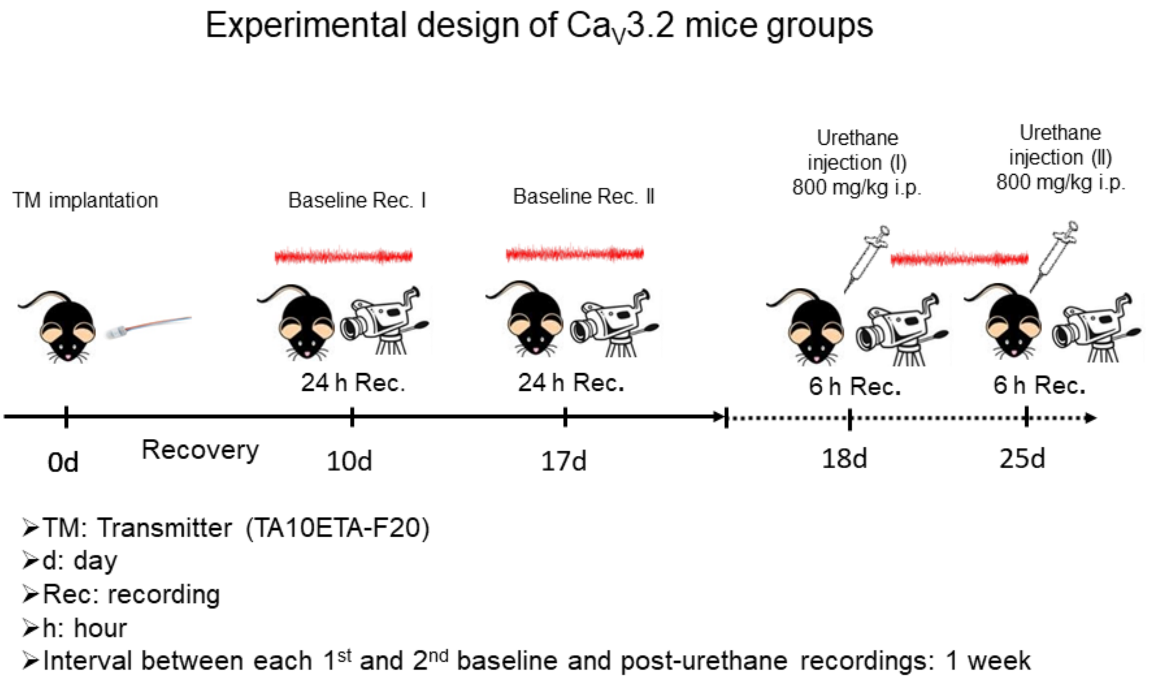

**Figure 3.7: Experimental design of Ca$_v$3.2 project - electrode implantation, R1 and R2 recordings, U1 and U2 recordings.**

### 3.2.7.3. Analysis of electrophysiological data

EEG data was exported to NeuroScore software (DSI, USA) and analyzed by FFT (Fast Fourier Transformation) based approach in the frequency range of 0.5-500 Hz. Each frequency range that was analyzed presented in Table 3.11.

**Table 3.11: Frequency ranges analyzed for the $Ca_v3.2$ project.**

| EEG oscillation (Frequency) | Frequency range |
|---|---|
| Delta 1 ($\delta_1$), Delta ($\delta_2$) | 0.5-4 Hz, 1-4 Hz |
| Theta 1 ($\theta_1$), Theta 2 ($\theta_2$) | 4-8 Hz, 4.1-12 Hz |
| Alpha ($\alpha$) | 8-12 Hz |
| Sigma ($\sigma$) | 12-16 Hz |
| Beta 1 ($\beta_1$), Beta 2 ($\beta_2$), Beta 3 ($\beta_3$) | 12.1-30 Hz, 16-24 Hz, 16-30 Hz |
| Gamma low ($\gamma_{low}$), Gamma mid ($\gamma_{mid}$), Gamma high ($\gamma_{high}$), Gamma ripples ($\gamma_{ripples}$), Gamma fast ripples ($\gamma_{fast\ ripples}$) | 30-50 Hz, 50-70 Hz, 70-100 Hz, 80-200 Hz, 200-500 Hz |

### 3.2.7.4. Radiotelemetric EEG data acquisition

EEG data acquisition was performed by Dataquest ART 4.2 software (DSI) at a nominal sampling rate of 1000 Hz (TA10ETA-F20 transmitter) with no priori filter cutoffs (Lundt, Wormuth, Siwek, Muller, et al., 2016; Papazoglou, Lundt, et al., 2016).

The length of the individual EEG epoch analyzed was 2 s (Lundt, Wormuth, Siwek, Müller, et al., 2016; Müller et al., 2017; Papazoglou, Lundt, et al., 2016). The actual TA10ETA-F20 transmitter (DSI, USA) bandwidth (B) is 200 Hz resulting in a nominal sampling rate (f) at 1000 Hz, (f = 5 X B). Thus, based on the Nyquist-Shannon theorem, the transmitter can only reliable record frequencies up to 500 Hz (Weiergraber, Papazoglou, Broich, & Muller, 2016).

Mean EEG relative power (%) of the individual frequency range was calculated for the dark/light circadian stages for the R1 and R2 recordings i.e. two dark (D1, D2) and two light cycles (L1, L2) and the two post urethane injections recordings U1 and U2.

Relative activity counts and temperature data were analyzed R1 and R2 as well as for U1 and U2. Importantly, mice active state (activity units > 0) or inactive state (activity units = 0) during the 12 h dark/light cycles were correlated with the relative EEG power of each individual frequency bands from the hippocampal deflections.

Further, power spectrum density (PSD) analysis for theta/alpha frequencies for both genotypes and from both baseline and post-urethane phases were also performed to get more insight into the hippocampal theta/alpha architecture.

Data were statistically analyzed and displayed as mean ± SEM. Statistics for frequencies, activity and temperature analysis were carried out using multiple Student's t-test, corrected for multiple comparison using the Holm-Sidak method ($*p < 0.05$; $**p < 0.01$; $***p < 0.001$). All statistics and graph presentations were performed with GraphPad Prism 6 (GraphPad Software, USA).

### 3.2.7.5. Quantitative Real Time PCR (qPCR)

Transcriptome analysis of hippocampi from control and $Ca_v3.2^{-/-}$ mice revealed various gene candidates that could be functionally related to altered thetagenesis (Papazoglou, Soos, et al., 2017). To investigate the molecular mechanism involved in the generation of hippocampal EEG oscillations in $Ca_v3.2$ deficient mice, hippocampal transcript levels of potential gene candidates, i.e. Dynein Light Chain Tctex-Type 1 (Dynlt1b), Neuronatin (Nnat), LLP homolog, long-term synaptic facilitation (Aplysia) (Llph), ATP synthase, $H^+$ transporting, mitochondrial F0 complex, subunit G (Atp5l) and 5-hydroxytryptamine receptor 2C (Htr2c) were analyzed using quantitative real time (RT) PCR (qPCR).

In a second approach, qPCR analysis of selected gene candidates of the GABAergic system was performed including GABA A receptor delta subunit (Gabrd), GABA A receptor gamma subunit (Gabrg2), GABA B1 receptor subunit (Gabbr1) and GABA B2 receptor subunit (Gabbr2). These subunits were selected for the following reasons: GABA A receptors are pentamers of four transmembrane domains that build up an intrinsic anion selective channel. In mammals, sequences of six α, three β, three γ, one δ, three ρ, one ε, one π and one θ GABA A receptor subunits have been described (Olsen & Sieghart, 2008, 2009; Sieghart, 2006; Sigel & Steinmann, 2012). Currently, 11 native GABA A receptors are classed as conclusively identified (i.e., α1β2γ2, α1βγ2, α3βγ2, α4βγ2, α4β2δ, α4β3δ, α5βγ2, α6βγ2, α6β2δ, α6β3δ and ρ) with further receptor isoforms occurring with high probability, or only tentatively (Olsen & Sieghart, 2008, 2009). Many GABA A receptor subtypes contain α-, β- and γ-subunits with a stoichiometry of 2α.2β.1γ (Korpi, Grunder, & Luddens, 2002; Olsen & Sieghart, 2008). It is assumed that the majority of GABA A receptors consist of a single type of α- and β -subunit variant. The α1β2γ2 hetero-oligomer represents the largest setting of GABA A receptors in the CNS, followed by the α2β3γ2 and α3β3γ2 isoforms. Receptors that incorporate the α4- α5-or α6-subunit, or the β1-, γ1-, γ3-, δ-, ε- and θ-subunits, are less numerous, but they may nonetheless serve important functions. Notably, GABA A receptors incorporating the γ2 subunit (except when associated with α5) cluster at the postsynaptic membrane (but may distribute dynamically between synaptic and extrasynaptic locations), whereas as those incorporating the δ subunit appear to be exclusively extrasynaptic (Z. W. Chen & Olsen, 2007; Jacob, Moss, & Jurd, 2008; Luscher, Fuchs, & Kilpatrick, 2011; Vithlani, Terunuma, & Moss, 2011). We have thus checked for the GABA A δ and γ subunit in my study. Functional GABA B receptors on the other hand are formed from the heterodimerization of two similar 7TM subunits termed GABA B1 and GABA B2 (Bowery et al., 2002; Emson, 2007; Pin et al., 2004; Pin et al., 2007; Ulrich & Bettler, 2007). GABA B receptors are widespread in the CNS and regulate both pre- and postsynaptic activity. Co-expression of GABA B1 and GABA B2 subunits allows transport of GABA B1 to the cell surface and generates a functional receptor that can couple to signal transduction pathways such as high-voltage-activated $Ca^{2+}$ channels ($Ca_v2.1$, $Ca_v2.2$), or inwardly rectifying potassium channels (Kir3) (Bettler, Kaupmann, Mosbacher, & Gassmann, 2004; Bowery et al., 2002; Bowery & Enna, 2000).

Finally, $Ca_v3.1$ (Cacna1g) and $Ca_v3.3$ (Cacna1i) were also analyzed to check for potential alterations in other LVA T-type $Ca^{2+}$ channel transcript levels. Forward and reverse primer sequences of candidate genes are displayed in Table 3.12.

Total RNA was extracted from the hippocampus of male $Ca_v3.2^{+/+}$ control animals (mean age: 19.32 ± 0.44 weeks, n = 8) and male $Ca_v3.2^{-/-}$ mice (mean age: 20.43 ± 0.41 weeks, n = 8). Additionally total hippocampal RNA was extracted from a female $Ca_v3.2^{+/+}$ mouse in the age of 24.14 weeks, which served as a calibrator in our analysis. First, hippocampal tissue was dissected in RNAprotect Tissue Reagent (Qiagen, Germany) and snap-frozen in liquid nitrogen. Total hippocampal RNA was extracted using RNeasy Lipid Tissue Mini Kit (Qiagen, Germany) including DNA degradation (additional DNase digestion step). Quality and quantity of the extracted RNA was evaluated using Nanodrop (Nanodrop 1000, Thermo Fisher Scientific, Germany). To obtain a 50µl cDNA volume, 1µg of total RNA from each animal was reversely transcribed in a two-step RT-PCR approach using both anchored-oligo $(dT)_{18}$ and hexamer primers (Transcriptor First Strand cDNA Synthesis Kit, Roche, Switzerland). Gene candidates were tested in triplicates in each animal using 2µl cDNA as a template. In addition, a triplicate of calibrator cDNA for normalization of potential inter-run variations was carried out. Duplicates of two negative controls, i.e. no template controls and no reverse transcriptase controls were performed to exclude false positive results. The animals that used for qPCR analysis did not undergo transmitter implantation and consequently EEG recordings.

qPCR was performed in a Light Cycler480 System (Roche, Switzerland) using the following protocol: 95°C (10 min, pre-incubation step); 95°C (10 s, denaturation step); 60°C (20 s, Annealing step); 72°C (30 s, extension step), 35 cycles. This protocol was applied to all studied primer pairs (Tab. 3.12). SYBR Green 1 Master (Roche, Switzerland) was used for signal detection and the specificity of amplification was checked by melting curve analysis.

The CP values received from the LightCycler 480 Software (Roche, Switzerland) were exported to qBase+ software (Biogazelle, Belgium) and analyzed based on a delta-Cq quantification model with qPCR efficiency correction, reference gene normalization considering the reference target stability of the selected housekeeping genes (HPRT, β-actin) and inter-run calibration (Hellemans, Mortier, De Paepe, Speleman, & Vandesompele, 2007). The results were determined as Calibrated Normalized Relative Quantity (CNRQ) and statistically analyzed using the Mann-Whitney test.

**Table 3.12: Sequence of primer pairs used for qPCR.**

| Gene | Forward sequence (5‘ - 3‘) | Reverse sequence (5‘ – 3‘) |
|---|---|---|
| **Htr2c**[1] | CGGTTCAATTCGCGGACTAAGG | GGTCATTGAGCACGCAGGTAGT |
| **Dynlt1b**[1] | GAAGAACGGTGCTGGGTTACAC | CAGATGGACAGTCCGAAGGTAC |
| **ATP5**[1] | CCTACAGCTATTCAGAGTGTGAAA | AAAACCACATCCACACCTCAGTG |
| **Nnat**[1] | GTGGTGGAGGAAGAGGGTTAAG | CACATTTTGGGGAGGGCTTTCG |
| **Gabrd**[2] | TCAAATCGGCTGGCCAGTTCCC | GCACGGCTGCCTGGCTAATCC |
| **Gabrg2**[2] | ACTTCTGGTGACTATGTGGTGAT | GGCAGGAACAGCATCCTTATTG |
| **Gabbr1**[1] | CGTGGGACTTTTCTATGAGACCG | GAACCAGTTGTCAGCATACCACC |
| **Gabbr2** | GGAACACTGCGAAAACACCC | ACCGAACAACATGAGGAGCC |
| **Ca$_v$3.1**[1] | GACCATGTGGTCCTCGTCATCA | TTTCAGCCAGGAAGACTGCCGT |
| **Ca$_v$3.3**[1] | GTCTTCACCAAGATGGACGACC | ACTTCGCACCAGTCAGGCTTGT |
| **Llph** | TGTTGTCTCTCAGGTGAAGCAT | CCCCGTCCACTCTGAGGATA |
| **Hprt**[3] | GCTGGTGAAAAGGACCTCT | CACAGGACTAGAACACCTGC |
| **Actb**[2] | GTCCACACCCGCCACCAGTTCG | ATGCCGGAGCCGTTGTCGAC |

[1] Origene Technologies.

[2] Mendu S.K. et al., PLoS One. 2012;7(8):e42959. doi: 10.1371/journal.pone.0042959. Epub 2012 Aug 21(Mendu, Bhandage, Jin, & Birnir, 2012).

[3] Weiergräber M. et al, Basic Res Cardiol. 2005 Jan;100(1):1-13. Epub 2004 Oct 20 (Weiergraber, Henry, Sudkamp, et al., 2005).

### 3.2.8. APPswePS1dE9 transgenic (TG) mice

#### 3.2.8.1. APP swePS1dE9 mice aged 12-16 weeks

In total, eight mice subgroups were analyzed in my study including four male (♂) and four female (♀) subgroups:

**Male (♂) mice subgroups**

- Wildtype (WT) DMSO (vehicle) treated ♂ controls (mean age: 11.17 ± 0.11weeks, mean weight: 24.03 ± 0.43 g, n = 7).
- Wildtype (WT) pantoprazole treated ♂ controls (mean age: 10.72 ± 0.13 weeks, mean weight: 22.80 ± 0.45 g, n = 6).
- DMSO (vehicle) treated ♂ APPswePS1dE9 transgenic (TG) mice (mean age: 11.03 ± 0.11 weeks, mean weight: 23.52 ± 0.49 g, n = 6).
- Pantoprazole treated ♂ APPswePS1dE9 transgenic (TG) mice (mean age: 10.96 ± 0.19 weeks, mean weight: 23.34 ± 0.43 g, n = 7) (Table 3.13).

**Female (♀) mice subgroups**

- Wildtype (WT) DMSO (vehicle) treated ♀ controls (mean age: 11.04 ± 0.16 weeks, mean weight: 19.80 ± 1.16 g, n = 4).
- Wildtype (WT) pantoprazole treated ♀ controls (mean age: 10.94 ± 0.22 weeks, mean weight: 20.16 ± 0.35 g, n = 5).
- DMSO (vehicle) treated ♀ APPswePS1dE9 transgenic (TG) mice (mean age: 10.93 ± 0.19 weeks, mean weight: 19.80 ± 1.24 g, n = 4).
- Pantoprazole treated ♀ APPswePS1dE9 transgenic (TG) mice (mean age: 10.50 ± 0.15 weeks, mean weight: 20.20 ± 0.60 g, n = 4) respectively (Table 3.13).

**Table 3.13: APPswePS1dE9 mice subgroups 12-16 weeks of age.**

| Gender | Genotype | Mice study subgroups | Group name |
|---|---|---|---|
| Male (♂) | Wild Type (WT) | DMSO: $H_2O$ (1:1) (untreated) | WT-DMSO |
| | | Pantoprazole (treated) | WT-Panto |
| | Transgenic (TG) APPswePS1dE9 | DMSO: $H_2O$ (1:1) (untreated) | APP(TG)-DMSO |
| | | Pantoprazole (treated) | APP(TG)-Panto |
| Female (♀) | Wild Type (WT) | DMSO: $H_2O$ (1:1) (untreated) | WT-DMSO |
| | | Pantoprazole (treated) | WT-Panto |
| | Transgenic (TG) APPswePS1dE9 | DMSO: $H_2O$ (1:1) (untreated) | APP(TG)-DMSO |
| | | Pantoprazole (treated) | APP(TG)-Panto |

### 3.2.8.2. APPswePS1dE9 mice subgroups 17-21 weeks of age

In total, four male (♂) mice subgroups were analyzed in this study including:

- Wildtype (WT) DMSO (vehicle) treated ♂ controls (mean age: 15.48 ± 0.31 weeks, mean weight: 25.70 ± 0.31 g, n = 3).
- Pantoprazole treated ♂ controls (mean age: 15.46 ± 0.04 weeks, mean weight: 26.43 ± 0.96 g, n = 4).
- DMSO (vehicle) treated ♂ APPswePS1dE9 transgenic (TG) mice (mean age: 15.38 ± 0.33 weeks, mean weight: 25.84 ± 0.26 g, n = 3).
- Pantoprazole treated ♂ APPswePS1dE9 transgenic (TG) mice (mean age: 15.43 ± 0.29 weeks, mean weight: 25.80 ± 0.57 g, n = 3) respectively (Table 3.14).

**Table 3.14: APPswePS1dE9 mice subgroups 17-21 weeks of age.**

| Gender | Genotype | Mice study subgroups | Group name |
|---|---|---|---|
| Male(♂) | Wild Type (WT) | DMSO: $H_2O$ (1:1)(untreated) | WT-DMSO |
| | | Pantoprazole (treated) | WT-Panto |
| | Transgenic (TG) APPswePS1dE9 | DMSO: $H_2O$ (1:1)(untreated) | APP(TG)-DMSO |
| | | Pantoprazole (treated) | APP(TG)-Panto |

### 3.2.8.3. Osmotic pumps

**Osmotic pump specifications and pantoprazole concentrations**

Pantoprazole was administered subcutaneously into the mice of APP swePS1dE9 aged 12-16 and 17-21 weeks by ALZET®minipumps (Charles River, Germany). ALZET®osmotic mini pumps (Charles River, Germany) deliver drugs with a constant, controlled and predetermined rate for minimum 3 days to maximum 4 weeks (Fig. 3.8A). In my study, we used the ALZET® 2002 pump (Charles River, Germany) which is a medium sized osmotic pump with a maximum use of 14 days, 200 µl volume of reservoir and average delivery rate of 0.5 µl/h (depending on the LOT Nr.) (Fig. 3.8D). The concentration of pantoprazole that was used in this study was calculated based on the standard pantoprazole human daily dose (40 mg/70kg/day) effectively used for gastroesophageal reflux disease (GERD) (Dabrowski et al., 2018; Mathews et al., 2010; Van Rensburg et al., 1999). Mouse daily pantoprazole administration was based on the assumption that average weight of an adult mouse is 25 g so the daily dose was calculated to

0.0143 mg/25g/day. Pantoprazole (Sigma-Aldrich, Germany) stock solution was prepared in DMSO: $H_2O$ (1:1) in a concentration of 1.25 mg/ml) and stored at -20°C until use.

### Osmotic pump preparation and implantation

ALZET®2002 osmotic pump (Charles River, Germany) were filled, weighed and primed (placed in 0.9% NaCl, at 37°C, overnight) according to the guidelines provided by ALZET®https://www.alzet.com/guide-to-use/filling-priming-alzet-pumps/) (Fig. 3.8B,C).

Untreated, control animals received pumps with DMSO: $H_2O$ (1:1) only and pantoprazole treated animals received pumps with 1.25 mg/ml pantoprazole prepared in DMSO: $H_2O$ (1:1). Mice were anesthetized by using isoflurane (Baxter, 100 % v/v) (2-3%) and carbogen (5% $CO_2$ and 95% $O_2$, 0.5-1 l/min and the lateral backside was shaved for a subcutaneous pump implantation. On the shaved side, antiseptic solution (Betaisodona®Solution, Mundipharma GmbH, Germany) was applied and a small incision was made to create a pouch. The pouch was flushed with normal saline (0.9% NaCl) and the osmotic pump was inserted into the pouch subcutaneously from the portal side. The incision was closed by over and over sutures (Ethilon, 6-0) and antiseptic (Betaisodona®Solution, Mundipharma GmbH, Germany) solution was applied.

Three osmotic pumps were implanted in the APPswePS1dE9 aged 12-16 weeks groups during the study (Fig. 3.9) in two weeks intervals. The first pump was implanted on the day of electrode implantation. Seven pumps were implanted in two weeks intervals in the APPswePS1dE9 mice aged 17-21 weeks (Fig. 3.10). All APPswePS1dE9 mice groups received the first osmotic pump at the same age (~11 weeks). Pantoprazole was administered continuously for six weeks in APPswePS1dE9 12-16 weeks of age while in APPswePS1dE9 mice 17-21 weeks of age for approximately thirteen weeks.

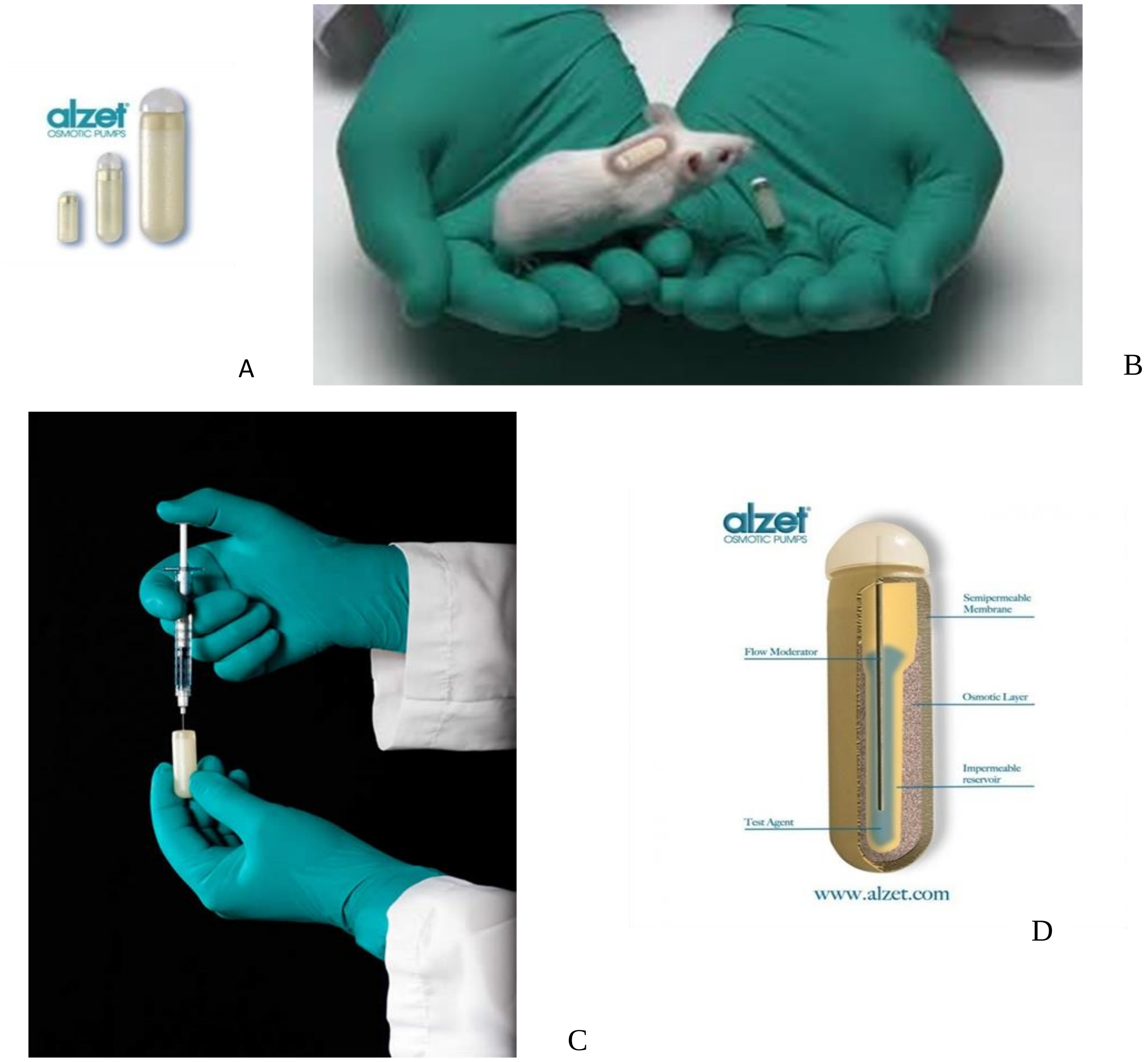

**Figure 3.8: (A) ALZET®osmotic minipump (B) Mouse with pump placement (C) Filling of osmotic pump with test solution (D) Structural and functional parts of ALZET®osmotic minipump**.

### 3.2.8.4. Radiotelemetric EEG data acquisition

EEG data acquisition from all APP swePS1dE9 mice groups were performed by the Dataquest ART 4.2 software (DSI) (Fig. 3.4) at a nominal sampling rate of 200 Hz (TL11M2-F20EET transmitter) with no priori filter cutoffs (Lundt, Wormuth, Siwek, Müller, et al., 2016; Papazoglou, Lundt, et al., 2016).

#### 3.2.8.5. Experimental design and EEG recording

**APP swePS1dE9 mice groups 12-16 weeks of age**

The 1st 24 h baseline recording was performed at day 10 (12th week of age) post-surgery from both motor cortex and the CA1 hippocampal regions. Subsequently, 2nd and 3rd 24 h baseline recordings were performed at day 24 (14th week of age) and 38 (16th week of age) post-implantation respectively (Fig. 3.9).

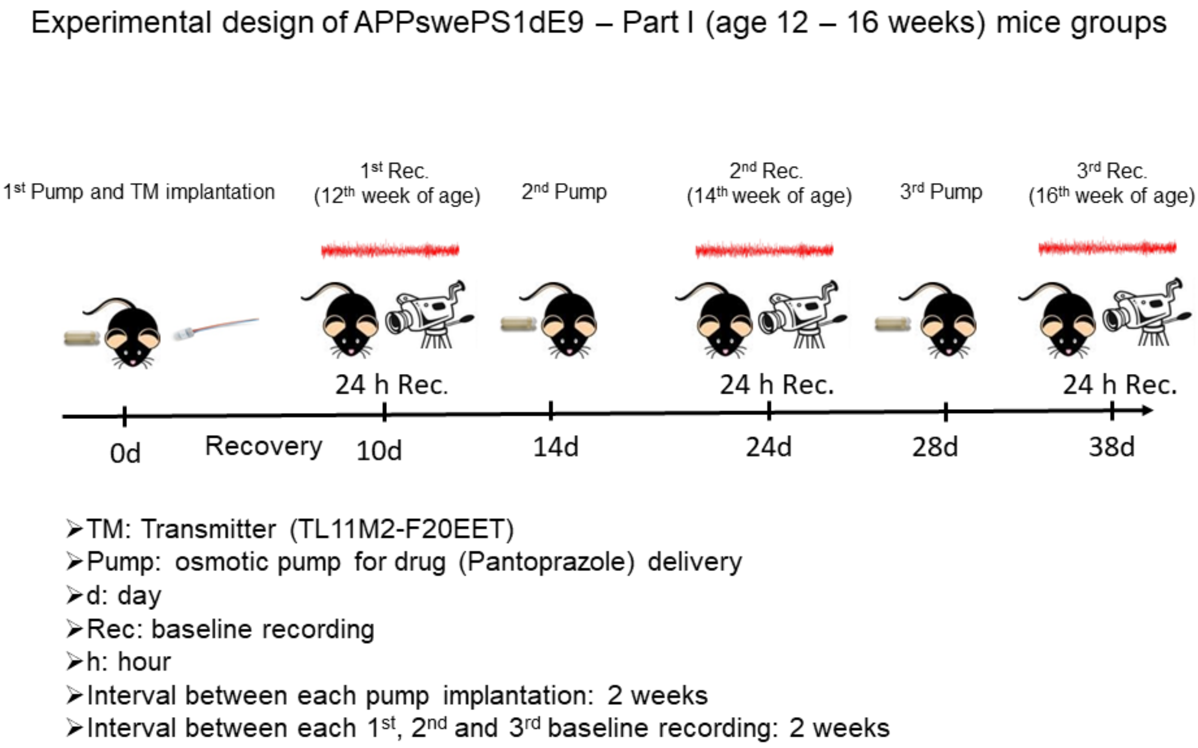

**Figure 3.9: Experimental design of osmotic pumps and electrode implantation of APPswePS1dE9 (age 12-16 weeks) groups.**

**APPswePS1dE9 mice groups 17-21 weeks of age**

We recorded five 24 h baseline recordings from both the motor cortex and the CA1 hippocampal regions. The 1st 24 h recording was performed at day 10 post-surgery (17th week of age). Followed by 2nd at day 17 (18th week of age), 3rd at day 24 (19th week of age), 4th at day 31 (20th week of age) and 5th at day 38 post surgery (21st week of age) respectively. Furthermore, after the 5th baseline recording, consecutive recordings of 1 h baseline, 1 h post-normal saline (0.9% NaCl), 1 h post-urethane injection (800 mg/kg freshly dissolved in 0.9% NaCl Sigma-Aldrich, Germany) and 3 h post-atropine injection (60 mg/kg Sigma-Aldrich, Germany, freshly dissolved in 0.9% NaCl) were also performed (Fig. 3.10).

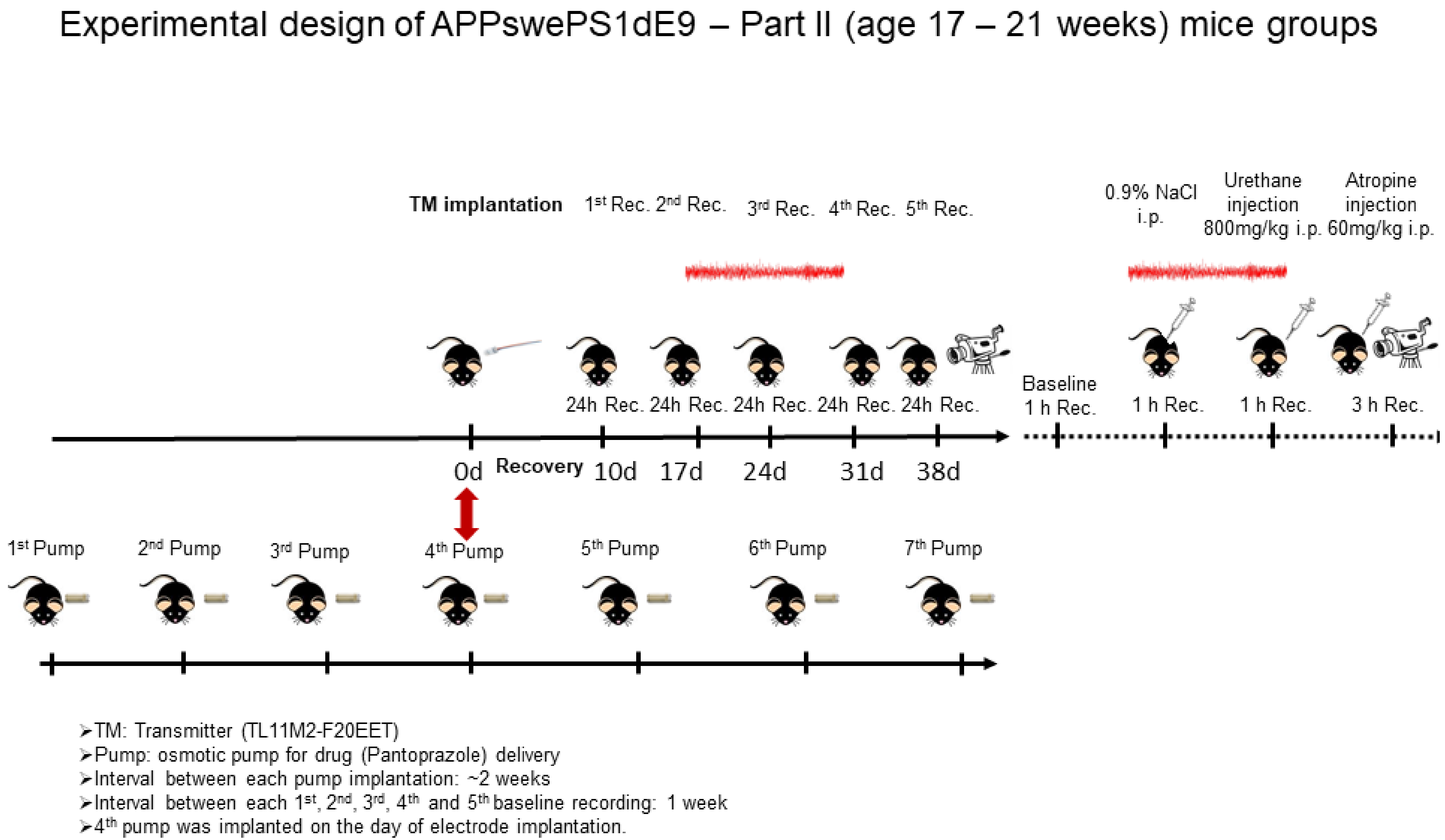

- TM: Transmitter (TL11M2-F20EET)
- Pump: osmotic pump for drug (Pantoprazole) delivery
- Interval between each pump implantation: ~2 weeks
- Interval between each 1st, 2nd, 3rd, 4th and 5th baseline recording: 1 week
- 4th pump was implanted on the day of electrode implantation.

**Figure 3.10: Experimental design of osmotic pumps and electrode implantation of APPswePS1dE9 (age 17-21 weeks) groups.**

### 3.2.8.6. EEG recording analysis of APPswePS1dE9 mice groups

EEG data were exported to NeuroScore software (DSI, USA) and analyzed by FFT (Fast Fourier Transformation) based approach in the frequency range of 0.5-70 Hz. The actual TL11M2-F20-EET transmitter (DSI, USA) bandwidth (B) is 50 Hz resulting in a nominal sampling rate (f) at 250 Hz, (f = 5 X B). Thus, based on the Nyquist-Shannon theorem, the transmitter can only reliable record frequencies up to 125 Hz (Weiergraber et al., 2016).

Each frequency and the range that were analyzed are presented Table 3.15.

The length of the individual EEG epochs that were FFT analyzed was 2 s (Lundt, Wormuth, Siwek, Müller, et al., 2016; Müller et al., 2017; Papazoglou, Lundt, et al., 2016).

**Table 3.15: Frequency ranges analyzed for the APPswePS1dE9 project.**

| EEG oscillation (Frequency) | Frequency range |
|---|---|
| Delta 1 ($\delta_1$) | 0.5-4 Hz |
| Theta 1 ($\theta_1$), Theta 2 ($\theta_2$) | 4-8 Hz, 4.1-12 Hz |
| Alpha ($\alpha$) | 8-12 Hz |
| Sigma ($\sigma$) | 12-16 Hz |
| Beta 1 ($\beta_1$), Beta 2 ($\beta_2$), Beta 3 ($\beta_3$) | 12.1-30 Hz, 16-24 Hz, 16-30 Hz |
| Gamma low ($\gamma_{low}$), Gamma mid ($\gamma_{mid}$), | 30-50 Hz, 50-70 Hz |

Activity data from the 12 h dark/light cycle of all three baseline recordings of APPswePS1dE9 mice 12-16 weeks of age and of all five baseline recordings as well as of 1 h baseline, 1 h post-normal saline, 1 h post-urethane and 3 h post-atropine recordings of APP swePS1dE9 mice 17-21 weeks of age were also analyzed from both the motor cortex (M1) and hippocampus (CA1) deflections. Additionally, temperature (°C) analysis was also performed for the same recording descript above.

Mean relative EEG power (%) of the individual frequency ranges was calculated for circadian stages, i.e. dark and light cycles for all the above descripted recording for all APPswePS1dE9 mice groups.

### 3.2.8.7. Electroencephalographic seizures analysis for all APPswePS1dE9 mice groups

Electroencephalographic seizures analysis was performed by using automated seizure detection and quantification modules of NeuroScore (DSI, USA). An EEG baseline amplitude for each animal and each recording was determined individually for both the hippocampal and cortical recordings. Based on the NeuroScore automated seizure detection module protocol, in order for as seizure like event to be scored, the amplitude threshold of ictal discharges was set to 1.5 X higher than the baseline (µV). Parameters for automated seizures detection, maximum amplitude was set at 1000 µV; minimum spike duration, 1 ms and maximum spike duration, 100 ms; spike trains parameters: minimum train duration, 0.5 s; minimum spike interval, 0.05 s; maximum spike interval, 0.3 s; train joint interval, 1 s; minimum number of spikes, 4 (Papazoglou, Lundt, et al., 2016).

The following seizures parameters including number of spike trains, spike trains duration (min) and number of single spikes were evaluated during both 12 h dark and light circadian phases for all three baseline recordings of APP swePS1dE9 mice 12-16 weeks of age (Fig. 3.9) and for all five baseline recordings of APP swePS1dE9 mice 17-21 weeks of age (Fig. 3.10).

#### 3.2.8.8. Euthanization, organ collection and animal perfusion

After EEG recordings, animals were anaesthetized by injecting ketamine hydrochloride and xylazine hydrochloride (200 mg/kg b/w Ketanest® Pfizer, USA; 25 mg/kg b/w Rompun® Bayer, Germany). Blood (~1 ml) was collected from all the animals by cardiac puncture followed by liver tissue collection. Then, the animals were cardiac perfused with using ice cold PBS (pH: 7.4). The descending aorta was closed with a surgical clamp at the diaphragm level before the upper part of the mouse body was perfused with 4% PFA in PBS. Subsequently, brains were extirpated and stored in 4% PFA for 3-4 h at room temperature. Brains were transferred to 30% sucrose in PBS for cryoprotection and stored at $4^oC$ until further use. Plasma was separated from the blood sample by centrifugation at 10,000 rpm for 10 minutes at $4^oC$. Plasma and liver samples were snap frozen in liquid nitrogen and stored at $-80^oC$ until further use.

#### 3.2.8.9. Statistical analysis

Frequency, activity and temperature analysis as well as seizure parameters results from all of APPswePS1dE9 mice groups were statistically analyzed and displayed as mean ± SEM for each individual male and female mice subgroups. Statistical comparison for mean ± SEM were carried out using two way ANOVA between all mice groups of each recording and also within the recordings of each group. Tukey's test was used as post-hoc analysis for multiple comparisons ($^{*}p < 0.05$; $^{**}p < 0.01$; $^{***}p < 0.001$). All statistics and graph presentations were performed with GraphPad Prism 6 (GraphPad Software, USA).

### 3.2.9. Liquid chromatographic and tandem mass spectrometric (LC-MS/MS) analysis of Pantoprazole

#### 3.2.9.1. Standard solutions

Pantoprazole concentration from plasma and liver tissue was determined by high liquid chromatography coupled with tandem mass spectrometry (LC-MS/MS).

The stable isotopically labeled Pantoprazole-d6 sodium salt (major Pantoprazole-d-6) was used as internal standard (molecular formula: $C_{16}H_7D_6F_2N_3NaO_4S$, Molecular Weight: 411.39, synthetic, purity ≥ 97%, Santa Cruz Biotechnology, USA). The stock solution of internal standard (0.1 µg/ml in DMSO: H2O (1:1 v/v)) was prepared, protected from light and stored at -20ºC until further use. The standard stock solution of Pantoprazole (100 µg/ml in DMSO: H2O (1:1 v/v), purity ≥ 98%, Sigma-Aldrich, Germany) was prepared, protected from light and stored at -20ºC until further use.

#### 3.2.9.2. Plasma samples analysis

**Calibration curve**

For the preparation of standard curve, fetal calf serum (FCS, sterile filtered, not heat-inactivated, Sigma, Germany) was used as matrix for the calibration of parameters. FCS was thawed in water bath and mixed by vortex before use. 3 µl of each pantoprazole dilution as shown in Table 3.16 was mixed with 297 µl of FCS. 900 µl (3x the volume) of ice-cold acetonitrile (≥ 99.9%) already mixed with deuterated-Pantoprazole (1.7 ng/ml) was added into each sample. The samples were vortexed to conduct protein precipitation and centrifuged for 5 minutes at room temperature and 16000 rcf. The supernatant was transferred to a 2 ml tube and evaporated by a nitrogen evaporator at 40ºC, for 1-2 h to form dried residues (evaporator system EVA-EC1-S, Germany). 100 µl of double distilled water (dd$H_2O$) was added to the dried residue of each sample and was vortexed until all precipitates were dissolved. Dissolved samples were centrifuged for 3 minutes at room temperature, at 16000 rcf to avoid any debris and lipid particles before LC-MS/MS analysis. Finally, the dissolved solution were transferred into a HPLC glass vial for further analysis and sealed. 5 µl from each sample were injected to the LC-MS/MS equipment. Blank solvents (deionized water and acetonitrile) and matrix blank were also run as controls to identify any possible contamination.

**Table 3.16: Standard curve of pantoprazole in FCS for the analysis of plasma samples.**

| Initial Pantoprazole Concentration | Plasma (FCS) Volume used [µl] | Final Concentration [ng/ml] |
|---|---|---|
| 3 µl (100 µg/ml) | 297 | 1000 |
| 3 µl (10 µg/ml) | 297 | 100 |
| 3 µl (5 µg/ml) | 297 | 50 |
| 3 µl (2.5 µg/ml) | 297 | 25 |
| 3 µl (1 µg/ml) | 297 | 10 |
| 3 µl (500 ng/ml) | 297 | 5 |
| 3 µl (250 ng/ml) | 297 | 2.5 |
| 3 µl (100 ng/ml) | 297 | 1 |
| 3 µl (50 ng/ml) | 297 | 0.5 |
| 3 µl (25 ng/ml) | 297 | 0.25 |
| 3 µl (10 ng/ml) | 297 | 0.1 |
| 3 µl (5 ng/ml) | 297 | 0.05 |
| 3 µl (DMSO: Water) | 297 | 0.0 |

### Analysis of APPswePS1dE9 (age 12-16 weeks) plasma samples

The plasma samples from every animal of each APP swePS1dE9 (age 12-16 weeks) mice group were thawed in water bath and transferred 100 µl of each plasma sample in 1.5 ml tubes. Then 300 µl (3x the volume) of ice-cold acetonitrile (≥ 99.9%) already mixed with deuterated-Pantoprazole (1.7 ng/ml) was added into each sample and vortexed them, precipitates were formed. Later, samples were centrifuged for 5 minutes at room temperature, 16000 rcf and transferred the supernatants in 2 ml tubes. The supernatants were evaporated by nitrogen evaporator at 40°C for 1-2 h to precipitate (evaporator system EVA-EC1-S, Germany). 100 µl of ddH$_2$O was added to the dried residue of each sample and vortexed them until all the precipitates were fully dissolved. Dissolved samples were centrifuged for 3 minutes at room temperature, at 16000 rcf to avoid any debris and lipid particles before LC-MS/MS analysis. Finally, the samples (without debris) were transferred in HPLC glass vials and closed for further analysis. 5 µl of each sample was injected into LC-MS/MS for analysis.

**Note:** It is better to analyze fresh samples to avoid any degradation. If this is not feasible then samples should be stored at -20°C and protected from light until further use as early as possible.

### 3.2.9.3. Liver tissue analysis

**Calibration Curve**

Untreated mouse (C57BL/J6) liver tissue was used as a matrix for the calibration curve. 50-60 mg untreated mouse liver tissue was mixed with 3 ml of ddH$_2$O water fortified with deuterated-pantoprazole (3 ng deuterated-Pantoprazole/ml) and it was homogenized on ice (Potter Elvehjem). Further, the tissue lysate was sheared with the help of a PTFE pistil (Polytetrafluoroethylene, Teflon®) and aliquot in 1.5 ml tubes (each 248 µl). 2 µl of each pantoprazole dilution (Table 3.17) was added in each lysate and incubated for 2 minutes at room temperature. 750 µl of ice-cold acetonitrile was added to each sample (≥ 99.9%) (~3x the volume of each lysate). The samples were vortexed to conduct protein precipitation and centrifuged for 5 minutes at room temperature and 16000 rcf. The supernatant was transferred to a 2 ml tube and evaporated by a nitrogen evaporator at 40°C for 1-2 h to form dried residues (evaporator system EVA-EC1-S, Germany). 100 µl of 2% acetic acid was added to the dried residue of each sample and was vortexed until all precipitates were dissolved. Finally, the dissolved solution was transferred into a HPLC glass vial for further analysis and sealed. 5 µl from each sample were injected to the LC-MS/MS equipment. Blank solvents (deionized water and acetonitrile) and matrix blank were also run as controls to identify any possible contamination.

**Table 3.17: Standard curve of pantoprazole in liver lysate for the analysis of liver samples.**

| Final concentration | Liver tissue lysate | Volume of stock solution |
|---|---|---|
| 80 ng/ml | 248 µl | 2µl (10 µg/ml) |
| 8 ng/ml | 248 µl | 2µl (1 µg/ml) |
| 0.8 ng/ml | 248 µl | 2µl (100 ng/ml) |
| 0.4 ng/ml | 248 µl | 2µl (50 ng/ml) |
| 0.2 ng/ml | 248 µl | 2µl (25 ng/ml) |
| 80 pg/ml | 248 µl | 2µl (10 ng/ml) |
| 40 pg/ml | 248 µl | 2µl (5 ng/ml) |
| 20 ng/ml) | 248 µl | 2µl (2.5 ng/ml) |
| 8 pg/ml) | 248 µl | 2µl (1 ng/ml) |
| 4 pg/ml) | 248 µl | 2µl (0.5 ng/ml) |
| 2 pg/ml) | 248 µl | 2µl (0.25 ng/ml) |
| 0.8 pg/ml) | 248 µl | 2µl (0.1 ng/ml) |

### Analysis of APPswePS1dE9 (age 12-16 weeks) liver samples

The mouse liver tissue samples (50-60 mg) for every animal of all APPswePS1dE9 (age 12-16 weeks) mice groups (Tab. 3.13) was mixed with 500 µl ddH$_2$O already fortified with deuterated-Pantoprazole (3 ng deuterated-Pantoprazole/ml) in 1.5 ml tubes and it was homogenized on ice (Potter Elvenjhem). The tissue lysate was sheared with the help of PTFE pistil (Polytetrafluoroethylene, Teflon®). 1.3-1.5 ml (~3x the volume of each lysate) of ice-cold acetonitrile was added into each sample (≥ 99.9%). The samples were vortexed for 5 s to conduct protein precipitation and centrifuged for 5 minutes at room temperature and 16000 rcf. The supernatant was transferred to a 2 ml tube and evaporated by a nitrogen evaporator (evaporator system EVA-EC1-S, Germany) at 40°C, for 1-2 h to form dried residues. 100 µl of 2% acetic acid was added to the dried residue of each sample and was vortexed until all precipitates were dissolved. Finally, the dissolved solution were transferred into a HPLC glass vial for further analysis and sealed. 5 µl from each sample were injected to the LC-MS/MS equipment. Blank solvents (deionized water and acetonitrile) and matrix blank were also run as controls to identify any possible contamination.

### 3.2.9.4. LC-MS/MS analysis

### Basic principle

For the analysis of samples by LC-MS/MS approach, the sample mixture was first injected into the liquid chromatograph that separates the sample mixture based on individual interaction to the stationary phase. The samples are further analyzed by means of MS/MS analysis, processed by tandem mass spectrometer, in which the specific analytes are ionized and separated further on the bases of their mass to charge ratio (m/z). The process of filtering and mass analysis is called multiple reaction monitoring (MRM). In MRM process, the analyte passes through different quadrupoles of MS optics from Q1, Q2, to Q3 to analyse the specific compound (Fig. 3.11). Different quadrupoles perform different MS/MS functions:

*m/z Q1: In quadrupole 1(Q1), the precursor ions are filtered based on mass to charge ratio (m/z) to form MS1 spectrum.

*In quadrupole 2 (Q2) (collision cell), the collision of the precursor ions with inert gas and applied voltage activate the fragmentation process of the precursor ions. The Q2 is only for collision, not for mass separation.

*m/z Q3: In quadrupole 3 (Q3), the selected product ions filtered based on mass to charge ratio (m/z) for detection to form MS2 spectrum.

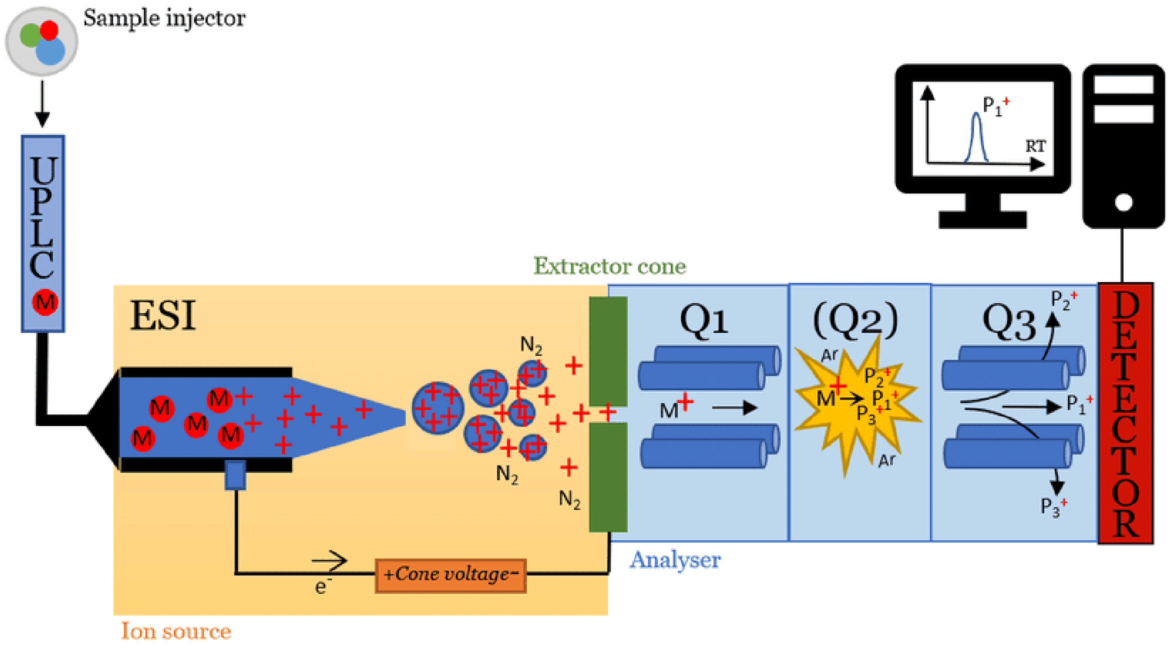

**Figure 3.11: Description of the sample analysis processed by liquid chromatography followed by MRM process using triple quadrupole of MS optics and finally the detection of analyte that appeared as mass spectrum** (Zimdahl Kahlin, 2020).

### Instrumentation and specifications

The analysis of samples were performed by Sciex QTRAP® 6500 MS coupled to a Shimadzu Nexera® UPLC. The chromatographic separation were achieved by Thermo Fisher Accucore® C8 (50x3mm, 2.7µm) equipped with a guard column. The running buffer consisted of 0.2% formic acid as aqueous phase (phase A) and acetonitrile as an organic phase (phase B). The gradient are shown in Table 3.18.

**Table 3.18: LC-MS running buffers.**

| Time [minute] | Phase A [%] | Phase B [%] |
|---|---|---|
| 0.2 | 99 | 1 |
| 10 | 0 | 100 |
| 10.1 | 99 | 1 |
| 12 | 99 | 1 |

**Table 3.19: Ion transitions for the MRM experiment.**

| **Q1 [*m/z*]** | **Q3 [*m/z*]** | **Compound** | **CE*** | **DP*** |
|---|---|---|---|---|
| 384.1 | 200.1 | Pantoprazole-1 | 25 | 100 |
| 384.1 | 138.1 | Pantoprazole-2 | 25 | 100 |
| 384.1 | 182 | Pantoprazole-3 | 25 | 100 |
| 390.1 | 206.1 | D6-Pantoprazole-1 | 25 | 100 |
| 390.1 | 143.1 | D6-Pantoprazole-2 | 25 | 100 |

For quantification, the ion transitions with *m/z* 384.1/200.1 and *m/z* 390.1/206.1 were used for pantoprazole and deuterated-pantoprazole, respectively. Calculations were done by Analyst® Software (Sciex, Singapore) and MultiQuant® software (Sciex, Singapore) (Tab. 3.19).

*CE (collision energy, eV): It is the amount of energy applied on the precursor ions when they facilitated into the collision cell for fragmentation.

*DP (Declustering potential, eV): Definitive potential for the particular ion, used to inhibit the clustering of ions and boost the entry of the analytes into the MS.

Data was statistically analyzed and displayed as mean ± SEM for all pantoprazole concentrations and for all individual male and female mice groups. Statistical comparison for mean ± SEM of all pantoprazole concentration ranges were carried out using one way ANOVA between all mice groups. Tukey's test was used as post-hoc analysis for multiple comparisons ($^{*} p < 0.05$; $^{**} p < 0.01$; $^{***} p < 0.001$; $^{****} p < 0.0001$). Most of the statistics and graph presentations were performed with GraphPad Prism 6 (GraphPad Software, USA).

**Metabolite analysis**

**Human liver microsome incubation**

183 µL of PBS was taken in 1.5 ml tube and then 2 µl of pantoprazole (0.1 mg/ml in DMSO: H2O stock solution) was added into it. Subsequently, 10 µl of 20 mM NADPH and 5 µl human liver microsomes (Gibco HLM, Thermo scientific, Germany) were also added and incubated for 30 min at 37°C. 600 µl of ice-cold acetonitrile (≥ 99.9%) was added into the mixture. The samples were vortexed and a precipitate was formed. The samples were then centrifuged and the supernatant was transferred into a 2 ml tube. The supernatant was evaporated by vacuum centrifuge under reduced pressure. 100 µl ddH$_2$O was added to dissolve the precipitate and the samples were

transferred into HPLC vials for analysis. Product ion experiment was performed to identify relevant ion transitions for metabolite identification (Tab. 3.20). Note that NADPH powder should be stored at -20 °C and NADPH solution in PBS at -80 °C. Furthermore, during evaporation, the centrifuge should be stopped and vacuum pump turned off after every 30 minutes.

**Table 3.20: MRM ion transitions of the measured metabolites**

| **Q1 [*m/z*]** | **Q3 [*m/z*]** | **Dwell time [msec]** | **ID** | **DP [eV]** | **CE [eV]** |
|---|---|---|---|---|---|
| 400.1 | 336.1 | 40 | Pantoprazolsulfone-1 | 100 | 30 |
| 400.1 | 216.1 | 40 | Pantoprazolsulfone-2 | 100 | 30 |
| 400.1 | 152.1 | 40 | Pantoprazolsulfone-3 | 100 | 30 |
| 400.1 | 304.1 | 40 | Pantoprazolsulfone-4 | 100 | 30 |
| 368.1 | 184.1 | 40 | Pantoprazolsulfane-1 | 100 | 30 |
| 368.1 | 335.1 | 40 | Pantoprazolsulfane-2 | 100 | 30 |
| 368.1 | 122.1 | 40 | Pantoprazolsulfane-3 | 100 | 30 |
| 368.1 | 152.1 | 40 | Pantoprazolsulfane-4 | 100 | 30 |

Statistical comparison of mean ± SEM area ratios of pantoprazole, pantoprazolesulfane and pantoprazolesulfone was performed between all mice groups and within each group by using one-way ANOVA. Tukey's test was used as post-hoc analysis for multiple comparisons ($^{*}\ p < 0.05$; $^{**}\ p < 0.01$; $^{***}\ p < 0.001$; $^{****}\ p < 0.0001$). Most of the statistics and graph presentations were performed with GraphPad Prism 6 (GraphPad Software, USA).

# 4. Results

## 4.1. Hippocampal EEG alterations in Ca$_v$3.2 mice

### 4.1.1. Representative EEG traces from Ca$_v$3.2$^{+/+}$ and Ca$_v$3.2$^{-/-}$ mice.

Representative 30 s EEG traces from the hippocampal CA1 region of Ca$_v$3.2$^{+/+}$ and Ca$_v$3.2$^{-/-}$ mice are shown in Fig. 4.1.1. During the light cycle, recording from Ca$_v$3.2$^{+/+}$ mice shows, i.e., typical large irregular amplitude (LIA) activity (Fig. 4.1.1A$_I$) while there is a general increase in EEG frequency during the dark cycle (Fig. 4.1.1A$_{II}$). In Ca$_v$3.2$^{-/-}$ mice, theta and alpha activity appears to be more prominent, particularly during the dark cycle (Fig. 4.1.1B$_{II}$).

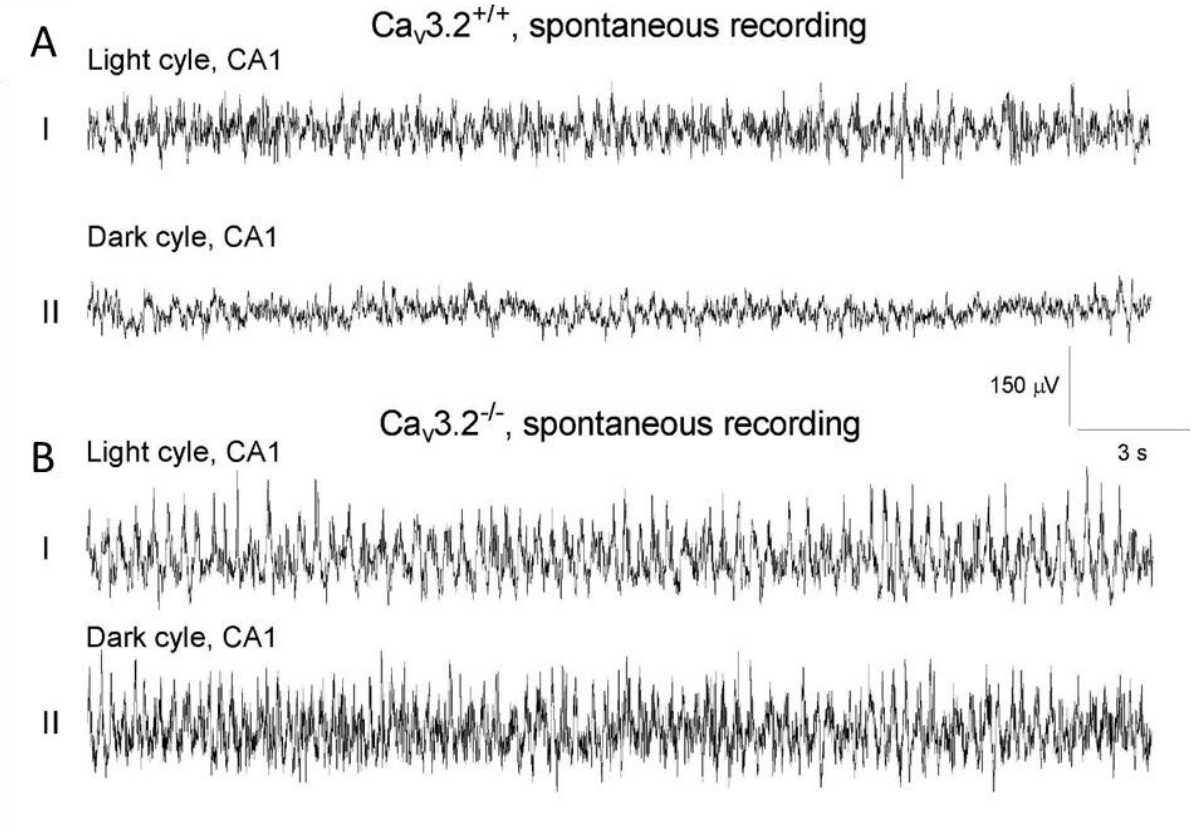

**Figure 4.1.1: Representative hippocampal CA1 EEG traces (30 s) during the dark and light cycles from Ca$_v$3.2$^{+/+}$ and Ca$_v$3.2$^{-/-}$ mice.** The EEG exhibits prominent theta oscillations in Ca$_v$3.2$^{-/-}$ mice (B) compared to Ca$_v$ 3.2$^{+/+}$ mice (A). Scale: Y-axis, 150 µV, X-axis, 3 s.

### 4.1.2. Activity analysis

The activity data provided by the radiofrequency transmitter was measured as mean relative activity units. The units were calculated by a binary system; with activity = 0 determining the inactive state and activity > 0 classifying the active state. The activity units represent the activity in the horizontal plane and integrate both trip distance, velocity and acceleration (Lundt, Wormuth, Siwek, Muller, et al., 2016).The mean relative activity was analyzed from both genotypes during the dark cycles (DC) and the light cycles (LC) of both baselines recordings (R1 & R2). In controls ($Ca_v3.2^{+/+}$) and transgenic ($Ca_v3.2^{-/-}$) mice, a significant increase in mean relative activity was observed in DC1 compared to LC1 at the 1st baseline (R1) recording ($Ca_v3.2^{+/+}$, n = 8, DC1: 0.070 ± 0.010 vs. LC1: 0.039 ± 0.003; p = 0.0084) ($Ca_v3.2^{-/-}$, n = 8, DC1: 0.078 ± 0.008 vs LC1: 0.042 ± 0.005; p = 0.0034) (Fig. 4.1.2A) and also at the 2nd baseline (R2) recording ($Ca_v3.2^{+/+}$, n = 8, DC2: 0.066 ± 0.007 vs LC2: 0.037 ± 0.006; p = 0.0104) ($Ca_v3.2^{-/-}$, n = 8, DC2: 0.075 ± 0.007 vs. LC2: 0.048 ± 0.011; p = 0.0382) (Fig. 4.1.2B). However, no significant difference in mean relative activity was detected between both genotypes during the dark and light cycles of both baseline recordings (R1 & R2) (Fig. 4.1.2).

Similarly, no significant differences in mean relative activity counts were found between both genotypes in the post urethane phase I (U1) ($Ca_v\,3.2^{+/+}$, n = 8: 0.014 ± 0.003 vs. $Ca_v\,3.2^{-/-}$, n = 8: 0.018 ± 0.004; p = 0.4433) and in post urethane phase II (U2) ($Ca_v\,3.2^{+/+}$: 0.019 ± 0.004 vs. $Ca_v\,3.2^{-/-}$, n = 8: 0.016 ± 0.002; p = 0.5281) (Fig. 4.1.3).

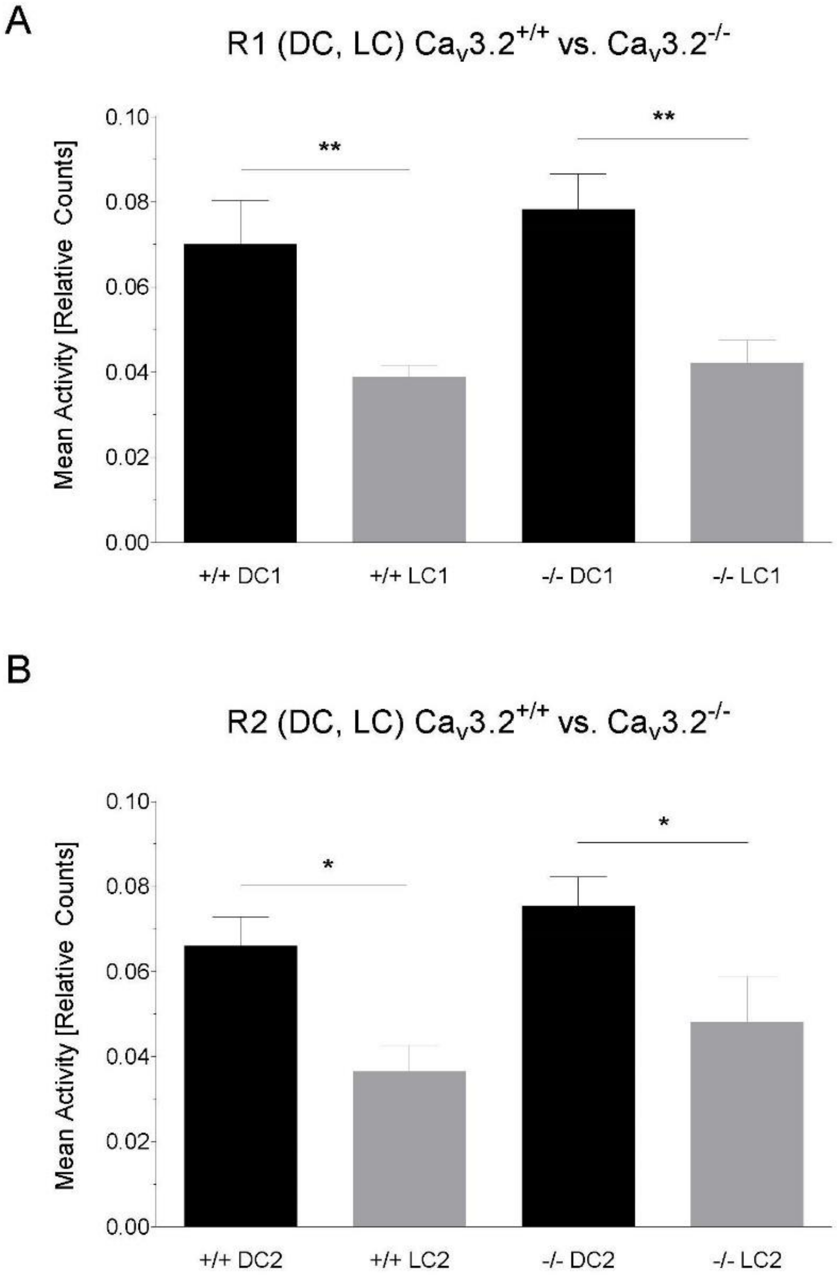

**Figure 4.1.2: Mean relative activity profile of $\mathrm{Ca_V3.2^{+/+}}$ and $\mathrm{Ca_V3.2^{-/-}}$ animals during the dark (DC) and light cycle (LC) for the first (R1, A) and second (R2, B) 24 h baseline recordings**.

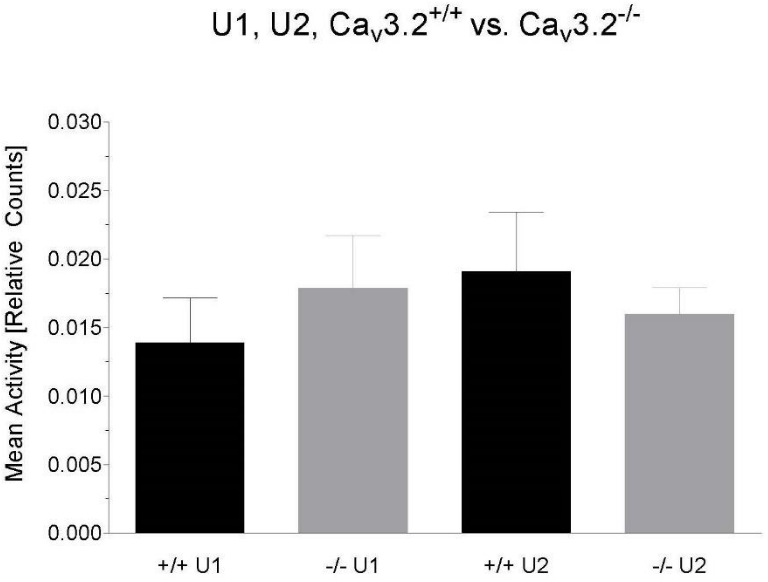

**Figure 4.1.3: Mean relative activity profile of $Ca_v3.2^{+/+}$ and $Ca_v3.2^{-/-}$ mice in post-urethane recordings (U1, U2).**

### 4.1.3. Temperature analysis

Besides biopotentials such as the EEG, the TA10ETAF20 transmitter is also capable of recording body temperature. As the transmitter was implanted in a subcutaneous pouch on the back of the experimental animals, temperature values do not represent body core temperature. Nevertheless, subcutaneous temperature values are comparable between both genotypes.

A significant increase in temperature was observed in both genotypes during DC1 compared to LC1 of the 1st baseline recording (R1) ($Ca_v3.2^{+/+}$), n = 7, DC1: 35.12 ± 0.13°C vs. LC1: 34.55 ± 0.11°C; $p < 0.0001$) ($Ca_v3.2^{-/-}$, n = 8, DC1: 34.70 ± 0.24°C vs. LC1: 34.04 ± 0.25°C; p = 0.0006) (Fig. 4.1.4A) and also at the 2nd baseline recordings (R2) ($Ca_v3.2^{+/+}$, n = 7, DC2: 34.80 ± 0.18°C vs LC2: 34.04 ± 0.16°C; p = 0.0002) ($Ca_v3.2^{-/-}$, n = 8, DC2: 34.60 ± 0.28°C vs. LC2: 33.94 ± 0.26°C; $p < 0.0001$) (Fig. 4.1.4B). However, no significant differences in temperature were observed between both genotypes within the dark and light cycle of the 1st and 2nd baseline recordings (R1 & R2) (Fig. 4.1.4). Similar to activity results, no significant differences were found in temperature profile at post urethane phase I (U1) ($Ca_v3.2^{+/+}$, n = 7: 33.11 ± 0.31°C vs. $Ca_v3.2^{-/-}$, n = 8: 32.91 ± 0.36°C; p = 0.6853) and post urethane phase II (U2) ($Ca_v3.2^{+/+}$, n = 7: 32.88 ± 0.33°C vs. $Ca_v3.2^{-/-}$, n = 8: 32.87 ± 0.40°C; p = 0.9809) (Fig. 4.1.5).

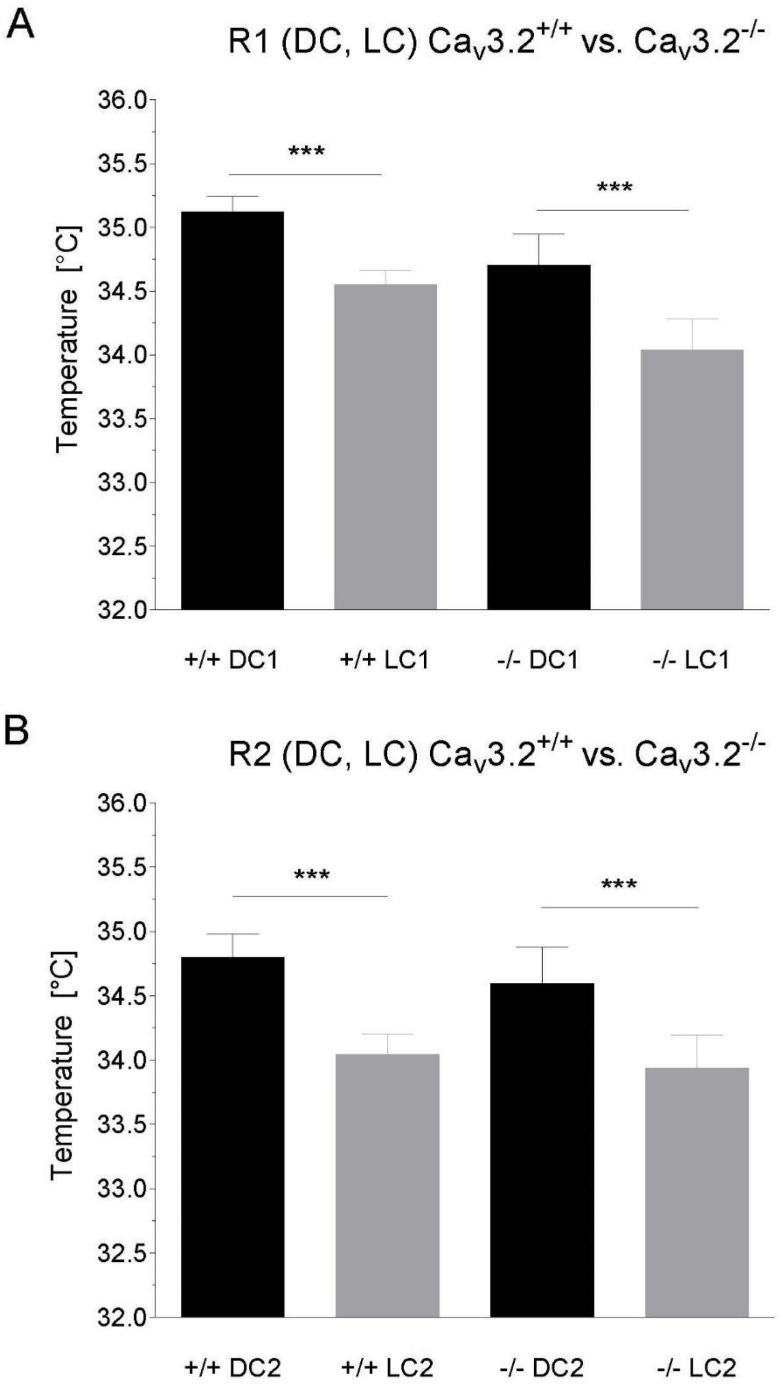

**Figure 4.1.4: Temperature profile of Ca$_v$3.2$^{+/+}$ and Ca$_v$3.2$^{-/-}$ during the dark cycle (DC) and light cycle (LC) for the first (R1, A) and the second (R2, B) 24 h baseline recordings.**

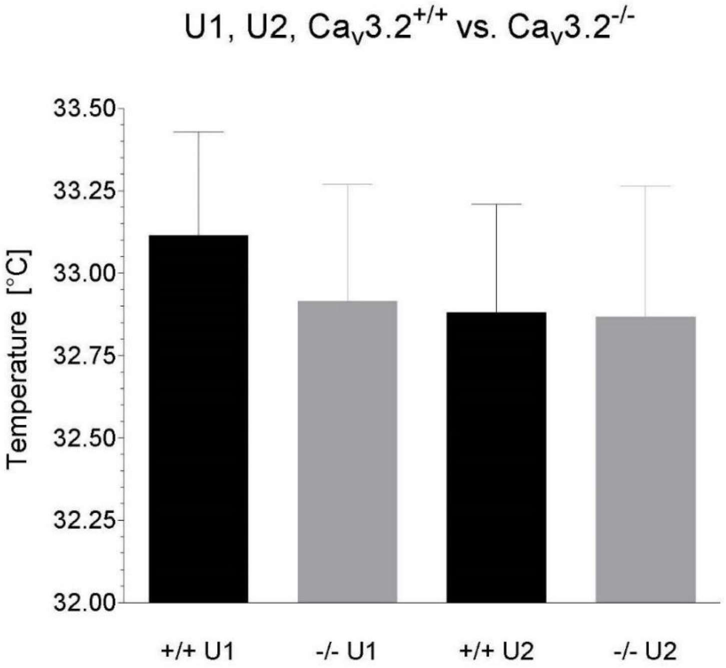

**Figure 4.1.5: Temperature profile of Ca$_v$3.2$^{+/+}$ and Ca$_v$3.2$^{-/-}$ mice during post-urethane recordings (U1, U2)**.

### 4.1.4. FFT based frequency analysis in controls (Ca$_v$3.2$^{+/+}$) and transgenic (Ca$_v$3.2$^{-/-}$) mice

In both control (Ca$_v$3.2$^{+/+}$) and transgenic (Ca$_v$3.2$^{-/-}$) animals, the FFT based relative EEG frequency analysis was performed from the CA1 region of the brain at the active state (AS) and non-active states (NAS) of dark/light cycles of both baseline (R1 & R2) and post-urethane (U1 & U2) recordings.

#### 4.1.4.1. EEG power analysis of R1/R2 during the active state of dark cycle

No significant differences were observed in $\delta_1$, $\delta_2$, α, σ, $\beta_1$, $\beta_2$, $\beta_3$, γ frequencies bands at the active phase of the DC of R1 (Fig. 4.1.6). Statistical trends were detected for $\theta_1$ (Ca$_v$3.2$^{+/+}$: 14.159 ± 1.764% vs. Ca$_v$3.2$^{-/-}$: 18.571 ± 1.533%; p = 0.0800), $\theta_2$ (Ca$_v$3.2$^{+/+}$: 28.215 ± 4.161% vs. Ca$_v$3.2$^{-/-}$: 37.766 ± 3.349%; p = 0.0954) and σ (Ca$_v$3.2$^{+/+}$: 4.312 ± 0.359% vs. Ca$_v$3.2$^{-/-}$: 5.267 ± 0.359%; p = 0.0811) between both genotypes (Fig. 4.1.6B,C).

Likewise, statistical trends in $\theta_2$, α and σ activities were observed in baseline recording R2 ($\theta_2$, Ca$_v$3.2$^{+/+}$: 28.877 ± 4.683% vs. Ca$_v$3.2$^{-/-}$: 40.321 ± 3.346%; p = 0.0667), (α, Ca$_v$3.2$^{+/+}$: 14.336 ± 2.576% vs. Ca$_v$3.2$^{-/-}$: 21.495 ± 2.452%; p = 0.0637) (σ, Ca$_v$3.2$^{+/+}$: 4.298 ± 0.519% vs. Ca$_v$3.2$^{-/-}$: 5.542 ± 0.289%; p = 0.0549) (Fig. 4.1.7B,C). No significant differences were observed for all other frequency bands in the dark cycle active phase of baseline recording R2 (Fig. 4.1.7).

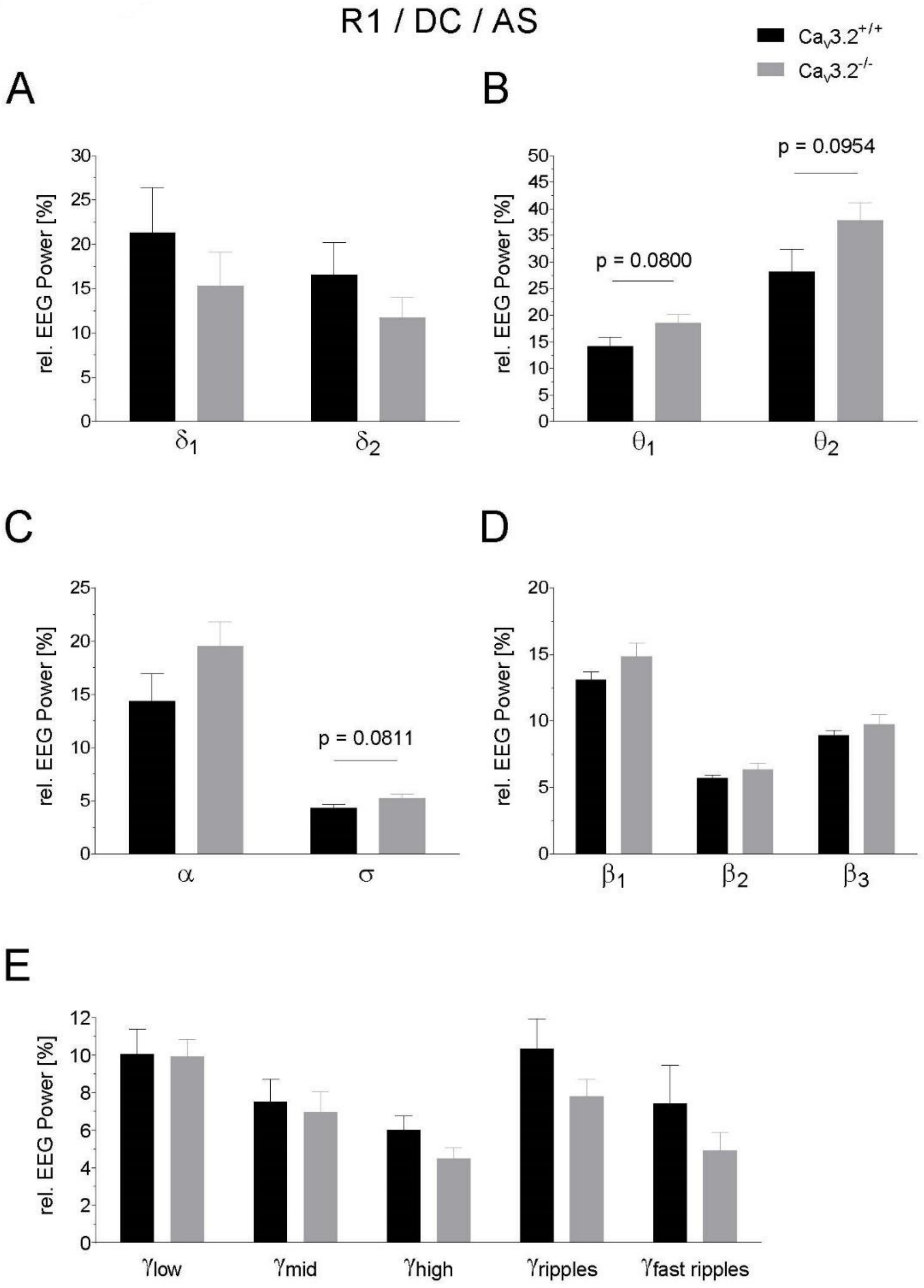

**Figure 4.1.6: EEG power analysis during the dark cycle active state of the 1st baseline recording (R1).** Relative EEG power (%) for $Ca_V3.2^{+/+}$ and $Ca_V3.2^{-/-}$ mice is displayed for the individual frequency ranges (A-E).

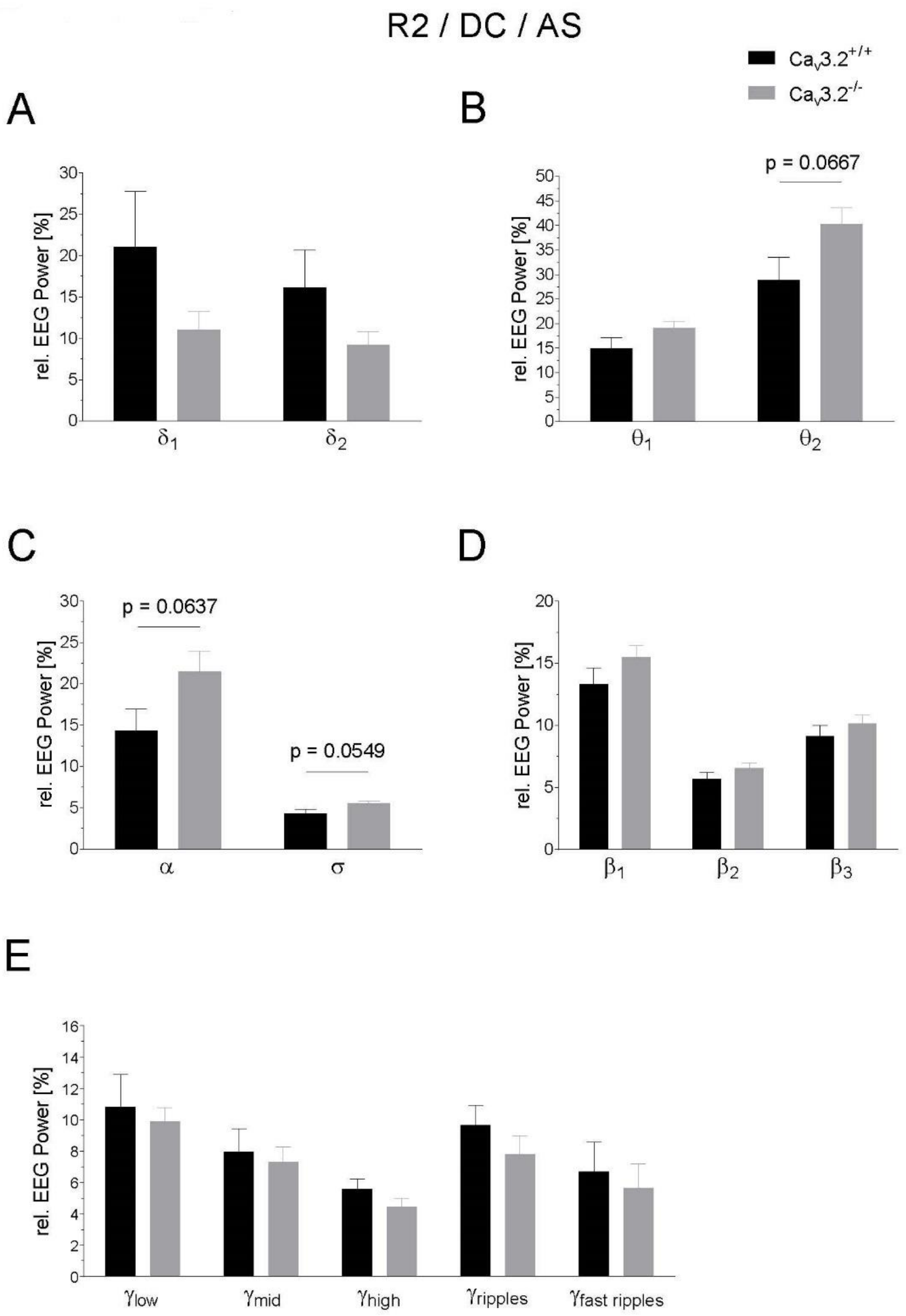

**Figure 4.1.7: EEG power analysis during the dark cycle active state of the 2nd baseline recording (R2).** Relative EEG power (%) for $Ca_V3.2^{+/+}$ and $Ca_V3.2^{-/-}$ mice is displayed for the individual frequency ranges (A-E).

### 4.1.4.2. EEG power analysis of R1/R2 during non-active state of the dark cycle

At dark cycle non-active state of baseline recording R1, a significant increase in relative $\theta_2$, $\alpha$ and $\sigma$ powers were observed in $\mathrm{Ca_v}3.2^{-/-}$ mice compared to controls ($\theta_2$, $\mathrm{Ca_v}3.2^{+/+}$: 33.344 ± 3.553% vs. $\mathrm{Ca_v}3.2^{-/-}$: 42.415 ± 2.047%; p = 0.0441) ($\alpha$, $\mathrm{Ca_v}3.2^{+/+}$:12.878 ± 1.458% vs. $\mathrm{Ca_v}3.2^{-/-}$: 17.287 ± 1.063%; p = 0.0284) ($\sigma$, $\mathrm{Ca_v}3.2^{+/+}$: 5.762 ± 0.543% vs. $\mathrm{Ca_v}3.2^{-/-}$: 7.214 ± 0.338%; p = 0.0395) (Fig. 4.1.8B,C). No significant differences were observed in $\delta_1$, $\delta_2$, $\theta_1$, $\beta_1$, $\beta_2$, $\beta_3$ and $\gamma$ frequency bands between both genotypes (Fig. 4.1.8).

Similarly, during the non-active state of the dark cycle during baseline recording R2, statistical increase in relative $\theta_2$ and $\alpha$ power was observed in $\mathrm{Ca_v}3.2^{-/-}$ mice compared to controls ($\theta_2$, $\mathrm{Ca_v}3.2^{+/+}$: 33.516 ± 4.177% vs. $\mathrm{Ca_v}3.2^{-/-}$: 44.078 ± 1.882%; p = 0.0370) ($\alpha$, $\mathrm{Ca_v}3.2^{+/+}$: 12.586 ± 1.675% vs. $\mathrm{Ca_v}3.2^{-/-}$: 18.159 ± 1.030%; p = 0.0132) (Fig. 4.1.9B,C). A statistical trend was detected for relative $\sigma$ power ($\mathrm{Ca_v}3.2^{+/+}$: 5.927 ± 0.717% vs. $\mathrm{Ca_v}3.2^{-/-}$: 7.426 ± 0.322%; p = 0.0773) (Fig. 4.1.9C). However, no significant changes were found in $\delta_1$, $\delta_2$, $\theta_1$, $\beta_1$, $\beta_2$, $\beta_3$ and $\gamma$ frequency bands between both genotypes (Fig. 4.1.9).

### 4.1.4.3. EEG power analysis of R1/R2 during active state of the light cycle

During the light cycle active state of baseline recording R1, a significant increase in relative $\sigma$ power was observed in $\mathrm{Ca_v}3.2^{-/-}$ mice compared to $\mathrm{Ca_v}3.2^{+/+}$ animals ($\sigma$, $\mathrm{Ca_v}3.2^{+/+}$: 4.143 ± 0.279% vs. $\mathrm{Ca_v}3.2^{-/-}$: 5.300 ± 0.286%; p = 0.0118) (Fig. 4.1.10C) and a statistical trend was found for $\theta_2$, $\beta_1$ and $\alpha$ ($\theta_2$, $\mathrm{Ca_v}3.2^{+/+}$: 27.758 ± 4.023% vs. $\mathrm{Ca_v}3.2^{-/-}$: 37.377 ± 3.223%; p = 0.0831) ($\beta_1$, $\mathrm{Ca_v}3.2^{+/+}$: 12.866 ± 0.615% vs. $\mathrm{Ca_v}3.2^{-/-}$: 15.022 ± 0.947%; p = 0.0767) ($\alpha$, $\mathrm{Ca_v}3.2^{+/+}$: 11.781 ± 1.701% vs. $\mathrm{Ca_v}3.2^{-/-}$: 16.724 ± 1.868%; p = 0.0706) (Fig. 4.1.10B,C,D). No significant changes were observed for $\delta_1$, $\delta_2$, $\theta_1$, $\beta_2$, $\beta_3$ and $\gamma$ frequency bands between both genotypes (Fig. 4.1.10).

Likewise, at light cycle active state of baseline recording R2, a significant increase in $\sigma$ and $\alpha$ relative powers was identified in knock out mice compared to controls ($\alpha$, $\mathrm{Ca_v}3.2^{+/+}$: 11.481 ± 1.925% vs. $\mathrm{Ca_v}3.2^{-/-}$:18.258 ± 2.341%; p = 0.0421) ($\sigma$, $\mathrm{Ca_v}3.2^{+/+}$: 4.090 ± 0.472% vs. $\mathrm{Ca_v}3.2^{-/-}$: 5.398 ± 0.356%; p = 0.0441) (Fig. 4.1.11C). Additionally, a statistical trend was observed in $\theta_2$ relative power ($\theta_2$, $\mathrm{Ca_v}3.2^{+/+}$: 27.886 ± 4.529% vs. $\mathrm{Ca_v}3.2^{-/-}$: 38.914 ± 3.762%; p = 0.0821) (Fig. 4.1.11B). However, no significant differences were identified for $\delta_1$, $\delta_2$, $\theta_1$, $\beta_1$, $\beta_2$, $\beta_3$ and $\gamma$ frequency bands between both genotypes (Fig. 4.1.11).

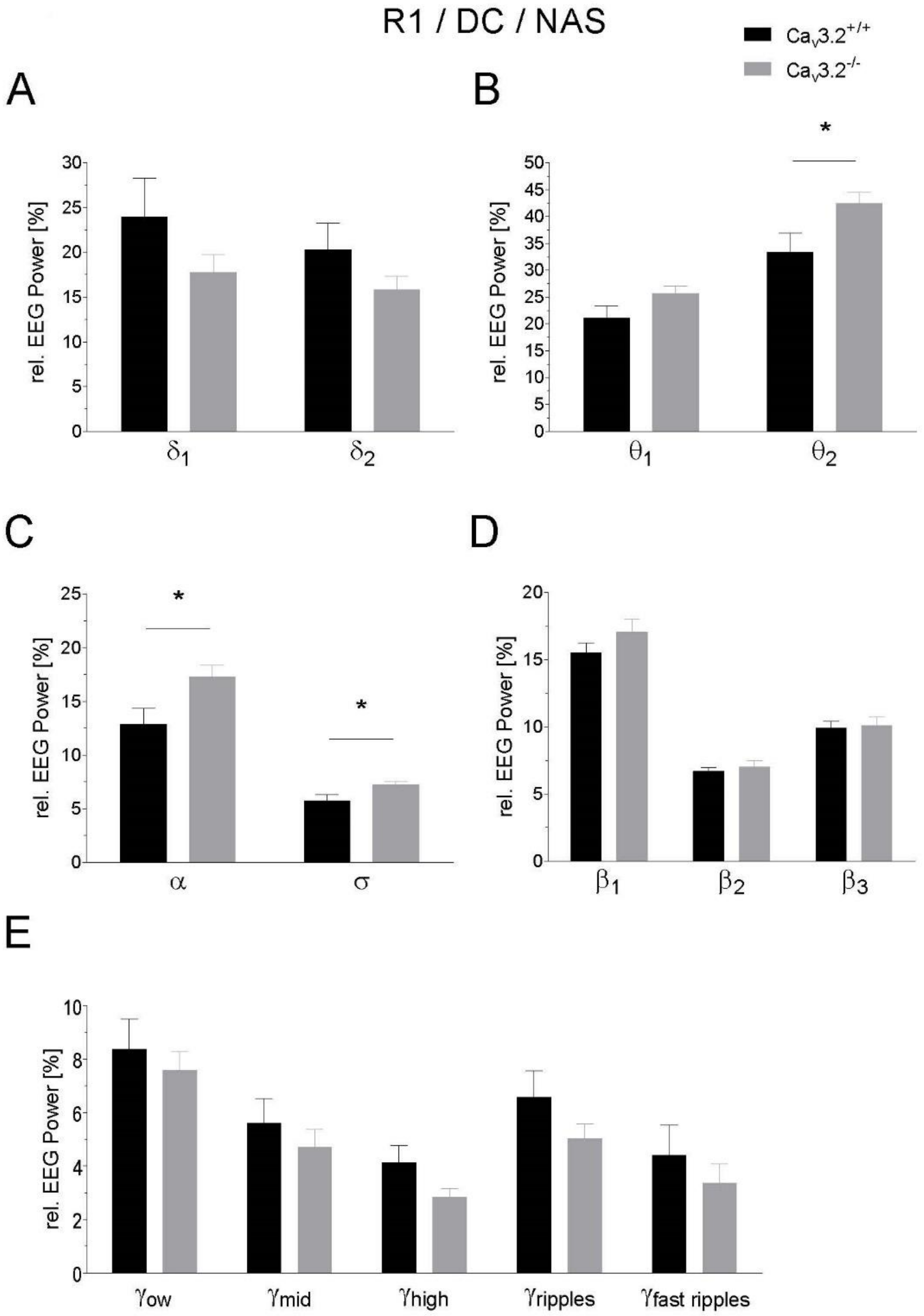

**Figure 4.1.8: EEG power analysis during the dark cycle non-active state of the 1st baseline recording (R1).** Relative EEG power (%) for Ca$_v$3.2$^{+/+}$ and Ca$_v$3.2$^{-/-}$ animals is displayed for the individual frequency ranges (A-E).

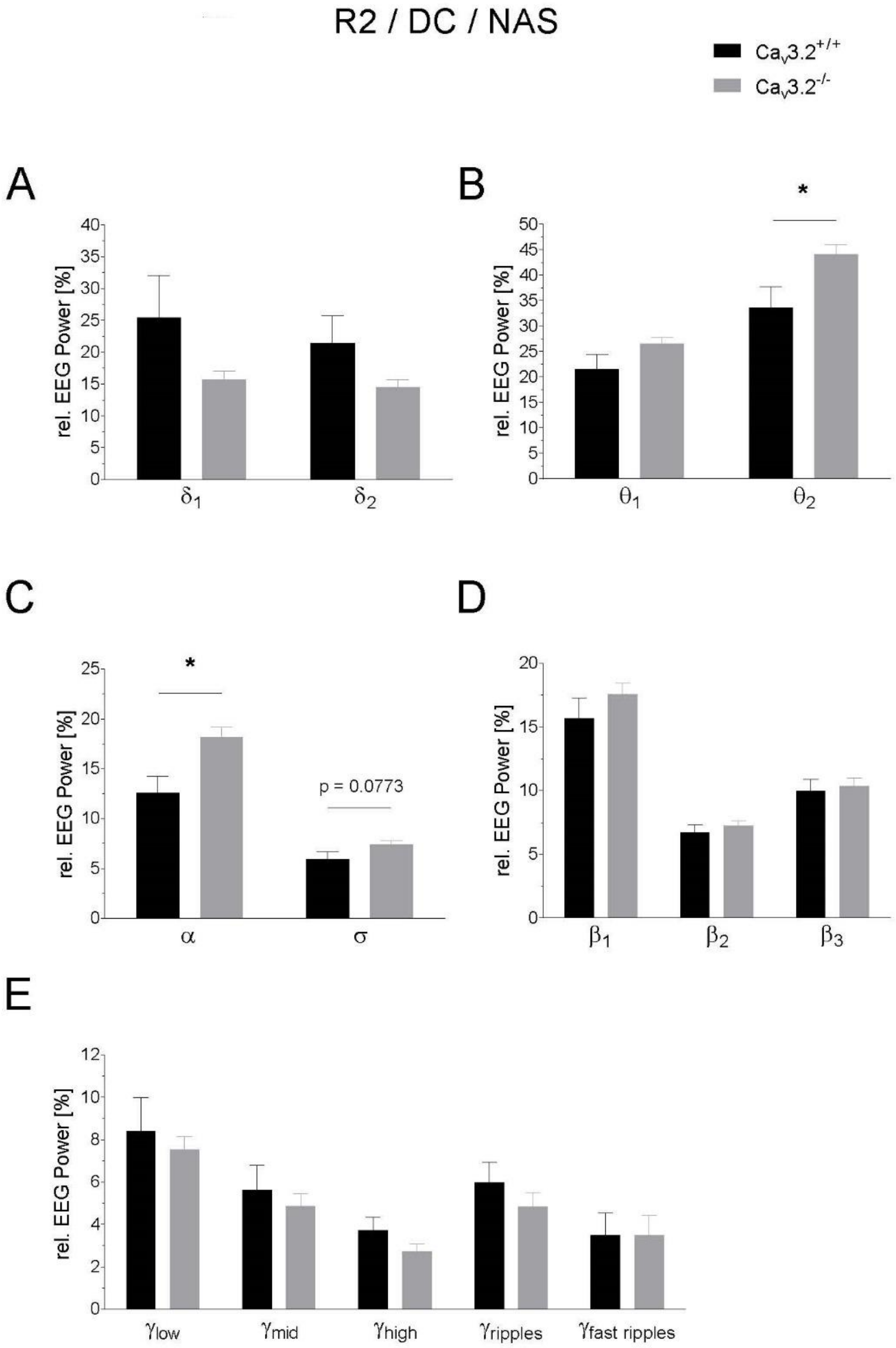

**Figure 4.1.9: EEG power analysis during the dark cycle non-active state of the 2nd baseline recording (R2).** Relative EEG power (%) for $Ca_V3.2^{+/+}$ and $Ca_V3.2^{-/-}$ mice is displayed for the individual frequency ranges (A-E).

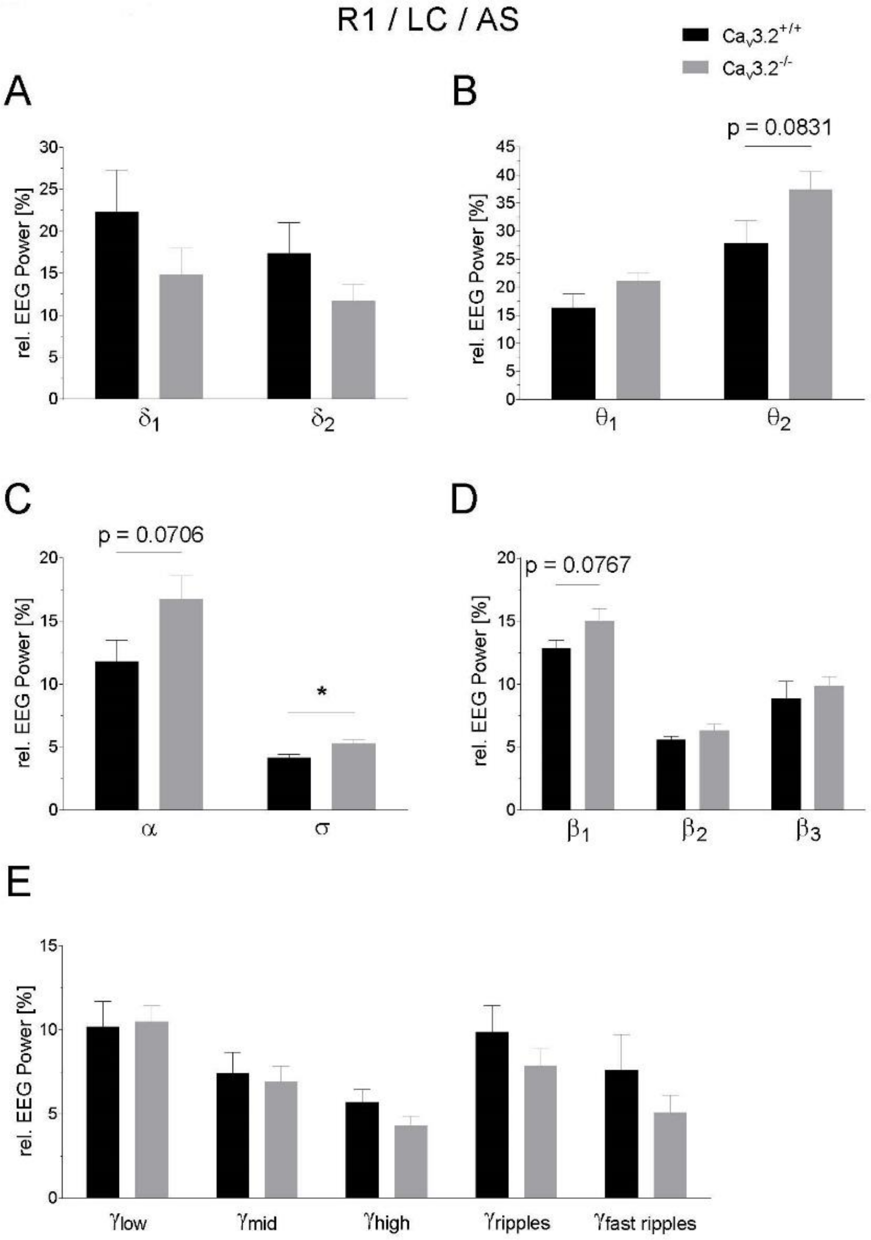

**Figure 4.1.10: EEG power analysis during the light cycle active state of the 1st baseline recording (R1).** Relative EEG power (%) for the $Ca_V3.2^{+/+}$ and $Ca_V3.2^{-/-}$ is displayed for the individual frequency ranges (A-E).

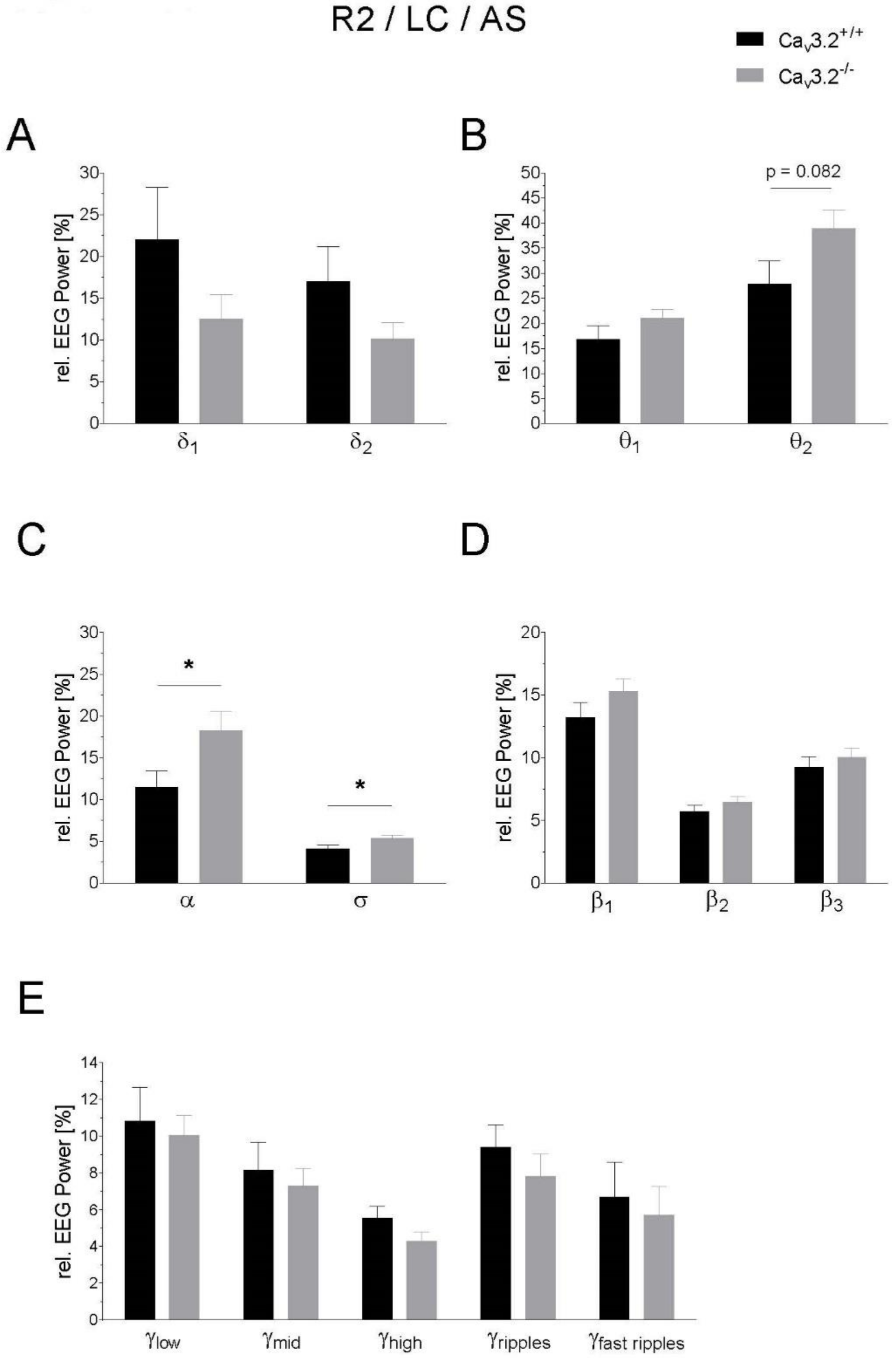

**Figure 4.1.11: EEG power analysis during the light cycle active state of the 2nd baseline recording (R2).** Relative EEG power (%) for Ca$_V$3.2$^{+/+}$ and Ca$_V$3.2$^{-/-}$ mice is displayed for the individual frequency ranges (A-E).

### 4.1.4.4. EEG power analysis of R1/R2 during the non-active state of the light cycle

During the non-active state of the light cycle of baseline recording R1, a significant increase in $\theta_2$, $\alpha$ and $\sigma$ relative EEG power was observed in $Ca_v3.2$ deficient mice compared to $Ca_v3.2^{+/+}$ animals ($\theta_2$, $Ca_v3.2^{+/+}$: 34.928 ± 3.521% vs. $Ca_v3.2^{-/-}$: 45.252 ± 1.730%; $p = 0.0197$) ($\alpha$, $Ca_v3.2^{+/+}$: 13.033 ± 1.309% vs. $Ca_v3.2^{-/-}$: 17.795 ± 0.794%; $p = 0.007$) ($\sigma$, $Ca_v3.2^{+/+}$: 6.208 ± 0.684% vs. $Ca_v3.2^{-/-}$: 8.039 ± 0.383%; $p = 0.0348$) (Fig. 4.1.12B,C). Moreover, a statistical trend was identified for θ1 and $\gamma_{high}$ between both genotypes ($\theta_1$, $Ca_v3.2^{+/+}$: 22.545 ± 2.534% vs. $Ca_v3.2^{-/-}$: 28.126 ± 1.396%; $p = 0.0742$) ($\gamma_{high}$, $Ca_v3.2^{+/+}$: 3.783 ± 0.815% vs. $Ca_v3.2^{-/-}$: 2.213 ± 0.272%; $p = 0.0891$) (Fig. 4.1.12B,E). No significant differences were observed for $\delta_1$, $\delta_2$, $\beta_1$, $\beta_2$, $\beta_3$, $\gamma_{low}$, $\gamma_{mid}$, $\gamma_{ripples}$ and $\gamma_{fast\ ripples}$ frequency bands between both genotypes (Fig. 4.1.12).

Similarly, during the light cycle non-active state of R2, a significant increase in $\theta_2$ and $\alpha$ relative powers was observed in $Ca_v3.2^{-/-}$ mice compared to $Ca_v3.2^{+/+}$ animals ($\theta_2$, $Ca_v3.2^{+/+}$: 34.707 ± 4.035% vs. $Ca_v3.2^{-/-}$: 46.247 ± 1.594%; $p = 0.0187$) ($\alpha$, $Ca_v3.2^{+/+}$: 12.671 ± 1.622% vs. $Ca_v3.2^{-/-}$: 18.189 ± 0.718%; $p = 0.0077$) (Fig. 4.1.13B,C). A statistical trend was found for $\theta_1$, $\sigma$ and $\gamma_{high}$ ($\theta_1$, $Ca_v3.2^{+/+}$: 22.674 ± 2.672% vs. $Ca_v3.2^{-/-}$: 28.692 ± 1.424%; $p = 0.0668$) ($\sigma$, $Ca_v3.2^{+/+}$: 6.563 ± 0.685% vs. $Ca_v3.2^{-/-}$: 8.018 ± 0.353%; $p = 0.0799$) ($\gamma_{high}$, $Ca_v3.2^{+/+}$: 3.558 ± 0.673% vs. $Ca_v3.2^{-/-}$: 2.232 ± 0.258%; $p = 0.0870$) (Fig. 4.1.13B,C,E). However, no significant changes were identified for $\delta_1$, $\delta_2$, $\beta_1$, $\beta_2$, $\beta_3$, $\gamma_{low}$, $\gamma_{mid}$, $\gamma_{ripples}$ and $\gamma_{fast\ ripples}$ frequency bands between both genotypes (Fig. 4.1.13).

In summary, a consistent finding from EEG power analysis turns out to be an increase in $\theta_2$ and $\alpha$ activity in $Ca_v3.2$ deficient animals.

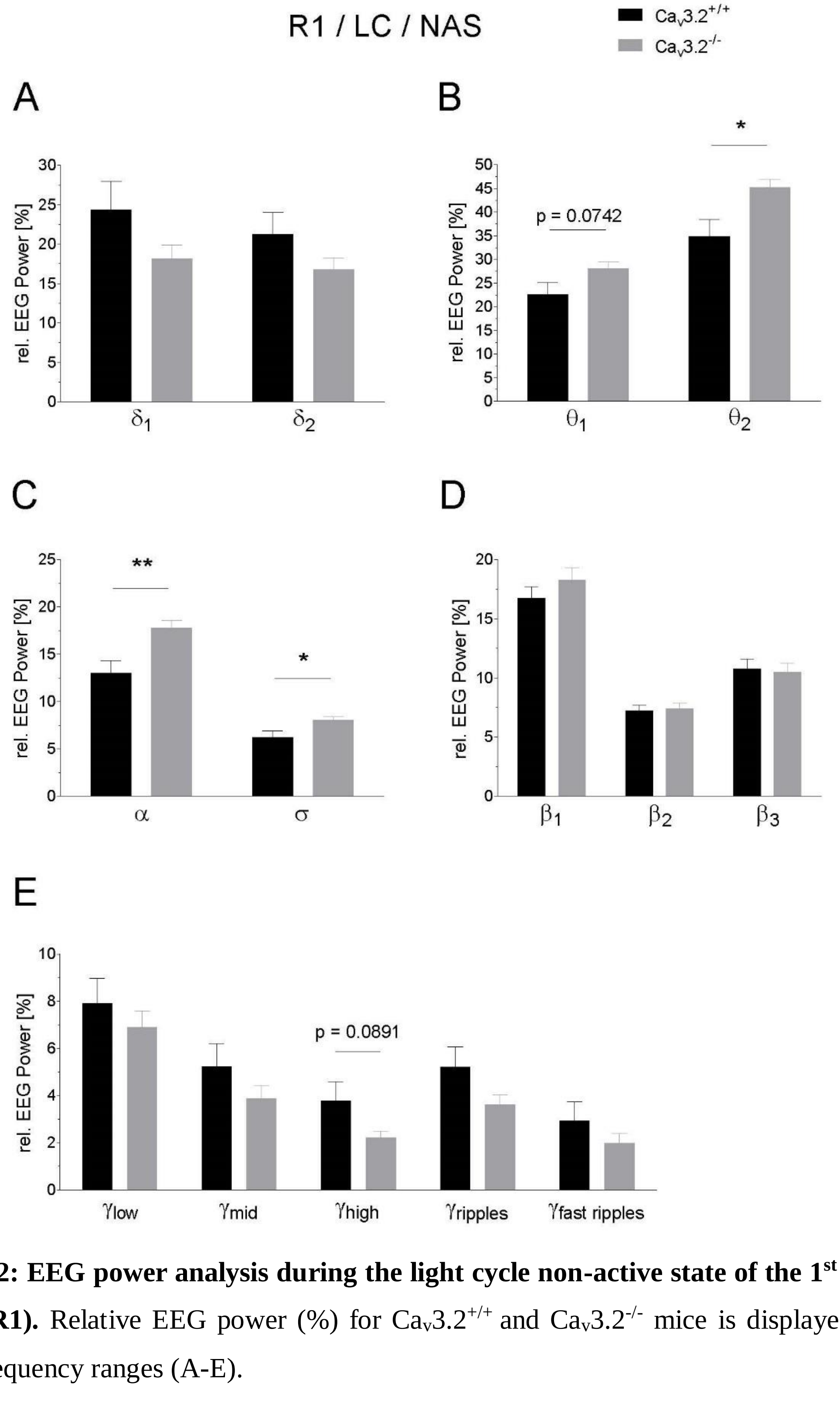

**Figure 4.1.12: EEG power analysis during the light cycle non-active state of the 1st baseline recording (R1).** Relative EEG power (%) for Ca$_V$3.2$^{+/+}$ and Ca$_V$3.2$^{-/-}$ mice is displayed for the individual frequency ranges (A-E).

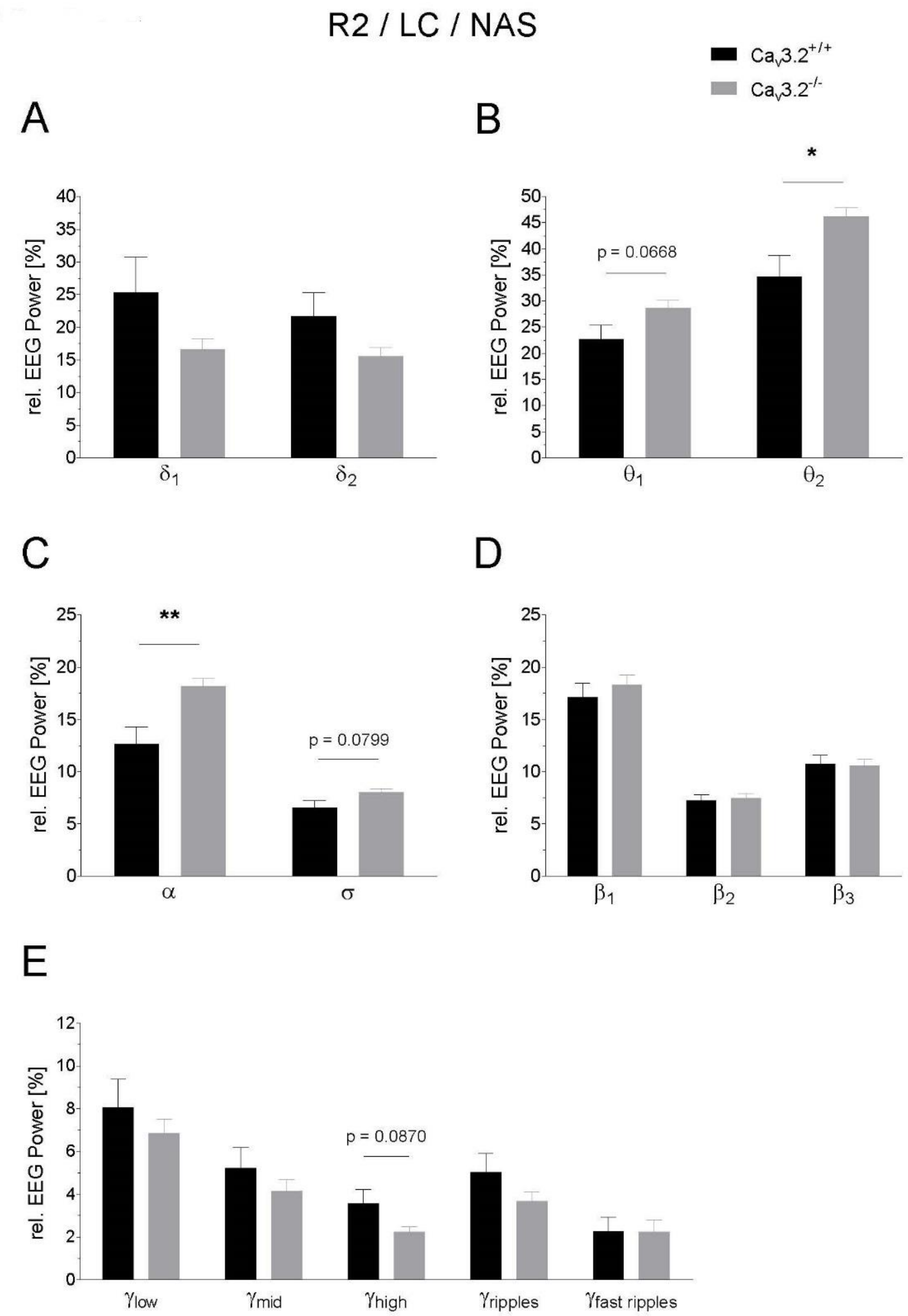

**Figure 4.1.13: EEG power analysis during the light cycle non-active state of the 2nd baseline recording (R2).** Relative EEG power (%) for the $Ca_V3.2^{+/+}$ and $Ca_V3.2^{-/-}$ animals is displayed for the individual frequency ranges (A-E).

### 4.1.4.5. EEG power analysis $Ca_v3.2^{+/+}$ and $Ca_v3.2^{-/-}$ post-urethane phases (U1 & U2)

Urethane is a multi-target drug that exerts narcotic effects that leads to hypolocomotion. At higher doses, it induces slow-wave sleep (~2 g/kg i.p.). In our studies, lower doses of urethane were used (800 mg/kg i.p.) to induce hippocampal type II theta oscillations. Baseline recordings from the hippocampal CA1 region of $Ca_v3.2^{+/+}$ mice (Fig. 4.1.14$A_I$) and $Ca_v3.2^{-/-}$ animals (Fig. 4.1.14$B_I$) show characteristics of LIA activity. Urethane is capable of inducing lower frequencies in controls (Fig. 4.1.14$A_{II}$) and even more prominent in $Ca_v3.2$ deficient mice (Fig. 4.1.14$B_{II}$).

Similar to our studies of spontaneous long-term EEG recordings (R1 & R2), we also analyzed EEGs at post-urethane phases (U1 & U2). For the 1st post-urethane phase (U1), a significant increase in $\theta_2$ and $\alpha$ relative power ($\theta_2$, $Ca_v3.2^{+/+}$: 33.424 ± 3.807% vs. $Ca_v3.2^{-/-}$: 44.941 ± 1.447%; p = 0.0134) ($\alpha$, $Ca_v3.2^{+/+}$:10.353 ± 1.232% vs. $Ca_v3.2^{-/-}$: 14.615 ± 0.623%; p = 0.0080) was observed in $Ca_v3.2^{-/-}$ mice compared to $Ca_v3.2^{+/+}$ mice (Fig. 4.1.15D,E). A statistical trend in $\theta_1$, $\sigma$ and $\gamma_{high}$ relative powers ($\theta_1$, $Ca_v3.2^{+/+}$: 23.950 ± 3.090% vs. $Ca_v3.2^{-/-}$: 31.111 ± 1.318%; p = 0.0512) ($\sigma$, $Ca_v3.2^{+/+}$: 5.408 ± 0.669% vs. $Ca_v3.2^{-/-}$: 6.783 ± 0.296%; p = 0.0811) ($\gamma_{high}$, $Ca_v3.2^{+/+}$: 3.511 ± 0.867% vs. $Ca_v3.2^{-/-}$: 1.891 ± 0.249%; p = 0.0939) between both genotypes (Fig. 4.1.15D,E,G). No significant differences were identified in $\delta_1$, $\delta_2$, $\beta_1$, $\beta_2$, $\beta_3$, $\gamma_{low}$, $\gamma_{mid}$, $\gamma_{ripples}$ and $\gamma_{fast\ ripples}$ frequency bands between both genotypes (Fig. 4.1.15).

Furthermore, at post-urethane phase 2 (U2), a significant increase in relative $\theta_1$, $\theta_2$ and $\alpha$ relative powers was observed in $Ca_v3.2^{-/-}$ mice compared to $Ca_v3.2^{+/+}$ animals ($\theta_1$, $Ca_v3.2^{+/+}$: 24.426 ± 3.129% vs. $Ca_v3.2^{-/-}$: 31.973 ± 1.308%; p = 0.0429) ($\theta_2$, $Ca_v3.2^{+/+}$: 33.650 ± 3.574% vs. $Ca_v3.2^{-/-}$: 46.371 ± 1.274%; p = 0.0047) ($\alpha$, $Ca_v3.2^{+/+}$: 10.204 ± 1.020% vs. $Ca_v3.2^{-/-}$: 15.180 ± 0.597%; p = 0.0008) (Fig. 4.1.16B,C). A statistical trend was identified for the relative $\sigma$ power between both genotypes ($\sigma$, $Ca_v3.2^{+/+}$: 5.267 ± 0.698% vs. $Ca_v3.2^{-/-}$: 6.884 ± 0.360%; p = 0.0586) (Fig. 4.1.16C). No significant difference was found for $\delta_1$, $\delta_2$, $\beta_1$, $\beta_2$, $\beta_3$, $\gamma_{low}$, $\gamma_{mid}$, $\gamma_{ripples}$ and $\gamma_{fast\ ripples}$ frequency bands between both genotypes (Fig. 4.1.16).

In summary, it was confirmed an increase theta/alpha activity observed in the CA1 hippocampal area of $Ca_v3.2$ deficient mice during both long-term baseline EEG recordings and post-urethane phases.

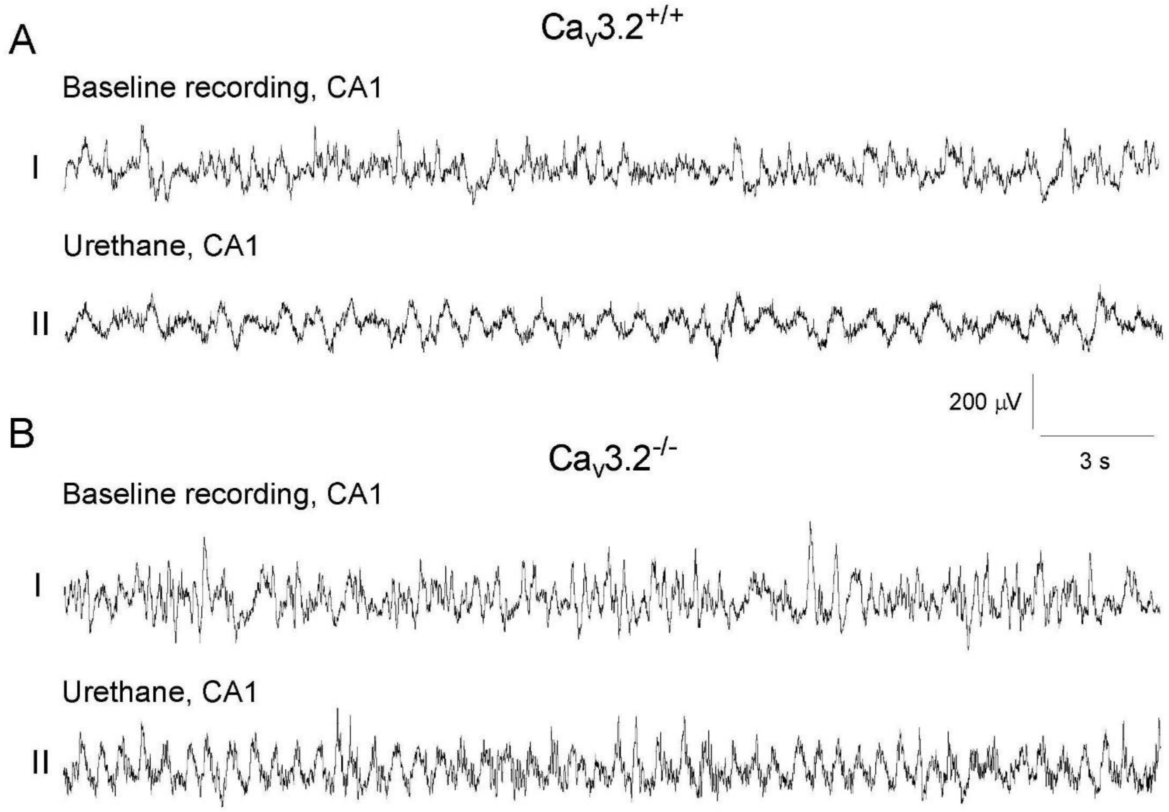

**Figure 4.1.14: Hippocampal CA1 EEG traces (30 s) from $Ca_v3.2^{+/+}$ and $Ca_v3.2^{-/-}$ mice prior to urethane injection baseline recording ($A_I$, $B_1$) and following urethane administration ($A_{II}$, $B_{1I}$).** The EEG exhibits prominent theta oscillations in $Ca_v3.2^{-/-}$ mice ($B_{II}$) compared to $Ca_v3.2^{+/+}$ mice. Scale: Y-axis, 200 µV, X-axis, 3 s.

### 4.1.5. Power spectrum density analysis of theta/alpha frequencies

In order to get a closer insight into the hippocampal theta/alpha architecture of $Ca_v3.2^{+/+}$ and $Ca_v3.2^{-/-}$ mice, we analyzed the power spectrum density (PSD) plots for theta/alpha peak frequencies from the baseline and post-urethane state (Fig. 4.1.17A). Particularly, the peak frequency was increased in $Ca_v3.2^{-/-}$ mice under baseline conditions ($Ca_v3.2^{+/+}$, 6.598 ± 0.300 Hz vs. $Ca_v3.2^{-/-}$, 7.676 ± 0.108 Hz; $p = 0.0045$) and post-urethane ($Ca_v3.2^{+/+}$, 5.134 ± 0.279 Hz vs. $Ca_v3.2^{-/-}$, 6.081 ± 0.279 Hz; $p = 0.0324$) (Fig. 4.1.17B,C).

These findings indicate that there is not only an increase in theta / alpha activity in $Ca_v3.2$ deficient mice but also a shift in theta peak frequency and thus in global theta architecture.

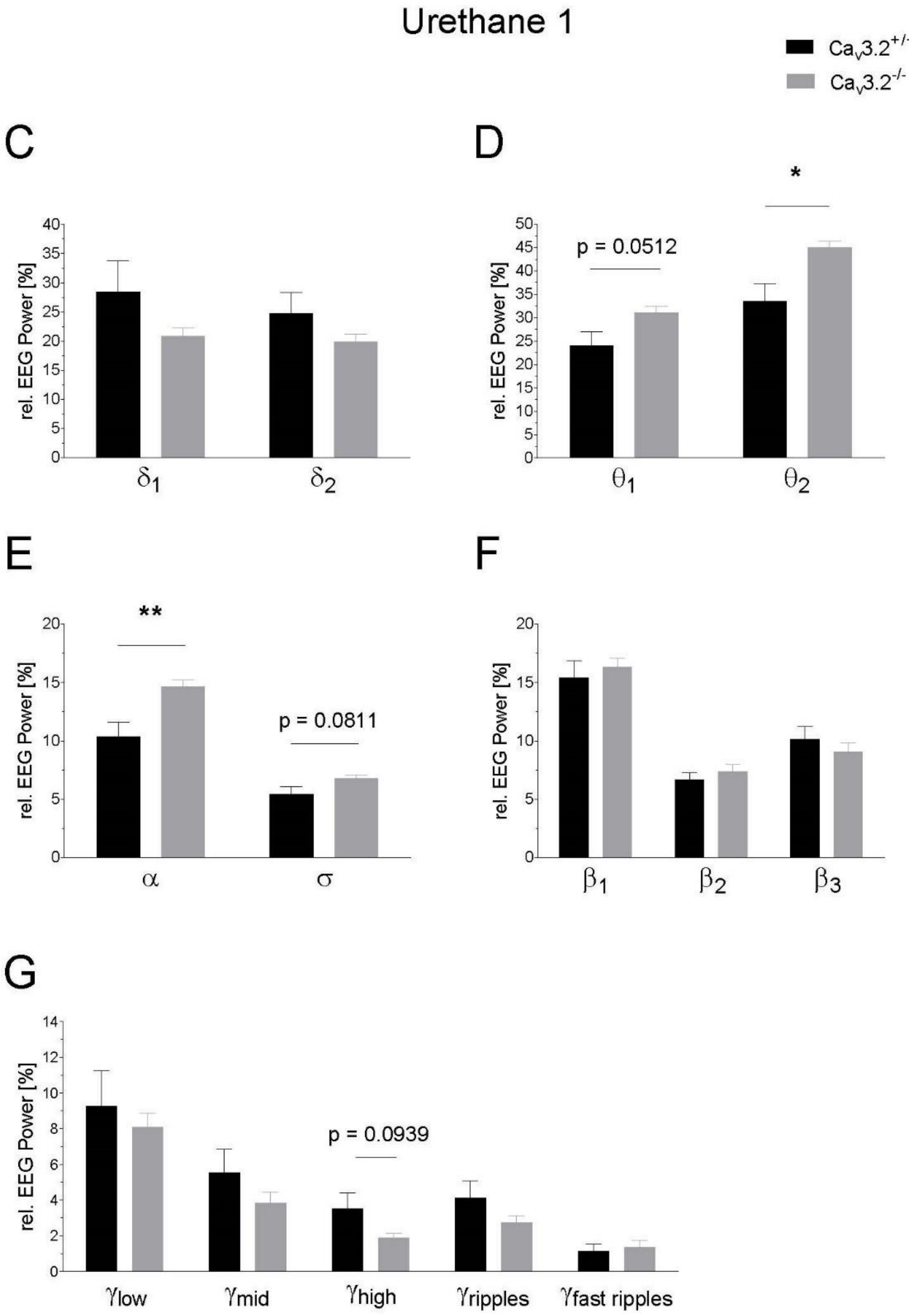

**Figure 4.1.15: EEG power analysis following the 1st urethane (U1) administration (800 mg/kg i.p.).** Relative EEG power (%) for the $Ca_V3.2^{+/+}$ and $Ca_V3.2^{-/-}$ mice is displayed for the individual frequency ranges (C-G).

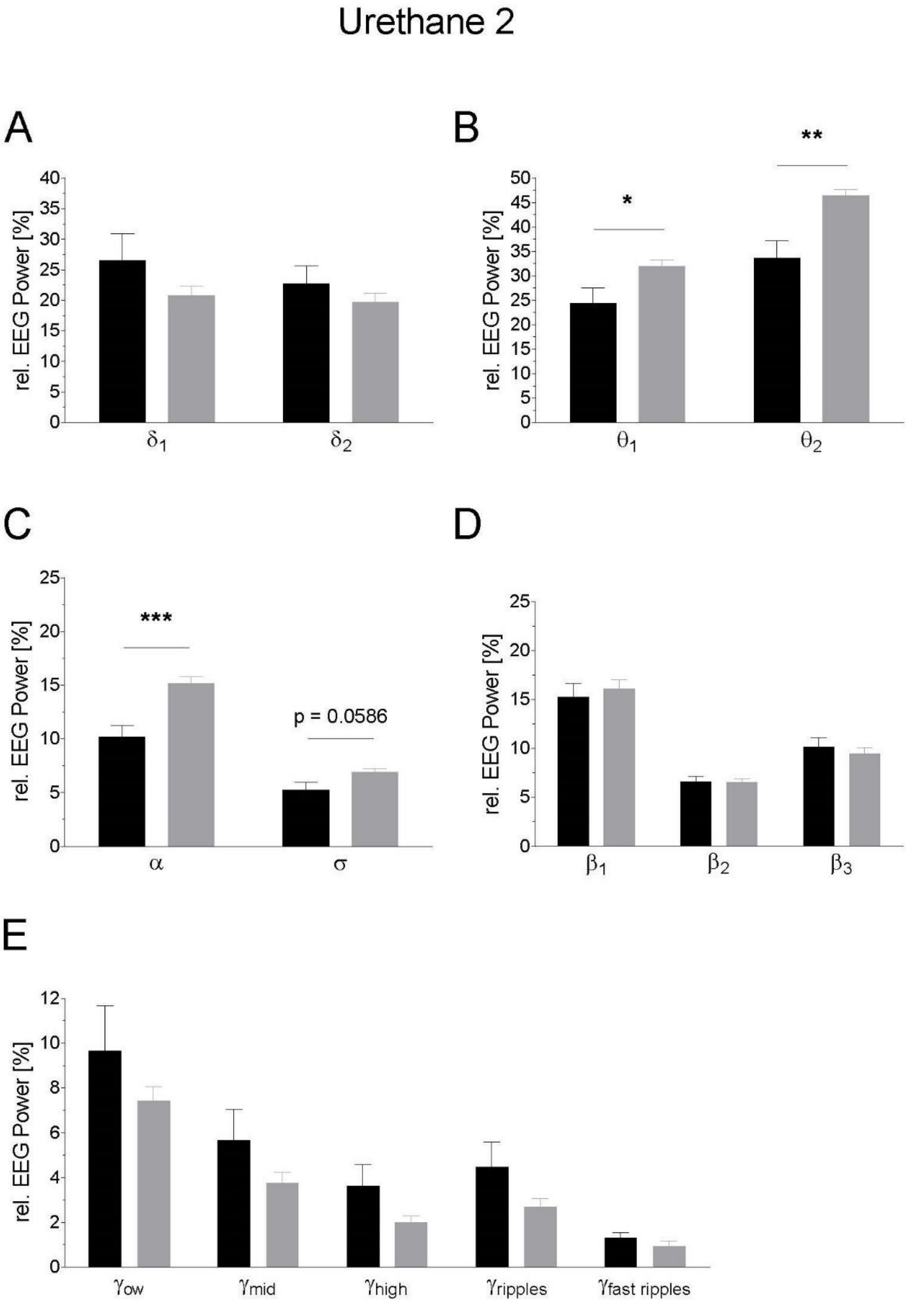

**Figure 4.1.16: EEG power analysis following the 2nd urethane (U2) administration (800 mg/kg i.p.).** Relative EEG power (%) for $Ca_V3.2^{+/+}$ and $Ca_V3.2^{-/-}$ animals is displayed for the individual frequency ranges (A-E).

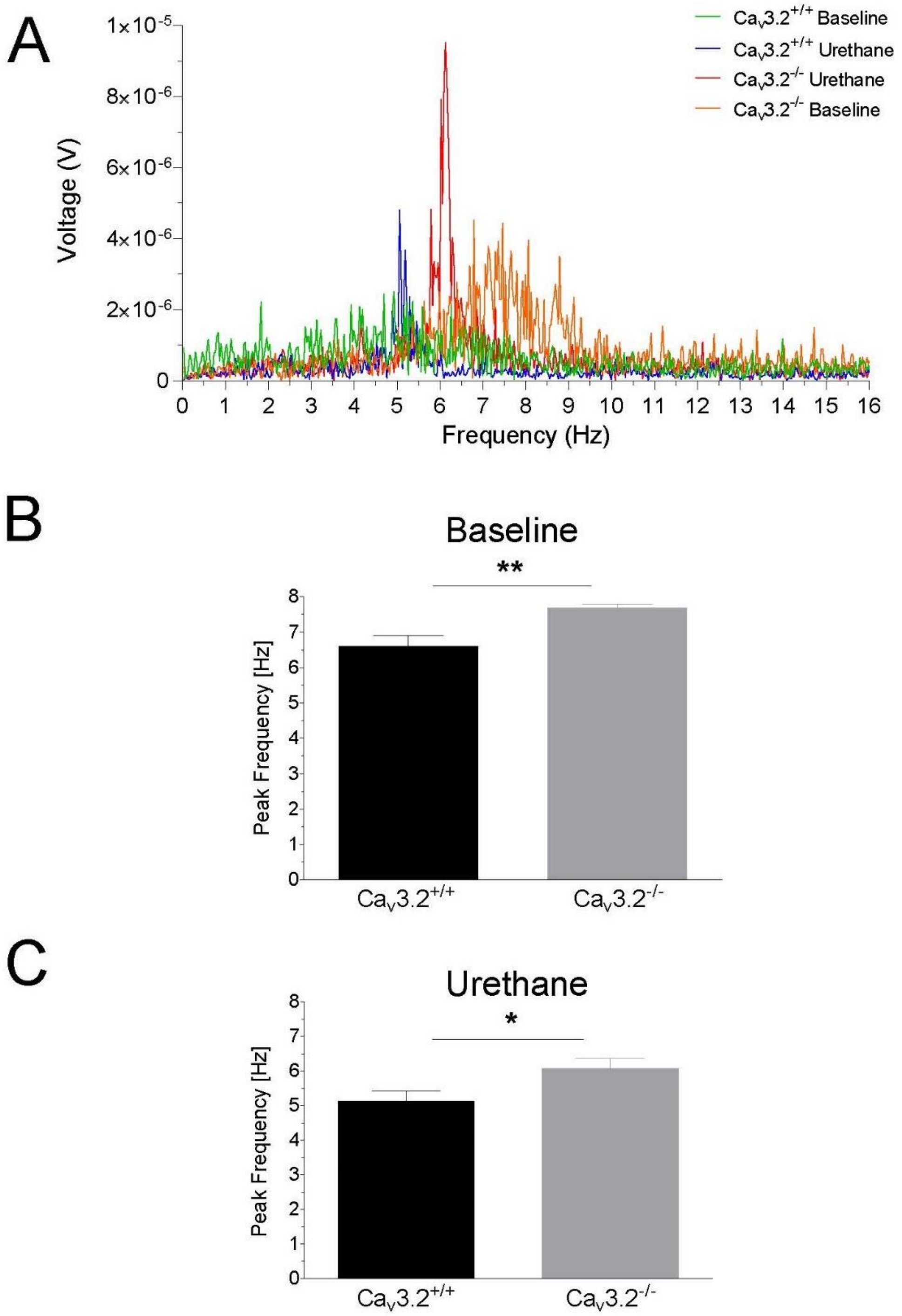

**Figure 4.1.17: Altered theta architecture in $\mathrm{Ca_v3.2^{+/+}}$ and $\mathrm{Ca_v3.2^{-/-}}$ mice.** (A) Power spectrum density (PSD) plots obtained from representative 30s EEG traces from baseline and post-urethane states from both genotypes. (B,C) PSD plots from the baselines (B) and post-urethane state (C) were analyzed for peak frequencies in the range of 0-16 Hz. Under both baseline and post-urethane conditions, $\mathrm{Ca_v3.2^{-/-}}$ mice exhibited a significant increase in theta peak frequencies.

### 4.1.6. Transcriptional alterations in the hippocampus of $Ca_v3.2$ deficient mice

Using quantitative real time PCR (qPCR), a significant decrease in transcript levels of dynein light chain Tctex-Type 1 (Dynlt1b) by a fold change (FC) of -5.208 (p = 0.0002) (Fig. 4.1.18B). A statistical trend in level of 5-hydroxytryptamine receptor 2C (Htr2c) (FC, +1.477; p = 0.065) was observed in $Ca_v3.2$ deficient mice (Fig. 4.1.18C). Furthermore, a significant decrease in Gabrd (FC, -1.385; p = 0.015) and Gabr1 (FC, -1.105; p = 0.010) was observed in $Ca_v3.2$ knock out mice (Fig. 4.1.19H,J). Additionally, a statistical trend was observed for Gabbr2 (FC, -1.088; p = 0.083) These findings correlate with the decrease in Tctex-Type 1 (Dynlt1b) transcripts suggesting an overall reduction in the GABA receptors transportome complex and synaptic and extrasynaptic GABA receptor density in the hippocampus, particularly in hippocampal interneurons.

We also checked for potential alteration in $Ca_v3.1$ and $Ca_v3.3$ $Ca^{2+}$ channel transcripts but no changes were observed between both genotypes (Fig. 4.1.18F; Fig. 4.1.19G).

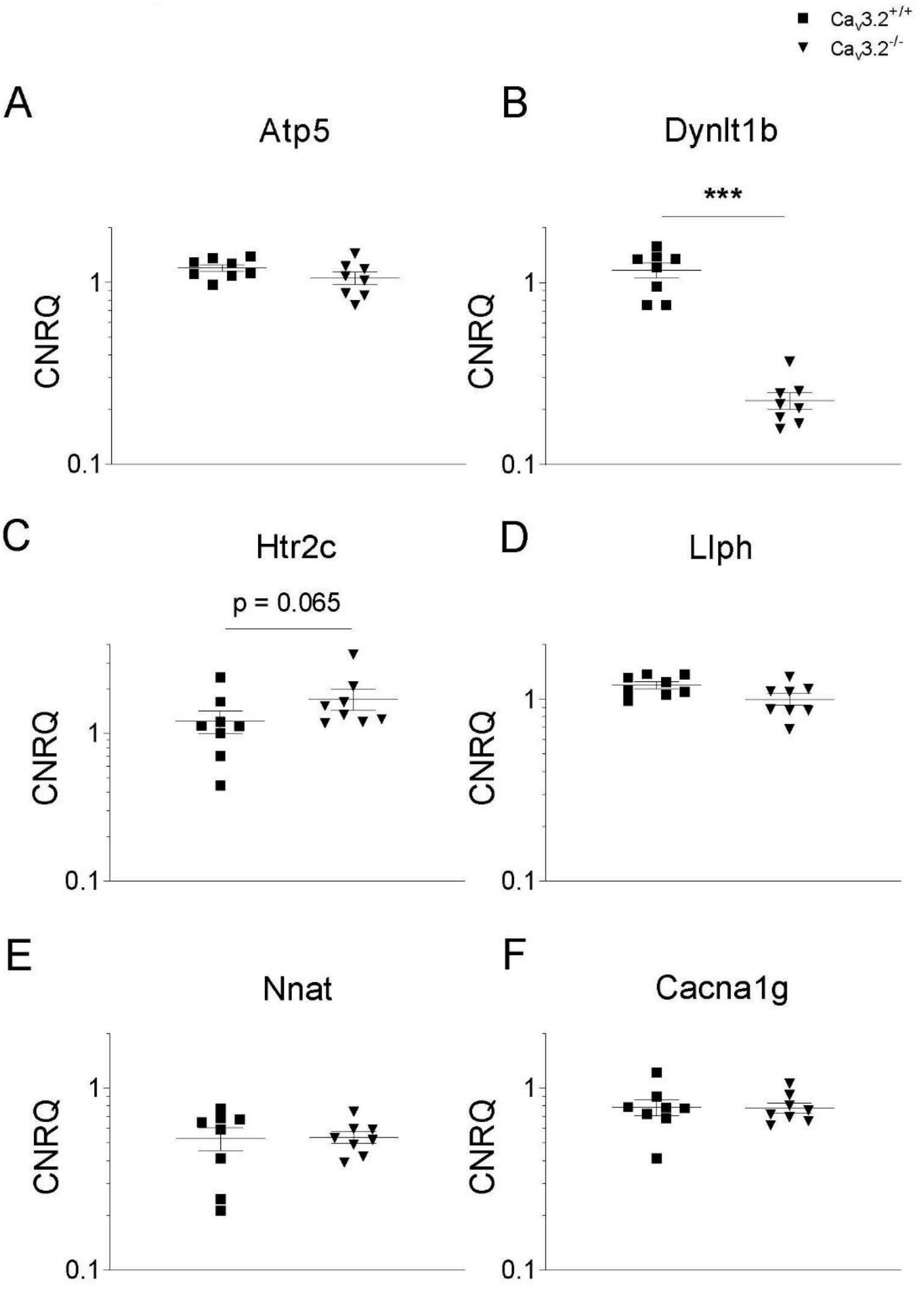

**Figure 4.1.18: qPCR analysis of gene candidates obtained from hippocampal transcriptome data in $Ca_v3.2^{+/+}$ and $Ca_v3.2^{-/-}$ mice.** The following gene candidates potentially relevant for hippocampal theta oscillations were analyzed using qPCR: (A) ATP synthase, $H^+$ transporting, mitochondrial F0 complex, subunit G (Atp5), (B) dynein light chain Tctex-Type1 (Dynlt1b), (C) 5-hydroxytryptamine receptor 2C (Htr2c), (D) LLP homologue, long term synaptic facilitation (Aplysia) (Llph), (E) Neuronatin (Nnat), (F) $Ca_v3.1$ (Cacna1g).

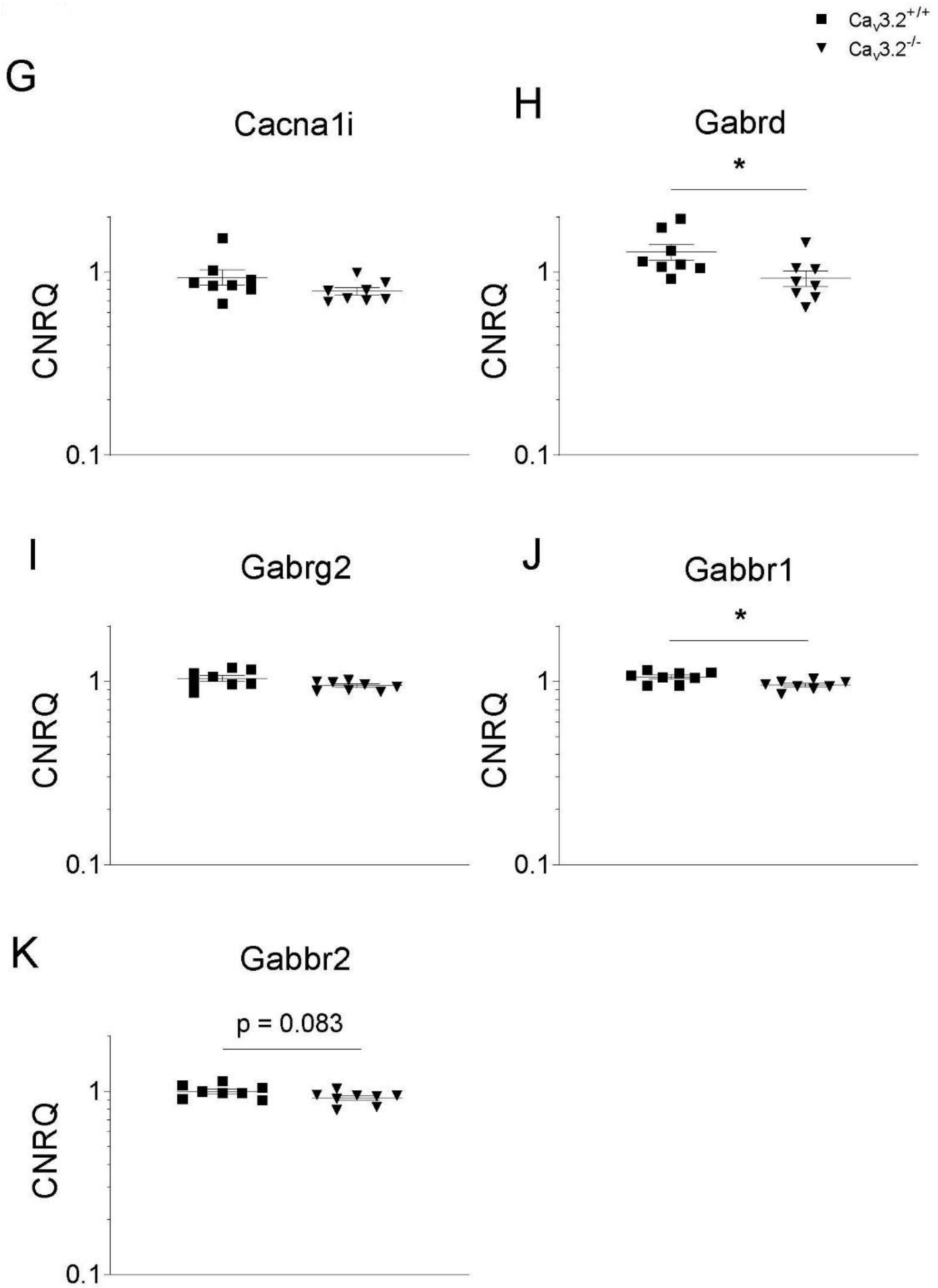

**Figure 4.1.19: qPCR analysis of gene candidates obtained from hippocampal transcriptome data from Ca$_V$3.2$^{+/+}$ and Ca$_V$3.2$^{-/-}$ mice.** The following gene candidates potentially relevant for hippocampal theta oscillations were analyzed using qPCR: (G) Ca$_V$3.3 (Cacna1i), (H) GABA A receptor delta subunit (Gabrd), (I) GABA A receptor gamma subunit (Gabrg2), (J) GABA B1 receptor subunit (Gabbr1), (K) GABA B2 receptor subunit (Gabbr2). A significant decrease in transcript levels of Dynlt1b, Gabrd and Gabbr1 was observed in Ca$_V$3.2$^{-/-}$ mice (B,H,J). A statistical trend was detected for Htr2c and Gabbr2 (C,K).

## 4.2. The effect of Pantoprazole in APPswePS1dE9 mice 12-16 weeks of age

### 4.2.1. Activity analysis – general aspects

The activity data provided by the radiofrequency transmitter was measured as mean relative activity units. The units were calculated by a binary system; with activity = 0 determining the inactive state and activity > 0 classifying the active state. The activity units represent the activity in the horizontal plane and integrate both trip distance, velocity and acceleration (Lundt, Wormuth, Siwek, Muller, et al., 2016).

#### 4.2.1.1. Activity analysis in male mice

Statistically, no significant differences were observed in the mean relative activity between all study groups (WT-DMSO vs. WT-Panto vs. APP(TG)-DMSO vs. APP(TG)-Panto) and all three recordings (at 12, 14 and 16 weeks of age) during the dark and light cycles (Fig. 4.2.1).

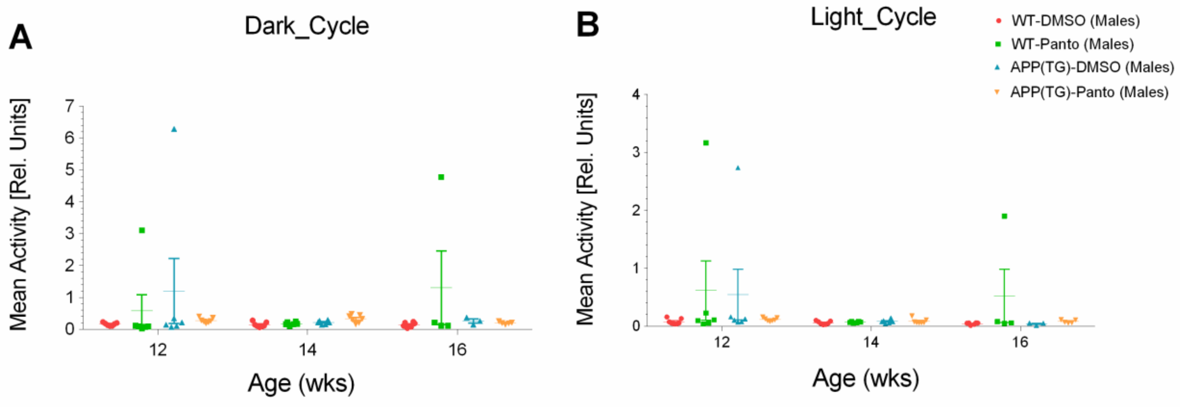

**Figure 4.2.1: Mean relative activity of WT-DMSO, WT-Panto, APP(TG)-DMSO and APP(TG)-Panto male mice groups during the dark/light cycle.**

#### 4.2.1.2. Activity analysis in female mice

A significant increase in the mean relative activity was detected for the WT-Panto group at 16 weeks of age compared to 14 weeks of age during the dark cycle (14 weeks, n = 5: 0.358 ± 0.089 vs. 16 weeks, n = 3: 2.616 ± 2.398; p = 0.0421). A statistical trend in the mean relative activity was found at week 16 for the WT-Panto group compared to the WT-DMSO group and the APP(TG)-DMSO group (WT-DMSO, n = 4: 0.197 ± 0.084 vs. WT-Panto, n = 3: 2.616 ± 2.398; p = 0.0642) (WT-Panto, n = 3: 2.616 ± 2.398 vs. APP(TG)-DMSO, n = 4: 0.262 ± 0.117; p = 0.0748).

No significant differences were observed for the mean relative activity between all other study groups (Fig. 4.2.2A).

During the light cycle, a significant increase in the mean relative activity was found for WT-Panto mice at 16 weeks compared to 14 weeks of age (14 weeks, n = 5: 0.116 ± 0.011 vs. 16 weeks, n = 3: 0.969 ± 0.648; p = 0.0307). There was a statistical trend in the mean relative activity at 16 week of age when the WT-Panto group was compared to the WT-DMSO, the APP(TG)-DMSO and the APP(TG)-Panto groups (WT-DMSO, n = 4: 0.133 ± 0.025 vs. WT-Panto, n = 3: 0.969 ± 0.648; p = 0.0783) (WT-Panto, n = 3, 0.969 ± 0.648 vs. APP(TG)-DMSO , n = 4: 0.129 ± 0.054; p = 0.0762) (WT-Panto, n = 3: 0.969 ± 0.648 vs. APP(TG)-Panto, n = 3: 0.090 ± 0.037; p = 0.0853). However, no other significant differences were observed for the mean relative activity between all other study groups (Fig. 4.2.2B).

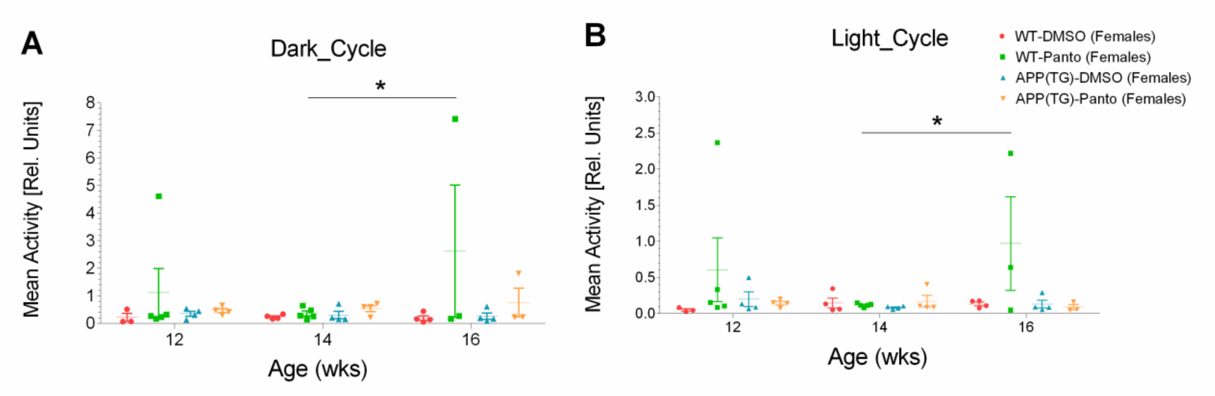

**Figure 4.2.2: Mean relative activity of WT-DMSO, WT-Panto, APP(TG)-DMSO and APP(TG)-Panto female mice and its dependence on the circadian rhythmicity (dark/light cycle)**. $^{*}p < 0.05$; $^{**}p < 0.01$; $^{***}p < 0.001$.

### 4.2.2. FFT based EEG frequency analysis

The Fast-Fourier-Transformation (FFT) based EEG frequency analysis was performed for wild-type controls (WT-DMSO and WT-Panto) and APPswePS1dE9 (APP(TG)-DMSO and APP(TG)-Panto) subgroups based on the EEG recordings from the hippocampal CA1 and motor cortex M1 regions of both genders.

### 4.2.2.1. FFT analysis in male mice

### Theta 1 frequency ($\theta_1$: 4-8 Hz)

### i) Hippocampal CA1 region

Dark cycle

A significant increase in relative theta 1 power was observed in the WT-Panto group compared to the WT-DMSO and APP(TG)-Panto groups at 12 weeks of age (WT-DMSO, n = 7: 21.522 ± 1.236% vs. WT-Panto, n = 6: 26.623 ± 1.050%; p = 0.0097) (WT-Panto, n = 6, 26.623 ± 1.050% vs. APP(TG)-Panto, n = 7: 21.250 ± 1.113%; p = 0.0058). A significant difference was also found for the WT-Panto group compared to the APP(TG)-DMSO and APP(TG)-Panto groups at 14 weeks of age (WT-Panto, n = 6: 29.127 ± 1.058% vs. APP(TG)-DMSO, n = 6: 24.745 ± 0.787%; p = 0.0434) (WT-Panto, n = 6: 29.127 ± 1.058% vs. APP(TG)-Panto, n = 7: 23.522 ± 1.521%; p = 0.0037). Also significant difference detected for the WT-Panto group compared to the APP(TG)-DMSO and the APP(TG)-Panto at 16 weeks of age (WT-Panto, n = 4: 31.055 ± 0.963% vs. APP(TG)-DMSO : n = 3: 24.806 ± 0.338%; p = 0.0253) (WT-Panto, n = 4: 31.055 ± 0.963% vs. APP(TG)-Panto, n = 5: 25.997 ± 1.064%; p = 0.0453).

Furthermore, an increase in theta 1 power was found at 14 weeks of age compared to 12 weeks for WT-DMSO group (12 weeks, n = 7: 21.522 ± 1.236% vs. 14 weeks, n = 7: 25.851 ± 1.053%; p = 0.015). Likewise, an increase in theta 2 power was observed at 16 weeks compared to 12 weeks of age for the WT-DMSO mice (12 weeks, n = 7: 21.522 ± 1.236% vs. 16 weeks, n = 6: 27.748 ± 1.428%; p = 0.0006).

Significant alterations were observed for WT-Panto mice at 16 weeks compared to 12 weeks of age (12 weeks, n = 6: 26.623 ± 1.050% vs. 16 weeks, n = 4: 31.055 ± 0.963%; p = 0.0454). Similarly, significant changes were detected at 16 weeks compared to 12 weeks of age for APP(TG)-Panto animals (12 weeks, n = 7: 21.250 ± 1.113% vs. 16 weeks, n = 5: 25.997 ± 1.064%; p = 0.0148). A statistical trend was detected between WT-Panto and APP(TG)-DMSO at 12 weeks of age (WT-Panto, n = 6: 26.623 ± 1.050% vs. APP(TG)-DMSO, n = 6: 22.491 ± 0.742%; p = 0.0905). Moreover, a statistical trend was observed at 16 weeks compared to 12 weeks of age for WT-Panto mice (12 weeks, n = 6: 26.201 ± 0.797% vs. 16 weeks, n = 6: 29.562 ± 0.748%; p = 0.0629).

No further significant differences in relative theta 1 power were observed between other study groups (Fig. 4.2.3A).

Light cycle

A significant increase in relative theta 1 power was observed in the WT-Panto group as compared to the APP(TG)-DMSO group at 14 weeks of age (WT-Panto, n = 6: 30.643 ± 0.889% vs. APP(TG)-DMSO, n = 6: 26.552 ± 0.328%; p = 0.0341). Furthermore, enhanced relative theta 2 power of the WT-DMSO group was detected at 14 and 16 weeks of age compared to 12 weeks (12 weeks, n = 7: 24.285 ± 0.860% vs. 14 weeks, n = 7: 27.558 ± 0.853%; p = 0.0485) (12 weeks, n = 7: 24.285 ± 0.860% vs. 16 weeks, n = 6: 28.800 ± 1.007%; p = 0.0061). Likewise, a significant increase was found at 14 and 16 weeks compared to 12 weeks of age for the WT-Panto group (12 weeks, n = 6: 26.091 ± 1.125% vs. 14 weeks, n = 6: 30.643 ± 0.890%; p = 0.0079) (12 weeks, n = 6: 26.091 ± 1.125% vs. 16 weeks, n = 4: 31.052 ± 1.646%; p = 0.0099). A statistical trend was identified between the WT-Panto group when compared to the APP(TG)-Panto group at 14 weeks of age (WT-Panto, n = 6: 30.643 ± 0.889% vs. APP(TG)-Panto, n = 7: 27.278 ± 1.451%; p = 0.0905) and at 16 weeks of age (WT-Panto, n = 4: 31.052 ± 1.646% vs. APP(TG)-Panto, n = 5: 26.854 ± 0.997%; p = 0.0752). In addition, the APP(TG)-DMSO group exhibited a significant difference between 16 weeks and 12 weeks of age (12 weeks, n = 6: 24.018 ± 0.926% vs. 16 week, n = 3: 28.176 ± 0.637%; p = 0.0605).

Furthermore, no significant differences in relative theta 1 power were observed between all other study groups (Fig. 4.2.3B).

### ii) Motor cortical M1 region

Dark cycle

A significant increase in relative theta 1 power was observed in WT-Panto compared to APP(TG)-Panto at 12 weeks of age (WT-Panto, n = 6: 28.256 ± 1.091% vs. APP(TG)-Panto, n = 7: 22.951 ± 0.738%; p = 0.0162) and at 14 weeks of age (WT-Panto, n = 6: 29.238 ± 1.689% vs. APP(TG)-Panto, n = 7: 24.456 ± 0.882%; p = 0.0361). In addition, at 16 weeks of age, an increased in theta 2 power was detected in the WT-Panto group compared to the WT-DMSO group (WT-DMSO, n = 7: 23.430 ± 2.063% vs. WT-Panto, n = 4: 28.587 ± 0.881%; p = 0.0485).

No significant differences in relative theta 1 power were detected between all other study groups (Fig. 4.2.3C).

Light cycle

No significant differences in relative theta 1 power were observed between all study groups (Fig. 4.2.3D).

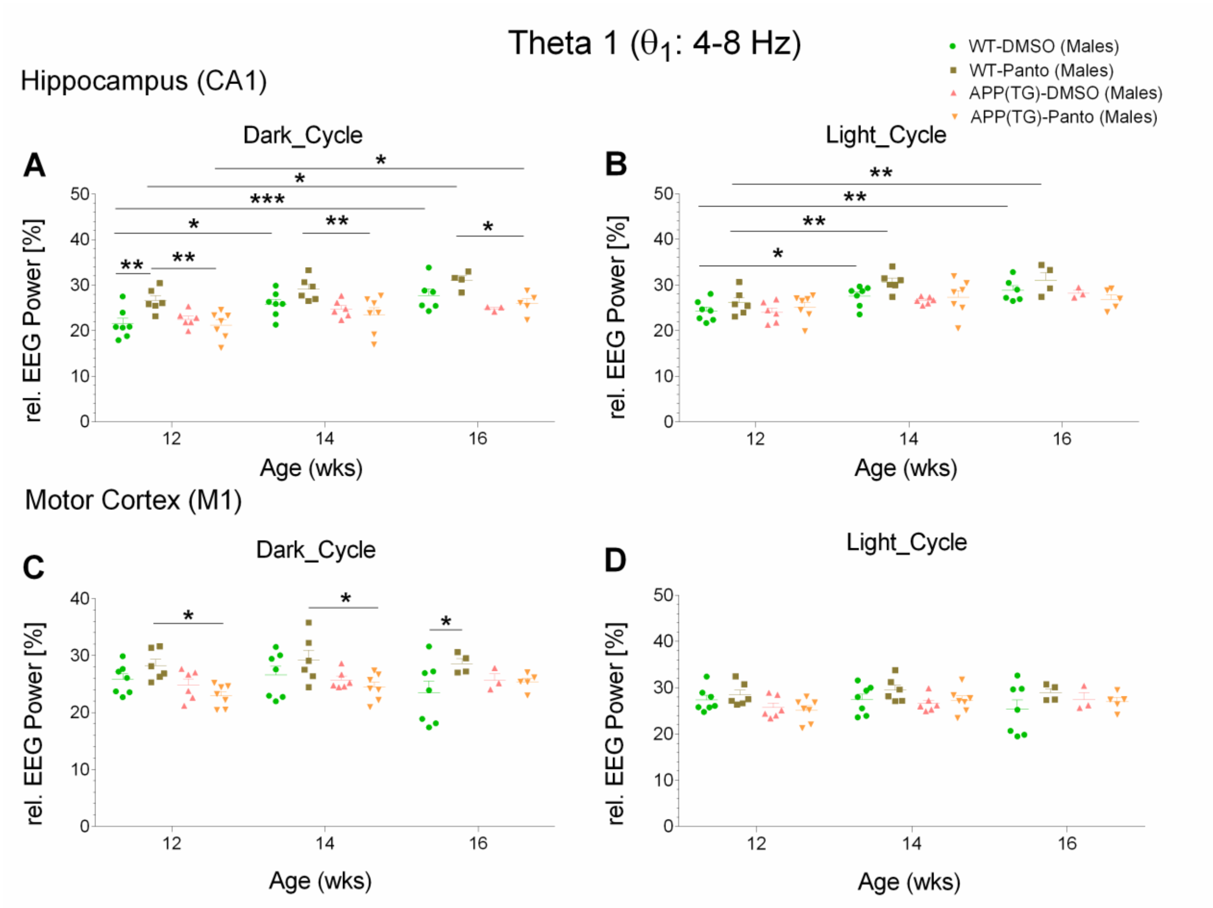

**Figure 4.2.3: Hippocampus (CA1) (A,B) and motor cortex (M1) (C,D) relative theta 1 power (%) ($\theta_1$: 4-8 Hz) in WT-DMSO, WT-Panto, APP(TG)-DMSO, and APP(TG)-Panto male mice.** Results are depicted considering the circadian rhythmicity (dark/light cycle). $^{*}$ $p < 0.05$; $^{**}$ $p < 0.01$; $^{***}$ $p < 0.001$.

### Theta 2 frequency ($\theta_2$: 4.1-12 Hz)

### i) Hippocampal CA1 region

Dark cycle

A significant increase in relative theta 2 power was observed in the WT-Panto group as compared to the WT-DMSO group at 12 weeks of age (WT-DMSO, n = 7: 35.021 ± 2.204% vs. WT-Panto, n = 6: 42.528 ± 1.692%; p = 0.0304) and at 14 weeks of age (WT-DMSO, n = 7: 39.330 ± 2.308% vs. WT-Panto, n = 6: 46.544 ± 1.331%; p = 0.0402). A significant increase was also detected at 16 weeks compared to 12 weeks of age for the WT-DMSO group (12 weeks, n = 7: 35.021 ± 2.204% vs. 16 weeks, n = 6: 42.094 ± 1.703%; p = 0.0255). However, no significant differences in relative theta 1 power were observed between all other study groups (Fig. 4.2.4A).

Light cycle

No significant differences in relative theta 2 power were detected between the analyzed study groups (Fig. 4.2.4B).

**ii) Motor cortical M1 region**

Dark cycle

A significant increase in relative theta 2 power was observed in the WT-Panto group compared to the WT-DMSO group at 16 weeks of age (WT-DMSO, n = 7: 34.156 ± 2.621% vs. WT-Panto, n = 4: 40.574 ± 1.264%; p = 0.0314). No further significant differences in relative theta 1 power were found between all other study groups (Fig. 4.2.4C).

Light cycle

No significant differences in relative theta 2 power were observed for all study groups (Fig. 4.2.4D).

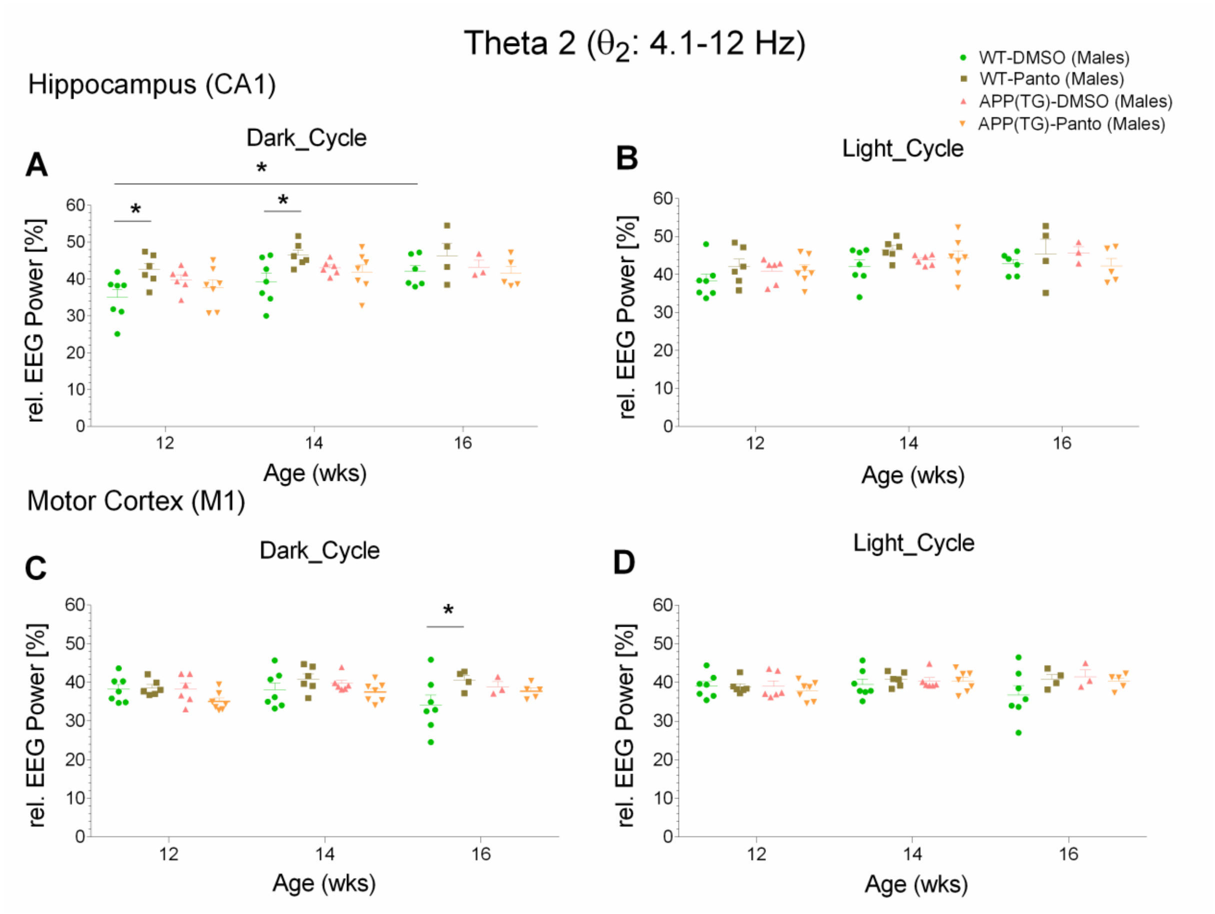

**Figure 4.2.4: Hippocampus (CA1) (A,B) and motor cortex (M1) (C,D) relative theta 2 power (%, $\theta_2$: 4.1-12 Hz) in WT-DMSO, WT-Panto, APP(TG)-DMSO, and APP(TG)-Panto male mice.** Results are depicted considering the circadian rhythmicity (dark/light cycle). $^{*}$ $p < 0.05$; $^{**}$ $p < 0.01$; $^{***}$ $p < 0.001$.

### Delta frequency (δ: 0.5-4 Hz)

### i) Hippocampal CA1 region

Dark cycle

A statistical trend in relative delta power was observed between the WT-DMSO group compared to the APP(TG)-Panto group at 14 weeks of age (WT-DMSO, n = 7: 32.852 ± 5.954% vs. APP(TG)-Panto, n = 7: 20.308 ± 2.071%; p = 0.0986).

No significant differences in the relative delta power were detected between all other study groups (Fig. 4.2.5A).

Light cycle

No significant differences in relative delta power were observed between all study groups (Fig. 4.2.5B).

**ii) Motor cortical M1 region**

Dark cycle

A significant increase in the relative delta power was observed in the WT-Panto group when compared to the APP(TG)-DMSO group at the 12 weeks of age (WT-Panto, n = 6: 36.523 ± 1.511% vs. APP(TG)-DMSO, n = 6: 25.774 ± 1.411%; p = 0.0247). In addition, a significant difference was also found in the WT-DMSO in comparison to the APP(TG)-DMSO at 14 weeks of age (WT-DMSO, n = 7: 34.453 ± 2.360% vs. APP(TG)-DMSO, n = 6: 23.995 ± 1.068%; p = 0.0229). Likewise, an enhanced delta power was identified at the 16 weeks in comparison to the 12 weeks of age for WT-DMSO mice (12 weeks, n = 7, 29.498 ± 1.154% vs. 16 weeks, n = 7: 38.781 ± 5.350%; p = 0.0226).

A statistical trend was also found between the WT-DMSO group as compared to the APP(TG)-DMSO and APP(TG)-Panto groups at the 16 weeks of age (WT-DMSO, n = 7, 38.781 ± 5.350% vs. APP(TG)-DMSO, n = 3: 27.805 ± 1.345%; p = 0.0709 ) (WT-DMSO, n = 7: 38.781 ± 5.350% vs. APP(TG)-Panto, n = 5: 29.947 ± 3.302%; p = 0.0947). However, no significant differences in relative delta power were observed between all other study groups (Fig. 4.2.5C).

Light cycle

A significant rise in the relative delta power was observed between the WT-Panto group as compared to the APP(TG)-DMSO group at the 12 weeks of age (WT-Panto, n = 6: 36.005 ± 1.960% vs. APP(TG)-DMSO , n = 6: 26.480 ± 1.072%; p = 0.0172).

A statistical trend was identified at the 12 weeks of age between the WT-Panto and the APP(TG)-Panto groups (WT-Panto, n = 6: 36.005 ± 1.959% vs. APP(TG)-Panto, n = 7: 28.426 ± 0.770%; p = 0.0663). Likewise, a statistical trend also detected at 14 weeks of age between WT-DMSO compared to the APP(TG)-DMSO mice and the WT-Panto compared to the APP(TG)-DMSO (WT-DMSO, n = 6: 32.780 ± 2.136% vs. APP(TG)-DMSO, n = 6: 25.431 ± 1.340%; p = 0.0791) (WT-Panto, n = 6: 33.640 ± 1.287% vs. APP(TG)-DMSO, n = 6: 25.431 ± 1.341%; p = 0.051). Furthermore, a statistical trend also found at 16 weeks of age between WT-DMSO compared to the APP(TG)-DMSO and APP(TG)-Panto mice (WT-DMSO, n = 7: 36.531 ± 4.789% vs. APP(TG)-DMSO, n = 3: 26.883 ± 2.441%; p = 0.0567) (WT-DMSO, n = 7: 36.531 ± 4.789% vs. APP(TG)-Panto, n = 5: 28.656 ± 1.606%; p = 0.0715).

However, no significant differences in the relative delta power were observed between all other study groups (Fig. 4.2.5D).

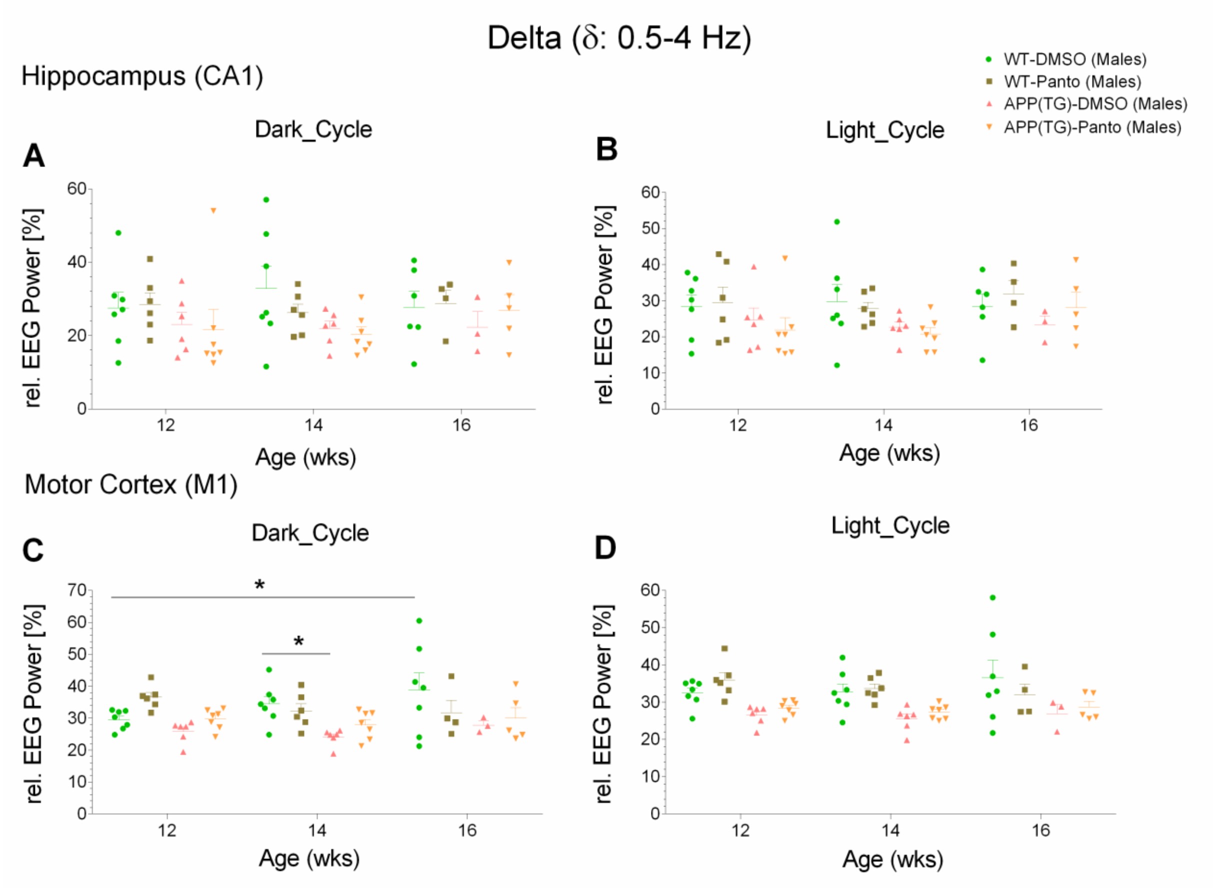

**Figure 4.2.5: Hippocampus (CA1) (A,B) and motor cortex (M1) (C,D) relative delta power (%) (δ: 0.5-4 Hz) in WT-DMSO, WT-Panto, APP(TG)-DMSO and APP(TG)-Panto male mice.** Results are depicted considering the circadian rhythmicity (dark/light cycle). $^{*}$ $p < 0.05$; $^{**}$ $p < 0.01$; $^{***}$ $p < 0.001$.

### Beta 1 frequency ($\beta_1$: 12.1-30 Hz)

### i) Hippocampal CA1 region

Dark cycle

A significant rise in relative beta 1 power was observed for the APP(TG)-Panto group compared to the WT-DMSO and WT-Panto groups at 14 weeks of age (WT-DMSO, n = 7: 14.568 ± 1.717% vs. APP(TG)-Panto, n = 7: 22.289 ± 1.467%: p = 0.0042) (WT-Panto, n = 6: 15.704 ± 0.587% vs. APP(TG)-Panto, n = 7: 22.289 ± 1.467%; p = 0.0258). However, a statistical trend was detected between APP(TG)-DMSO and WT-DMSO at 14 weeks of age (WT-DMSO, n = 7: 14.568 ± 1.717% vs. APP(TG)-DMSO, n = 6: 20.039 ± 1.559%; p = 0.0852).

No further significant differences in relative beta 1 power were found between all other study groups (Fig. 4.2.6A).

Light cycle

A significant increase in relative beta 1 power was identified in APP(TG)-Panto group compared to the WT-Panto mice at 12 weeks of age (WT-Panto, n = 6: 16.646 ± 0.992% vs. APP(TG)-Panto, n = 7: 22.465 ± 2.052%; p = 0.0359). Likewise, a significant alteration was detected for the APP(TG)-Panto group compared to the WT-DMSO and WT-Panto groups at 14 weeks of age (WT-DMSO, n = 7: 16.079 ± 1.406% vs. APP(TG)-Panto, n = 7: 22.907 ± 1.424%; p = 0.0066) (WT-Panto, n = 6: 16.071 ± 0.527% vs. APP(TG)-Panto, n = 7: 22.907 ±1.424%; p = 0.0097).

No significant differences in relative beta 1 power were observed between all other study groups (Fig. 4.2.6B).

### ii) Motor cortex (M1)

Dark cycle

A significant increase in relative beta 1 power was observed in APP(TG)-DMSO and APP(TG)Panto groups compared to WT-Panto mice at 12 weeks of age (WT-Panto, n = 6: 13.588 ± 0.698% vs. APP(TG)-DMSO, n = 6: 18.583 ± 0.482%; p = 0.004) (WT-Panto, n = 6: 13.588 ± 0.698% vs. APP(TG)-Panto, n = 7: 17.750 ± 0.504%; p = 0.0154).

Significant differences were identified at 14 weeks of age between APP(TG)-DMSO group compared to the WT-DMSO and WT-Panto groups (WT-DMSO, n = 7: 14.226 ± 0.721% vs. APP(TG)-DMSO, n = 6: 19.290 ± 0.286%; p = 0.0021) (WT-Panto, n = 6: 14.198 ±1.029% vs. APP(TG)-DMSO, n = 6: 19.290 ± 0.286%; p = 0.003). Likewise, significant alterations were also observed between APP(TG)-Panto group compared to the WT-DMSO and WT-Panto groups (WT-DMSO, n = 7: 14.226 ± 0.721% vs. APP(TG)-Panto, n = 7: 17.924 ± 0.755%; p = 0.0287) (WT-Panto, n = 6: 14.198 ± 1.029% vs. APP(TG)-Panto, n = 7: 17.924 ± 0.755%; p = 0.036).

Furthermore, a significant change was observed at 16 weeks of age in APP(TG)-Panto compared to WT-DMSO (WT-DMSO, n = 7: 14.262 ± 1.867% vs. APP(TG)-Panto, n = 5: 18.235 ± 1.446%; p = 0.033).

No significant differences in relative beta 1 power were detected between all other study groups (Fig. 4.2.6C).

Light cycle

A significant increase in relative beta 1 power was observed in APP(TG)-Panto group compared to WT-DMSO and WT-Panto groups at 12 weeks of age (WT-DMSO, n = 7: 15.871 ± 0.724% vs. APP(TG)-Panto, n = 7: 19.032 ± 0.422%; p = 0.0429) (WT-Panto, n = 6: 13.533 ± 0.950% vs. APP(TG)-DMSO, n = 6: 19.074 ± 0.350%; p = 0.0003). Likewise, a significant difference was also observed between APP(TG)-DMSO compared to WT-Panto mice (WT-Panto, n = 6: 13.533 ± 0.950% vs. APP(TG)-Panto, n = 7: 19.032 ± 0.422%; p = 0.0002).

Furthermore, an enhanced in relative beta 1 power was identified in APP(TG)-DMSO group compared to WT-DMSO and WT-Panto groups at 14 weeks of age (WT-DMSO, n = 7: 15.647 ± 0.606% vs. APP(TG)-DMSO, n = 6: 20.309 ± 0.235%; p = 0.0017) (WT-Panto, n = 6: 15.099 ± 0.795% vs. APP(TG)-DMSO, n = 6: 20.309 ± 0.235%; p = 0.0007). Similarly, a significant increase was also observed in APP(TG)-Panto group compared to WT-DMSO and WT-Panto groups at 14 weeks of age (WT-DMSO, n = 7: 15.647 ± 0.606% vs. APP(TG)-Panto, n = 7: 19.584 ± 0.721%; p = 0.0071) (WT-Panto, n = 6: 15.099 ± 0.795% vs. APP(TG)-Panto, n = 7: 19.584 ± 0.721%; p = 0.0027). In addition, a significant difference was identified between APP(TG)-DMSO compared to WT-DMSO mice at 16 weeks of age (WT-DMSO, n = 7: 15.643 ± 1.845% vs. APP(TG)-DMSO, n = 3: 20.033 ± 0.186%; p = 0.0254). A statistical trend was detected between APP(TG)-DMSO compared to WT-DMSO mice at 12 weeks of age (WT-DMSO, n = 7: 15.871 ± 0.724% vs. APP(TG)-DMSO, n = 6: 19.074 ± 0.350%; p = 0.0511). Additionally, significant difference was also observed between APP(TG)-Panto compared to WT-DMSO groups at 16 weeks of age (WT-DMSO, n = 7: 15.643 ± 1.846% vs. APP(TG)-Panto, n = 5: 18.990 ± 0.842%; p = 0.0536).

Further, no significant differences in relative beta 1 power were detected between all other study groups (Fig. 4.2.6D).

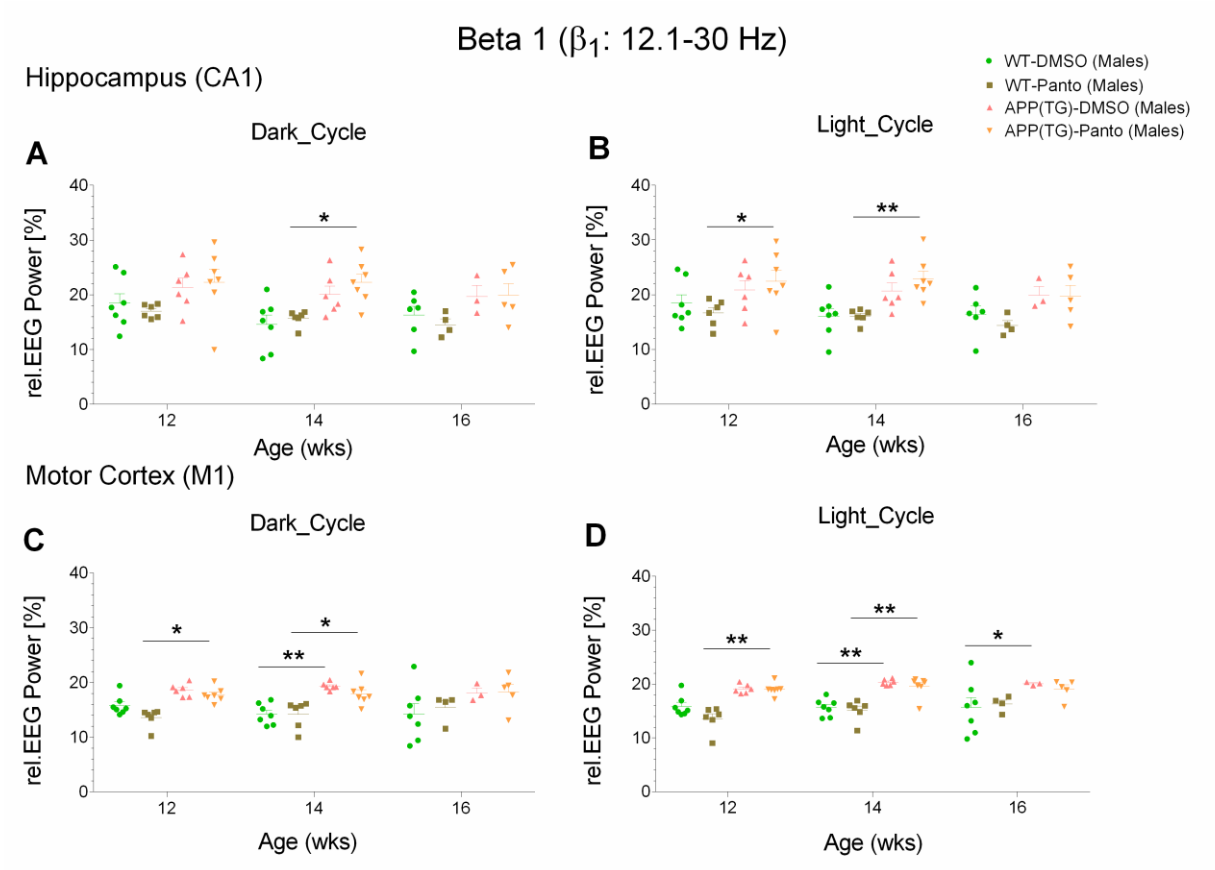

**Figure 4.2.6: Hippocampus (CA1) (A,B) and motor cortex (M1) (C,D) relative beta 1 power (%) ($\beta_1$: 12.1-30 Hz) in WT-DMSO, WT-Panto, APP(TG)-DMSO and APP(TG)-Panto male mice.** Results are depicted considering the circadian rhythmicity (dark/light cycle). $^{*}$ $p < 0.05$; $^{**}$ $p < 0.01$; $^{***}$ $p < 0.001$.

### Beta 2 ($\beta_2$: 16-24 Hz)

### i) Hippocampal CA1 region

Dark cycle

A significant increase in relative beta 2 power was observed in APP(TG)-Panto animals compared to WT-DMSO and WT-Panto mice at 14 weeks of age (WT-DMSO, n = 7: 5.898 ± 0.735% vs. APP(TG)-Panto, n = 7: 9.511 ± 0.744%; p = 0.0027) (WT-Panto, n = 6: 6.334 ± 0.301% vs. APP(TG)-Panto, n = 7: 9.511 ± 0.744%; p = 0.0146). A statistical trend was identified between APP(TG)-Panto and WT-Panto at 12 weeks of age (WT-Panto, n = 6: 6.923 ± 0.258% vs. APP(TG)-Panto, n = 7: 9.512 ± 1.089%; p = 0.0639) and between APP(TG)-DMSO and WT-DMSO at 14 weeks of age (WT-DMSO, n = 7: 5.898 ± 0.735% vs. APP(TG)-DMSO, n = 6: 8.319 ± 0.689%; p = 0.093).

No significant differences in relative beta 2 power were detected between all other analyzed groups (Fig. 4.2.7A).

Light cycle

A significant increase in relative beta 2 power was observed in APP(TG)-Panto compared to WT-Panto mice at 12 weeks of age (WT-Panto, n = 6: 6.788 ± 0.468% vs. APP(TG)-Panto, n = 7: 9.527 ± 0.968%; p = 0.028). Likewise, significant differences were also detected in APP(TG)-Panto group compared to WT-DMSO and WT-Panto groups at 14 weeks of age (WT-DMSO, n = 7: 6.416 ± 0.626% vs. APP(TG)-Panto, n = 7: 9.622 ± 0.695%; p = 0.0048) (WT-Panto, n = 6: 6.414 ± 0.265% vs. APP(TG)-Panto, n = 7: 9.622 ± 0.695%; p = 0.0072).

However, no significant differences in relative beta 2 power were detected between all other study groups (Fig. 4.2.7B).

**ii) Motor cortical M1 region**

Dark cycle

A significant increase in relative beta 2 power was observed in APP(TG)-DMSO and APP(TG)-Panto groups compared to WT-Panto group at 12 weeks of age (WT-Panto, n = 6: 5.401 ± 0.312% vs. APP(TG)-DMSO, n = 6: 7.588 ± 0.245%; p = 0.0124) (WT-Panto, n = 6: 5.401 ± 0.312% vs. APP(TG)-Panto, n = 7: 7.228 ± 0.217%; p = 0.0383). In addition, significant changes were also identified in APP(TG)-DMSO mice compared to WT-DMSO and WT-Panto animals at 14 weeks of age (WT-DMSO, n = 7: 5.721 ± 0.296% vs. APP(TG)-DMSO, n = 6: 7.917 ± 0.130%; p = 0.0085) (WT-Panto, n = 6: 5.677 ± 0.428% vs. APP(TG)-DMSO , n = 6: 7.917 ± 0.130%; p = 0.010). A statistical trend was observed at 14 weeks of age between APP(TG)-Panto compared to WT-DMSO and WT-Panto (WT-DMSO, n = 7: 5.721 ± 0.296% vs. APP(TG)-Panto, n = 7: 7.336 ± 0.354%; p = 0.0652) (WT-Panto, n = 6: 5.677 ± 0.428% vs. APP(TG)-Panto, n = 7: 7.336 ± 0.354%; p = 0.0705).

No significant differences in relative beta 2 power were detected between all other analyzed groups (Fig. 4.2.7C).

Light cycle

A significant increase in relative beta 2 power observed in APP(TG)-DMSO and APP(TG)-Panto groups as compared to WT-Panto group at 12 weeks of age (WT-Panto, n = 7: 5.412 ± 0.396% vs. APP(TG)-DMSO, n = 6: 7.801 ± 0.163%; p = 0.0024) (WT-Panto, n = 6: 5.412± 0.396% vs. APP(TG)-Panto, n = 7: 7.905 ± 0.245%; p = 0.0009). Additionally, a significant rise in beta 2 power were identified in APP(TG)-DMSO group compared to WT-DMSO and WT-Panto groups at 14 weeks of age (WT-DMSO, n = 7: 6.292 ± 0.305% vs. APP(TG)-DMSO, n = 6: 8.314 ± 0.091%; p = 0.0092) (WT-Panto, n = 6: 5.941 ± 0.330% vs. APP(TG)-DMSO, n = 6: 8.314 ± 0.0901%; p = 0.0025). Likewise, significant differences were also detected in APP(TG)-Panto mice compared to WT-DMSO and WT-Panto animals at 14 weeks of age (WT-DMSO, n = 7: 6.291 ± 0.359% vs. APP(TG)-Panto, n = 7: 7.892 ± 0.337%; p = 0.0435) (WT-Panto, n = 6: 5.9401 ± 0.330% vs. APP(TG)-Panto, n = 7: 7.892 ± 0.337%; p = 0.0128).

A statistical trend was observed between APP(TG)-Panto compared to WT-DMSO group at 12 weeks of age (WT-DMSO, n = 7: 6.372 ± 0.318% vs. APP(TG)-Panto, n = 7: 7.905 ± 0.245%; p = 0.0573).

No significant differences in relative beta 2 power were detected between all other study groups (Fig. 4.2.7D).

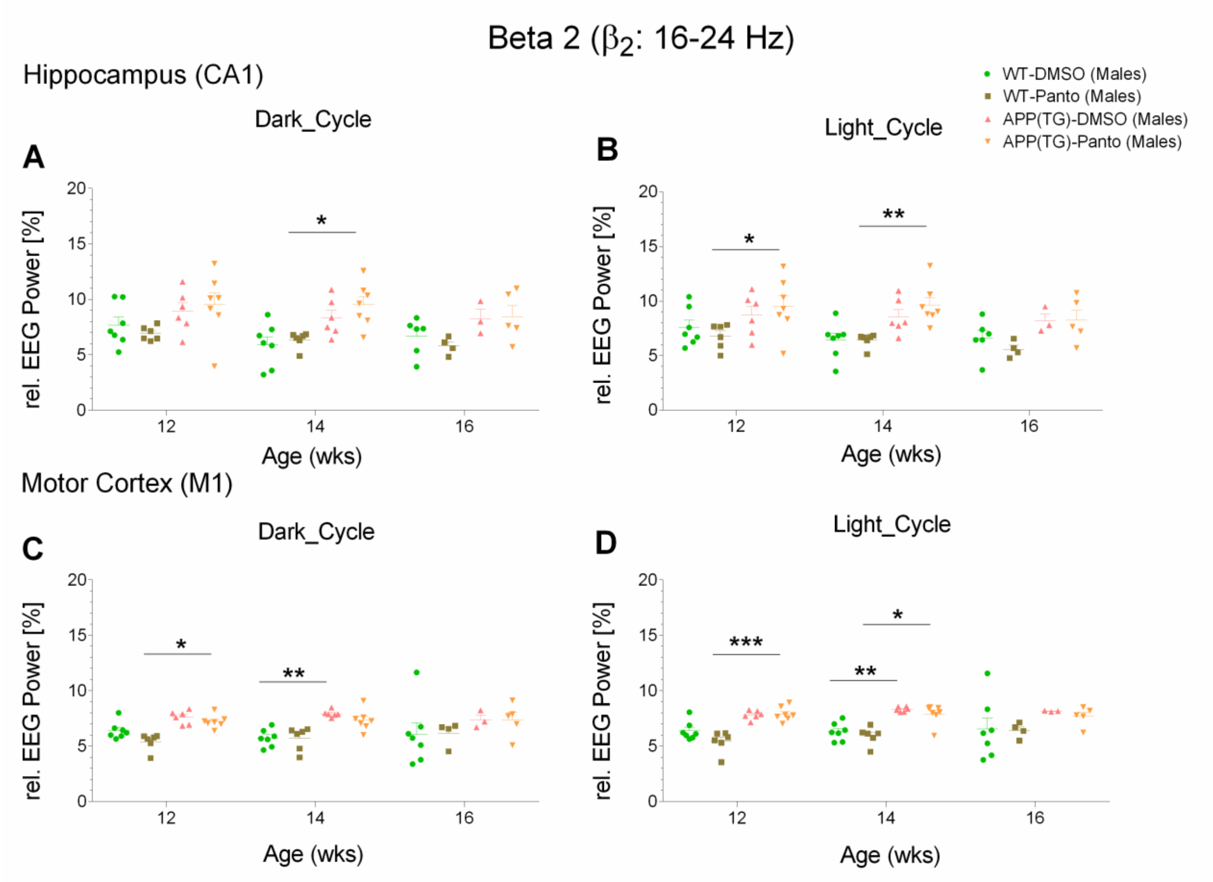

**Figure 4.2.7: Hippocampus (CA1) (A,B) and motor cortex (M1) (C,D) relative beta 2 power (%) ($\beta_2$: 16-24 Hz) in WT-DMSO, WT-Panto, APP(TG)-DMSO and APP(TG)-Panto male mice.** Results are illustrated considering the circadian rhythmicity (dark/light cycle). * $p < 0.05$; ** $p < 0.01$; *** $p < 0.001$.

### Beta 3 ($\beta_3$: 16-30 Hz)

### i) Hippocampal CA1 region

Dark cycle

A significant increase in relative beta 3 power was observed in APP(TG)-Panto compared to WT-Panto mice at 12 weeks of age (WT-Panto, n = 6: 10.397 ± 0.504% vs. APP(TG)-Panto, n = 7: 14.906 ± 1.758%; p = 0.0425). Furthermore, significant differences were also detected in APP(TG)-Panto group compared to WT-DMSO and WT-Panto groups at 14 weeks of age (WT-DMSO, n = 7: 9.102 ± 1.294% vs. APP(TG)-Panto, n = 7: 14.624 ± 1.263%; p = 0.0055) (WT-Panto, n = 6: 9.468 ± 0.553% vs. APP(TG)-Panto, n = 7: 14.624 ± 1.263%; p = 0.0153)
No significant differences in relative beta 3 power were detected between all other analyzed groups (Fig. 4.2.8A).

Light cycle

A significant increase in relative beta 3 power was observed in APP(TG)-Panto compared to WT-Panto mice at 12 weeks of age (WT-Panto, n = 6: 10.179 ± 0.801% vs. APP(TG)-Panto, n = 7: 14.401 ± 1.482%; p = 0.0329). Likewise, significant changes were detected in APP(TG)-Panto group compared WT-DMSO and WT-Panto groups at 14 weeks of age (WT-DMSO, n = 7: 9.775 ± 1.132% vs. APP(TG)-Panto, n = 7: 14.264 ± 1.051%; p = 0.0148) (WT-Panto, n = 6: 9.432 ± 0.498% vs. APP(TG)-Panto, n = 7: 14.264 ± 1.051%; p = 0.011).
However, no significant differences in relative beta 3 power were identified between all other study groups (Fig. 4.2.8B).

### ii) Motor cortical M1 region

Dark cycle

A significant increase in relative beta 3 power was detected in APP(TG)-DMSO and APP(TG)-Panto groups compared to WT-Panto group at 12 weeks of age (WT-Panto, n = 6: 7.902 ± 0.460% vs. APP(TG)-DMSO, n = 6: 11.312 ± 0.313%; p = 0.0062) (WT-Panto, n = 6: 7.902 ± 0.460% vs. APP(TG)-Panto, n = 7: 11.078 ± 0.358%; p = 0.0087). Additionally, significant differences were also observed for the APP(TG)-DMSO group compared to the WT-DMSO and WT-Panto groups at 14 weeks of age (WT-DMSO, n = 7: 8.521 ± 0.430% vs. APP(TG)-DMSO, n = 6: 11.865 ± 0.144%; p = 0.0052) (WT-Panto, n = 6: 8.386 ± 0.655% vs. APP(TG)-DMSO, n = 6: 11.865 ± 0.144%; p = 0.0051). Likewise, significant alterations were also identified for the APP(TG)-Panto mice compared to the WT-DMSO and WT-Panto animals at 14 weeks of age (WT-DMSO, n = 7:

8.521 ± 0.430% vs. APP(TG)-Panto, n = 7: 11.182 ± 0.573%; p = 0.0277) (WT-Panto, n = 6: 8.386 ± 0.655% vs. APP(TG)-Panto, n = 7: 11.182 ± 0.573%; p = 0.0258).

However, no significant differences in relative beta 3 power were detected between all other analyzed study groups (Fig. 4.2.8C).

Light cycle

A significant increase in relative beta 3 power was observed in APP(TG)-DMSO and APP(TG)-Panto compared to WT-Panto mice at 12 weeks of age (WT-Panto, n = 6: 7.930 ± 0.563% vs. APP(TG)-DMSO, n = 6: 11.440 ± 0.227%; p = 0.003) (WT-Panto, n = 6: 7.930 ± 0.563% vs. APP(TG)-Panto, n = 7: 11.492 ± 0.326%; p = 0.0017). In addition, a significant increase was observed in APP(TG)-DMSO group compared to the WT-DMSO and WT-Panto groups at 14 weeks of age (WT-DMSO, n = 7: 9.196 ± 0.526% vs. APP(TG)-DMSO, n = 6: 12.033 ± 0.166%; p = 0.0169) (WT-Panto, n = 6: 8.561 ± 0.471% vs. APP(TG)-DMSO, n = 6: 12.033 ± 0.166%; p = 0.0034). Furthermore, a significant difference was also detected for the APP(TG)-Panto compared to the WT-Panto mice at 14 weeks of age (WT-Panto, n = 6: 8.561 ± 0.471% vs. APP(TG)-Panto, n = 7: 11.447 ± 0.443%; p = 0.0146).

A statistical trend was observed between APP(TG)-Panto group compared to WT-DMSO group at 12 weeks of age (WT-DMSO, n = 7: 9.290 ± 0.480% vs. APP(TG)-Panto, n = 7: 11.492 ± 0.326%; p = 0.0746) and at 14 weeks of age (WT-DMSO, n = 7: 9.196 ± 0.526% vs. APP(TG)-Panto, n = 7: 11.447 ± 0.443%; p = 0.0656).

No significant differences in relative beta 3 power were identified between all other study groups (Fig. 4.2.8D).

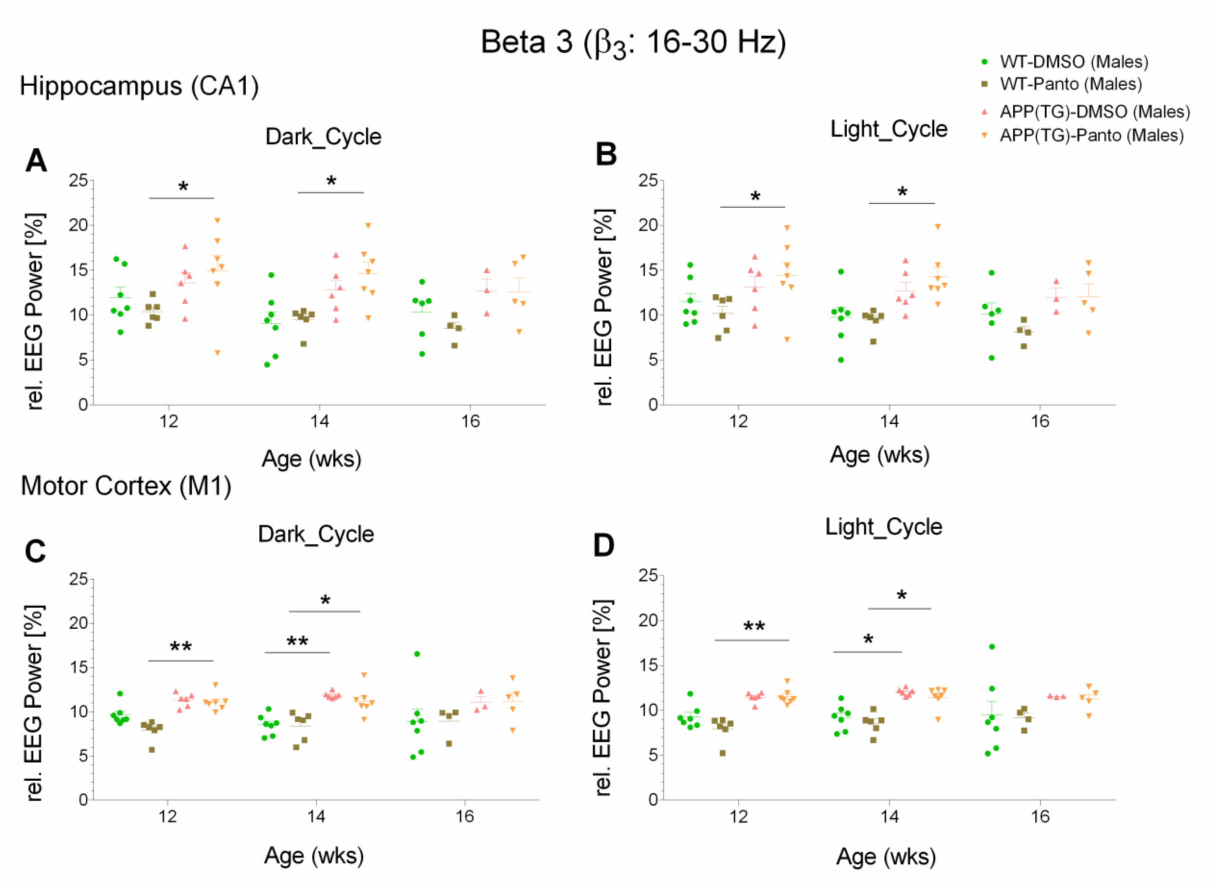

**Figure 4.2.8: Hippocampus (CA1) (A, B) and motor cortex (M1) (C, D) relative beta 3 power (%) ($\beta_3$: 16-30 Hz) in WT-DMSO, WT-Panto, APP(TG)-DMSO and APP(TG)-Panto male mice**. Results are depicted considering the circadian rhythmicity (dark/light cycle). $^{*}$ $p < 0.05$; $^{**}$ $p < 0.01$; $^{***}$ $p < 0.001$.

**Alpha (α: 8-12 Hz)**

**i) Hippocampal CA1 region**

Dark cycle

A statistical trend in relative alpha power was detected between APP(TG)-DMSO compared to WT-DMSO and at 14 weeks of age (WT-DMSO, n = 7: 14.200 ± 1.400% vs. APP(TG)-DMSO, n = 6: 18.884 ± 0.652%; p = 0.0686). Likewise, significant alteration was also identified between APP(TG)-Panto compared to WT-DMSO at 14 weeks of age (WT-DMSO, n = 7: 14.200 ± 1.400% vs. APP(TG)-Panto, n = 7: 18.860 ± 0.920%; p = 0.0556).

No significant differences in relative alpha power were observed between all other analyzed groups (Fig. 4.2.9A).

Light cycle

No significant differences in relative theta power obtained between all analyzed groups (Fig. 4.2.9B).

**ii) Motor cortical M1 region**

Dark cycle

A significant increase in relative alpha power was observed in APP(TG)-DMSO compared to WT-Panto mice at 12 weeks of age (WT-Panto, n = 6: 11.286 ± 0.357% vs. APP(TG)-DMSO, n = 6: 14.045 ± 0.554%; p = 0.0376). However, a statistical trend was identified between APP(TG)-DMSO group compared to WT-DMSO group at 14 weeks of age (WT-DMSO, n = 7: 12.371 ± 0.635% vs. APP(TG)-DMSO, n = 6: 14.720 ± 0.311%; p = 0.0809).

No significant differences in relative alpha power were detected between all study groups (Fig. 4.2.9C).

Light cycle

A significant increase in relative alpha power was observed in APP(TG)-DMSO and APP(TG)-Panto groups compared to WT-Panto group at 12 weeks of age (WT-Panto, n = 6: 11.401 ± 0.510% vs. APP(TG)-DMSO, n = 6: 14.076 ± 0.459%; p = 0.0089) (WT-Panto, n = 6: 11.401 ± 0.510% vs. APP(TG)-Panto, n = 7: 13.520 ± 0.431%; p = 0.043). Furthermore, a significant increase was detected in APP(TG)-DMSO compared to WT-Panto mice at 14 weeks of age (WT-Panto, n = 6: 12.340 ± 0.487% vs. APP(TG)-DMSO, n = 6: 14.631 ± 0.320%; p = 0.0322). A statistical trend was identified between APP(TG)-DMSO compared to WT-DMSO mice at 16 weeks of age (WT-DMSO, n = 7: 12.378 ± 1.014% vs. APP(TG)-DMSO, n = 3: 14.902 ± 0.439%; p = 0.0558).

However, no significant differences in relative alpha power were detected between all analyzed groups (Fig. 4.2.9D).

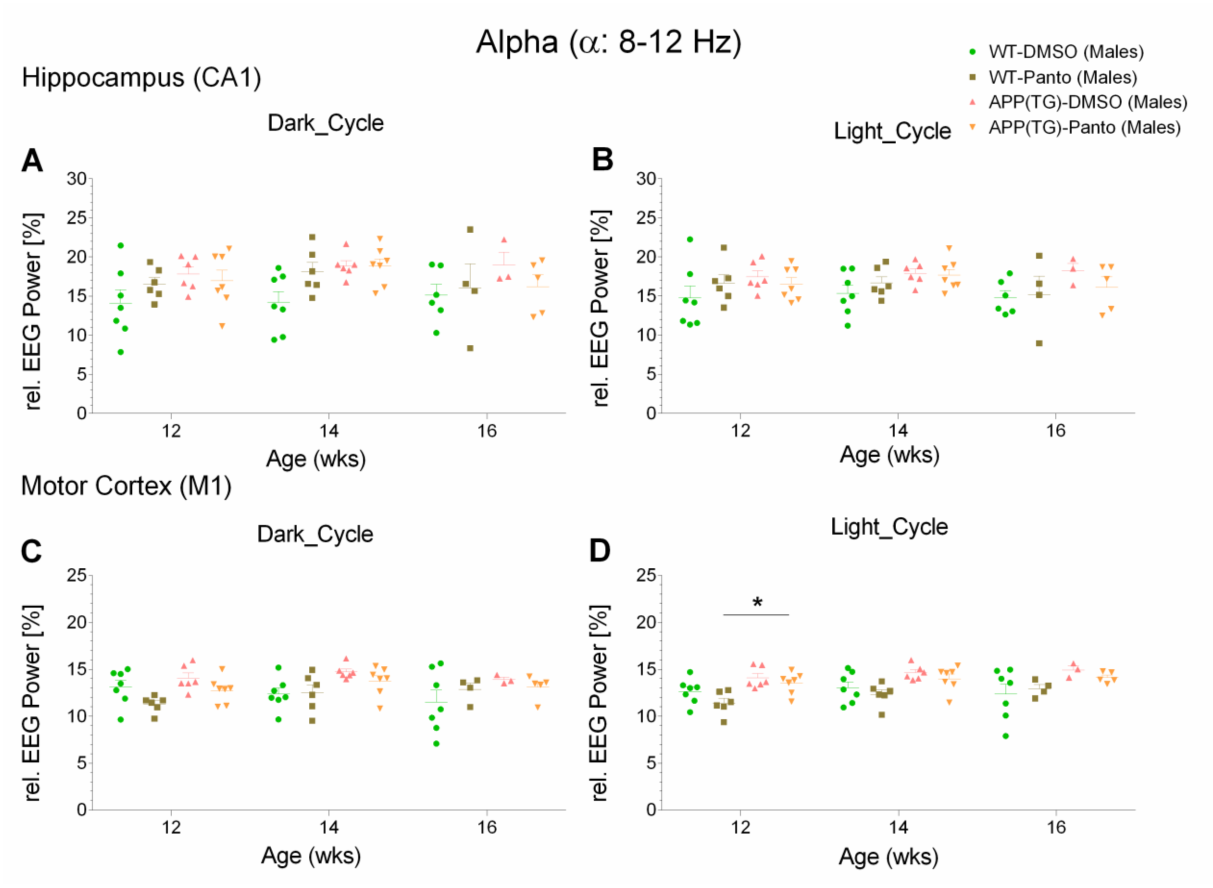

**Figure 4.2.9: Hippocampus (CA1) (A,B) and motor cortex (M1) (C,D) relative alpha power (%) (α: 8-12 Hz) in WT-DMSO, WT-Panto, APP(TG)-DMSO and APP(TG)-Panto male mice.** Results are depicted considering the circadian rhythmicity (dark/light cycle). $^{*}$ $p < 0.05$; $^{**}$ $p < 0.01$; $^{***}$ $p < 0.001$.

### Sigma (σ: 12-16 Hz)

#### i) Hippocampal CA1 region

Dark cycle

A significant increase in relative sigma power found in APP(TG)-Panto compared to WT-DMSO mice at 14 weeks of age (WT-DMSO, n = 7: 5.282 ± 0.453% vs. APP(TG)-Panto, n = 7: 7.426 ± 0.229%; p = 0.0102). A statistical trend in relative sigma power was detected between APP(TG)-DMSO group compared to WT-DMSO group at 14 weeks of age (WT-DMSO, n = 7: 5.2823 ± 0.4529% vs. APP(TG)-DMSO, n = 7: 7.048846 ± 0.5364%; p = 0.0599).

No significant differences in relative sigma power were identified between all other study groups (Fig. 4.2.10A).

Light cycle

A significant increase in relative sigma power was observed in APP(TG)-Panto mice compared to WT-DMSO and WT-Panto animals at 14 weeks of age (WT-DMSO, n = 7: 6.097 ± 0.366% vs. APP(TG)-Panto, n = 7: 8.382 ± 0.385%; p = 0.0055) (WT-Panto, n = 6: 6.420 ± 0.288% vs. APP(TG)-Panto, n = 7: 8.382 ± 0.385%; p = 0.0295).

However, no significant differences in relative sigma power were observed between all other study groups (Fig. 4.2.10B).

### ii) Motor cortical M1 region

Dark cycle

A significant increase in relative sigma power was observed in APP(TG)-DMSO compared to WT-Panto mice at 12 weeks of age (WT-Panto, n = 6: 5.499 ± 0.252% vs. APP(TG)-DMSO, n = 6: 7.038 ± 0.209%; p = 0.0101). Similarly, significant increase was also detected in APP(TG)-DMSO group compared to WT-DMSO and WT-Panto groups at 14 weeks of age (WT-DMSO, n = 7: 5.491 ± 0.361% vs. APP(TG)-DMSO, n = 6: 7.188 ± 0.163%; p = 0.0025) (WT-Panto, n = 6: 5.623 ± 0.391% vs. APP(TG)-DMSO, n = 6: 7.188 ± 0.163%; p = 0.0086).

Moreover, significant changes were also identified in APP(TG)-DMSO and APP(TG)-Panto groups compared to WT-DMSO group at 16 weeks of age (WT-DMSO, n = 6: 5.163 ± 0.533% vs. APP(TG)-DMSO, n = 3: 6.808 ± 0.251%; p = 0.0258) (WT-DMSO, n = 6: 5.163 ± 0.533% vs. APP(TG)-Panto, n = 5: 6.897 ± 0.477%; p = 0.0035).

However, a statistical trend was observed in relative sigma power between APP(TG)-DMSO compared WT-DMSO mice at 12 weeks of age (WT-DMSO, n = 7: 5.936 ± 0.275% vs. APP(TG)-DMSO, n = 6: 7.038 ± 0.209%; p = 0.0852). In addition, a significant difference was found between APP(TG)-Panto group compared to WT-DMSO group at 14 weeks of age (WT-DMSO, n = 7: 5.491 ± 0.361% vs. APP(TG)-Panto, n = 7: 6.525 ± 0.193%; p = 0.0971). However, no significant differences in relative sigma power were observed between all other analyzed groups (Fig. 4.2.10C).

Light cycle

A significant increase in relative sigma power was observed in APP(TG)-DMSO and APP(TG)-Panto groups compared to WT-Panto group at 12 weeks of age (WT-Panto, n = 6: 5.420 ± 0.380% vs. APP(TG)-DMSO, n = 6: 7.392 ± 0.227%; p < 0.0001) (WT-Panto, n = 6: 5.420 ± 0.380% vs. APP(TG)-Panto, n = 7: 7.294 ± 0.170%; p < 0.0001). Additionally, significant differences were observed for the APP(TG)-DMSO compared to the WT-DMSO and WT-Panto mice at 14 weeks of age (WT-DMSO, n = 7: 6.228 ± 0.187% vs. APP(TG)-DMSO, n = 6: 8.019 ± 0.130%; p = 0.0002) (WT-Panto, n = 6: 6.327 ± 0.365% vs. APP(TG)-DMSO, n = 6:8.019 ± 0.130%; p = 0.0007). Likewise, significant alterations were identified for the APP(TG)-Panto group compared to the WT-DMSO and WT-Panto groups at 14 weeks of age (WT-DMSO, n = 7: 6.228 ± 0.187% vs. APP(TG)-Panto, n = 7: 7.884 ± 0.288%; p = 0.0003) (WT-Panto, n = 6: 6.327 ± 0.365% vs. APP(TG)-Panto, n = 7: 7.884 ± 0.288%; p = 0.0012). Furthermore, a significant increase was also observed in APP(TG)-DMSO and APP(TG)-Panto groups compared to WT-DMSO group at 16 weeks of age (WT-DMSO, n = 7: 5.957 ± 0.410% vs. APP(TG)-DMSO, n = 3: 8.220 ± 0.173%; p = 0.0001) (WT-DMSO, n = 7: 5.957 ± 0.410% vs. APP(TG)-Panto, n = 5: 7.503 ± 0.333%; p = 0.0025).

Moreover, a significant increase in relative sigma power was identified at 16 weeks compared to 12 weeks of age for the WT-Panto mice (12 weeks, n = 6: 5.420 ± 0.380% vs. 16 weeks, n = 4: 6.941 ± 0.196%; p = 0.0044).

However, a statistical trend was detected in relative sigma power between WT-DMSO compared to WT-Panto and APP(TG)-DMSO mice at 12 weeks of age (WT-DMSO, n = 7: 6.363 ± 0.282% vs. WT-Panto, n = 6: 5.420 ± 0.380%; p = 0.0915) (WT-DMSO, n = 7: 6.363 ± 0.282% vs. APP(TG)-DMSO, n = 6: 7.392 ± 0.227%; p = 0.0553). Additionally, a statistical trend was also observed between APP(TG)-DMSO compared to WT-Panto mice at 16 weeks of age (WT-Panto, n = 4: 6.941 ± 0.196% vs. APP(TG)-DMSO, n = 3: 8.220 ± 0.173%; p = 0.0972). Furthermore, a statistical trend in relative sigma power was also identified at 14 weeks compared to 12 weeks of age for the WT-Panto mice (12 weeks, n = 6: 5.420 ± 0.380% vs. 14 weeks, n = 6: 6.327 ± 0.365%; p = 0.0779).

No significant differences in relative sigma power were observed between all other study groups (Fig. 4.2.10D).

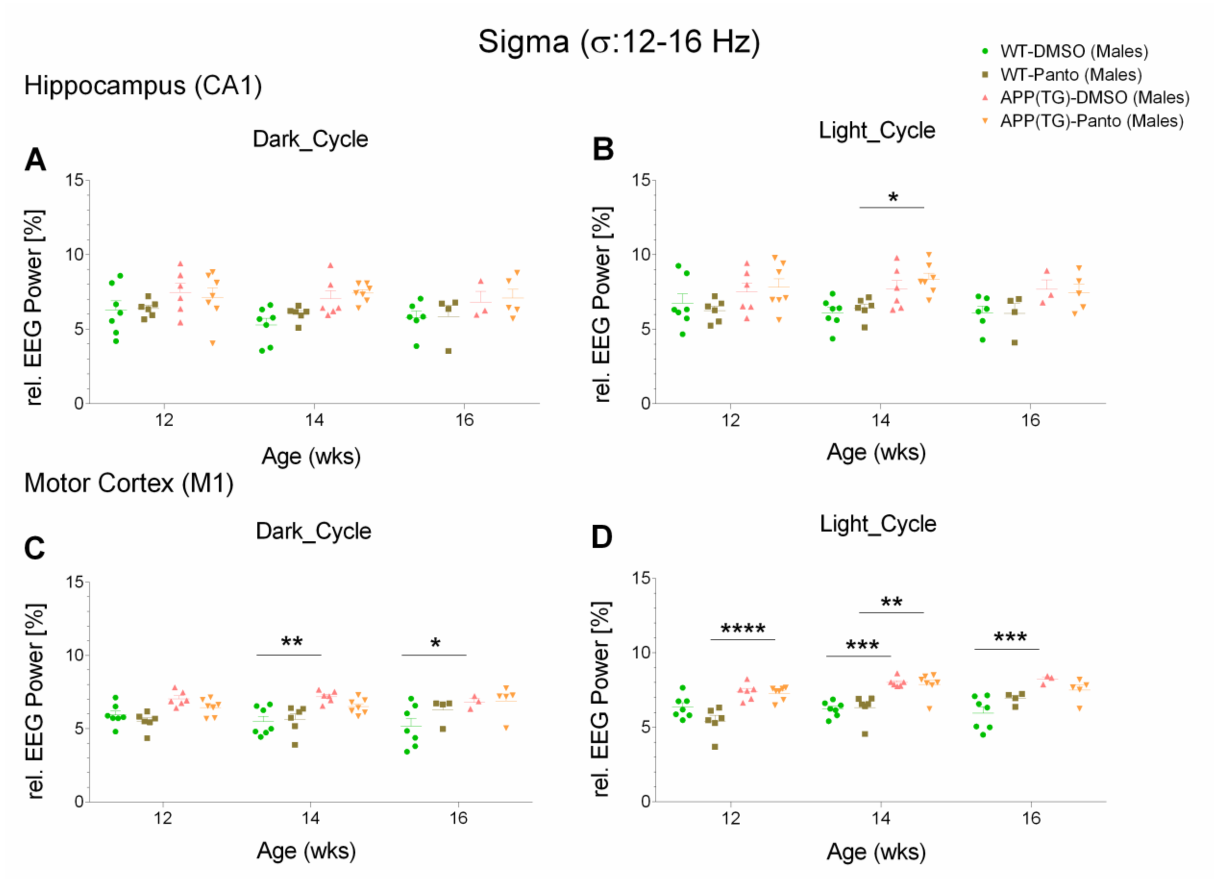

**Figure 4.2.10: Hippocampus (CA1) (A,B) and motor cortex (M1) (C,D) relative sigma power (%) (σ: 12-16 Hz) in WT-DMSO, WT-Panto, APP(TG)-DMSO and APP(TG)-Panto male mice.** Results are depicted considering the circadian rhythmicity (dark/light cycle). $^{*}$ $p < 0.05$; $^{**}$ $p < 0.01$; $^{***}$ $p < 0.001$.

### Gamma low ($\gamma_{low}$: 30-50 Hz)

### i) Hippocampal CA1 region

Dark cycle

A significant increase in relative gamma low power was observed in APP(TG)-Panto as compared to WT-Panto mice at 12 weeks of age (WT-Panto, n = 6: 7.063 ± 0.820% vs. APP(TG)-Panto, n = 7: 11.782 ± 1.779%; p = 0.0361). However, a statistical trend was detected in relative gamma low power between 12 weeks compared to 16 weeks of age for the APP(TG)-Panto mice (12 weeks, n = 7: 11.782 ± 1.779 % vs. 16 weeks, n = 5: 7.556 ± 1.122%; p = 0.0553).

However, no significant differences in relative gamma low power were detected between all other study groups (Fig. 4.2.11A).

Light cycle

A statistical trend in relative gamma low power was identified between 12 weeks compared to 16 weeks of age for the APP(TG)-Panto mice (12 weeks, n = 7: 9.435 ± 1.205% vs. 16 weeks, n = 5: 6.414 ± 0.988%; p = 0.097).

No significant differences in relative gamma low power were detected between all other analyzed groups (Fig. 4.2.11B).

**ii) Motor cortical M1 region**

Dark cycle

A significant increase in relative gamma low power was identified in WT-DMSO, APP(TG)-DMSO and APP(TG)-Panto groups compared to WT-Panto group at 12 weeks of age (WT-DMSO, n = 7: 7.691 ± 0.529% vs. WT-Panto, n = 6: 5.202 ± 0.446%; p = 0.0475) (WT-Panto, n = 6: 5.202 ± 0.446% vs. APP(TG)-DMSO, n = 6: 8.667 ± 0.336%; p = 0.0038) (WT-Panto, n = 6: 5.202 ± 0.446% vs. APP(TG)-Panto, n = 7: 9.075 ± 0.499%; p = 0.0006). Likewise, a significant increase was also detected in APP(TG)-Panto mice compared to the WT-DMSO and WT-Panto animals at 14 weeks of age (WT-DMSO, n = 7: 6.129 ± 0.630% vs. APP(TG)-Panto, n = 7: 8.700 ± 0.634%; p = 0.0287) (WT-Panto, n = 6: 5.885 ± 0.581% vs. APP(TG)-Panto, n = 7: 8.700 ± 0.634%; p = 0.0193). In addition, a significant difference was also observed for the APP(TG)-DMSO compared to the WT-Panto mice at 14 weeks of age (WT-Panto, n = 6: 5.885 ± 0.581% vs. APP(TG)-DMSO, n = 6: 8.544 ± 0.248%; p = 0.0391).

A statistical trend in relative gamma low power was observed at 14 weeks of age between APP(TG)-DMSO compared to WT-DMSO mice (WT-DMSO, n = 7: 6.129 ± 0.630% vs. APP(TG)-DMSO, n = 6: 8.544 ± 0.248%; p = 0.0575).

However, no significant differences in relative gamma low power were observed between all other study groups (Fig. 4.2.11C).

Light cycle

A significant increase in relative gamma low power was observed in APP(TG)-DMSO and APP(TG)-Panto compared to WT-Panto mice at 12 weeks of age (WT-Panto, n = 6: 5.269 ± 0.337% vs. APP(TG)-DMSO, n = 6: 7.9344 ± 0.390%; p = 0.0078) (WT-Panto, n = 6: 5.269 ± 0.337% vs. APP(TG)-Panto, n = 7: 7.751 ± 0.336%; p = 0.0107). Additionally, a significant increase was also detected in APP(TG)-DMSO group compared to WT-Panto group at 14 weeks of age (WT-Panto, n = 6: 4.924 ± 0.390% vs. APP(TG)-DMSO, n = 6: 7.3630 ± 0.324%; p = 0.0173). A statistical trend in relative gamma low power was identified at 12 weeks of age between

WT-DMSO compared to APP(TG)-DMSO and APP(TG)-Panto mice (WT-DMSO, n = 7: 5.969 ± 0.474% vs. APP(TG)-DMSO, n = 6: 7.934 ± 0.390%; p = 0.0618) (WT-DMSO, n = 7: 5.969 ± 0.474% vs. APP(TG)-Panto, n = 7: 7.751 ± 0.336%; p = 0.086). Furthermore, a statistical trend was also detected at 14 weeks of age between APP(TG)-Panto compared to WT-Panto mice (WT-Panto, n = 6: 4.924 ± 0.390% vs. APP(TG)-Panto, n = 7: 6.923 ± 0.335%; p = 0.056).

However, no significant differences in relative gamma low power were observed between all other analyzed groups (Fig. 4.2.11D).

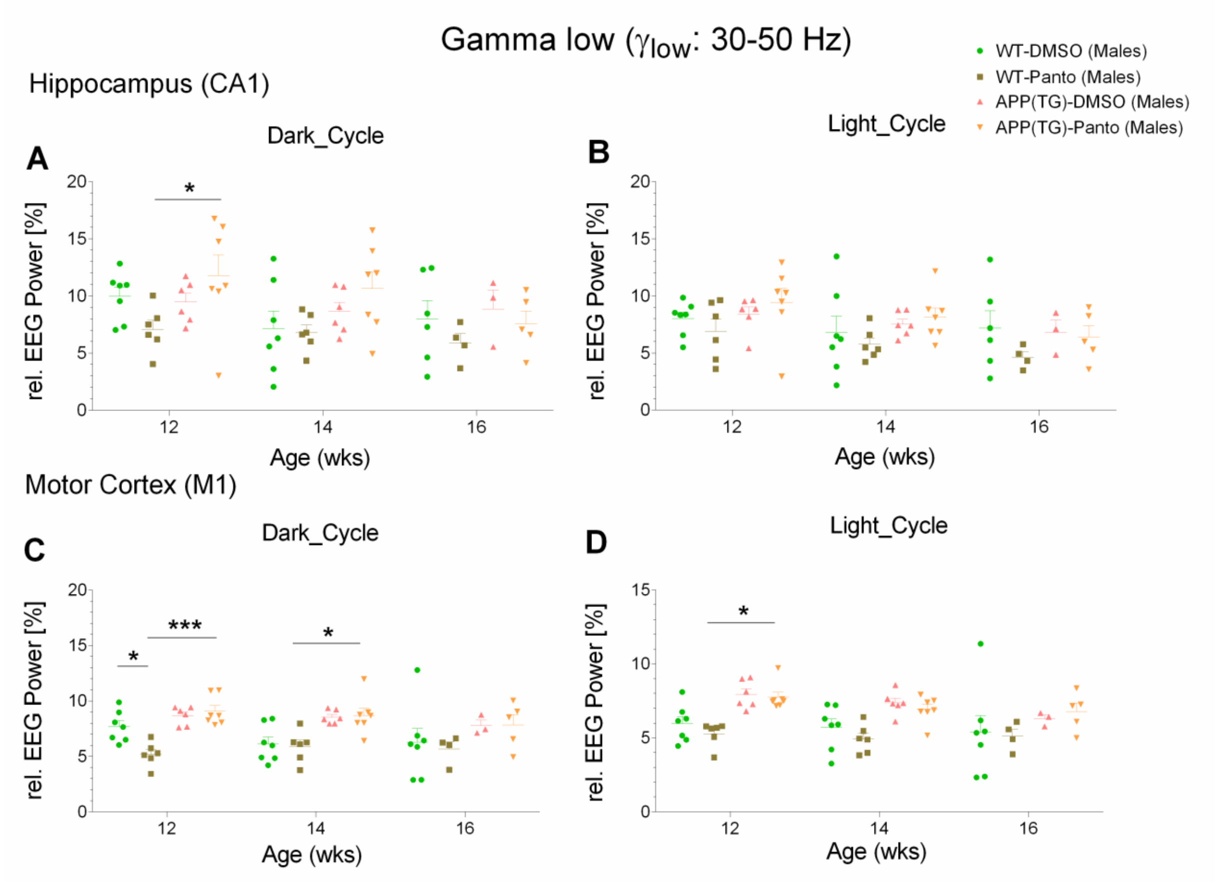

**Figure 4.2.11: Hippocampus (CA1) (A,B) and motor cortex (M1) (C,D) relative gamma low power (%) ($\gamma_{low}$: 30-50 Hz) in WT-DMSO, WT-Panto, APP(TG)-DMSO and APP(TG)-Panto male mice.** Results are illustrated considering the circadian rhythmicity (dark/light cycle). $^{*}$ $p < 0.05$; $^{**}$ $p < 0.01$; $^{***}$ $p < 0.001$.

### Gamma mid ($\gamma_{mid}$: 50-70 Hz)

### i) Hippocampal CA1 region

Dark cycle

A significant rise in relative gamma mid power was observed in WT-DMSO compared to WT-Panto at 12 weeks of age (WT-DMSO, n = 7: 4.936 ± 0.454% vs. WT-Panto, n = 6: 2.853 ± 0.357%; p = 0.0285). Likewise, a significant increase was also detected at 12 weeks compared to 16 weeks of age for the APP(TG)-Panto mice (12 weeks, n = 7: 4.257 ± 0.635% vs. 16 weeks, n = 5: 2.342 ± 0.260%; p = 0.0392).

However, a statistical trend in relative gamma mid power was observed at 12 weeks compared to 14 weeks of age for the WT-DMSO mice (12 weeks, n = 7: 4.936 ± 0.454% vs. 14 weeks, n = 7: 3.319 ± 0.724%; p = 0.0611).

No significant differences in relative gamma mid power were detected between all other study groups (Fig. 4.2.12A).

Light cycle

No significant differences in relative gamma mid power were observed in all analyzed groups (Fig. 4.2.12B).

### ii) Motor cortical M1 region

Dark cycle

A significant increase in relative gamma mid power was observed in WT-DMSO, APP(TG)-DMSO and APP(TG)-Panto groups compared to WT-Panto group at 12 weeks of age (WT-DMSO, n = 7: 4.045 ± 0.140% vs. WT-Panto, n = 6: 2.676 ± 0.278%; p = 0.0279) (WT-Panto, n = 6: 2.676 ± 0.278% vs. APP(TG)-DMSO, n = 6: 4.568 ± 0.296%; p = 0.0017) (WT-Panto, n = 6: 2.676 ± 0.278% vs. APP(TG)-Panto, n = 7: 4.281 ± 0.376%; p = 0.0071). Additionally, a significant increase was detected in APP(TG)-DMSO compared to WT-DMSO and WT-Panto mice at 14 weeks of age (WT-DMSO, n = 7: 3.201 ± 0.320% vs. APP(TG)-DMSO, n = 6: 4.544 ± 0.215%; p = 0.0321) (WT-Panto, n = 6: 3.172 ± 0.409% vs. APP(TG)-DMSO, n = 6: 4.544 ± 0.215%; p = 0.0359).

A statistical trend in relative gamma mid power was identified between 12 weeks compared to 16 weeks of age for the WT-DMSO mice (12 weeks, n = 7: 4.045 ± 0.140% vs. 16 weeks, n = 7: 2.983 ± 0.575%; p = 0.0604) and APP(TG)-Panto (12 weeks, n = 7: 4.281 ± 0.376% vs. 16 weeks, n = 5: 3.195 ± 0.337%; p = 0.0851).

However, no significant differences in relative gamma mid power were detected between all other study groups (Fig. 4.2.12C).

Light cycle

A statistical trend in relative gamma mid power was observed between APP(TG)-DMSO compared to WT-Panto mice at 12 weeks of age (WT-Panto, n = 6: 2.767 ± 0.300% vs. APP(TG)-DMSO, n = 6: 3.923 ± 0.138%; p = 0.0549).

However, no significant differences in relative gamma mid power were identified between all other study groups (Fig. 4.2.12D).

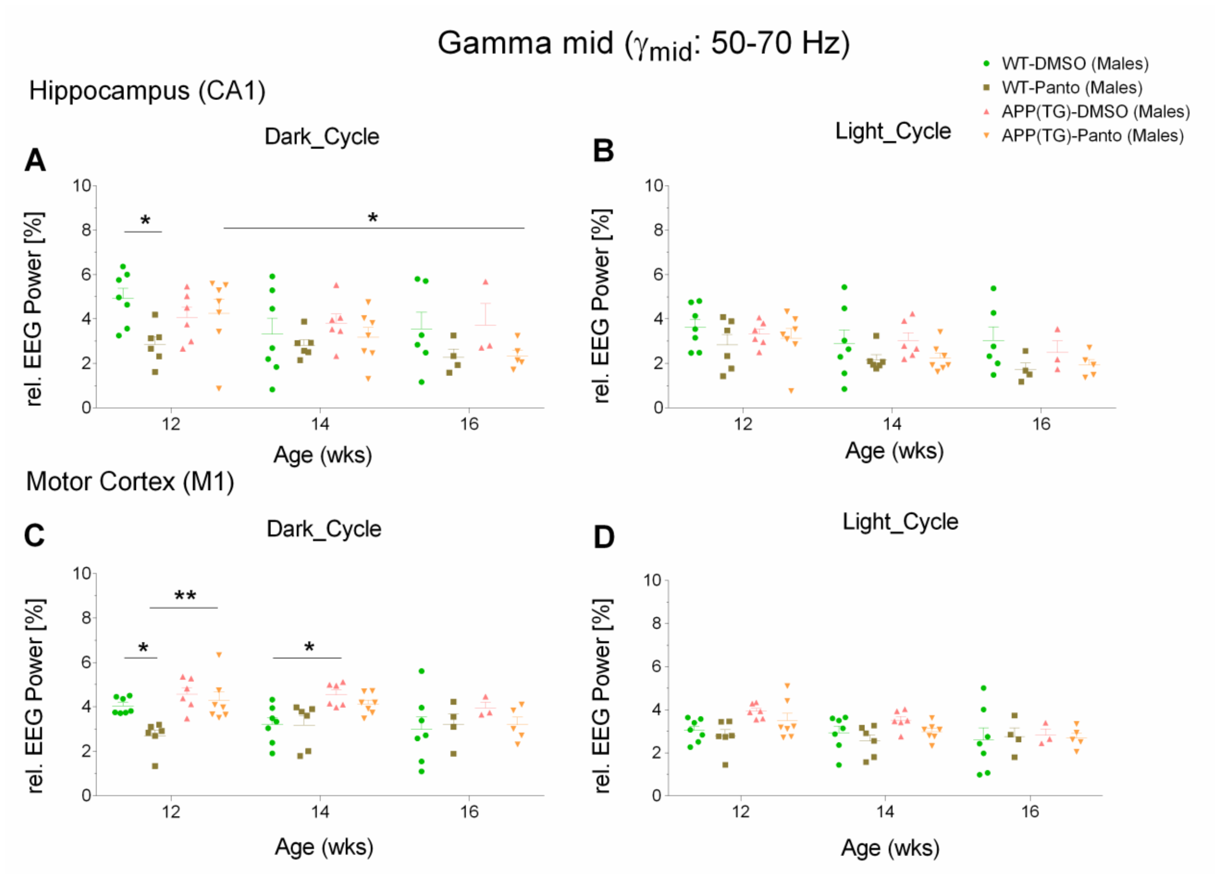

**Figure 4.2.12: Hippocampus (CA1) (A,B) and motor cortex (M1) (C,D) relative gamma mid power (%) ($\gamma_{mid}$: 50-70 Hz) in WT-DMSO, WT-Panto, APP(TG)-DMSO and APP(TG)-Panto male mice.** Results are depicted considering the circadian rhythmicity (dark/light cycle). $^{*}$ $p < 0.05$; $^{**}$ $p < 0.01$; $^{***}$ $p < 0.001$.

#### 4.2.2.2. Female mice groups

##### Theta 1 ($\theta_1$: 4-8 Hz)

No significant differences in relative theta 1 power were observed between all study groups analyzed from hippocampal CA1 and motor cortical M1 regions at both dark and light cycles (Fig. 4.2.13).

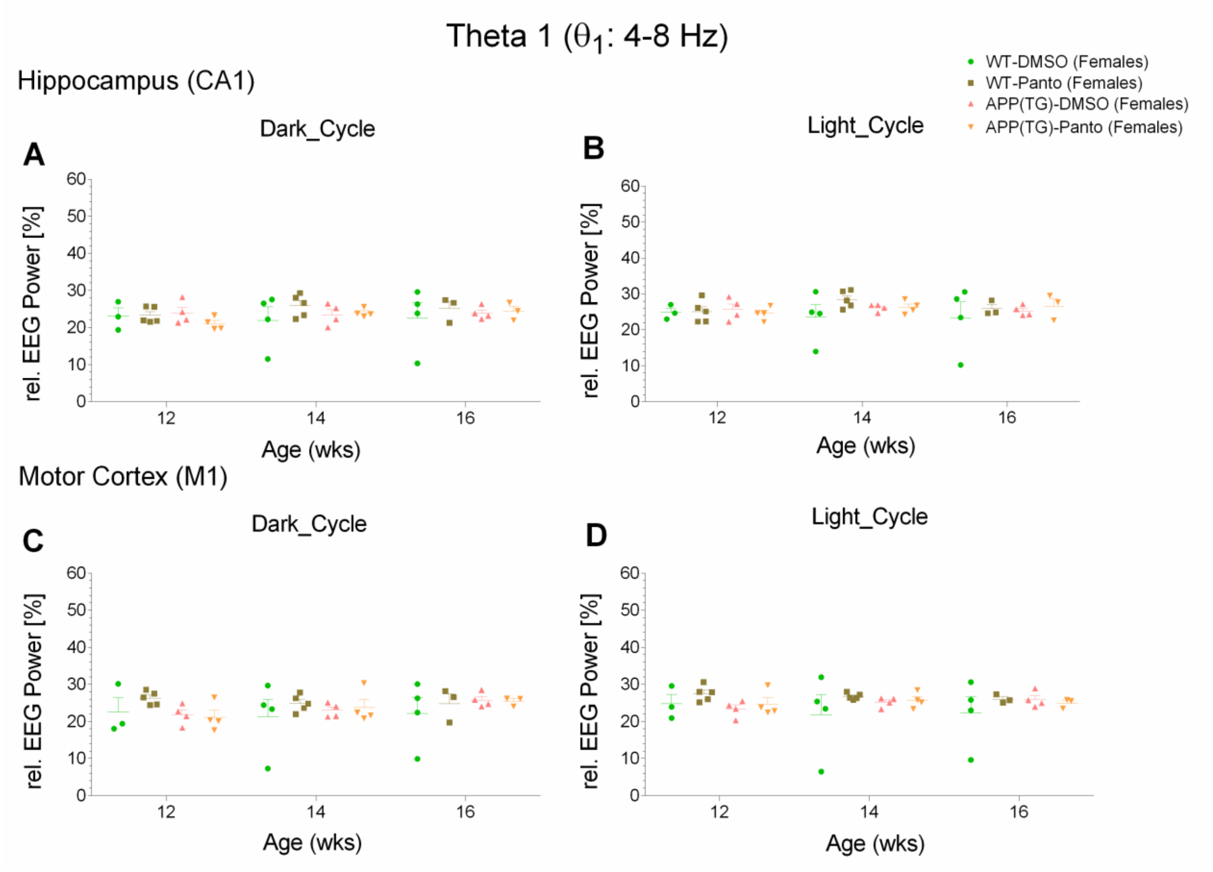

**Figure 4.2.13: Hippocampus (CA1) (A,B) and motor cortex (M1) (C,D) relative theta 1 power (%) ($\theta_1$: 4-8 Hz) in WT-DMSO, WT-Panto, APP(TG)-DMSO and APP(TG)-Panto female mice.** Results are depicted considering the circadian rhythmicity (dark/light cycle). $^{*}$ $p < 0.05$; $^{**}$ $p < 0.01$; $^{***}$ $p < 0.001$.

##### Theta 2 ($\theta_2$: 4.1-12 Hz)

No significant differences in relative theta 2 power were observed between all study groups analyzed from hippocampal CA1 and motor cortical M1 regions during both dark and light cycles (Fig. 4.2.14).

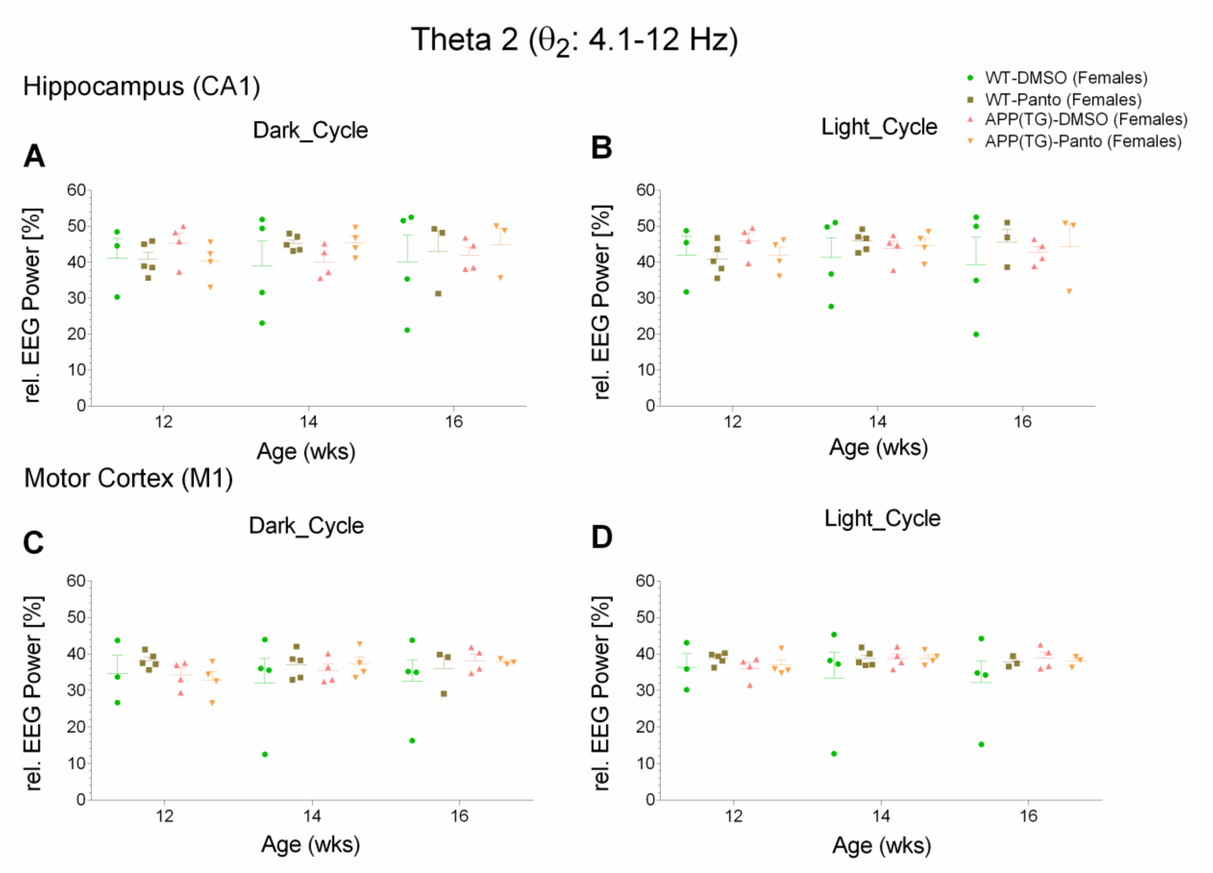

**Figure 4.2.14: Hippocampal (A,B) and motor cortex (C,D) relative theta 2 power (%) ($\theta_2$: 4.1-12 Hz) in WT-DMSO, WT-Panto, APP(TG)-DMSO and APP(TG)-Panto female mice.** Results are illustrated considering the circadian rhythmicity (dark/light cycle). $^{*}$ $p < 0.05$; $^{**}$ $p < 0.01$; $^{***}$ $p < 0.001$.

### Delta (δ: 0.5-4 Hz)

#### i) Hippocampal CA1 region

No significant differences in relative delta power were detected between all study groups analyzed from hippocampal CA1 region during both dark and light cycles (Fig. 4.2.15A,B).

#### ii) Motor cortical M1 region

Dark cycle

No significant differences in relative delta power were observed between all study groups (Fig. 4.2.15C).

Light cycle

A significant increase in relative delta power were identified in WT-DMSO as compared to

APP(TG)-Panto mice at 16 weeks of age (WT-DMSO, n = 4: 41.709 ± 6.816% vs. APP(TG)-Panto, n = 3: 27.238 ± 2.185%; p = 0.0167).

A statistical trend in relative delta power was detected between WT-DMSO and APP(TG)-DMSO mice at 16 weeks of age (WT-DMSO, n = 4: 41.709 ± 6.816% vs. APP(TG)-DMSO, n = 4: 30.647 ± 2.005%; p = 0.062).

However, no significant differences in relative delta power were identified between all other study groups (Fig. 4.2.15D).

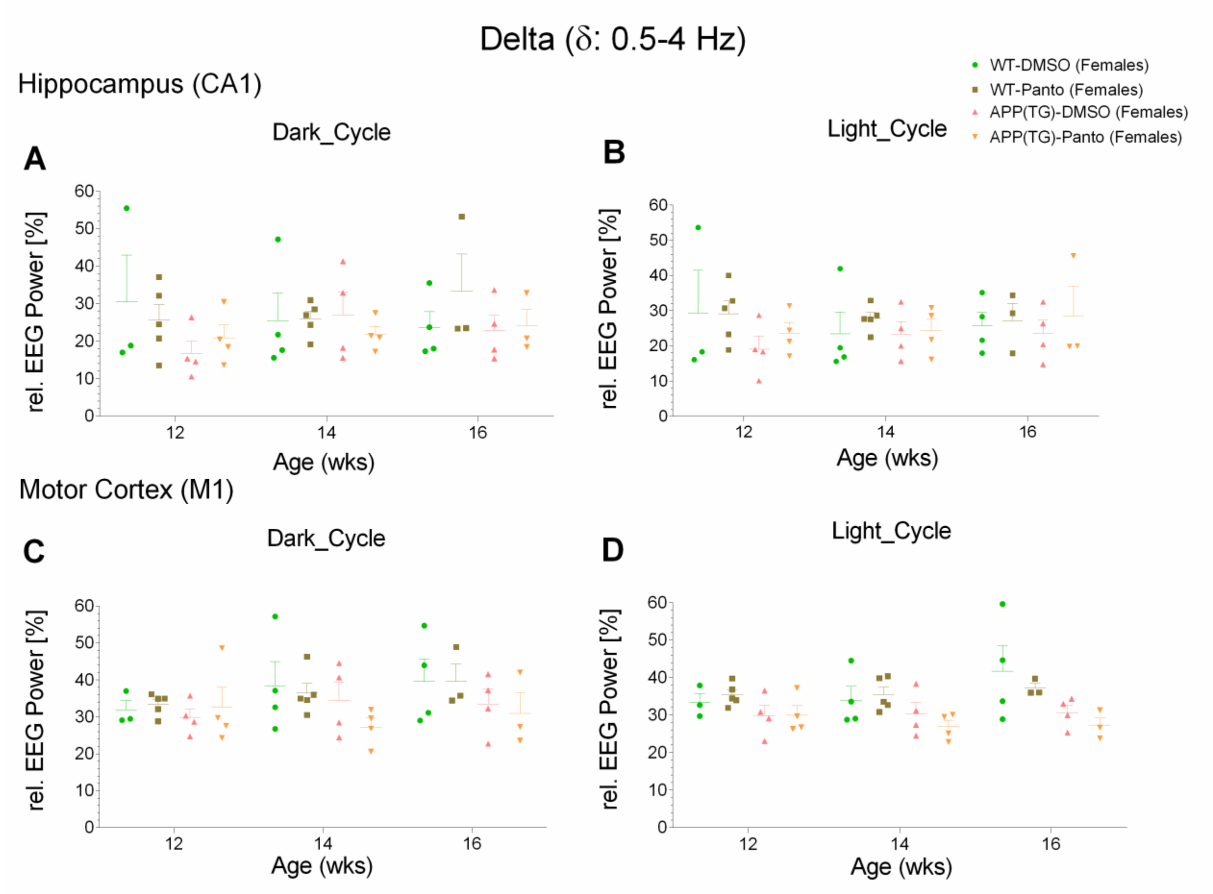

**Figure 4.2.15: Hippocampus (CA1) (A,B) and motor cortex (M1) (C,D) relative delta power (%) (δ: 0.5-4 Hz) in WT-DMSO, WT-Panto, APP(TG)-DMSO and APP(TG)-Panto female mice.** Results are depicted considering the circadian rhythmicity (dark/light cycle). $^{*}$ $p < 0.05$; $^{**}$ $p < 0.01$; $^{***}$ $p < 0.001$.

**Beta 1 (β$_1$: 12.1-30 Hz)**

**i) Hippocampal CA1 region**

Dark cycle

A statistical trend in relative beta power was observed between APP(TG)-DMSO and WT-DMSO mice at 12 weeks of age (WT-DMSO, n = 3: 14.687 ± 3.996% vs. APP (TG)-DMSO, n = 4: 21.526 ± 1.1582%; p = 0.0558). Likewise, a statistical trend was observed between APP(TG)-DMSO and WT-Panto mice at 16 weeks of age (WT-Panto, n = 3: 14.319 ± 2.670% vs. APP(TG)-DMSO, n = 4: 20.924 ± 1.744%; p = 0.0683).

No significant differences in relative beta 1 power were detected between all other study groups (Fig. 4.2.16A)

Light cycle

A statistical trend in relative beta 1 power was observed between APP(TG)-DMSO and WT-Panto mice at 14 weeks of age (WT-Panto, n = 5: 15.376 ± 0.992% vs. APP(TG)-DMSO, n = 4: 21.398 ± 1.168%; p = 0.059)

No significant differences in relative beta 1 power were identified between all other study groups (Fig. 4.2.16B).

**ii) Motor cortical M1 region**

Dark cycle

A statistical trend in relative beta 1 power was observed between APP(TG)-Panto and WT-Panto mice at 14 weeks of age (WT-Panto, n = 5: 13.501 ± 0.573% vs. APP(TG)-Panto, n = 4: 18.261 ± 1.089%; p = 0.0501).

No significant differences in relative beta 1 power were detected between all other study groups (Fig. 4.2.16C).

Light cycle

A significant increase in relative beta 1 power was observed in APP(TG)-DMSO and APP(TG)-Panto compared to WT-Panto mice at 12 weeks of age (WT-Panto, n = 5: 14.260 ± 0.730% vs. APP(TG)-DMSO, n = 4: 18.621 ± 0.992%; p = 0.0100) (WT-Panto, n = 5: 14.260 ± 0.730% vs. APP(TG)-Panto, n = 4: 18.745 ± 0.956%; p = 0.007). In addition, a significant increase was also detected in APP(TG)-Panto compared to WT-DMSO and WT-Panto mice at 14 weeks of age (WT-DMSO, n = 4: 15.551 ± 1.176% vs. APP(TG)-Panto, n = 4: 20.345 ± 0.865%; p = 0.0068) (WT-Panto, n = 5: 14.999 ± 0.481% vs. APP(TG)-Panto, n = 4: 20.345 ± 0.865%; p = 0.0012). Likewise, a significant difference was also identified in APP(TG)-DMSO compared to WT-Panto mice at 14 weeks of age (WT-Panto, n = 5: 14.999 ± 0.481% vs. APP(TG)-DMSO, n = 4: 18.919 ± 1.147%; p = 0.0235).

Furthermore, an increase in relative beta 1 power was observed in APP(TG)-DMSO compared to WT-Panto and WT-DMSO mice at 16 weeks of age (WT-DMSO, n = 4: 13.965 ± 1.769% vs. APP(TG)-DMSO, n = 4: 19.265 ± 0.863%; p = 0.0025) (WT-Panto, n = 3: 14.9964 ± 0.1032% vs. APP(TG)-DMSO, n = 4: 19.2650 ± 0.8631%; p = 0.0324). In addition, significant alterations were detected in APP(TG)-Panto compared to WT-Panto and WT-DMSO mice at 16 weeks of age (WT-DMSO, n = 4: 13.965 ± 1.769% vs. APP(TG)-Panto, n = 3: 20.819 ± 0.656%; p = 0.0003) (WT-Panto, n = 3: 14.996 ± 0.103% vs. APP(TG)-Panto, n = 3: 20.819 ± 0.656%; p = 0.0042).

However, a statistical trend in relative beta 1 power was identified between APP(TG)-DMSO and WT-DMSO at 14 weeks of age (WT-DMSO, n = 4: 15.551 ± 1.176% vs. APP(TG)-DMSO, n = 4: 18.919 ± 1.147%; p = 0.0849).

No significant differences in relative beta 1 power were detected between all other study groups (Fig. 4.2.16D).

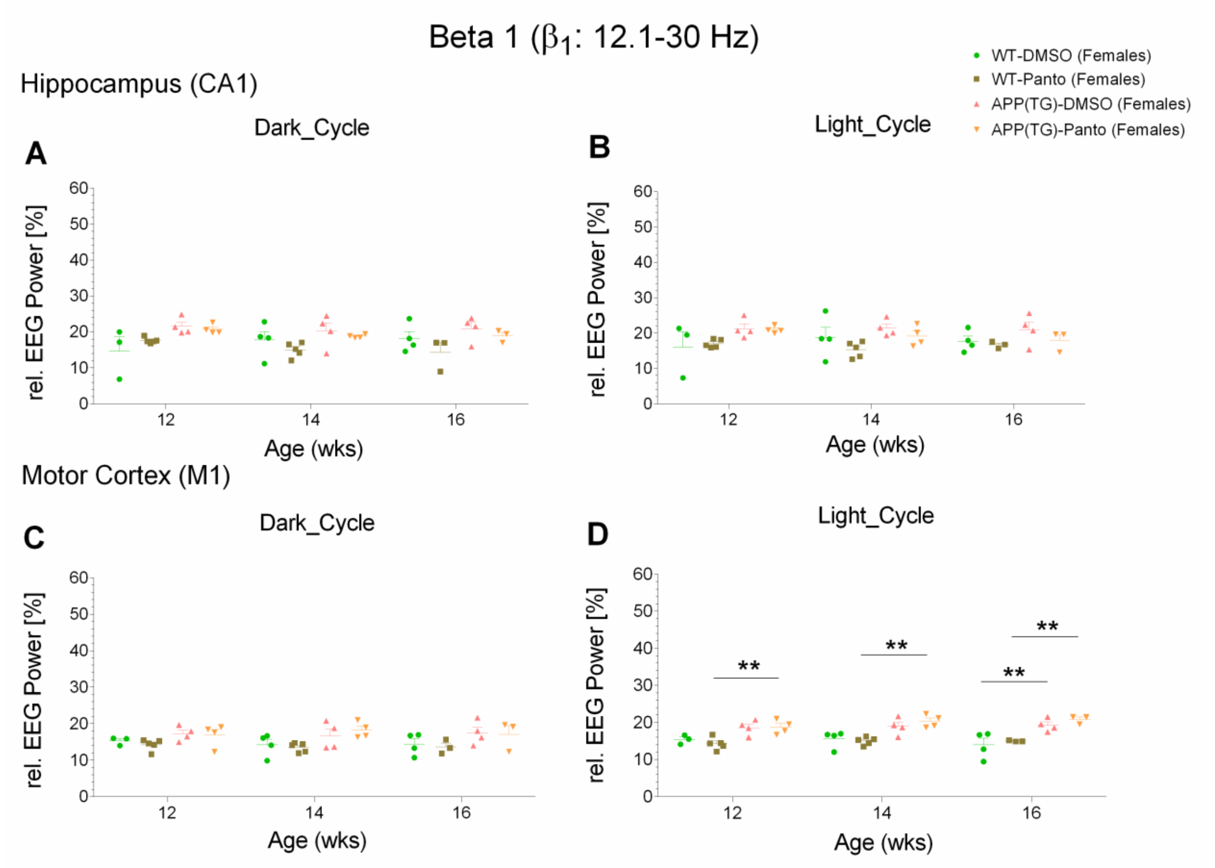

**Figure 4.2.16: Hippocampus (CA1) (A,B) and motor cortex (M1) (C,D) relative beta 1 power (%) ($\beta_1$: 12.1-30 Hz) in WT-DMSO, WT-Panto, APP(TG)-DMSO and APP(TG)-Panto female mice.** Results are depicted considering the circadian rhythmicity (dark/light cycle). $^{*}$ $p < 0.05$; $^{**}$ $p < 0.01$; $^{***}$ $p < 0.001$.

**Beta 2 ($\beta_2$: 16-24 Hz)**

**i) Hippocampal CA1 region**

<u>Dark cycle</u>

A significant increase in relative beta 2 power was observed in APP(TG)-DMSO compared to WT-DMSO mice at 12 weeks of age (WT-DMSO, n = 3: 5.880 ± 1.632% vs. APP(TG)-DMSO, n = 4: 9.156 ± 0.468%; p = 0.0269). Additionally, a significant increase was observed in APP(TG)-DMSO group compared to WT-Panto group at 14 weeks of age (WT-Panto, n = 5: 5.976 ± 0.376% vs. APP(TG)-DMSO, n = 4: 8.627 ± 1.025%; p = 0.0467). Moreover, a significant difference was detected in APP(TG)-DMSO compared to WT-Panto at 16 weeks of age (WT-Panto, n = 3: 5.653 ± 1.058% vs. APP(TG)-DMSO, n = 4: 8.804 ± 0.782%; p = 0.0354). However, a statistical trend was observed between APP(TG)-Panto and WT-DMSO at 12 weeks of age (WT-DMSO, n = 3: 5.880 ± 1.632% vs. APP(TG)-Panto, n = 4: 8.726 ± 0.297%; p = 0.0664).

No significant differences in relative beta 2 power were detected between all other study groups (Fig. 4.2.17A).

Light cycle

A significant increase in relative beta 2 power was observed in APP(TG)-DMSO compared to WT-Panto at 14 weeks of age (WT-Panto, n = 5: 6.082 ± 0.460% vs. APP(TG)-DMSO, n = 4: 8.884± 0.531%; p = 0.0444).

No significant differences in relative beta 2 power were identified between all other study groups (Fig. 4.2.17B).

**ii) Motor cortical M1 region**

Dark cycle

A significant increase in relative beta power was observed in APP(TG)-Panto compared to WT-Panto mice at 14 weeks of age (WT-Panto, n = 5: 5.362 ± 0.218% vs. APP(TG)-Panto, n = 4: 7.624 ± 0.429%; p = 0.0128).

No significant differences in relative beta 2 power were detected between all other study groups (Fig. 4.2.17C).

Light cycle

A significant increase in relative beta power was detected in APP(TG)-DMSO compared to WT-DMSO and WT-Panto mice at 12 weeks of age (WT-DMSO, n = 3: 6.214 ± 0.276% vs. APP(TG)-DMSO, n = 4: 7.774 ± 0.382%; p = 0.0425) (WT-Panto, n = 5: 5.649 ± 0.238% vs. APP(TG)-DMSO, n = 4: 7.774 ± 0.382%; p = 0.0007). Similarly, a significant increase was observed in APP(TG)-Panto compared to WT-Panto mice at 12 weeks of age (WT-Panto, n = 5: 5.649 ± 0.238% vs. APP(TG)-Panto, n = 4: 7.650 ± 0.485%; p = 0.0015).

Furthermore, an increase in relative beta 2 power was identified in APP(TG)-Panto compared to WT-DMSO mice at 14 weeks of age (WT-DMSO, n = 4: 6.851 ± 0.219% vs. APP(TG)-Panto, n = 4: 8.389 ± 0.376%; p = 0.0277). Additionally, a significant increase was also detected in APP(TG)-Panto and APP(TG)-DMSO groups compared to WT-Panto groups at 14 weeks of age (WT-Panto, n = 5: 5.859 ± 0.193% vs. APP(TG)-DMSO, n = 4: 7.789 ± 0.516%; p = 0.0023) (WT-Panto, n = 5: 5.859 ± 0.193% vs. APP(TG)-Panto, n = 4: 8.389 ± 0.376%; p < 0.0001).

Moreover, significant alterations were observed for the APP(TG)-DMSO group compared to the WT-DMSO and WT-Panto groups at 16 weeks of age (WT-DMSO, n = 4: 5.754 ± 0.621% vs. APP(TG)-DMSO, n = 4:7.865 ± 0.382%; p = 0.0015) (WT-Panto, n = 3: 5.880 ± 0.032% vs.

APP(TG)-DMSO, n = 4: 7.865 ± 0.382%; p = 0.0064). Likewise, significant changes were also detected for the APP(TG)-Panto group compared to the WT-DMSO and WT-Panto groups at 16 weeks of age (WT-DMSO, n = 4:5.754 ± 0.621% vs. APP(TG)-Panto, n = 3: 8.714 ± 0.227%; p < 0.0001) (WT-Panto, n = 3: 5.880 ± 0.032% vs. APP(TG)-Panto, n = 3: 8.714 ± 0.227%; p = 0.0002).

However, a statistical trend was identified between APP(TG)-Panto compared to WT-DMSO mice at 12 weeks of age (WT-DMSO, n = 3: 6.214 ± 0.276% vs. APP(TG)-Panto, n = 4: 7.650 ± 0.485%; p = 0.0697).

No significant differences in relative beta 2 power were observed between all other analyzed groups (Fig. 4.2.17D).

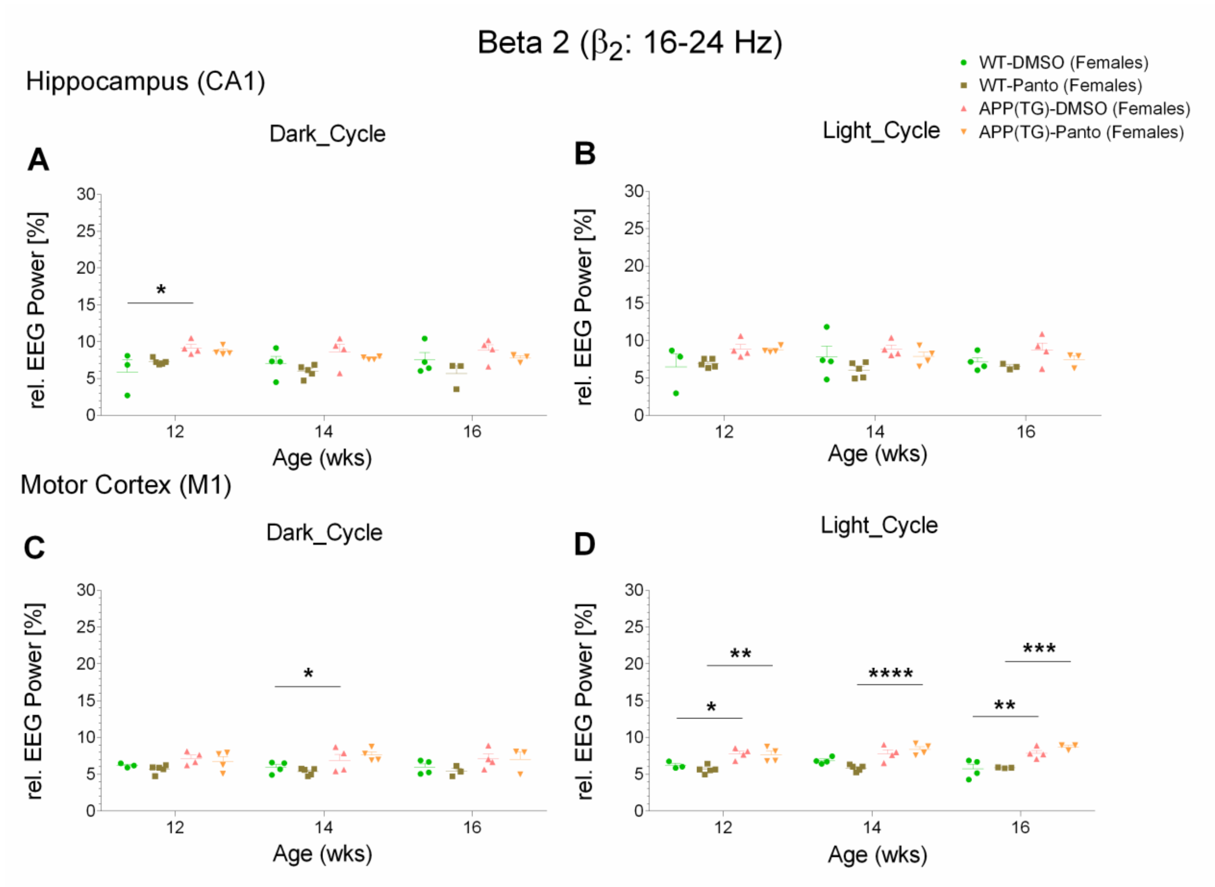

**Figure 4.2.17: Hippocampus (CA1) (A,B) and motor cortex (M1) (C,D) relative beta 2 power (%) ($\beta_2$: 16-24 Hz) in WT-DMSO, WT-Panto, APP(TG)-DMSO and APP(TG)-Panto female mice.** Results are depicted considering the circadian rhythmicity (dark/light cycle). $^{*}p < 0.05$; $^{**}p < 0.01$; $^{***}p < 0.001$.

**Beta 3 ($\beta_3$: 16-30 Hz)**

**i) Hippocampal CA1 region**

Dark cycle

A statistical trend in relative beta 3 power was observed between APP(TG)-DMSO compared to WT-DMSO mice and between APP(TG)-Panto compared to WT-DMSO mice at 12 weeks of age (WT-DMSO, n = 3: 9.021 ± 2.579% vs. APP(TG)-DMSO, n = 4: 13.930 ± 0.648%; p = 0.0613) (WT-DMSO, n = 3: 9.021 ± 2.579% vs. APP(TG)-Panto, n = 4: 13.670 ± 0.445%; p = 0.0828). Likewise, a statistical trend was identified between APP(TG)-DMSO and WT-Panto mice at 16 weeks of age (WT-Panto, n = 3: 8.525 ± 1.685% vs. APP(TG)-DMSO, n = 4: 13.3771 ± 1.104%; p = 0.0655).

No significant differences in relative beta 3 power were detected between all other study groups (Fig. 4.2.18A).

Light cycle

No significant differences in relative beta 3 power were observed between all study groups (Fig. 4.2.18B).

**ii) Motor cortical M1 region**

Dark cycle

A significant increase in relative beta 3 power was identified in APP(TG)-Panto compared to WT-Panto mice at 14 weeks of age (WT-Panto, n = 5: 7.922 ± 0.326% vs. APP(TG)-Panto, n = 4: 11.500 ± 0.719%; p = 0.010). A statistical trend found in relative beta 3 power between APP(TG)-Panto group and WT-DMSO group at 14 weeks of age (WT-DMSO, n = 4: 8.755 ± 0.619% vs. APP(TG)-Panto, n = 4: 11.500 ± 0.719%; p = 0.088).

No significant differences in relative beta 3 power were observed between all other study groups (Fig. 4.2.18C).

Light cycle

A significant increase in relative beta 3 power was observed in APP(TG)-DMSO group compared to WT-DMSO and WT-Panto groups at 12 weeks of age (WT-DMSO, n = 3: 9.046 ± 0.401% vs. APP(TG)-DMSO, n = 4: 11.423 ± 0.567%; p = 0.0241) ) (WT-Panto, n = 5: 8.212 ± 0.380% vs. APP(TG)-DMSO, n = 4: 11.423 ± 0.567%; p = 0.0003). Similarly, a significant increase was detected in APP(TG)-Panto mice compared to WT-DMSO and WT-Panto animals at 12 weeks of age (WT-DMSO, n = 3: 9.046 ± 0.401% vs. APP(TG)-Panto, n = 4: 11.293 ± 0.626 %; p = 0.0357)

(WT-Panto, n = 5: 8.212 ± 0.380% vs. APP(TG)-Panto, n = 4: 11.293 ± 0.626%; p = 0.0005). Furthermore, significant increase was identified in APP(TG)-Panto group compared to WT-DMSO and WT-Panto groups at 14 weeks of age (WT-DMSO, n = 4: 9.757 ± 0.246% vs. APP(TG)-Panto, n = 4: 12.163 ± 0.457%; p = 0.0118) (WT-Panto, n = 5: 8.396 ± 0.312% vs. APP(TG)-Panto, n = 4: 12.163 ± 0.457%; p < 0.0001). Likewise, a significant difference was detected for the APP(TG)-DMSO compared to the WT-Panto mice at 14 weeks of age (WT-Panto, n = 5: 8.396 ± 0.312% vs. APP(TG)-DMSO, n = 4: 11.205 ± 0.757%; p = 0.0015).

Moreover, a significant increase in relative beta 3 power were observed in APP(TG)-DMSO mice compared to WT-DMSO and WT-Panto animals at 16 weeks of age (WT-DMSO, n = 4: 8.448 ± 0.846% vs. APP(TG)-DMSO, n = 4: 11.156 ± 0.569%; p = 0.0039) (WT-Panto, n = 3: 8.416 ± 0.104% vs. APP(TG)-DMSO, n = 4: 11.156 ± 0.569%; p = 0.0074). Similarly, a significant increase was also detected in APP(TG)-Panto group compared to WT-DMSO and WT-Panto groups at 16 weeks of age (WT-DMSO, n = 4: 8.448 ± 0.846% vs. APP(TG)-Panto, n = 3: 12.434 ± 0.295%; p < 0.0001) (WT-Panto, n = 3: 8.416 ± 0.104% vs. APP(TG)-Panto, n = 3: 12.434 ± 0.295%; p = 0.0002).

No significant differences in relative beta 3 power were identified between all other analyzed groups (Fig. 4.2.18D).

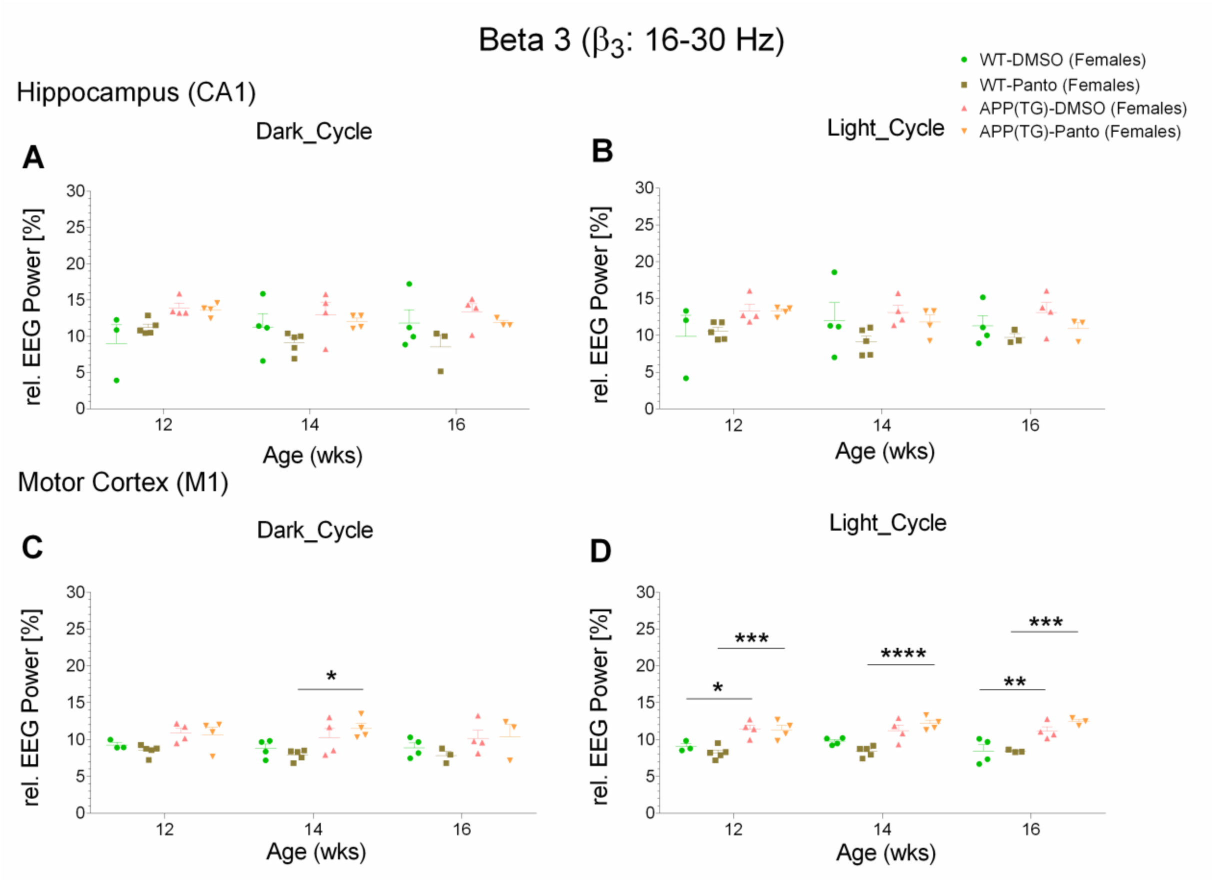

**Figure 4.2.18: Hippocampus (CA1) (A,B) and motor cortex (M1) (C,D) relative beta 3 power (%) (β3: 16-30 Hz) in WT-DMSO, WT-Panto, APP(TG)-DMSO and APP(TG)-Panto female mice.** Results are illustrated considering the circadian rhythmicity (dark/light cycle). $^{*}$ $p < 0.05$; $^{**}$ $p < 0.01$; $^{***}$ $p < 0.001$.

### Alpha (α: 8-12 Hz)

No significant differences in relative alpha power were observed between all study groups analyzed from hippocampal CA1 and motor cortical M1 regions during both dark and light cycles (Fig. 4.2.19).

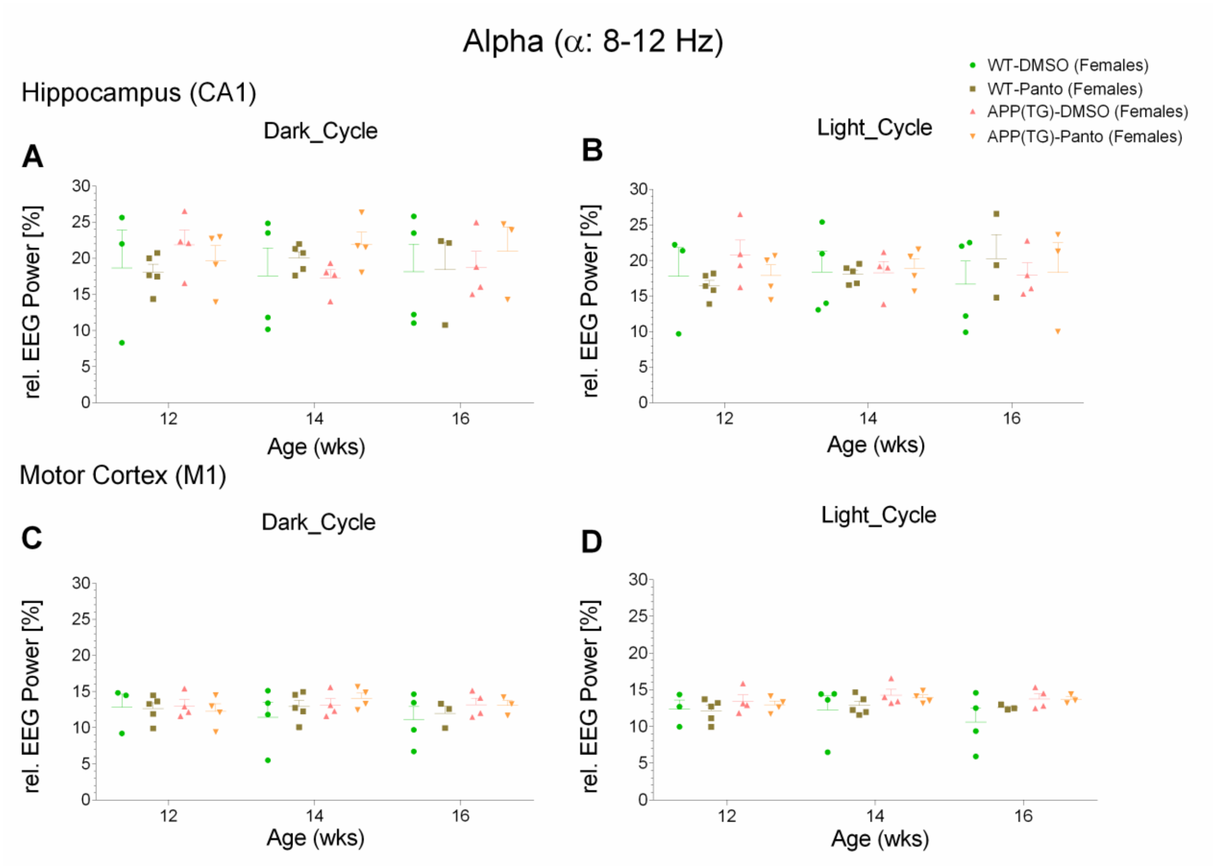

**Figure 4.2.19: Hippocampus (CA1) (A,B) and motor cortex (M1) (C,D) relative alpha power (%) (α: 8-12 Hz) in WT-DMSO, WT-Panto, APP(TG)-DMSO and APP(TG)-Panto female mice.** Results are illustrated considering the circadian rhythmicity (dark/light cycle). $^{*}$ $p < 0.05$; $^{**}$ $p < 0.01$; $^{***}$ $p < 0.001$.

### Sigma (12-16 Hz)

### i) Hippocampus

Dark cycle

No significant differences in relative sigma power were observed between all study groups (Fig. 4.2.20A).

Light cycle

A statistical trend in relative sigma power was observed between APP(TG)-DMSO compared to WT-Panto at 14 weeks of age (WT-Panto, n = 5: 6.049 ± 0.281% vs. APP(TG)-DMSO, n = 4: 8.019 ± 0.362%; p = 0.0544).

No significant differences in relative sigma power were detected between all other analyzed groups (Fig. 4.2.20B).

### ii) Motor cortical M1 region

Dark cycle

No significant differences in relative sigma power were identified between all study groups (Fig. 4.2.20C).

Light cycle

A significant increase in relative sigma power was observed in APP(TG)-Panto compared to WT-DMSO mice at 14 weeks of age (WT-DMSO, n = 4: 5.586 ± 1.274% vs. APP(TG)-Panto, n = 4: 7.922 ± 0.447%; p = 0.0304). Likewise, a significant increase was detected in APP(TG)-DMSO and APP(TG)-Panto groups compared to WT-DMSO group at 16 weeks of age (WT-DMSO, n = 4: 5.322 ± 0.969% vs. APP(TG)-DMSO, n = 4: 7.858 ± 0.385%; p = 0.0164) (WT-DMSO, n = 4: 5.322 ± 0.969% vs. APP(TG)-Panto, n = 3: 8.134 ± 0.392%; p = 0.0133).

No significant differences in relative sigma power were detected between all other study groups (Fig. 4.2.20D).

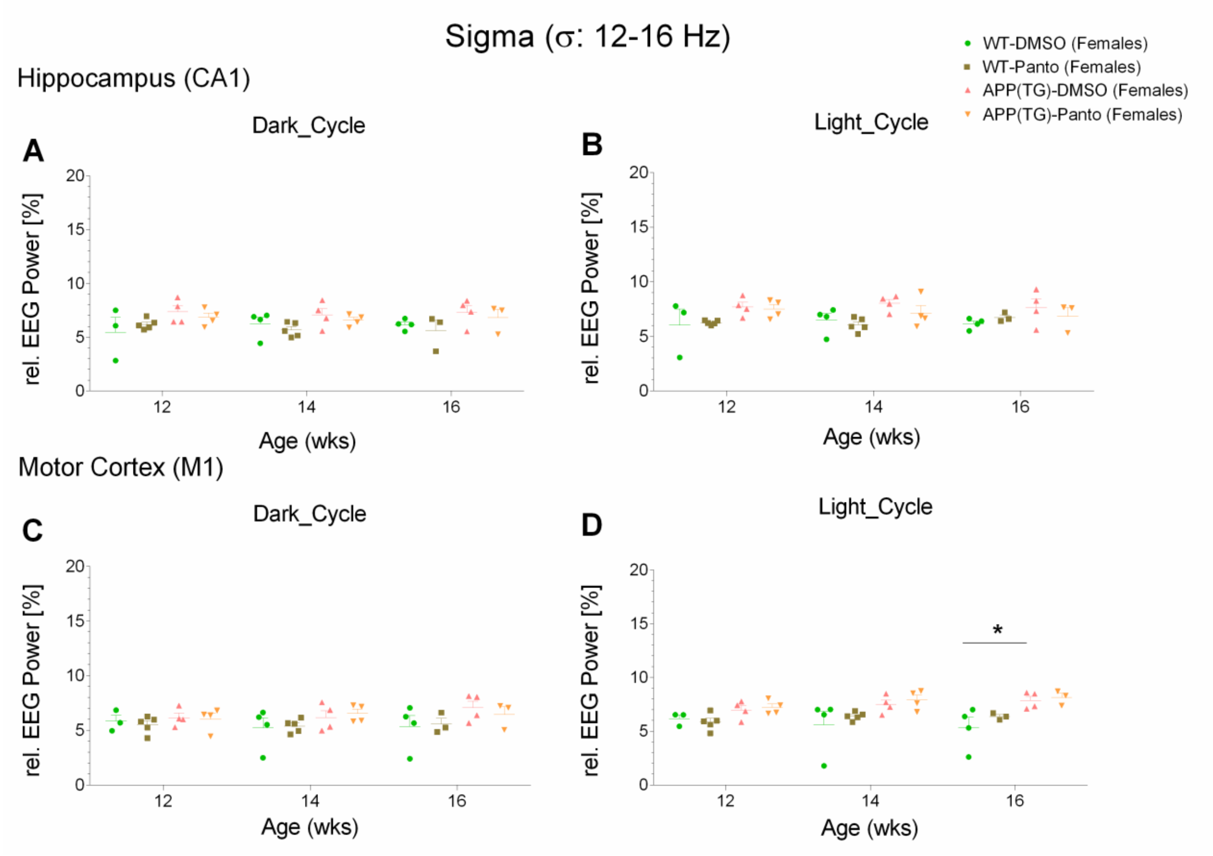

**Figure 4.2.20: Hippocampus (CA1) (A,B) and motor cortex (M1) (C,D) relative sigma power (%) (σ: 12-16 Hz) in WT-DMSO, WT-Panto, APP(TG)-DMSO and APP(TG)-Panto female mice**. Results are illustrated considering the circadian rhythmicity (dark/light cycle). $^{*}$ $p < 0.05$; $^{**}$ $p < 0.01$; $^{***}$ $p < 0.001$.

### Gamma low ($\gamma_{low}$: 30-50 Hz)

### i) Hippocampal CA1 region

No significant differences in relative gamma low power were observed between all study groups analyzed from hippocampal CA1 region during both dark and light cycles (Fig. 4.2.21A,B).

### ii) Motor cortical M1 region

Dark cycle

A significant increase in relative gamma low power was observed in APP(TG)-DMSO compared to WT-Panto mice at 12 weeks of age (WT-Panto, n = 5: 6.525 ± 0.252% vs. APP(TG)-DMSO, n = 4: 9.399 ± 0.691%; p = 0.0388). Additionally, a significant increase was detected in APP(TG)-Panto group compared to WT-Panto group at 14 weeks of age (WT-Panto, n = 5: 5.733 ± 0.470% vs. APP(TG)-Panto, n = 4: 8.843 ± 0.579%; p = 0.0222). Furthermore, a significant increase in relative gamma low power was detected in 12 week of age compared to 16 weeks of age for the APP(TG)-DMSO mice (12 weeks, n = 4, 9.399 ± 0.691% vs. 16 weeks, n = 4, 5.774 ± 0.838%; p = 0.0053).

However, a statistical trend in relative gamma low power was identified between APP(TG)-Panto compared to WT-Panto mice at 12 weeks of age (WT-Panto, n = 5: 6.525 ± 0.252% vs. APP(TG)-Panto, n = 7: 9.111 ± 1.116%; p = 0.0733) and also between 14 weeks compared to 12 weeks of age for the APP(TG)-DMSO group (12 weeks, n = 4, 9.399 ± 0.691% vs. 14 weeks, n = 4, 7.064 ± 0.869%; p = 0.0918).

No significant differences in relative gamma low power were identified between all other study groups (Fig. 4.2.21C).

Light cycle

A significant increase in relative gamma low power was observed in APP(TG)-DMSO compared to WT-Panto mice at 12 weeks of age (WT-Panto, n = 5: 5.363 ± 0.235% vs. APP(TG)-DMSO, n = 4: 7.961 ± 0.487%; p = 0.0197). In addition, a significant increase was detected in APP(TG)-Panto compared to WT-Panto at 14 weeks of age (WT-Panto, n = 5: 5.005 ± 0.347%, vs. APP(TG)-Panto, n = 4: 7.611 ± 0.552%; p = 0.0193).

However, a statistical trend in relative gamma low power was identified between APP(TG)-Panto and WT-Panto mice at 12 weeks of age (WT-Panto, n = 5: 5.363 ± 0.235% vs. APP(TG)-Panto, n = 4: 7.615 ± 0.614; p = 0.0526). Likewise, a statistical trend was detected between WT-DMSO and WT-Panto groups at 14 weeks of age (WT-DMSO, n = 4: 7.173 ± 1.338% vs. WT-Panto, n = 5: 5.005 ± 0.348%; p = 0.0659) and also between APP(TG)-Panto compared to WT-Panto at 16 weeks of age (WT-Panto, n = 3: 4.905 ± 0.448% vs. APP(TG)-Panto, n = 3: 7.514 ± 0.645%; p = 0.0701).

However, no significant differences in relative gamma low power were observed between all other analyzed groups (Fig. 4.2.21D).

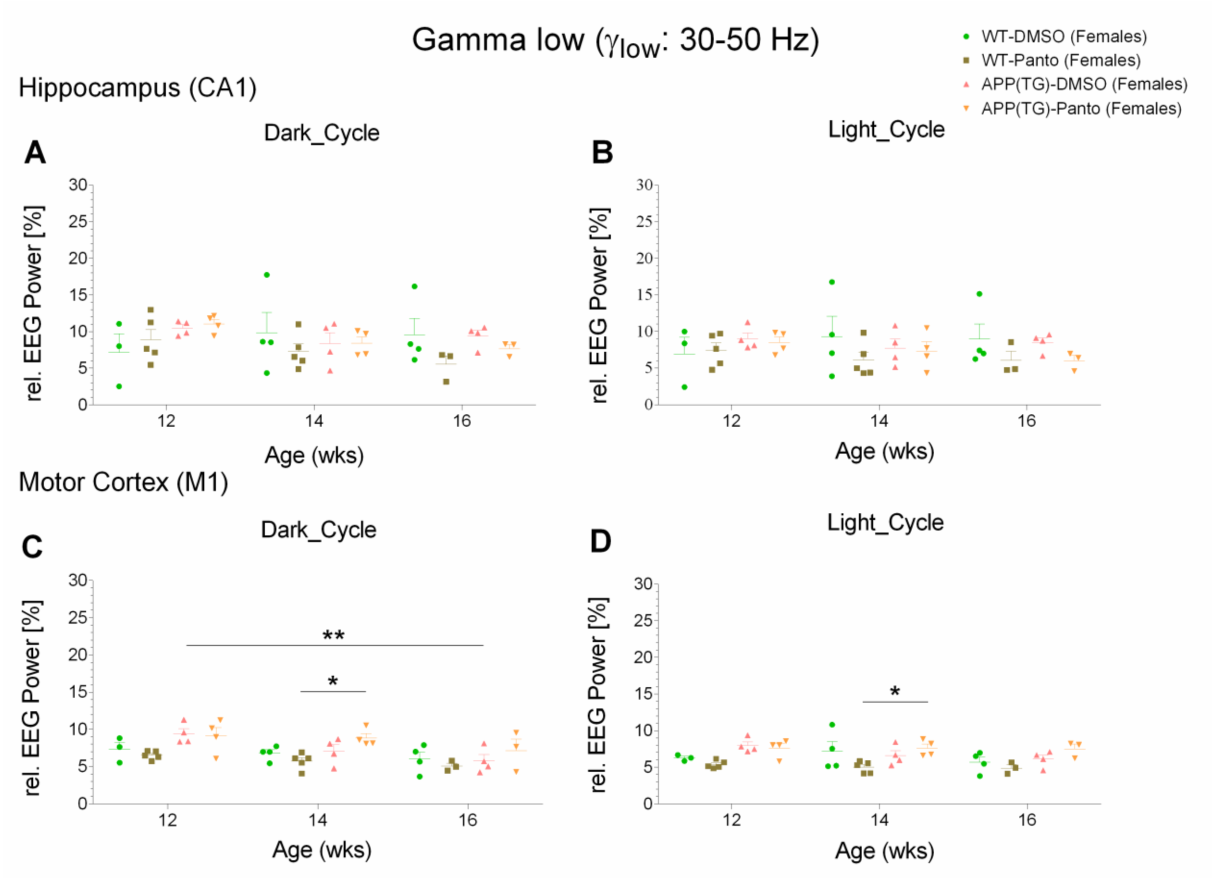

**Figure 4.2.21: Hippocampus (CA1) (A,B) and motor cortex (M1) (C,D) relative gamma low power (%) ($\gamma_{low}$: 4.1-12 Hz) in WT-DMSO, WT-Panto, APP(TG)-DMSO and APP(TG)-Panto female mice.** Results are depicted considering the circadian rhythmicity (dark/light cycle). $^{*}$ $p < 0.05$; $^{**}$ $p < 0.01$; $^{***}$ $p < 0.001$.

### Gamma mid ($\gamma_{mid}$: 50-70 Hz)

### i) Hippocampal CA1 region

No significant differences in relative gamma mid power were observed between all study groups analyzed from hippocampal CA1 region during both dark and light cycles (Fig. 4.2.22A,B).

### ii) Motor cortical M1 region

<u>Dark cycle</u>

A significant increase in relative gamma mid power was observed at 12 weeks compared to 16 weeks of age for the APP(TG)-DMSO mice (12 weeks, n = 4: 4.677 ± 0.252% vs. 16 weeks, n = 4: 2.574 ± 0.417%; p = 0.0135).

A statistical trend in relative gamma mid power was detected at 12 weeks compared to 16 weeks of age for the WT-DMSO mice (12 weeks, n = 3: 4.784 ± 1.123% vs. 16 weeks of age, n = 4: 3.132 ± 0.716%; p = 0.089).

However, no significant differences in relative gamma mid power were identified between all other study groups (Fig. 4.2.22C).

### Light cycle

A statistical trend in relative gamma mid power was observed between WT-DMSO compared to WT-Panto mice at 14 weeks of age (WT-DMSO, n = 4: 4.124 ± 1.090% vs. WT-Panto, n = 5: 2.547 ± 0.208%; p = 0.0638).

No significant differences in relative gamma mid power were detected between all other study groups (Fig. 4.2.22D).

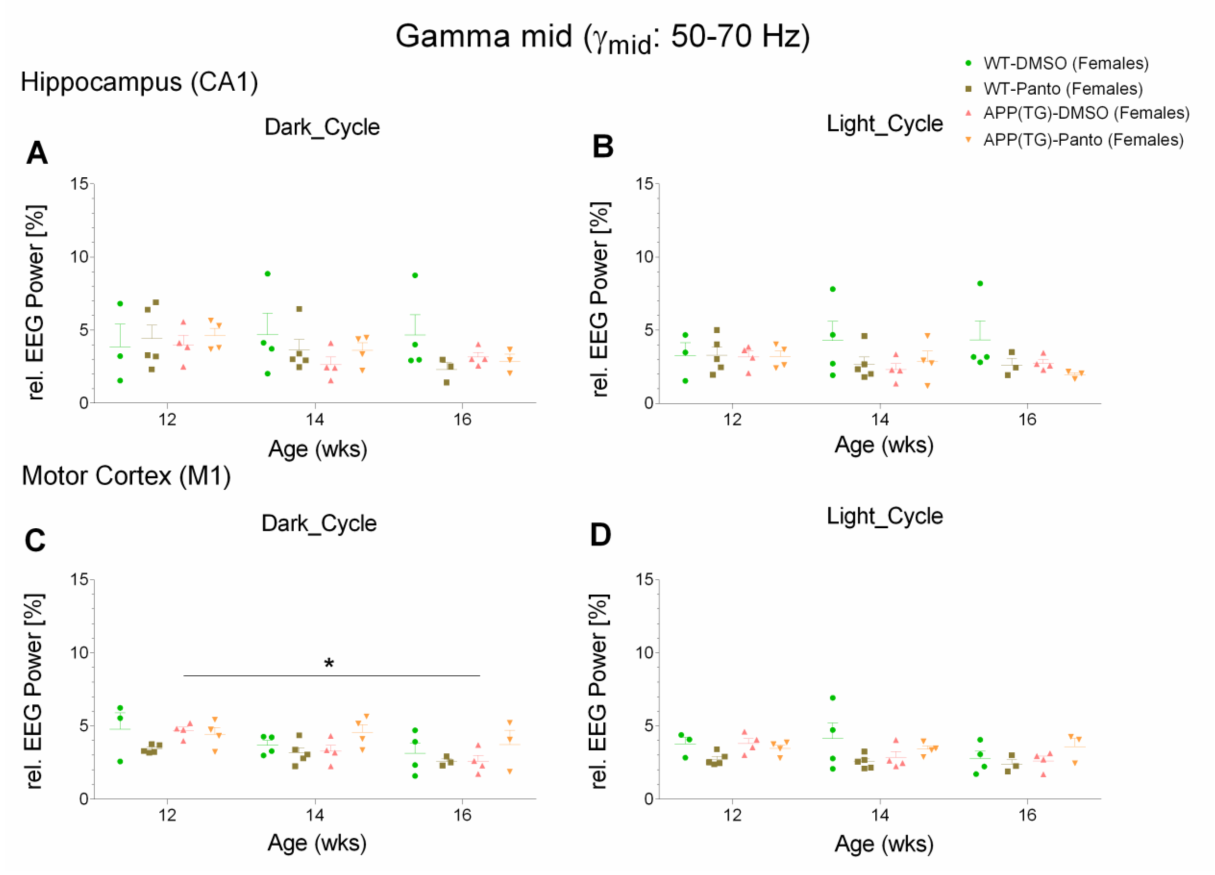

**Figure 4.2.22: Hippocampus (CA1) (A,B) and motor cortex (M1) (C,D) relative gamma mid power (%) ($\gamma_{mid}$: 50-70 Hz) in WT-DMSO, WT-Panto, APP(TG)-DMSO and APP(TG)-Panto female mice.** Results are illustrated considering the circadian rhythmicity (dark/light cycle). $^{*}p < 0.05$; $^{**}p < 0.01$; $^{***}p < 0.001$.

### 4.2.3 Electroencephalographic seizures analysis

Electroencephalographic seizures analysis was performed for wild-type controls (WT-DMSO and WT-Panto) and APPswePS1dE9 (APP(TG)-DMSO and APP(TG)-Panto) subgroups based on the EEG recordings from the hippocampal CA1 and motor cortical M1 regions of both genders.

#### 4.2.3.1 Seizures analysis in male mice

**Number of spike trains**

**i) Hippocampal CA1 region**

No significant differences observed in number of spike trains between all study groups analyzed from hippocampal CA1 region during both dark and light cycles (Fig 4.2.23A,B).

**ii) Motor cortical M1 region**

Dark cycle

A significant increase in number of spike trains was observed in APP(TG)-DMSO group compared to WT-DMSO and WT-Panto groups at 14 weeks of age (WT-DMSO, n = 7: 5.571 ± 4.048 vs. APP(TG)-DMSO, n = 6: 53.667 ± 17.927; p = 0.0017) (WT-Panto, n = 6: 1.75 ± 0.804 vs. APP(TG)-DMSO, n = 6: 53.667 ± 17.927; p = 0.0010). Likewise, a significant increase was detected at 14 weeks compared to 16 weeks of age for the APP(TG)-DMSO mice (14 weeks, n = 6: 53.667 ± 17.927 vs. 16 weeks, n = 3: 12.667 ± 5.207; p = 0.0335).

However, a statistical trend in number of spike trains was observed between APP(TG)-DMSO and APP(TG)-Panto at 14 weeks of age (APP(TG)-DMSO, n = 6: 53.667 ± 17.927 vs. APP(TG)-Panto, n = 6: 22.357 ± 9.342; p = 0.0711). Additionally, a statistical trend was also detected between 14 weeks compared to 12 weeks of age for the APP(TG)-DMSO group (12 weeks, n = 6: 24.083 ± 12.605 vs. 14 weeks, n = 6: 53.667 ± 17.927; p = 0.0678).

However, no significant differences in number of spike trains were observed between all other study groups (Fig. 4.2.23C).

Light cycle

A significant increase in number of spike trains was observed in APP(TG)-DMSO group compared to WT-DMSO, WT-Panto and APP(TG)-Panto groups at 14 weeks of age (WT-DMSO, n = 7: 5.357 ± 4.045 vs. APP(TG)-DMSO, n = 6: 77.167 ± 32.250; p = 0.0004) (WT-Panto, n = 6: 2.167 ± 1.216 vs. APP(TG)-DMSO, n = 6: 77.167 ± 32.250; p = 0.0003) (APP(TG)-DMSO, n = 6: 77.167 ± 32.250 vs. APP(TG)-Panto, n = 6: 27.357 ± 10.582; p = 0.0212). Furthermore, a significant increase in number of spike trains was also observed at 14 weeks compared to 12 weeks and 16 weeks of age for the APP(TG)-DMSO mice (12 weeks, n = 6: 22.000 ± 9.470 vs. 14 weeks, n = 6: 77.167 ± 32.250; p = 0.0065) (14 weeks, n = 6: 77.167 ± 32.250 vs. 16 weeks, n = 3: 15.000 ± 8.145; p = 0.0133).

However, no significant differences in number of spike trains were detected between all other study groups (Fig. 4.2.23D).

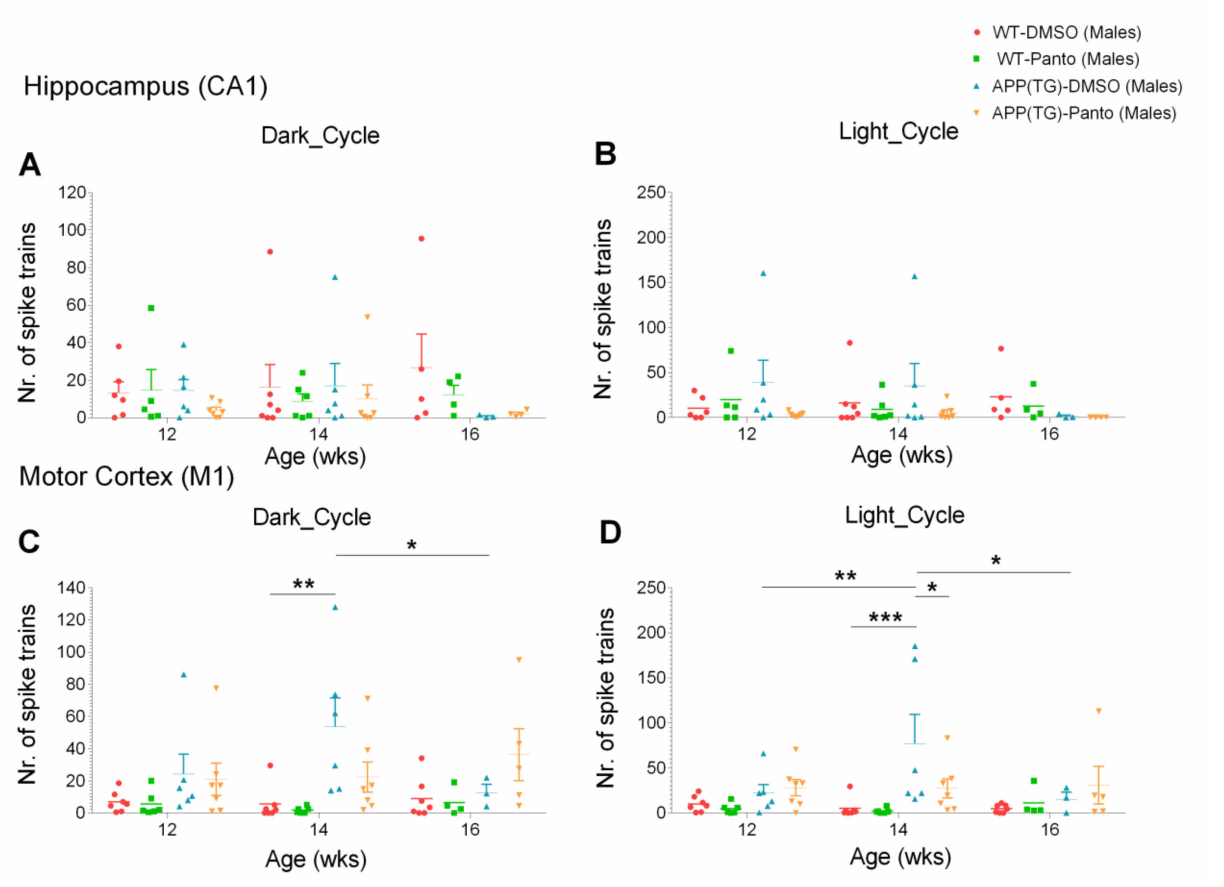

**Figure 4.2.23: Hippocampus (CA1) (A,B) and motor cortex (M1) (C,D) number of spike trains in WT-DMSO, WT-Panto, APP(TG)-DMSO and APP(TG)-Panto male mice.** Results are depicted considering the circadian rhythmicity (dark/light cycle). $^{*}$ $p < 0.05$; $^{**}$ $p < 0.01$; $^{***}$ $p < 0.001$.

### Number of single spikes

### i) Hippocampal CA1 region

Dark cycle

No significant differences in total number of single spikes were identified between all analyzed groups (Fig. 4.2.24A).

Light cycle

A statistical trend in number of single spikes was identified between 12 weeks compared to 16 weeks of age for the APP(TG)-DMSO group (12 weeks, n = 6: 5635.584 ± 1968.024 vs. 16 weeks, n = 6: 932.333 ± 639.087; $p = 0.092$).

No significant differences in number of single spikes were observed between all other study groups (Fig. 4.2.24B).

### ii) Motor cortical M1 region

Dark cycle

A significant increase in number of single spikes was identified in APP(TG)-DMSO compared to WT-Panto at 14 weeks of age (WT-Panto, n = 6: 960.833 ± 172.838 vs. APP(TG)-DMSO, n = 6: 3079.833 ± 397.771; $p = 0.040$). A statistical trend in number of single spikes was detected at 14 weeks of age between APP(TG)-DMSO compared to WT-DMSO mice and APP(TG)-Panto compared to WT-Panto mice (WT-DMSO, n = 6: 1268.000 ± 435.261 vs. APP(TG)-DMSO, n = 6: 3079.833 ± 397.771; $p = 0.0832$) (WT-Panto, n = 6: 960.833 ± 172.838 vs. APP(TG)-Panto, n = 7: 2861.714 ± 716.919; $p = 0.0632$).

However, no significant differences in number of single spikes were identified between all other study groups (Fig. 4.2.24C).

Light cycle

A significant increase in number of single spikes was observed in APP(TG)-DMSO group compared to WT-DMSO and WT-Panto groups at 14 weeks of age (WT-DMSO, n = 7: 1084.643 ± 416.240 vs. APP(TG)-DMSO, n = 6: 4228.417 ± 729.876; $p < 0.0001$) (WT-Panto, n = 6: 883.333 ± 174.783 vs. APP(TG)-DMSO, n = 6: 4228.417 ± 729.876; $p < 0.0001$). Likewise, a significant increase was observed in APP(TG)-Panto group compared to WT-DMSO and WT-Panto groups (WT-DMSO, n = 7: 1084.643 ± 416.240 vs. APP(TG)-Panto, n = 7: 3099.072 ± 407.148; $p = 0.0077$) (WT-Panto, n = 6: 883.333 ± 174.783 vs. APP(TG)-Panto, n = 7: 3099.072 ± 407.148; $p = 0.0044$). Additionally, a significant increase was also detected in APP(TG)-Panto compared to WT-DMSO mice at 16 weeks of age (WT-DMSO, n = 7: 824.857 ± 235.311 vs. APP(TG)-Panto, n = 5: 2954.200 ± 735.738; $p = 0.0107$). Furthermore, a significant increase in number of single spikes was identified at 14 weeks compared to 12 weeks of age for the APP(TG)-DMSO mice (12 weeks, n = 6: 2360.333 ± 401.702 vs. 14 weeks, n = 6: 4228.417 ± 729.876; $p = 0.0154$).

A statistical trend in number of single spikes was detected between APP(TG)-Panto and WT-Panto mice 12 weeks of age (WT-Panto, n = 6: 1669.083 ± 268.003 vs. APP(TG)-Panto, n = 7: 3185.286 ± 568.986; p = 0.0847). Moreover, a significant trend was also observed at 14 weeks compared to 16 weeks of age for the APP(TG)-DMSO mice (14 weeks, n = 6: 4228.417 ± 729.876 vs. 16 weeks, n = 3: 2347.167 ± 663.979; p = 0.0554).

However, no significant differences in number of single spikes were identified between all other study groups (Fig. 4.2.24D).

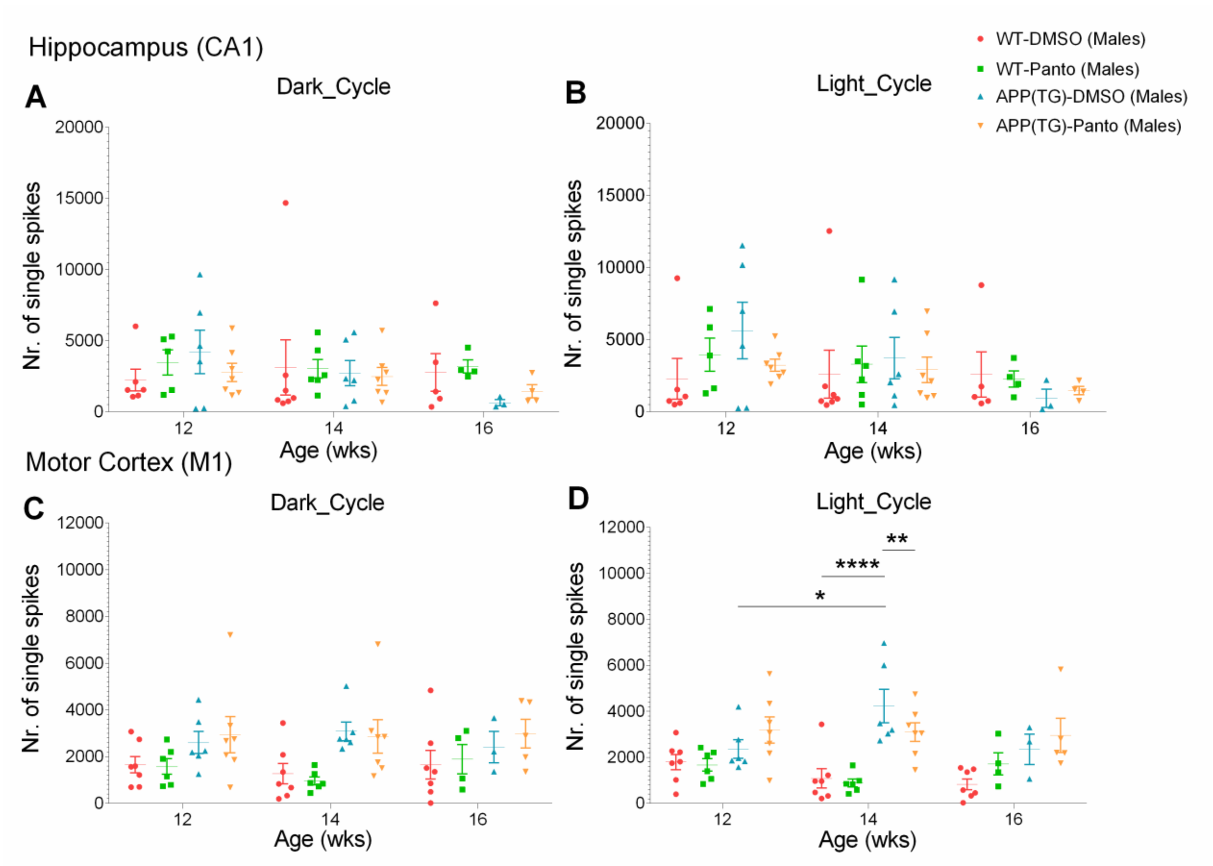

**Figure 4.2.24: Hippocampus (CA1) (A,B) and motor cortex (M1) (C,D) total number of single spikes in WT-DMSO, WT-Panto, APP(TG)-DMSO and APP(TG)-Panto male mice.** Results are depicted considering the circadian rhythmicity (dark/light cycle). $^{*}$ $p < 0.05$; $^{**}$ $p < 0.01$; $^{***}$ $p < 0.001$.

## Spike trains duration (min)

### i) Hippocampal CA1 region

No significant differences in spike trains duration (min) were identified between all study groups analyzed from hippocampal CA1 region during both dark and light cycles (Fig 4.2.25A,B).

### ii) Motor cortical M1 region

Dark cycle

A significant increase in spike trains duration (min) was observed in APP(TG)-DMSO group compared to WT-DMSO and WT-Panto groups at 14 weeks of age (WT-DMSO, n = 7: 0.069 ± 0.046 vs. APP(TG)-DMSO, n = 6: 0.677 ± 0.240; p = 0.0023) (WT-Panto, n = 6: 0.017 ± 0.008 vs. APP(TG)-DMSO, n = 6: 0.677 ± 0.240; p = 0.0014). In addition, a significant increase was detected at 14 weeks compared to 16 weeks of age for the APP(TG)-DMSO mice (14 weeks, n = 6: 0.677 ± 0.240 vs. 16 weeks, n = 3: 0.159 ± 0.062; p = 0.0393).

A statistical trend in spike trains duration (min) was observed at 14 weeks of age between APP(TG)-DMSO and APP(TG)-Panto mice (APP(TG)-DMSO, n = 6: 0.677 ± 0.240 vs. APP(TG)-Panto, n = 6: 0.275 ± 0.120; p = 0.075). Additionally, a statistical trend was identified between 14 weeks compared to 12 weeks of age for the APP(TG)-DMSO mice (12 weeks, n = 6: 0.282 ± 0.153 vs. 14 weeks, n = 6: 0.677 ± 0.240; p = 0.0582).

However**,** no significant differences in spike trains duration (min) were observed between all other study groups (Fig 4.2.25C).

Light cycle

A significant increase in spike trains duration (min) was observed in APP(TG)-DMSO group compared to WT-DMSO and WT-Panto groups at 14 weeks of age (WT-DMSO, n = 7: 0.064 ± 0.048 vs. APP(TG)-DMSO, n = 6: 0.990 ± 0.432; p = 0.0013) (WT-Panto, n = 6: 0.024 ± 0.014 vs. APP(TG)-DMSO, n = 6: 0.990 ± 0.432; p = 0.0012). Likewise, a significant increase in spike trains duration (min) was detected at 14 weeks as compared to 12 weeks and 16 weeks of age for the APP(TG)-DMSO mice (12 weeks, n = 6: 0.263 ± 0.122 vs. 14 weeks, n = 6: 0.990 ± 0.432; p = 0.0119) (14 weeks, n = 6: 0.990 ± 0.432 vs. 16 weeks, n = 3: 0.176 ± 0.097; p = 0.0233).

No significant differences in spike trains duration (min) were observed between all other study groups (Fig 4.2.25D).

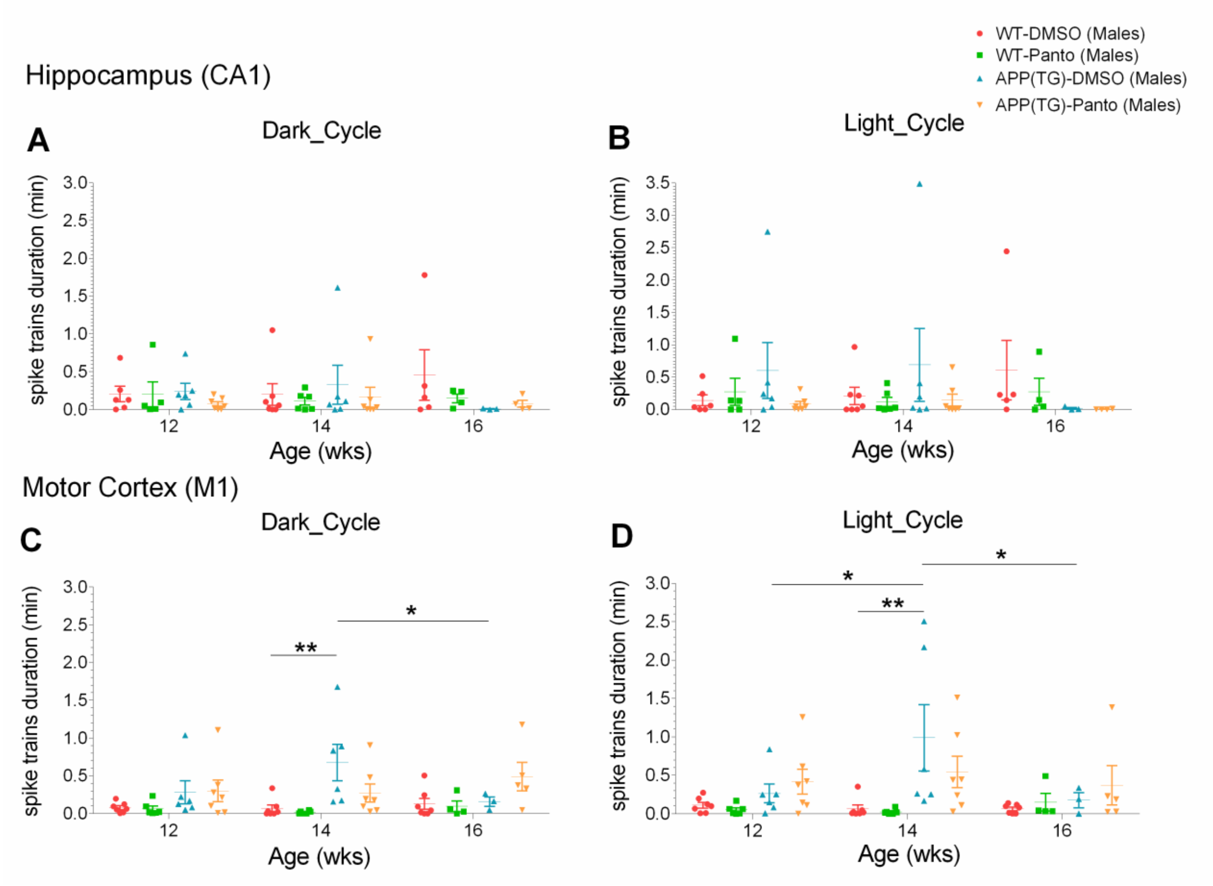

**Figure 4.2.25: Hippocampus (CA1) (A,B) and motor cortex (M1) (C,D) spike trains duration (min) in WT-DMSO, WT-Panto, APP(TG)-DMSO and APP(TG)-Panto male mice.** Results are depicted considering the circadian rhythmicity (dark/light cycle). * $p < 0.05$; ** $p < 0.01$; *** $p < 0.001$.

### 4.2.3.2. Seizures analysis in female mice

**Number of spike trains**

**i) Hippocampal CA1 region**

No significant differences in number of spike trains were observed between all study groups analyzed from hippocampal CA1 region during both dark and light cycles (Fig 4.2.26A,B).

**ii) Motor cortical M1 region**

Dark cycle

A significant increase in number of spike trains was observed in APP(TG)-DMSO compared to WT-DMSO mice at 16 weeks of age (WT-DMSO, n = 3: 8.833 ± 4.781 vs. APP(TG)-DMSO, n = 4: 82.000 ± 42.457; p = 0.0166). Additionally, a significant increase in number of spike trains was also detected at 16 weeks compared to 12 weeks of age for the APP(TG)-DMSO mice (12 weeks, n = 4: 8.000 ± 1.969 vs. 16 weeks, n = 4: 82.000 ± 42.457; p = 0.0042).

No significant differences in number of spike trains were identified between all other study groups (Fig. 4.2.26C).

Light cycle

A significant increase in number of spike trains was observed in APP(TG)-DMSO group compared to WT-DMSO, WT-Panto and APP(TG)-Panto groups at 14 weeks of age (WT-DMSO, n = 4: 8.000 ± 4.628 vs. APP(TG)-DMSO, n = 4: 46.375 ± 19.368; p = 0.0135) (WT-Panto, n = 5: 2.100 ± 0.678 vs. APP(TG)-DMSO, n = 4: 46.375 ± 19.368; p = 0.0021) (APP(TG)-DMSO, n = 4: 46.375 ± 19.368 vs. APP(TG)-Panto, n = 4: 12.000 ± 6.0999; p = 0.0312). Furthermore, a significant increase in number of spike trains was detected at 14 weeks compared to 12 weeks of age for the APP(TG)-DMSO mice (12 weeks, n = 4: 15.750 ± 5.044 vs. 14 weeks, n = 4: 46.375 ± 19.368; p = 0.0368).

No significant differences in number of spike trains were identified between all other analyzed groups (Fig. 4.2.26D).

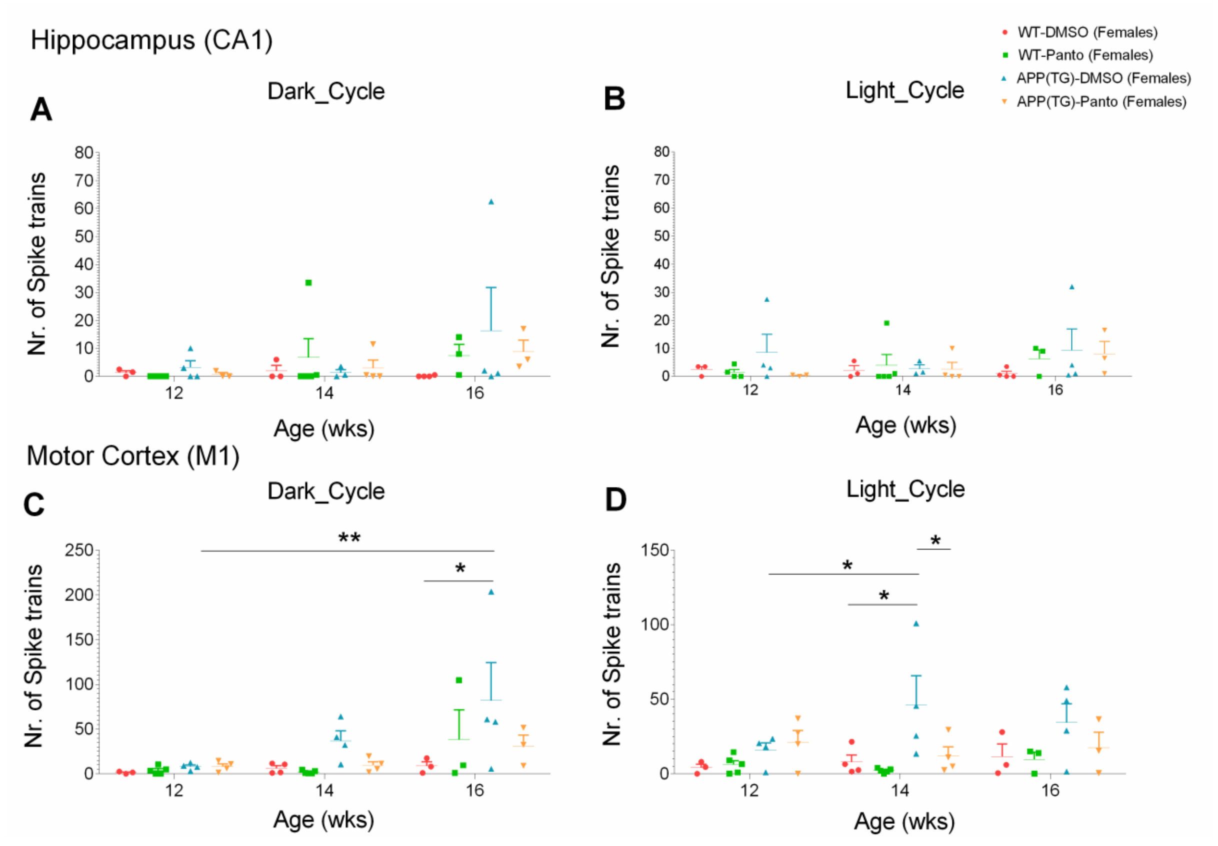

**Figure 4.2.26: Hippocampus (CA1) (A,B) and motor cortex (M1) (C,D) number of spike trains in WT-DMSO, WT-Panto, APP(TG)-DMSO and APP(TG)-Panto female mice.** Results

are depicted considering the circadian rhythmicity (dark/light cycle). $^{*}$ $p < 0.05$; $^{**}$ $p < 0.01$; $^{***}$ $p < 0.001$.

### Number of single spikes

### i) Hippocampal CA1 region

Dark cycle

A statistical trend in number of single spikes was observed between APP(TG)-DMSO and WT-DMSO groups at 16 weeks of age (WT-DMSO, n = 4: 333.125 ± 102.810 vs. APP(TG)-DMSO, n = 4: 3049.750 ± 1084.182; p = 0.0791). No significant differences in number of single spikes were detected between all study groups (Fig. 4.2.27A).

Light cycle

A statistical trend in number of single spikes was identified between APP(TG)-Panto compared to WT-DMSO mice at 16 weeks of age (WT-DMSO, n = 4: 461.250 ± 192.761 vs. APP(TG)-Panto, n = 3: 3272.667 ± 1091.513; p = 0.0675). No significant differences in number of single spikes were observed between all study groups (Fig. 4.2.27B).

### ii) Motor cortical M1 region

Dark cycle

A statistical trend in number of single spikes was observed between 16 weeks compared to 12 weeks of age for the APP(TG)-DMSO mice (12 weeks, n = 4: 1834.000 ± 256.294 vs. 16 weeks, n = 4: 4682.000 ± 2058.677; p = 0.0764). No significant differences in number of single spikes were detected between all study groups (Fig. 4.2.27C).

Light cycle

A significant increase in number of single spikes was observed in APP(TG)-DMSO compared to WT-Panto mice at 14 weeks of age (WT-Panto, n = 5: 986.700 ± 179.315 vs. APP(TG)-DMSO, n = 4: 3899.250 ± 551.964; p = 0.0119). A statistical trend in number of single spikes was identified between APP(TG)-DMSO and WT-DMSO groups at 14 weeks of age (WT-DMSO, n = 4: 1585.750 ± 689.511 vs. APP(TG)-DMSO, n = 4: 3899.250 ± 551.964; p = 0.0812). However, no significant differences in number of single spikes were detected between all other analyzed groups (Fig. 4.2.27D).

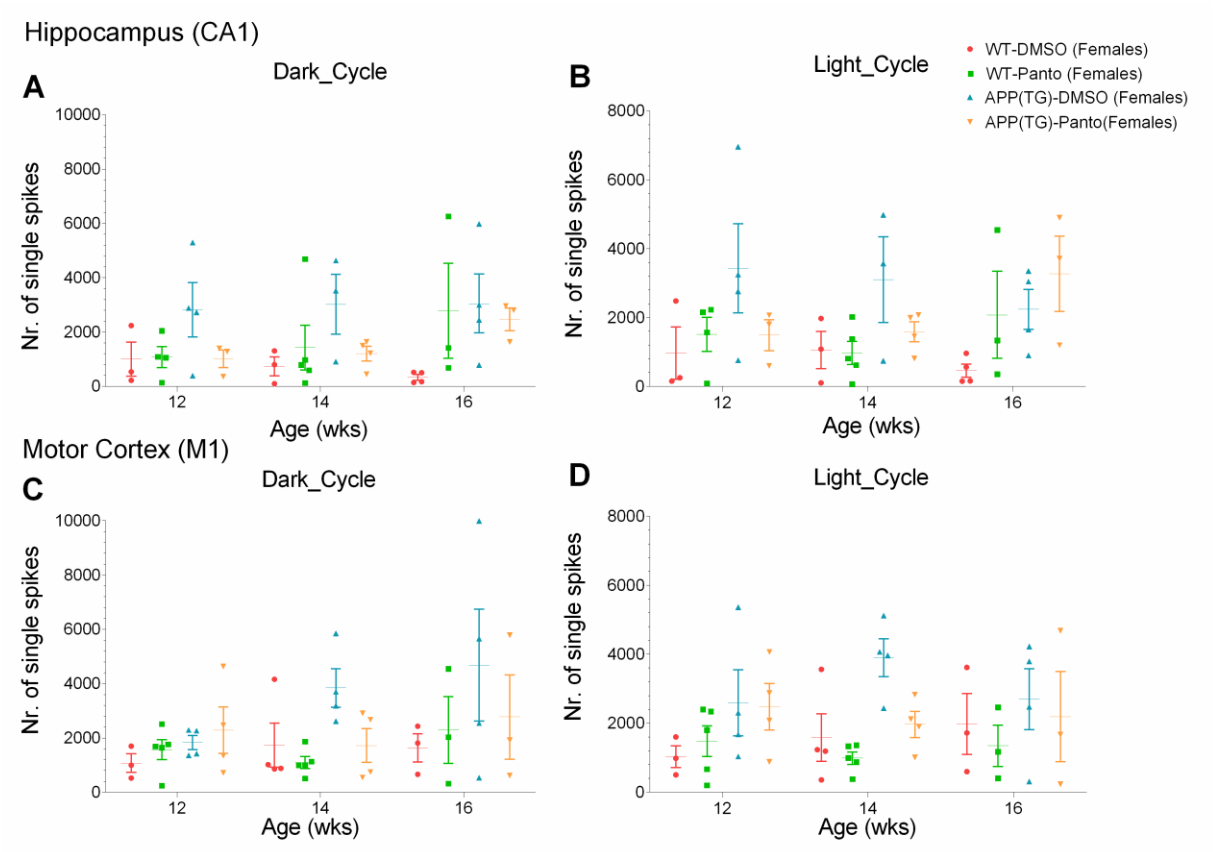

**Figure 4.2.27: Hippocampus (CA1) (A,B) and motor cortex (M1) (C,D) total number of single spikes in WT-DMSO, WT-Panto, APP(TG)-DMSO and APP(TG)-Panto female mice.** Results are depicted considering the circadian rhythmicity (dark/light cycle). $^{*}$ $p$ < 0.05; $^{**}$ $p$ < 0.01; $^{***}$ $p$ < 0.001.

### Spike trains duration (min)

### i) Hippocampal CA1 region

No significant differences in spike trains duration (min) were observed between all study groups analyzed from hippocampal CA1 region during both dark and light cycles (Fig 4.2.28A,B).

### ii) Motor cortical M1 region

Dark cycle

A significant increase in spike trains duration (min) was observed in APP(TG)-DMSO compared to WT-DMSO mice at 16 weeks of age (WT-DMSO, n = 3: 0.135 ± 0.090 vs. APP(TG)-DMSO, n = 4: 1.4603 ± 0.867; p = 0.0342). Additionally, a significant increase in spike trains duration (min) was identified at 16 weeks compared to 12 weeks of age for the APP(TG)-DMSO mice (12 weeks, n = 4: 0.090 ± 0.025 vs. 16 weeks, n = 4: 1.460 ± 0.867; p = 0.0082). A statistical trend in spike trains duration (min) was observed between 16 weeks compared to 14 weeks of age for the APP(TG)-DMSO group (14 weeks, n = 4: 0.470 ± 0.148 vs. 16 weeks, n = 4: 1.460 ± 0.867; p = 0.0677).

However, no significant differences in spike trains duration (min) were detected between all other study groups (Fig. 4.2.28C).

Light cycle

A significant increase in spike trains duration (min) was observed in APP(TG)-DMSO group compared to WT-DMSO, WT-Panto and APP(TG)-Panto groups at 14 weeks of age (WT-DMSO, n = 4: 0.101 ± 0.056 vs. APP(TG)-DMSO, n = 4: 0.656 ± 0.273; p = 0.0167) (WT-Panto, n = 5: 0.024 ± 0.007 vs. APP(TG)-DMSO, n = 4: 0.656 ± 0.273; p = 0.0032) (APP(TG)-DMSO, n = 4: 0.656 ± 0.273 vs. APP(TG)-Panto, n = 4: 0.131 ± 0.069; p = 0.0256).

No significant differences in spike trains duration (min) were detected between all other study groups (Fig. 4.2.28D).

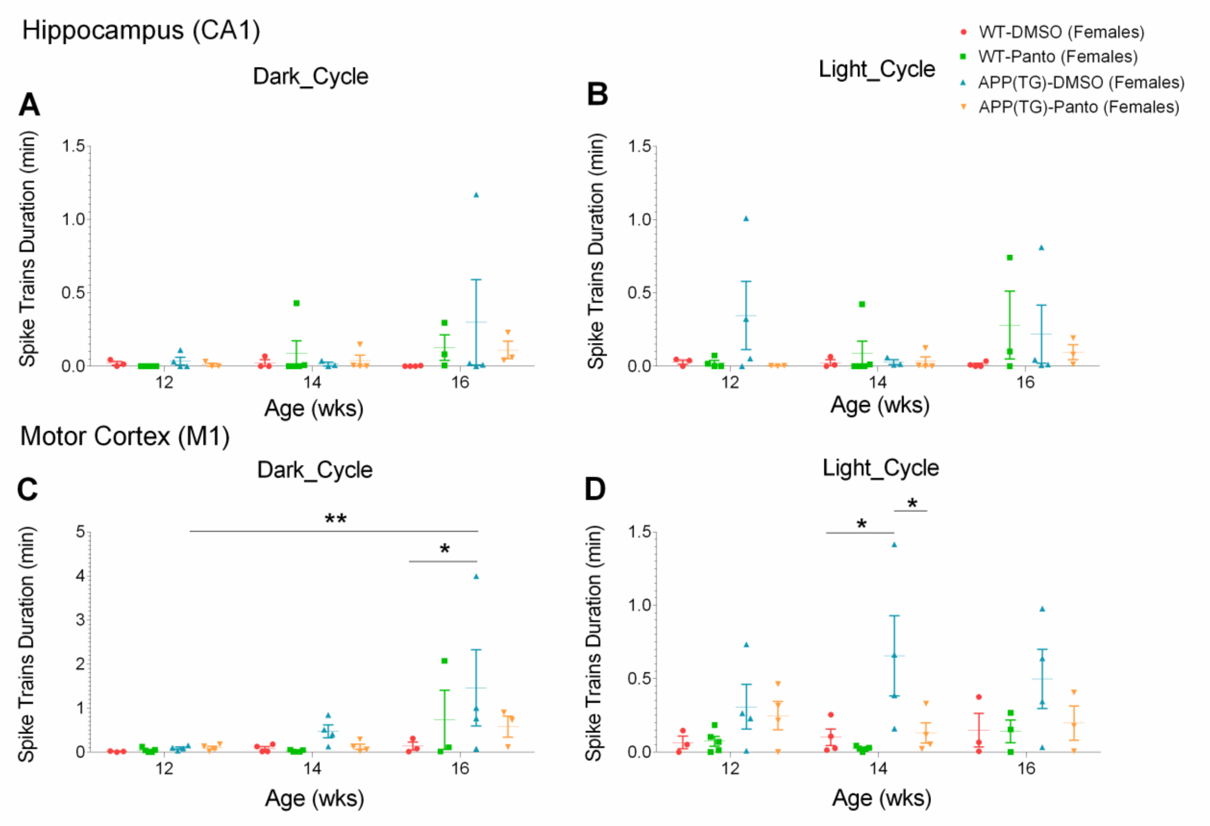

**Figure 4.2.28: Hippocampus (CA1) (A,B) and motor cortex (M1) (C,D) spike trains duration (min) in WT-DMSO, WT-Panto, APP(TG)-DMSO and APP(TG)-Panto female mice.** Results are depicted considering the circadian rhythmicity (dark/light cycle). $^{*}$ $p < 0.05$; $^{**}$ $p < 0.01$; $^{***}$ $p < 0.001$.

### 4.2.4. LC-MS/MS analysis of Pantoprazole concentration in plasm and liver

### 4.2.4.1. Calibration Curves

The standard curves for the liver and plasma samples were constructed by plotting peak areas against corresponding different known liver and plasma concentrations using linear regression statistics as follows:

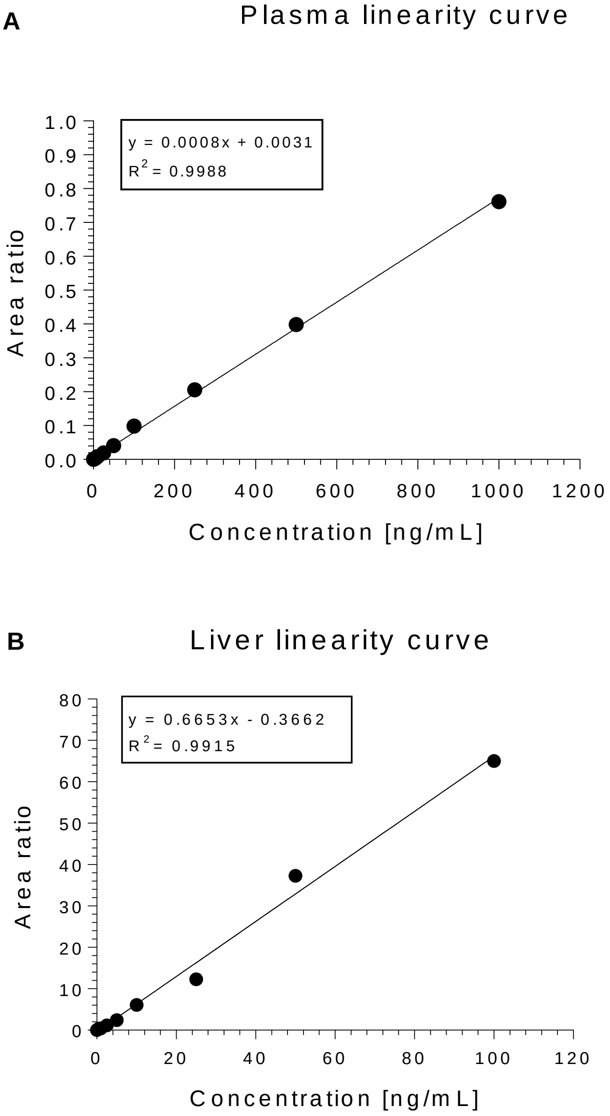

**Figure 4.2.29: (A) Representation standard curve using linear regression statistics for plasma; (B) Representation standard curve using linear regression statistics for liver.**

#### 4.2.4.2. Pantoprazole plasma concentration

**Table 4.2.1: Pantoprazole plasma concentration (mean ± SEM).**

| APP swePS1dE9-Part I Mice sub groups | Plasma drug concentration [ng/mL] (Males; (♂) | Plasma drug concentration [ng/mL] (Females; (♀) |
|---|---|---|
| WT-DMSO | 0.0 ± 0.0, n = 7 | 0.002 ± 0.002, n = 4 |
| WT-Panto | 0.592 ± 0.068, n = 6 | 0.064 ± 0.018, n = 5 |
| APP(TG)-DMSO | 0.016 ± 0.012, n = 5 | 0.056 ± 0.042, n = 4 |
| APP(TG)-Panto | 0.145 ± 0.036, n = 6 | 0.970 ± 0.856, n = 4 |

**Table 4.2.2: Statistical analysis of pantoprazole plasma concentration**.

| Mice groups | Males (♂) | Females; (♀) |
|---|---|---|
| **Tukey's multiple comparisons test** | **P-Value** | **P-Value** |
| WT-DMSO vs. WT-Panto | < 0.0001 | 0.9995 |
| WT-DMSO vs. APP(TG)-DMSO | 0.9916 | 0.9997 |
| WT-DMSO vs. APP(TG)-Panto | 0.058 | 0.3816 |
| WT-Panto vs. APP(TG)-DMSO | < 0.0001 | > 0.9999 |
| WT-Panto vs. APP(TG)-Panto | < 0.0001 | 0.3926 |
| APP(TG)-DMSO vs. APP(TG)-Panto | 0.1498 | 0.4289 |

#### 4.2.4.3. Pantoprazole liver concentration

**Table 4.2.3: Pantoprazole liver concentration (mean ± SEM)**

| APP swePS1dE9-Part I Mice sub groups | Plasma drug concentration [ng/mL] (Males; (♂) | Plasma drug concentration [ng/mL] (Females; (♀) |
|---|---|---|
| WT-DMSO | 0.0371 ± 0.0162, n = 6 | 0.0118 ± 0.0061, n = 4 |
| WT-Panto | 0.6325 ± 0.1544, n = 6 | 0.1251 ± 0.0314, n = 5 |
| APP(TG)-DMSO | 0.0557 ± 0.0088, n = 6 | 0.0694 ± 0.0583, n = 3 |
| APP(TG)-Panto | 0.3282 ± 0.1035, n = 6 | 0.5307 ± 0.2557, n = 4 |

**Table 4.2.4: Statistical analysis of pantoprazole liver concentration.**

| **Mice groups** | **Males (♂)** | **Females; (♀)** |
|---|---|---|
| **Tukey's multiple comparisons test** | **P-Value** | **P-Value** |
| WT-DMSO vs. WT-Panto | 0.0011 | 0.9156 |
| WT-DMSO vs. APP(TG)-DMSO | 0.999 | 0.9913 |
| WT-DMSO vs. APP(TG)-Panto | 01563 | 0.067 |
| WT-Panto vs. APP(TG)-DMSO | 0.0016 | 0.991 |
| WT-Panto vs. APP(TG)-Panto | 0.1307 | 0.1511 |
| APP(TG)-DMSO vs. APP(TG)-Panto | 0.1992 | 0.1516 |

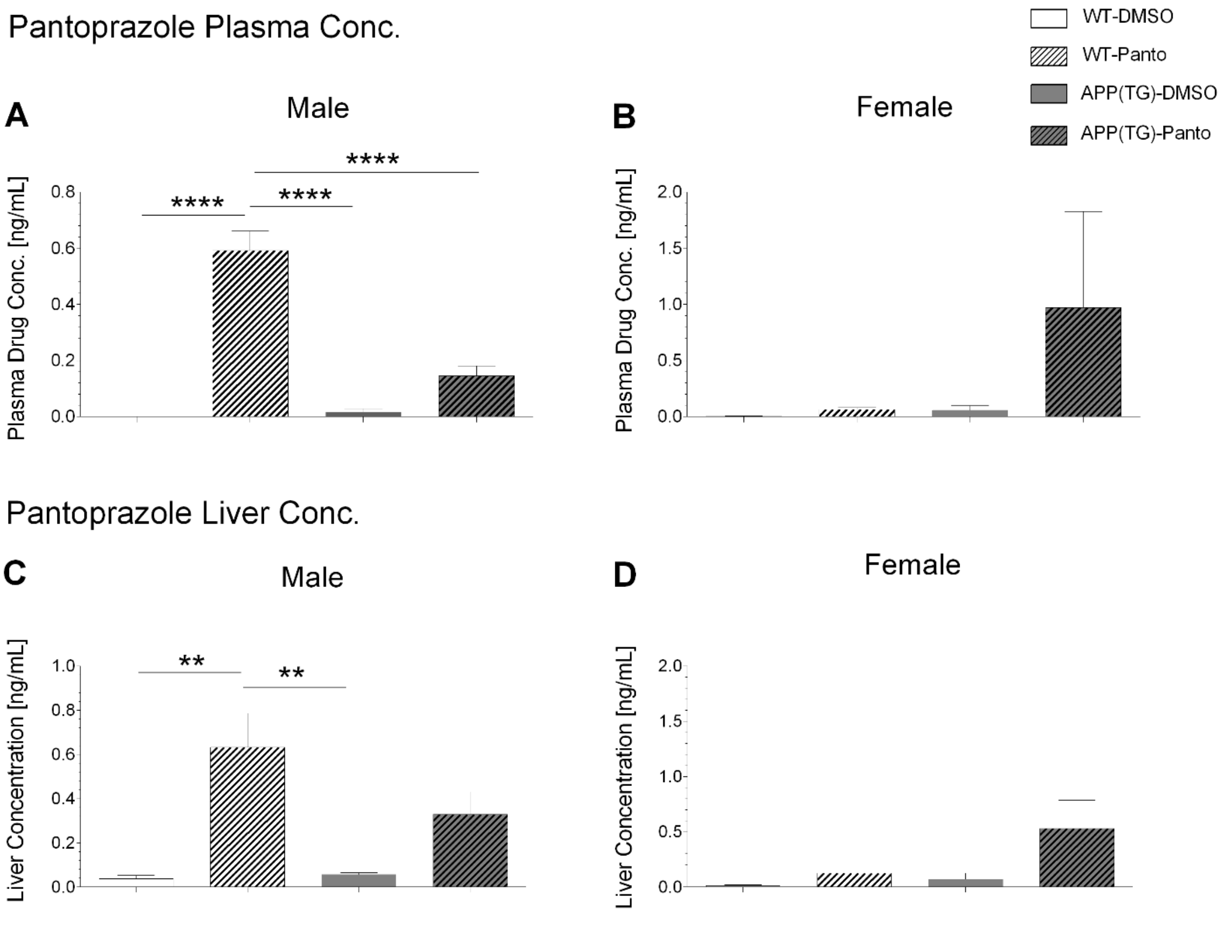

**Figure 4.2.30: (A) pantoprazole plasma concentration in male subgroups; (B) pantoprazole plasma concentration in female subgroups; (C) pantoprazole liver concentration in male subgroups; (D) pantoprazole liver concentration in female subgroups**. $*p < 0.05$; $**p < 0.01$; $***p < 0.001$; $****p < 0.0001$.

#### 4.2.4.4. Pantoprazole metabolite analysis

#### Human liver microsome incubation

Human liver microsome (HLM) incubation analysis was performed for qualitative analysis of pantoprazole metabolites in order to investigate the metabolic tendency of the mice. With regards to the parent ion masses and deduced fragmentation pattern, Pantoprazolesulfane and pantoprazolesulfone were the two major pantoprazole metabolites detected (Fig. 4.2.31). Unfortunately, no reference substances were available to confirm the nature of the metabolites. In prior experiments, additional metabolites like Desmethylpantoprazole and Desmethylpantoprazolesulfate have been confirmed, but did not occur in the here presented HLM approach. Therefore, the calculated ratios and semi-quantitative metabolic results should be interpreted carefully.

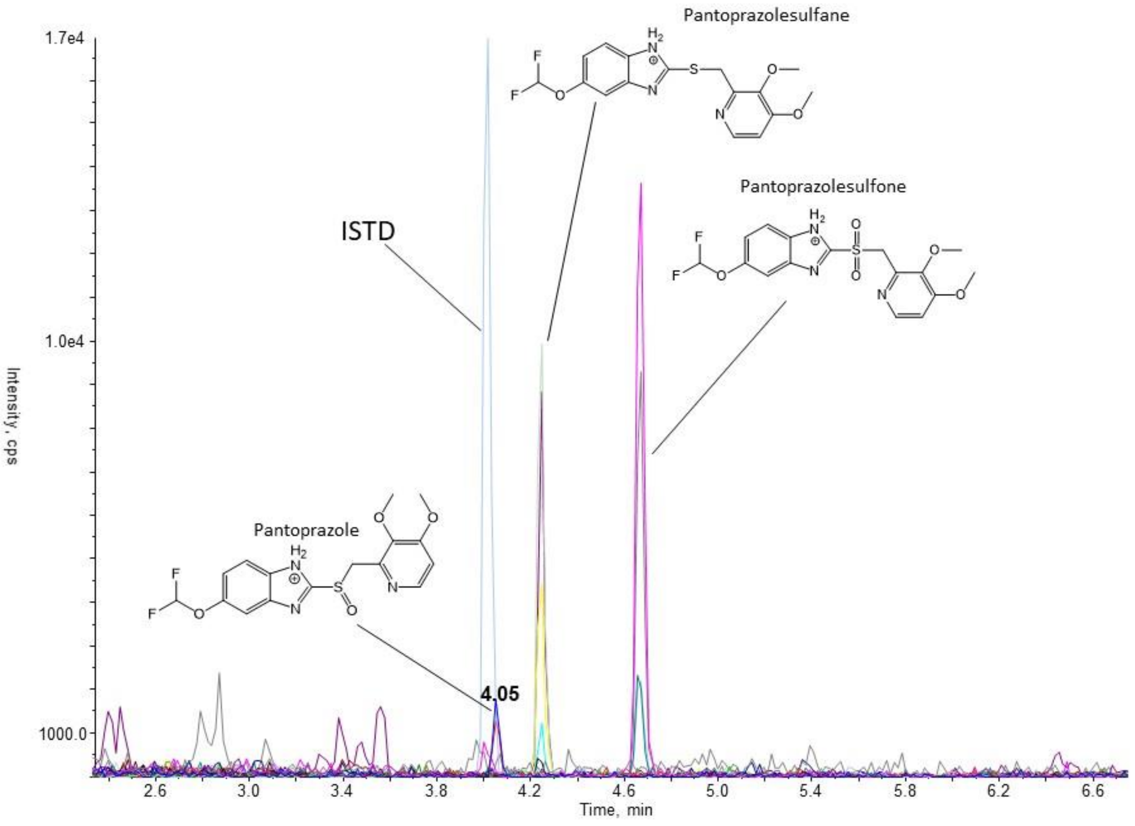

**Figure 4.2.31: Extracted ion chromatogram of (+) MRM from liver tissue lysate.**

**Semi-quantitative metabolic estimation of mice for pantoprazole**

Additionally, plasma and liver pantoprazole, pantoprazolesulfane and pantoprazolesulfone area ratios were measured and statistically analyzed. (Fig. 4.2.32).

Pantoprazolesulfone liver area ratio was significant higher compared to pantoprazole and pantoprazolesulfane in both male and female mice. As expected, higher metabolite amounts were observed in the liver samples, rather in the plasma samples. Pantoprazolesulfone was the most intense one. The presence of metabolites is one factor, which can explain the low content of pantoprazole in female mice. All semi-quantitative statistical calculations in figure 4.2.32 have been made with the assumption of identical ionization tendency of pantoprazole, pantoprazolesulfane and pantoprazolesulfone during the LC-MS measurement.

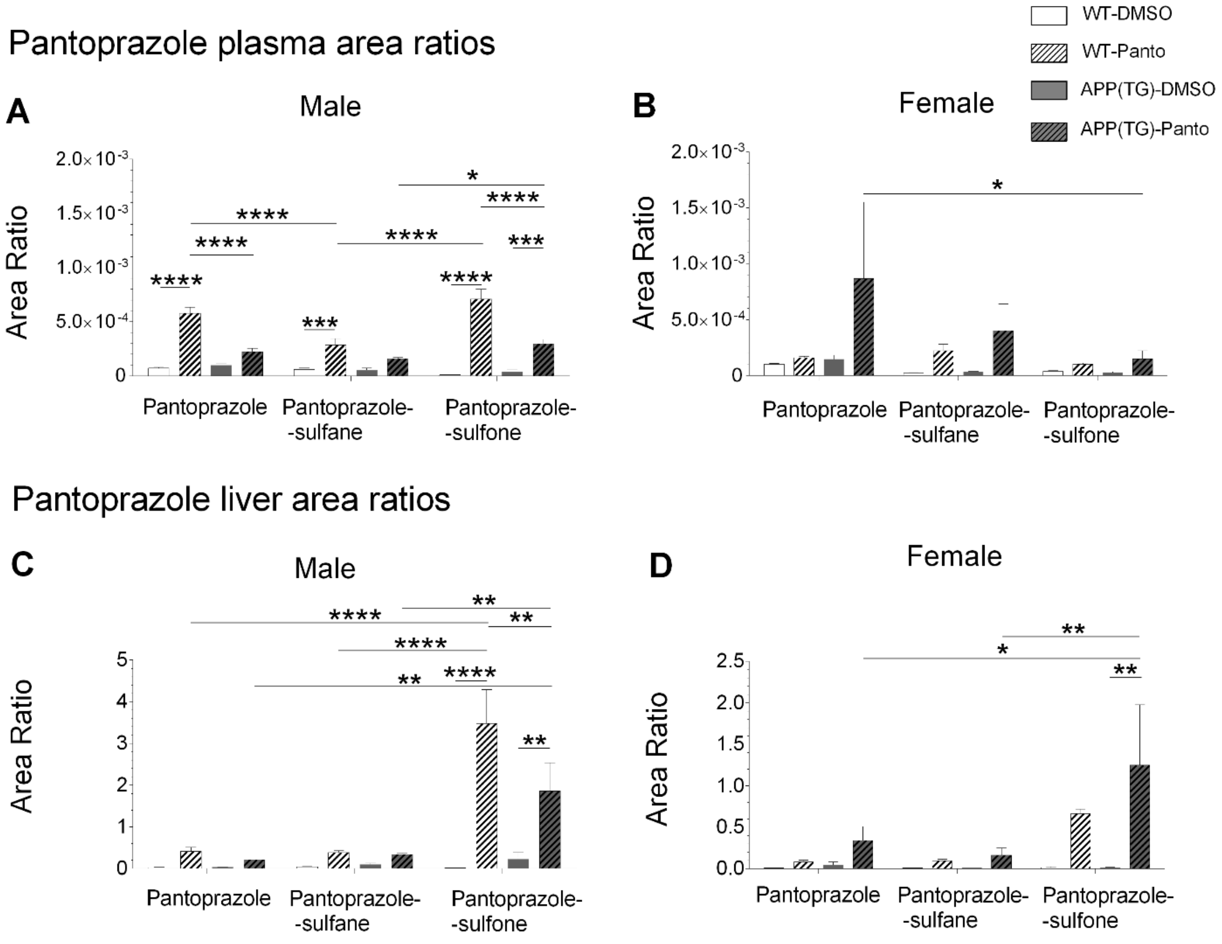

**Figure 4.2.32: Pantoprazole, pantoprazolesulfane and pantoprazolesulfone area ratios with deuterated-pantoprazole in** (A) plasma of male mice groups; (B) female mice groups; (C) in liver tissues of male mice groups; (D) in liver tissues of female mice groups. $*p < 0.05$; $**p < 0.01$; $***p < 0.001$; $****p < 0.0001$.

# 4.3. The effect of Pantoprazole in APPswePS1dE9 mice 17-21 weeks of age

## 4.3.1. Activity analysis in male mice

### 4.3.1.1. Baseline recordings

No significant differences in mean relative activity (units) were observed between all study groups (WT-DMSO vs. WT-Panto vs. APP(TG)-DMSO vs. APP(TG)-Panto) and all five recordings (at 17, 18, 19, 20 and 21 weeks of age) during the dark and light cycles (Fig. 4.3.1A,B).

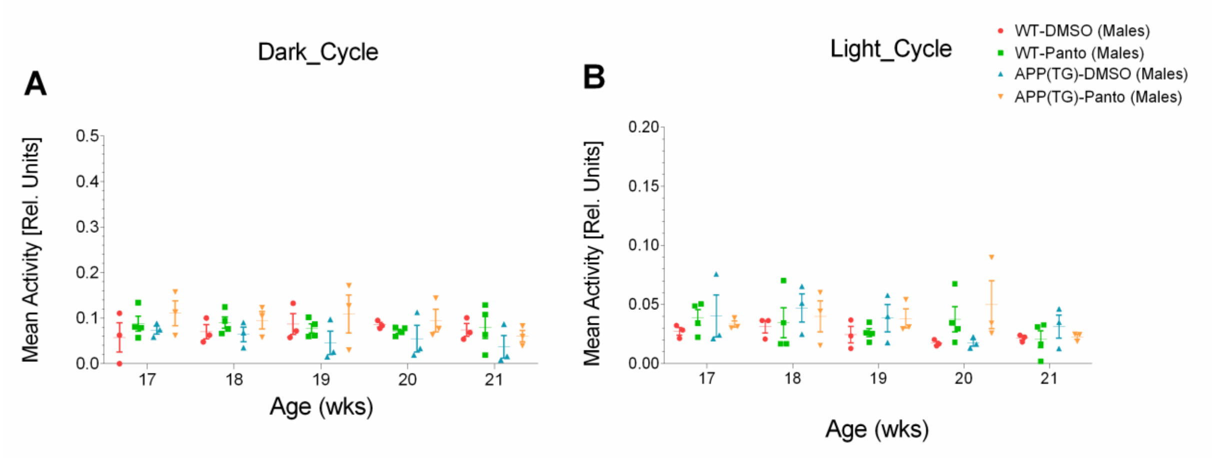

**Figure 4.3.1: Mean relative activity (units) in WT-DMSO, WT-Panto, APP(TG)-DMSO and APP(TG)-Panto male mice groups during the dark/light cycle.**

### 4.3.1.2. Post-urethane and post-atropine analysis

A significant increase in mean relative activity (units) was observed between WT-Panto and WT-DMSO mice during baseline (1 h) recording (WT-DMSO, n = 3: 0.006 ± 0.003 vs. WT-Panto, n = 4: 0.008 ± 0.003; p = 0.0002). Likewise, a significant increase was also detected in APP(TG)-DMSO and APP(TG)-Panto groups compared to WT-Panto group during baseline (1 h) recording (WT-Panto, n = 4: 0.008 ± 0.003 vs. APP(TG)-DMSO, n = 3: 0.024 ± 0.014; p = 0.0003) (WT-Panto, n = 4: 0.008 ± 0.003 vs. APP(TG)-Panto, n = 3: 0.028 ± 0.009; p < 0.0001).

Furthermore, an increase in mean relative activity (units) was identified in APP(TG)-Panto compared to WT-Panto at post-normal saline (1 h) recording (WT-Panto, n = 4: 0.038 ± 0.001 vs. APP(TG)-Panto, n = 3: 0.046 ± 0.028; p = 0.019). In addition, a significant increase in mean relative activity (units) was observed in APP(TG)-DMSO and APP(TG)-Panto mice compared to WT-Panto mice during post-atropine (3 h) recording (WT-Panto, n = 4: 0.0007 ± 0.0003 vs. APP(TG)-DMSO, n = 3: 0.003 ± 0.003; p = 0.0468) (WT-Panto, n = 4: 0.0007 ± 0.0003 vs. APP(TG)-Panto, n = 3: 0.002 ± 0.001; p = 0.0132). Moreover, a significant increase in post-urethane (1 h) compared to baseline (1 h) recordings for the WT-Panto mice (baseline (1 h), n = 4: 0.008 ± 0.003 vs. post-urethane (1 h), n = 4: 0.013 ± 0.004; p = 0.0007).

A statistical trend was detected between WT-DMSO and WT-Panto during post-normal saline (1 h) recording (WT-DMSO, n = 3: 0.071 ± 0.007 vs. WT-Panto, n = 4: 0.038 ± 0.013; p = 0.0823). Additionally, a statistical trend was also identified during post-normal saline (1 h) compared to baseline (1 h) and post-urethane (1 h) compared to post-atropine (3 h) recordings for the WT-Panto group (baseline, n = 4: 0.008 ± 0.003 vs. post-normal saline, n = 4: 0.038 ± 0.013; p = 0.0624) (post-urethane, n = 4: 0.013 ± 0.004 vs. post-atropine, n = 4: 0.0007 ± 0.0003; p = 0.0717). However, no significant differences in mean relative activity (units) were observed between all other study groups (Fig. 4.3.2).

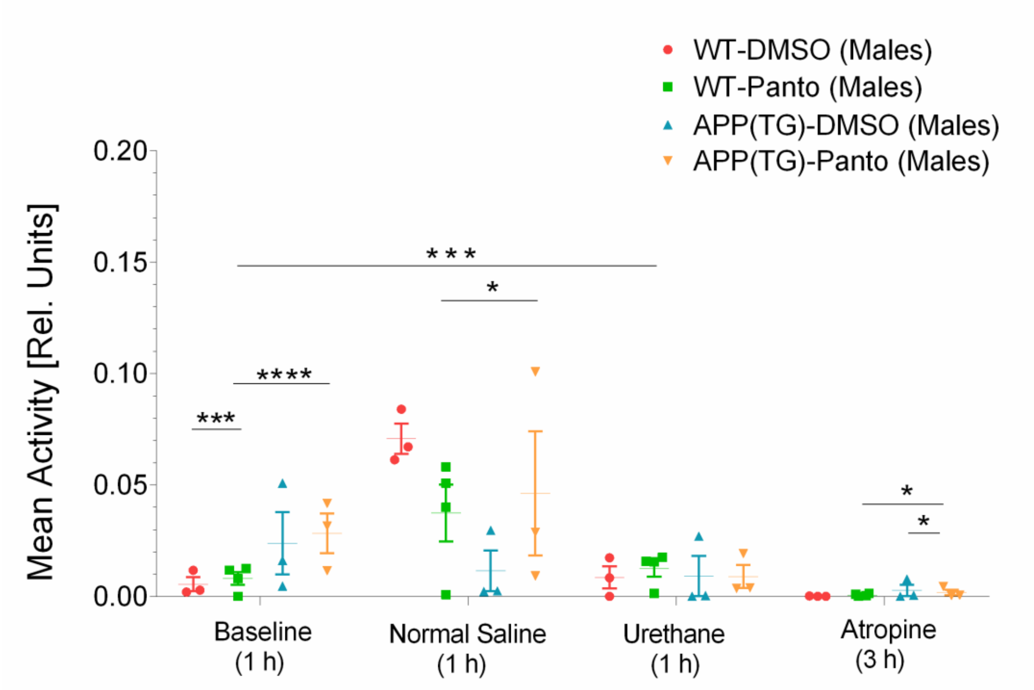

**Figure 4.3.2: Mean relative activity (units) of WT-DMSO, WT-Panto, APP(TG)-DMSO and APP(TG)-Panto male mice groups is presented for baseline (1 h), post-normal saline (1 h), post-urethane (1 h) and post-atropine (3 h) recordings**. $*p < 0.05$; $**p < 0.01$; $***p < 0.001$.

## 4.3.2. Temperature analysis

### 4.3.2.1. Baseline recordings

Dark cycle

No significant differences in temperature (°C) were identified between all study groups (Fig. 4.3.3A).

Light Cycle

A significant increase in temperature (°C) was observed in APP(TG)-DMSO compared to WT-Panto at 19 weeks of age (WT-Panto, n = 4: 32.854 ± 0.238 vs. APP(TG)-DMSO, n = 3: 34.412 ± 0.366; p = 0.0207). However, a statistical trend was detected in temperature (°C) analysis between 17 weeks and 21 weeks of age for the WT-Panto mice (17 weeks, n = 4: 33.751 ± 0.306 vs. 21 weeks, n = 4: 32.455 ± 0.172; p = 0.0669).

No significant differences in temperature (°C) were identified between all other study groups (Fig. 4.3.3B).

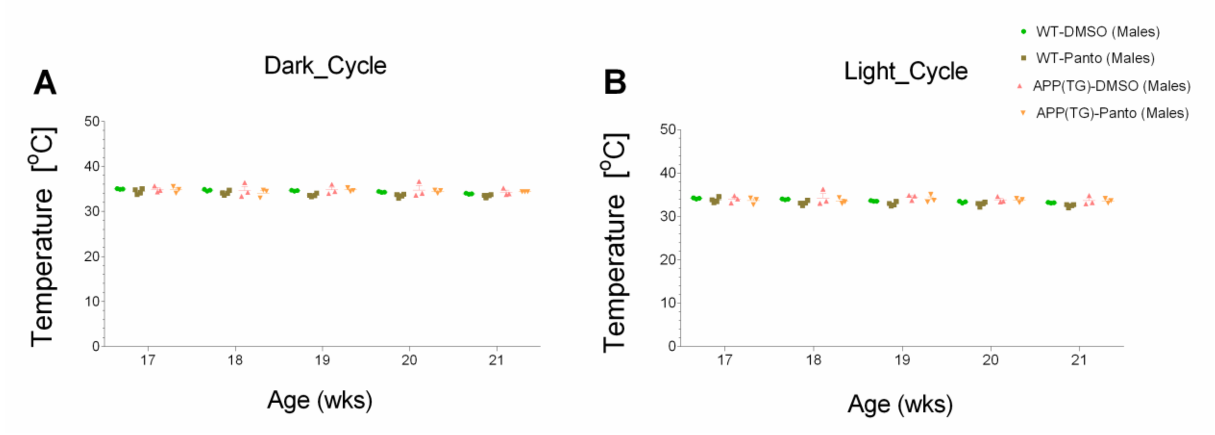

**Figure 4.3.3: Temperature (°C) analysis of WT-DMSO, WT-Panto, APP(TG)-DMSO, APP(TG)-Panto male mice groups during the dark/light cycle.** $*p < 0.05$; $**p < 0.01$; $***p < 0.001$.

### 4.3.2.2. Post-urethane and post-atropine recordings

A significant increase in temperature (°C) was observed in APP(TG)-Panto group compared to WT-DMSO, WT-Panto and APP(TG)-DMSO groups during baseline (1 h) recording (WT-DMSO, n = 3: 33.088 ± 0.201 vs. APP(TG)-Panto, n = 3: 33.585 ± 0.297; p = 0.0003) (WT-Panto, n = 4: 32.478 ± 0.390 vs. APP(TG)-Panto, n = 3: 33.585 ± 0.297; p < 0.0001) (APP(TG)DMSO, n = 3: 32.986 ± 1.260 vs. APP(TG)-Panto, n = 3: 33.585 ± 0.297; p = 0.0016). Furthermore, a significant increase in temperature (°C) was detected in APP(TG)-Panto mice compared to WT-DMSO, WT-Panto and APP(TG)-DMSO mice during post-urethane (1 h) recording (WT-DMSO, n = 3: 32.414 ± 1.162 vs. APP(TG)-Panto, n = 3: 33.401 ± 0.442; p = 0.0075) (WT-Panto, n = 4: 32.168 ± 0.320 vs. APP(TG)-Panto, n = 3: 33.401 ± 0.442; p = 0.0002) (APP(TG)-DMSO, n = 3: 33.209 ± 0.433 vs. APP(TG)-Panto, n = 3: 33.401 ± 0.442; p = 0.0045).

Additionally, a significant increase was observed during post-normal saline (1 h) compared to baseline (1 h) recordings for the APP(TG)-Panto mice (baseline, n = 3: 33.585 ± 0.297 vs. post-normal saline, n = 3: 33.836 ± 0.225; p = 0.0143). Similarly, a significant difference was also detected during baseline (1 h) compared to post-atropine (3 h) recordings for the APP(TG)-Panto group (baseline, n = 3: 33.585 ± 0.297 vs. post-atropine (3 h), n = 3: 31.759 ± 1.055; p = 0.0076). However, a statistical trend was observed between post-urethane (1 h) compared to post-atropine (3 h) recordings for the APP(TG)-Panto group (post-urethane, n = 3: 33.401 ± 0.442 vs. post-atropine, n = 3: 31.759 ± 1.055; p = 0.0927).

No significant differences in temperature (°C) were detected between all other study groups (Fig. 4.3.4).

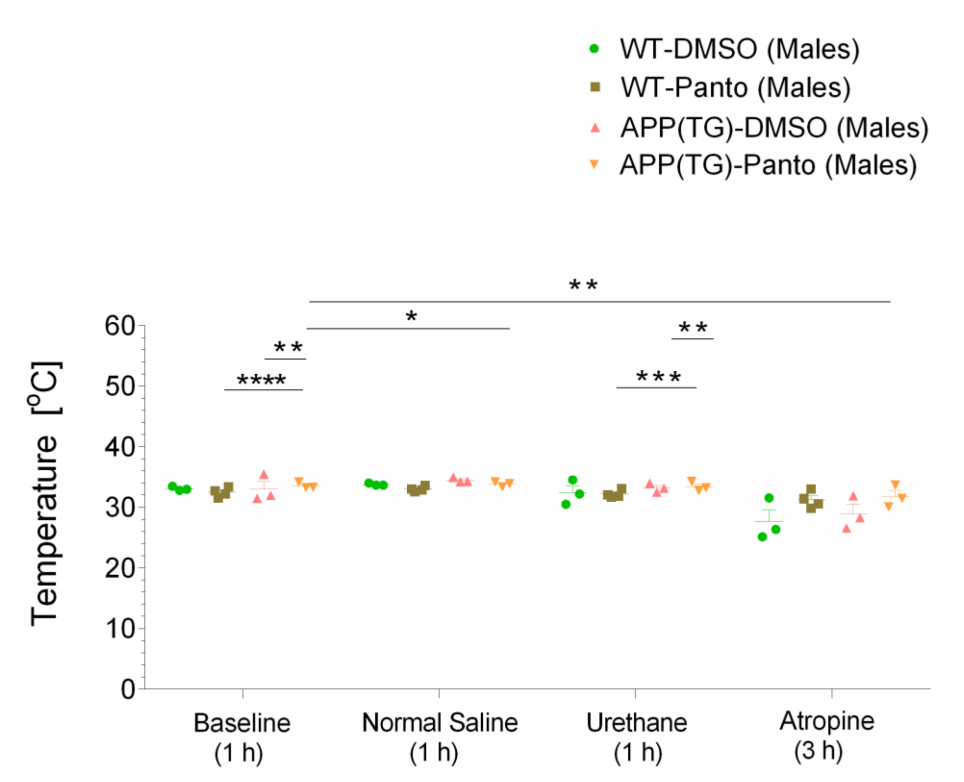

**Figure 4.3.4: Temperature (°C) analysis of WT-DMSO, WT-Panto, APP(TG)-DMSO and APP(TG)-Panto male mice groups is presented for baseline (1 h), post-normal saline (1 h), post-post-urethane (1 h) and post-atropine (3 h) recordings.** $*p < 0.05$; $**p < 0.01$; $***p < 0.001$.

### 4.3.3. FFT based EEG frequency analysis in male mice

The Fast-Fourier-Transformation (FFT) based EEG frequency analysis was performed for wild-type controls (WT-DMSO and WT-Panto) and APPswePS1dE9 (APP(TG)-DMSO and APP(TG)-Panto) subgroups based on the EEG recordings from the hippocampal CA1 and motor cortex M1 regions of male mice.

### Theta 1 ($\theta_1$: 4-8 Hz)

### i) Hippocampal CA1 region

Dark cycle

A significant increase in relative theta 1 power was observed in WT-DMSO compared to APP(TG)-DMSO mice at 21 weeks of age (WT-DMSO, n = 3: 30.625 ± 2.322% vs. APP(TG)-DMSO, n = 3: 22.843 ± 2.734%; p = 0.0313).

No significant differences in relative theta power were detected between all other study groups (Fig. 4.3.5A).

Light cycle

No significant differences in relative theta 1 power were identified between all study groups (Fig. 4.3.5B).

### ii) Motor cortical M1 region

Dark cycle

A statistical trend in relative theta 1 power was observed between WT-Panto and APP(TG)-Panto mice at 20 weeks of age (WT-Panto, n = 4: 30.313 ± 1.825% vs. APP(TG)-Panto, n = 3: 23.373 ± 1.462%; p = 0.0766). Additionally, a statistical trend was detected between WT-Panto and APP(TG)-DMSO groups at 21 weeks of age (WT-Panto, n = 4: 28.630 ± 1.366% vs. APP(TG)-DMSO, n = 3: 21.876 ± 3.471%; p = 0.0886).

No significant differences in relative theta power were identified between all other study groups (Fig. 4.3.5C).

Light cycle

A statistical trend in relative theta 1 power was observed between WT-Panto compared to APP(TG)-DMSO mice at 20 weeks of age (WT-Panto, n = 4: 30.138 ± 1.253% vs. APP(TG)-DMSO, n = 3: 23.835 ± 6.004%; p = 0.0789).

No significant differences in relative theta 1 power were detected between all other study groups (Fig. 4.3.5D).

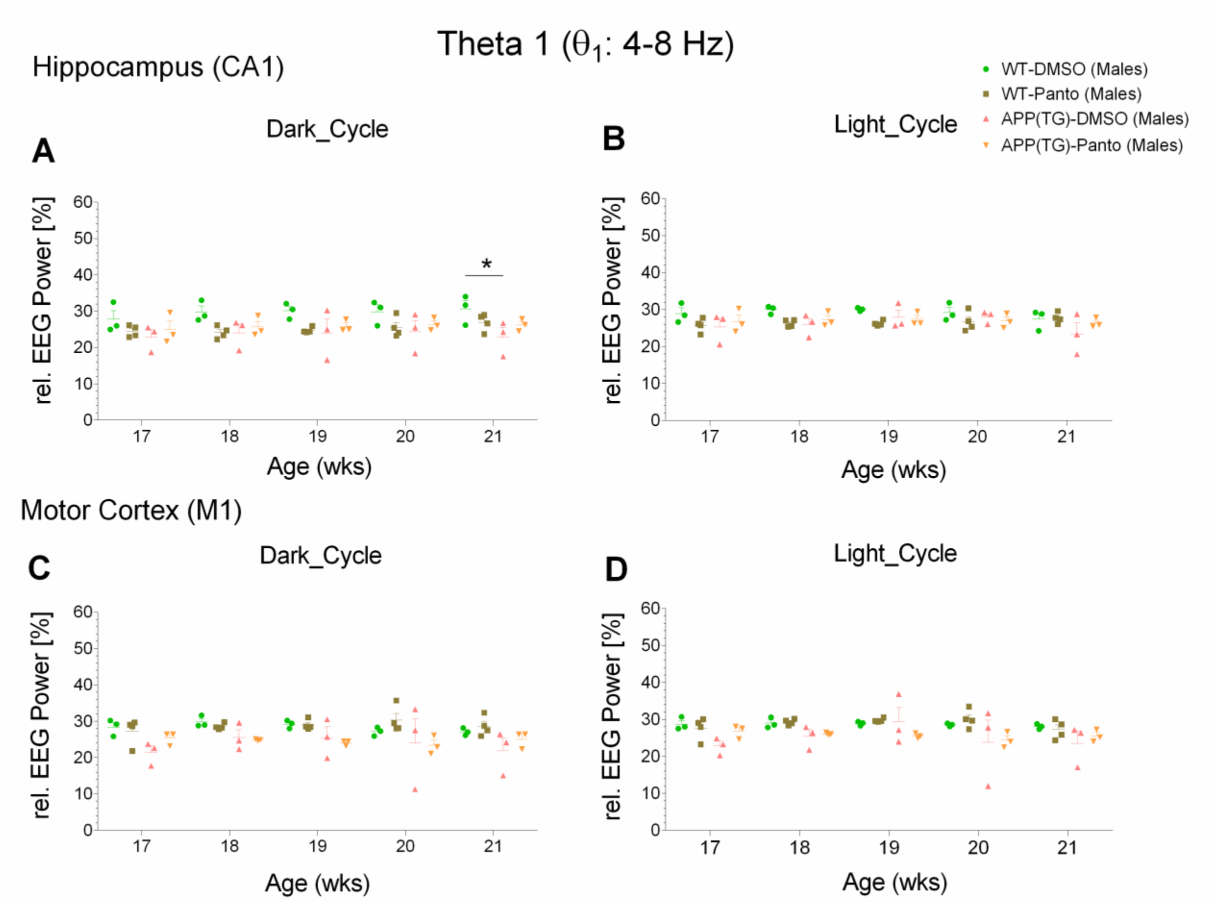

**Figure 4.3.5: Hippocampus (CA1) (A,B) and motor cortex (M1) (C,D) relative theta 1 power (%) ($\theta_1$: 4-8 Hz) in WT-DMSO, WT-Panto, APP(TG)-DMSO, and APP(TG)-Panto male mice.** Results are depicted considering the circadian rhythmicity (dark/light cycle). $^{*}$ $p < 0.05$; $^{**}$ $p < 0.01$; $^{***}$ $p < 0.001$.

### Theta 2 ($\theta_2$: 4.1-12 Hz):

### i) Hippocampal CA1 region

Dark cycle

A statistical trend in relative theta 2 power was observed between WT-DMSO and APP(TG)-DMSO mice at 19 weeks of age (WT-DMSO, n = 3: 47.768 ± 1.217% vs. APP(TG)-DMSO, n = 3: 36.751 ± 7.435%; p = 0.0662).

No significant differences in relative theta 2 power were identified between all other study groups (Fig. 4.3.6A).

Light cycle

A significant increase in relative theta 2 power was observed in WT-Panto compared to APP(TG)-DMSO mice at 21 weeks of age (WT-Panto, n = 4: 41.727 ± 1.594% vs. APP(TG)-DMSO, n = 3:

34.100 ± 5.368%; p = 0.0323). Furthermore, a significant increase was observed in 18 weeks and 19 weeks compared to 21 weeks of age for the WT-DMSO group (18 weeks, n = 3: 45.625 ± 1.450% vs. 21 weeks, n = 3: 36.727 ± 1.845%; p = 0.0258) (19 weeks, n = 3: 45.519 ± 1.356% vs. 21 weeks, n = 3: 36.727 ± 1.845%; p = 0.0283).

A statistical trend in relative theta 2 power was identified between 17 weeks compared to 21 weeks of age for the WT-DMSO mice (17 weeks, n = 3: 44.719 ± 0.626% vs. 21 weeks, n = 3: 36.727 ± 1.845%; p = 0.0564). Additionally, a statistical trend was detected between 19 weeks and 21 weeks of age for the APP(TG)-DMSO group (19 weeks, n = 3: 42.044 ± 2.975% vs. 21 weeks, n = 3: 34.100 ± 5.368%; p = 0.0587). Likewise, a statistical trend was observed between 20 weeks and 21 weeks of age for the APP(TG)-DMSO mice (20 weeks, n = 3: 42.148 ± 0.768% vs. 21 weeks, n = 3: 34.100 ± 5.368%; p = 0.0538).

However, no significant differences in relative theta 2 power were observed between all other analyzed groups (Fig. 4.3.6B).

### ii) Motor cortical M1 region

No significant differences in relative theta 2 power were observed between all study groups analyzed from motor cortical M1 region during both dark and light cycles (Fig. 4.3.6C,D).

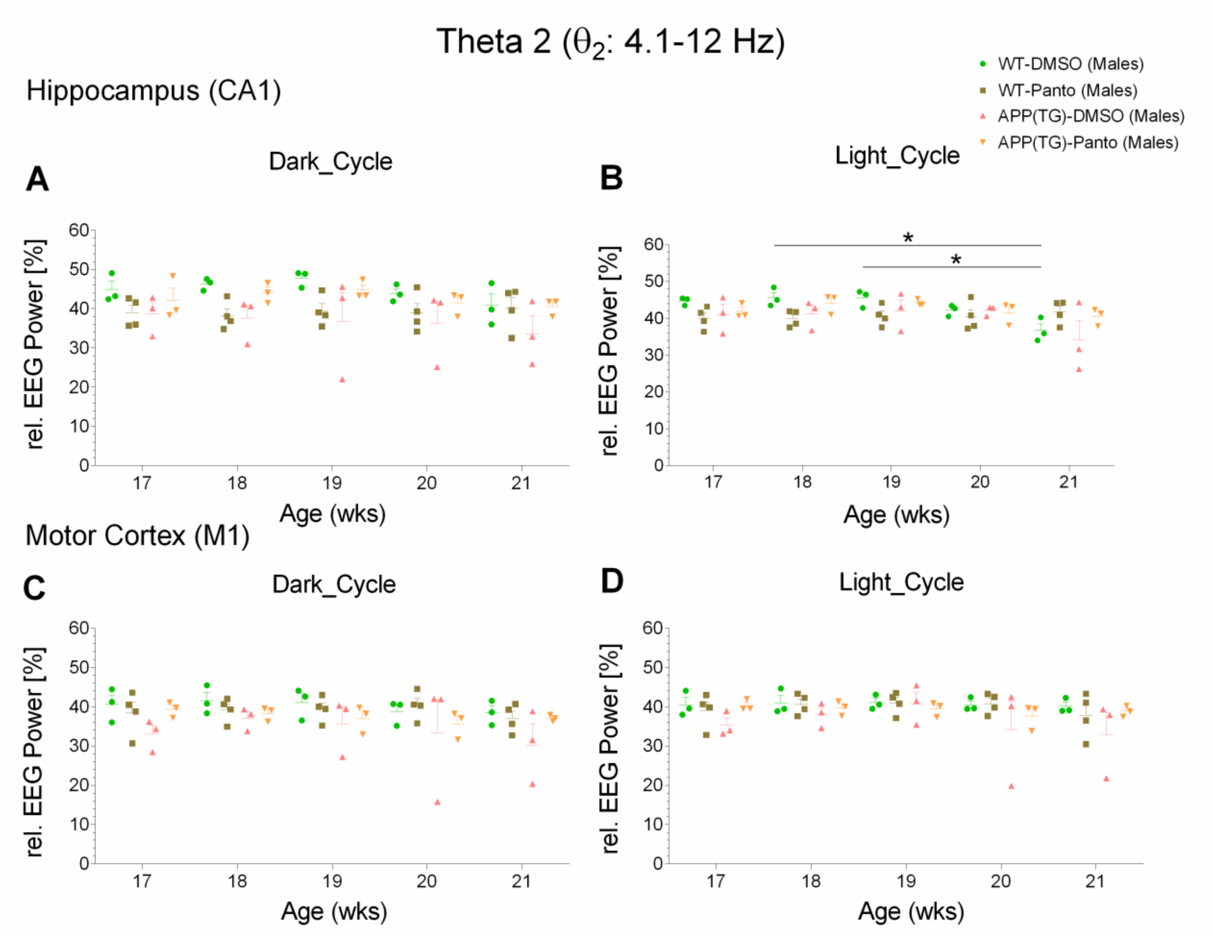

**Figure 4.3.6: Hippocampus (CA1) (A,B) and motor cortex (M1) (C,D) relative theta 2 power (%) ($\theta_2$: 4.1-12 Hz) in WT-DMSO, WT-Panto, APP(TG)-DMSO, and APP(TG)-Panto male mice.** Results are depicted considering the circadian rhythmicity (dark/light cycle). $^{*}$ $p < 0.05$; $^{**}$ $p < 0.01$; $^{***}$ $p < 0.001$.

### Delta (δ: 0.5-4 Hz)

No significant differences in relative delta power were observed between all study groups analyzed from hippocampal CA1 and motor cortical M1 regions during both dark and light cycles (Fig. 4.3.7).

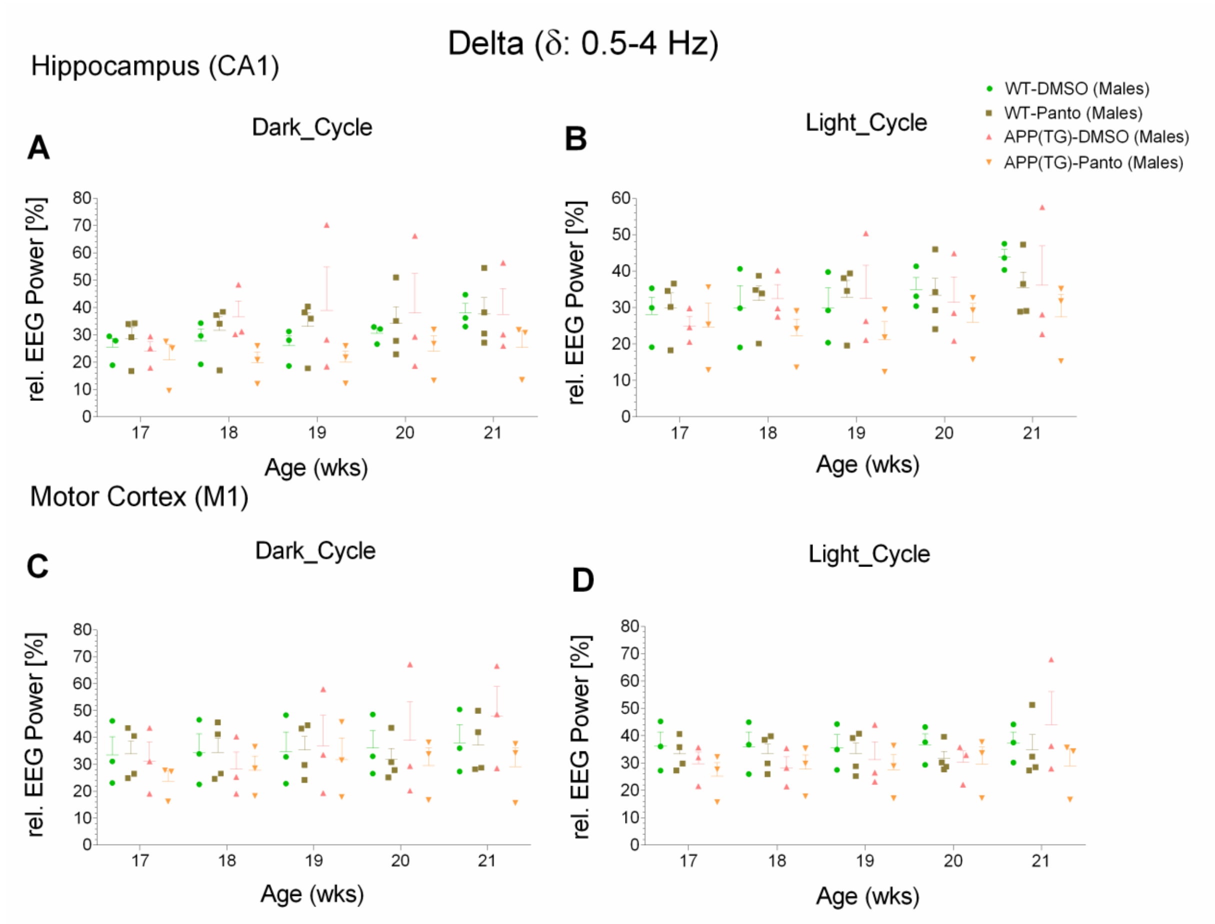

**Figure 4.3.7: Hippocampus (CA1) (A,B) and motor cortex (M1) (C,D) relative delta power (%) (δ: 0.5-4 Hz) in WT-DMSO, WT-Panto, APP(TG)-DMSO and APP(TG)-Panto male mice.** Results are depicted considering the circadian rhythmicity (dark/light cycle). $^{*}p < 0.05$; $^{**}p < 0.01$; $^{***}p < 0.001$.

### Beta 1 ($\beta_1$: 12.1-30 Hz)

### i) Hippocampal CA1 region

Dark cycle

No significant differences in relative beta 1 power were identified between all study groups (Fig. 4.3.8A).

Light cycle

A statistical trend in relative beta 1 power was observed between APP(TG)-Panto compared to WT-DMSO mice at 21 weeks of age (WT-DMSO, n = 3: 11.701 ± 0.205% vs. APP(TG)-Panto, n = 3: 21.023 ± 3.886%; p = 0.0889).

No significant differences in relative beta 1 power were detected between all other study groups (Fig. 4.3.8B).

**ii) Motor cortical M1 region**

No significant differences in relative beta 1 power were detected between all study groups analyzed from motor cortical M1 region during both dark and light cycles (Fig. 4.3.8C,D).

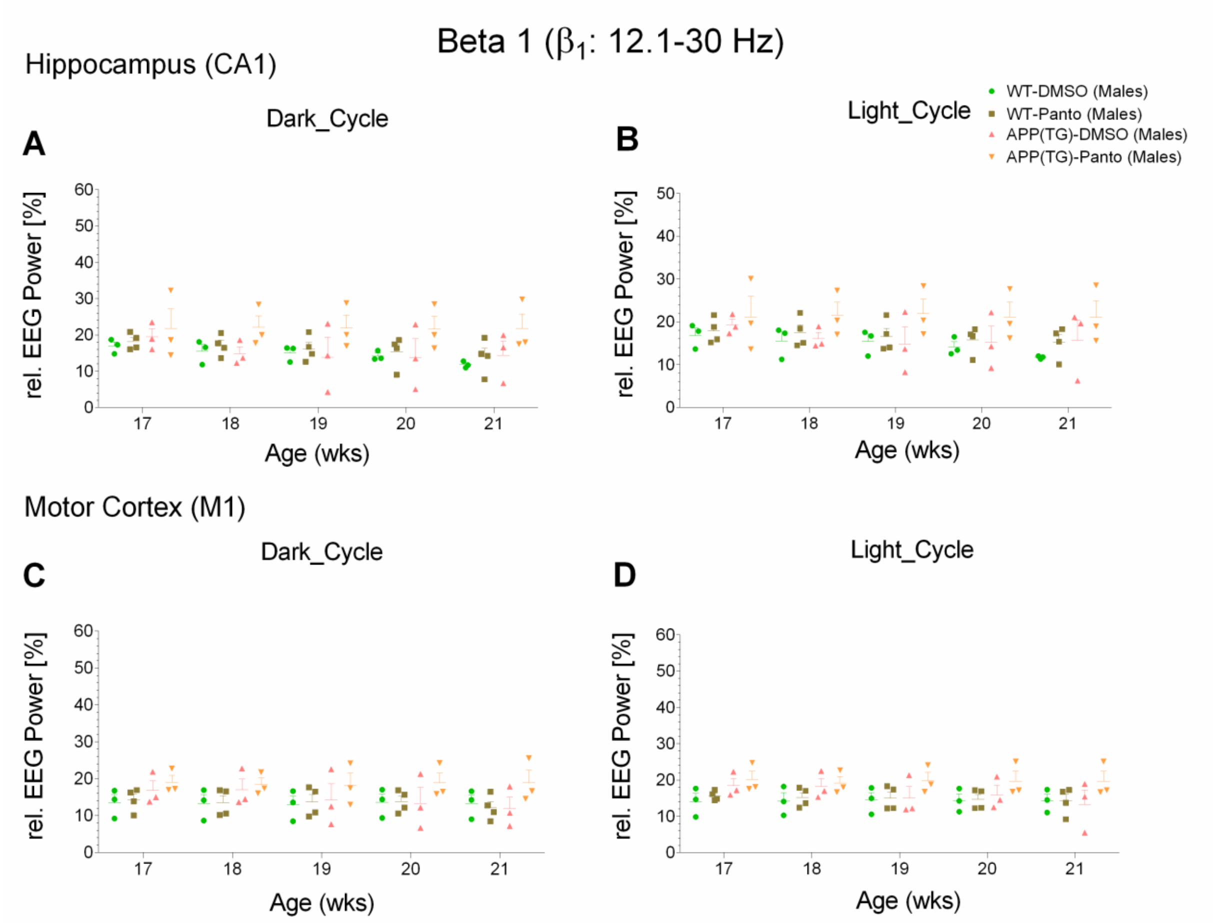

**Figure 4.3.8: Hippocampus (CA1) (A,B) and motor cortex (M1) (C,D) relative beta 1 power (%) ($\beta_1$: 12.1-30 Hz) in WT-DMSO, WT-Panto, APP(TG)-DMSO and APP(TG)-Panto male mice.** Results are depicted considering the circadian rhythmicity (dark/light cycle). $^{*}$ $p < 0.05$; $^{**}$ $p < 0.01$; $^{***}$ $p < 0.001$.

**Beta 2 ($\beta_2$: 16-24 Hz)**

No significant differences in relative beta 2 power were identified between all study groups analyzed from hippocampal CA1 and motor cortical M1 regions during both dark and light cycles (Fig. 4.3.9).

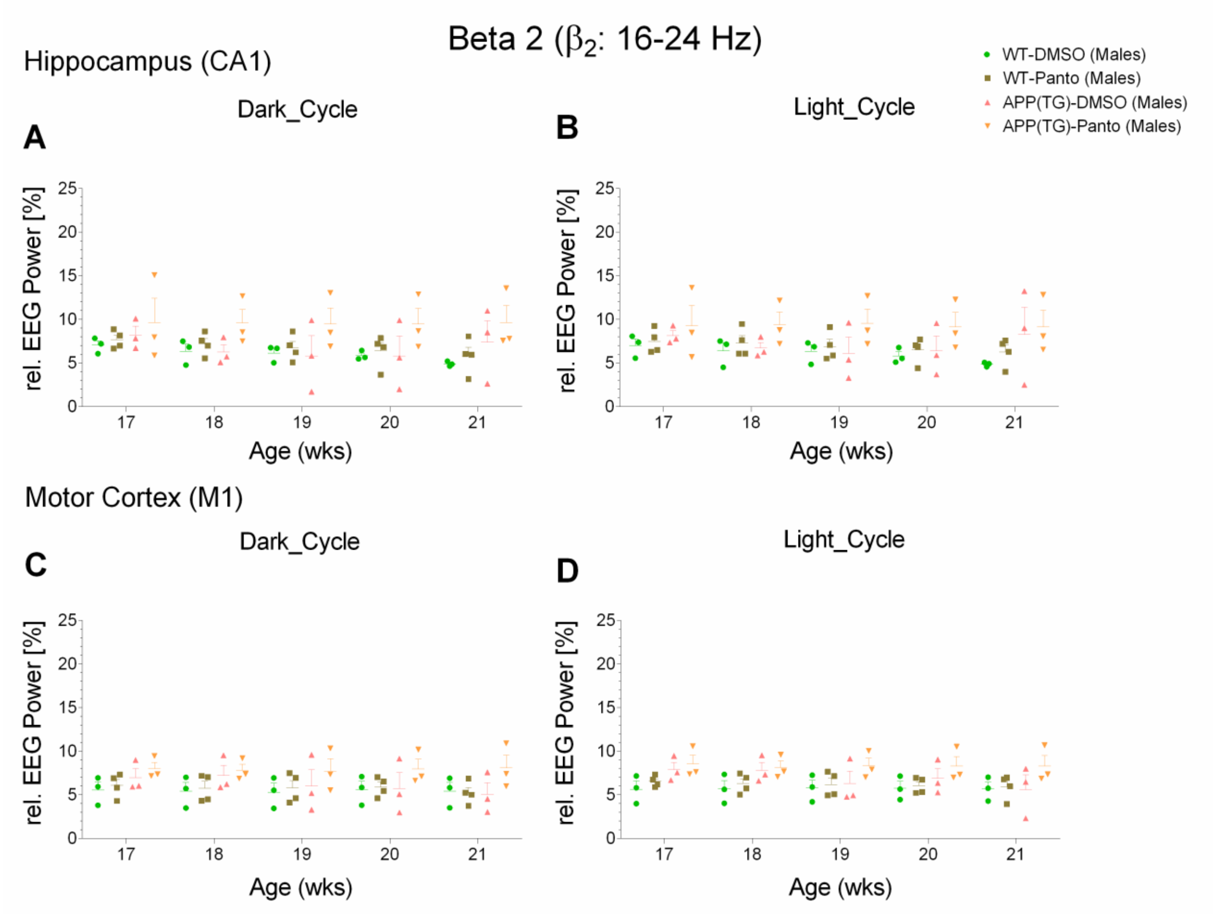

**Figure 4.3.9: Hippocampus (CA1) (A,B) and motor cortex (M1) (C,D) relative beta 2 power (%) ($\beta_2$: 16-24 Hz) in WT-DMSO, WT-Panto, APP(TG)-DMSO and APP(TG)-Panto male mice.** Results are illustrated considering the circadian rhythmicity (dark/light cycle). $^{*}$ $p < 0.05$; $^{**}$ $p < 0.01$; $^{***}$ $p < 0.001$.

### Beta 3 ($\beta_3$: 16-30 Hz)

No significant differences in relative beta 3 power were detected between all study groups analyzed from hippocampal CA1 and motor cortical M1 regions during both dark and light cycles (Fig. 4.3.10).

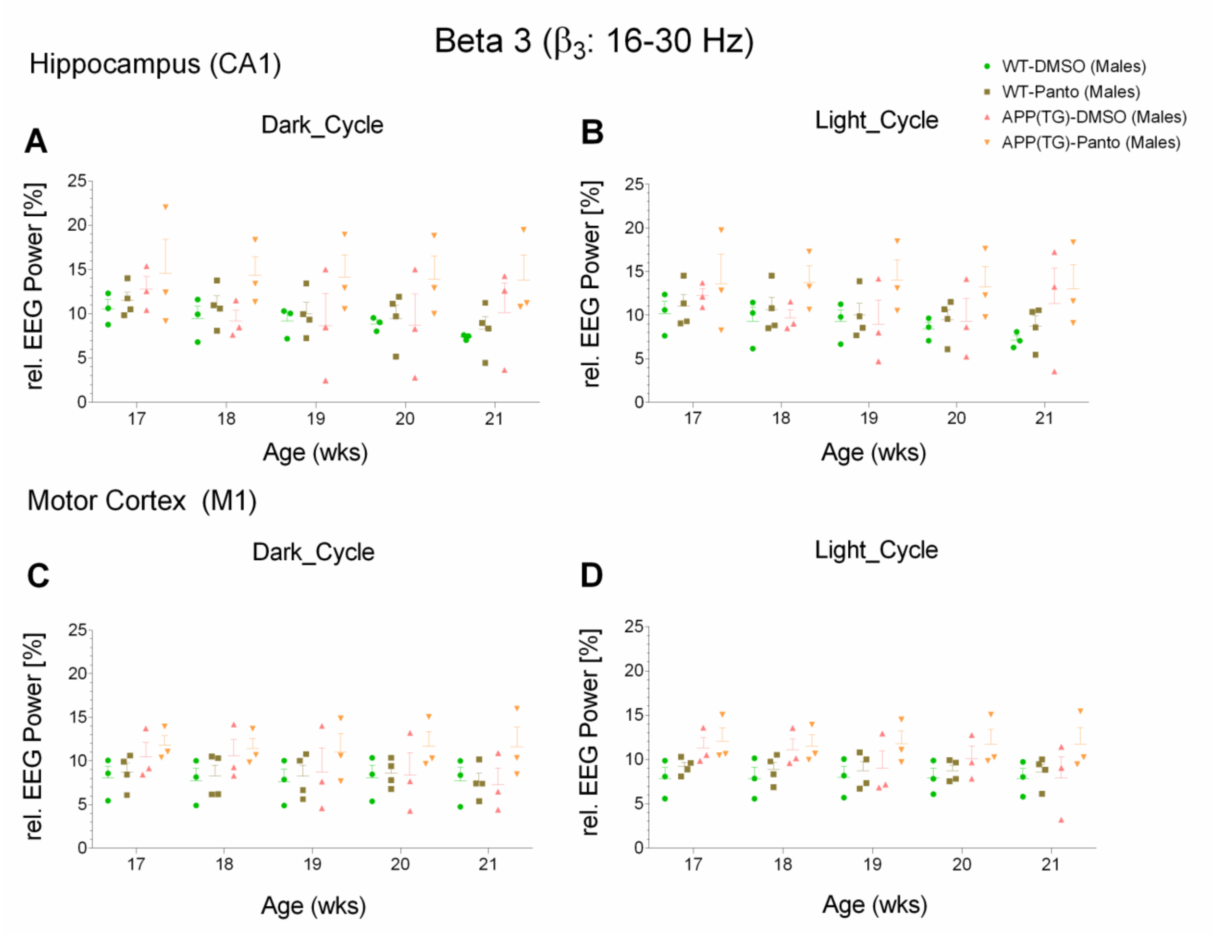

**Figure 4.3.10: Hippocampus (CA1) (A,B) and motor cortex (M1) (C,D) relative beta 3 power (%) (β3: 16-30 Hz) in WT-DMSO, WT-Panto, APP(TG)-DMSO and APP(TG)-Panto male mice.** Results are depicted considering the circadian rhythmicity (dark/light cycle). $^{*}$ $p < 0.05$; $^{**}$ $p < 0.01$; $^{***}$ $p < 0.001$.

### Alpha (α: 8-12 Hz)

### i) Hippocampal CA1 region

Dark cycle

A significant increase in relative alpha power was observed in 19 weeks compared to 21 weeks of age for the WT-DMSO mice (19 weeks, n = 3: 18.469 ± 0.431% vs. 21 weeks, n = 3: 11.399 ± 2.439%; p = 0.0317). A statistical trend in relative alpha power was detected between APP(TG)-Panto compared to APP(TG)-DMSO mice at 19 weeks of age (APP(TG)-DMSO, n = 3: 13.409 ± 3.840% vs. APP(TG)-Panto, n = 3: 19.417 ± 0.486%; p = 0.0625). Additionally, a statistical trend was also detected between 17 weeks and 21 weeks of age for the WT-DMSO groups (17 weeks, n = 3: 17.785 ± 0.207% vs. 21 weeks, n = 3: 11.399 ± 2.439%; p = 0.0646). However, no significant differences in relative alpha power were identified between all other analyzed groups (Fig. 4.3.11A).

Light cycle

A significant increase in relative alpha power was observed in WT-Panto compared to WT-DMSO mice at 21 weeks of age (WT-DMSO, n = 3: 10.392 ± 1.254% vs. WT-Panto, n = 4: 14.824 ± 1.017%; p = 0.0358). In addition, a significant increase was detected in 17 weeks, 18 weeks and 19 weeks of age compared to 21 weeks of age for the WT-DMSO group (17 weeks, n = 3: 16.502 ± 1.034% vs. 21 weeks, n = 3: 10.392 ± 1.254%; p = 0.0064) (18 weeks, n = 3: 16.450 ± 1.473% vs. 21 weeks, n = 3: 10.392 ± 1.254%; p = 0.007) (19 weeks, n = 3: 16.255 ± 1.291% vs. 21 weeks, n = 3: 10.392 ± 1.254%; p = 0.0096).

However, a statistical trend in relative alpha power was identified between APP(TG)-Panto and WT-DMSO mice at 21 weeks of age (WT-DMSO, n = 3: 10.392 ± 1.254% vs. APP(TG)-Panto, n = 3: 14.865 ± 1.364%; p = 0.0521). Additionally, a statistical trend was observed between 17 weeks compared to 21 weeks of age and 18 weeks compared to 21 weeks of age for the APP(TG)-DMSO mice respectively (17 weeks, n = 3: 16.263 ± 1.046% vs. 21 weeks, n = 3: 11.584 ± 2.330%; p = 0.059) (18 weeks, n = 3: 15.953 ± 0.562% vs. 21 weeks, n = 3: 11.584 ± 2.330%; p = 0.0897).

However, no significant differences in relative alpha power were detected between all other study groups (Fig. 4.3.11B).

**ii) Motor cortical M1 region**

No significant differences in relative alpha power were identified between all study groups analyzed from motor cortical M1 region during both dark and light cycles (Fig. 4.3.11C,D).

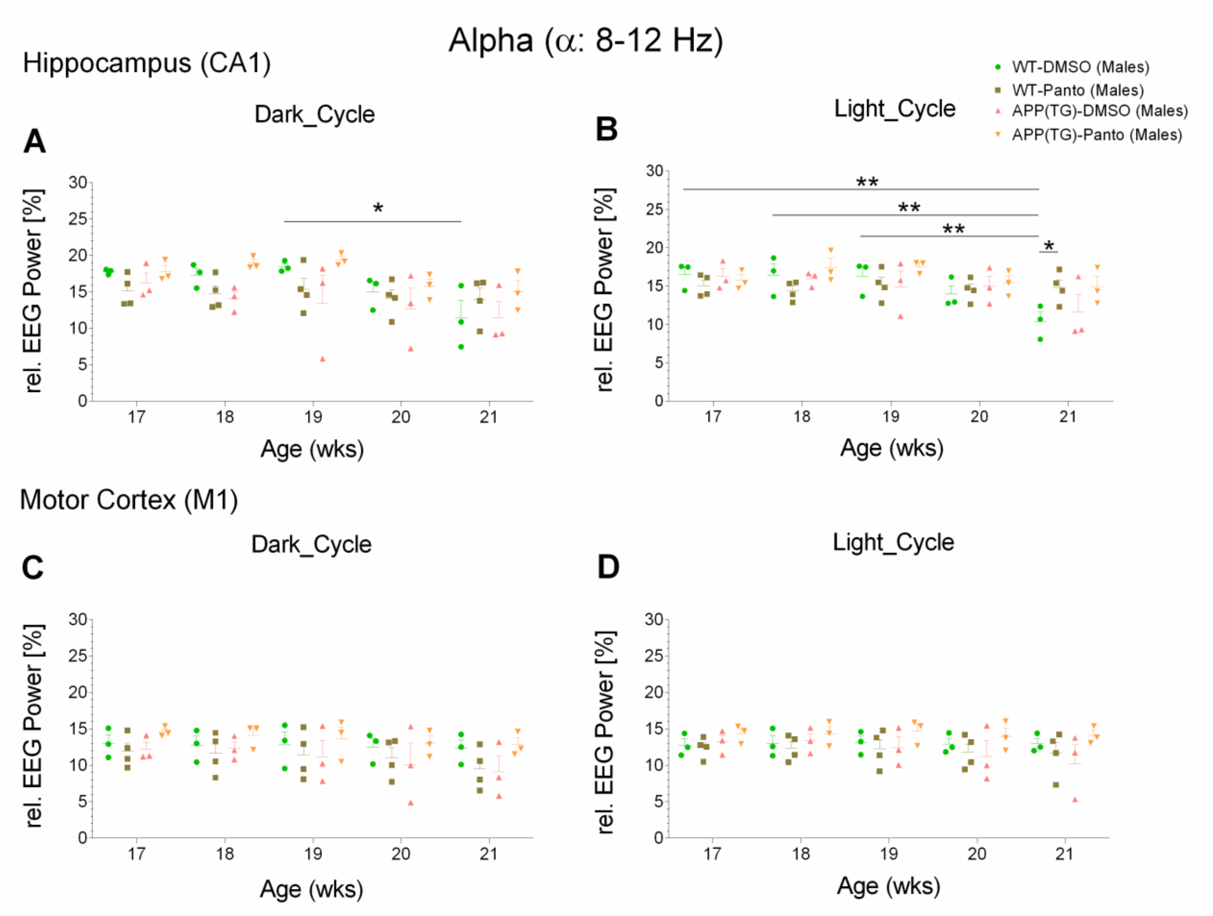

**Figure 4.3.11: Hippocampus (CA1) (A,B) and motor cortex (M1) (C,D) relative alpha power (%) (α: 8-12 Hz) in WT-DMSO, WT-Panto, APP(TG)-DMSO and APP(TG)-Panto male mice.** Results are depicted considering the circadian rhythmicity (dark/light cycle). $^{*}$ $p < 0.05$; $^{**}$ $p < 0.01$; $^{***}$ $p < 0.001$.

**Sigma (σ: 12-16 Hz)**

**i) Hippocampal CA1 region**

Dark cycle

A significant increase in relative sigma power was observed in APP(TG)-Panto compared to APP(TG)-DMSO mice at 21 weeks of age (APP(TG)-DMSO, n = 3: 4.413 ± 1.558% vs. APP(TG)-Panto, n = 3: 8.201 ± 1.231%; p = 0.0475). A statistical trend in relative sigma power was detected between APP(TG)-Panto and WT-DMSO at 21 weeks of age (WT-DMSO, n = 3: 4.607 ± 0.532% vs. APP(TG)-Panto, n = 3: 8.201 ± 1.231%; p = 0.0654).

No significant differences in relative sigma power were identified between all other study groups (Fig. 4.3.12A).

Light cycle

A significant increase in relative sigma power was observed in APP(TG)-Panto group compared to APP(TG)-DMSO and WT-DMSO groups at 21 weeks of age (WT-DMSO, n = 3: 4.713 ± 0.339% vs. APP(TG)-Panto, n = 3: 8.257 ± 1.144%; p = 0.0362) (APP(TG)-DMSO, n = 3: 4.526 ± 1.779% vs. APP(TG)-Panto, n = 3: 8.257 ± 1.144%; p = 0.025).

However, no significant differences in relative sigma power were detected between all other study groups (Fig. 4.3.12B).

### ii) Motor cortical M1 region

No significant differences in relative sigma power were identified between all study groups analyzed from motor cortical M1 region during both dark and light cycles (Fig. 4.3.12C,D).

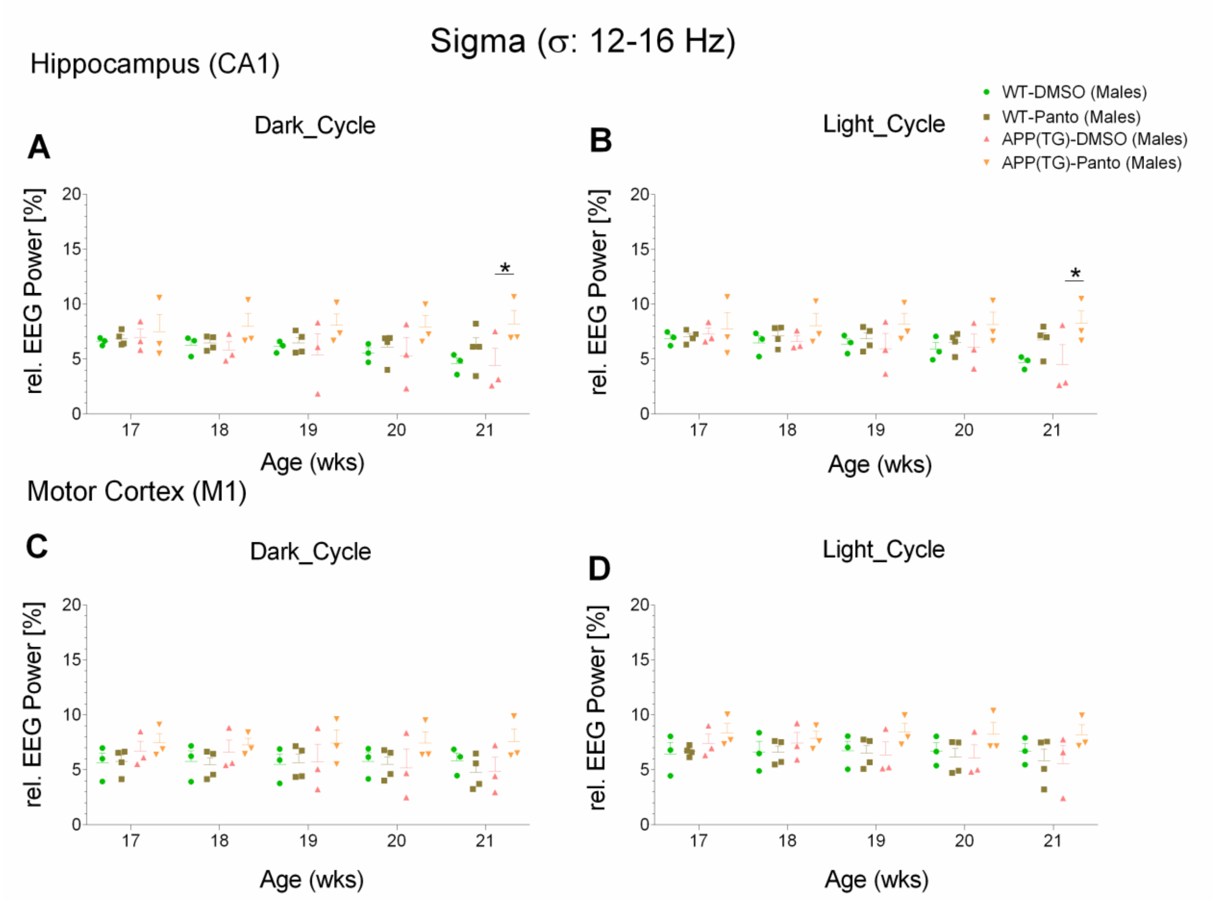

**Figure 4.3.12: Hippocampus (CA1) (A,B) and motor cortex (M1) (C,D) relative sigma power (%) (σ: 12-16 Hz) in WT-DMSO, WT-Panto, APP(TG)-DMSO and APP(TG)-Panto male mice.** Results are depicted considering the circadian rhythmicity (dark/light cycle). $^{*}$ $p < 0.05$; $^{**}$ $p < 0.01$; $^{***}$ $p < 0.001$.

### Gamma low ($\gamma_{low}$: 30-50 Hz)

### i) Hippocampal CA1 region

No significant differences in relative gamma low power were detected between all study groups analyzed from hippocampal CA1 region during both dark and light cycles (Fig. 4.3.13A,B).

### ii) Motor cortical M1 region

Dark cycle

No significant differences in relative gamma low power were detected between all study groups (Fig. 4.3.13C).

Light cycle

A statistical trend in relative gamma low power was observed between APP(TG)-DMSO and WT-DMSO mice at 17 weeks of age (WT-DMSO, n = 3: 4.205 ± 0.680% vs. APP(TG)-DMSO, n = 3: 8.063 ± 0.507%; p = 0.0508) and at 20 weeks of age (WT-DMSO, n = 3: 4.053 ± 0.707% vs. APP(TG)-DMSO, n = 3: 7.660 ± 1.085%; p = 0.0757).

However, no significant differences in relative gamma low power were detected between all other study groups (Fig. 4.3.13D).

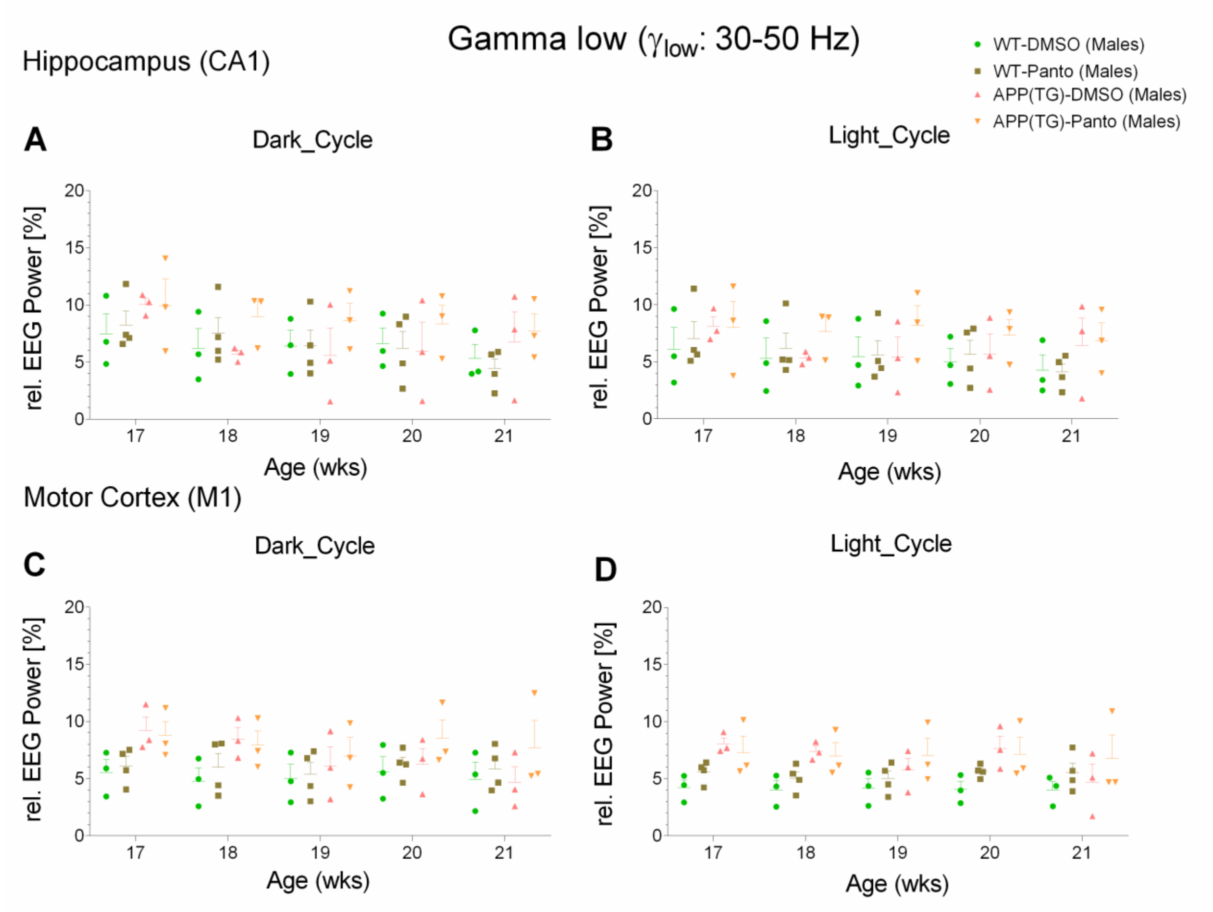

**Figure 4.3.13: Hippocampus (CA1) (A,B) and motor cortex (M1) (C,D) relative gamma low power (%) ($\gamma_{low}$: 30-50 Hz) in WT-DMSO, WT-Panto, APP(TG)-DMSO and APP(TG)-Panto male mice**. Results are illustrated considering the circadian rhythmicity (dark/light cycle). $^{*}$ $p < 0.05$; $^{**}$ $p < 0.01$; $^{***}$ $p < 0.001$.

### Gamma mid ($\gamma_{mid}$: 50-70 Hz)

### i) Hippocampal CA1 region

No significant differences in relative gamma mid power were identified between all study groups analyzed from hippocampal CA1 region during both dark and light cycles (Fig. 4.3.14A,B).

### ii) Motor cortical M1 region

Dark cycle

No significant differences in relative gamma mid power were detected between all study groups (Fig. 4.3.14C).

Light cycle

A significant increase in relative gamma mid power was observed in APP(TG)-DMSO compared to WT-DMSO mice at 20 weeks of age (WT-DMSO, n = 3: 1.813 ± 0.350% vs. APP(TG)-DMSO, n = 3: 4.836 ± 1.221%; p = 0.0073). A statistical trend in relative gamma mid power was identified between 20 weeks and 21 weeks of age for the APP(TG)-DMSO group (20 weeks, n = 3: 4.836 ± 1.221% vs. 21 weeks, n = 3: 2.331 ± 0.774%; p = 0.0519).

However, no significant differences in relative gamma mid power were detected between all other study groups (Fig. 4.3.14D).

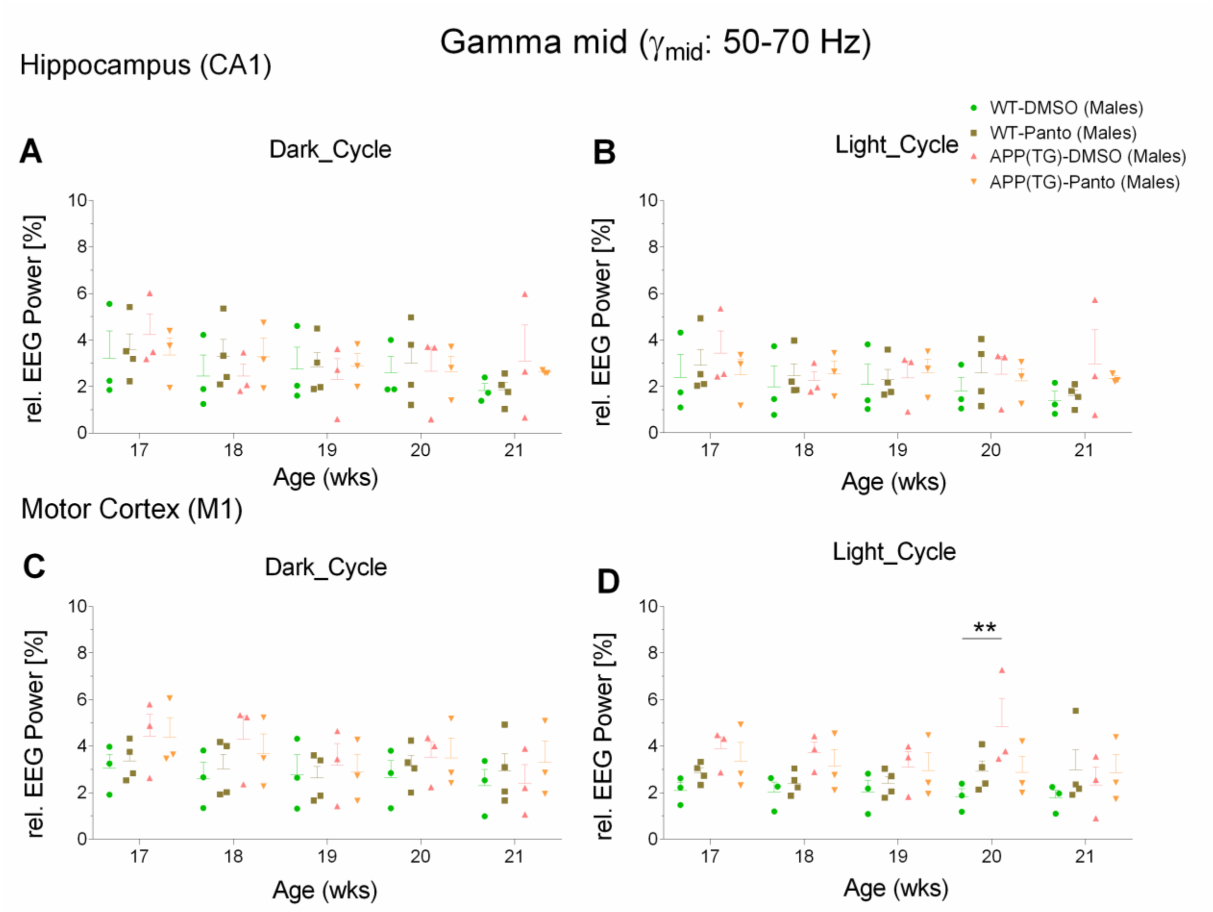

**Figure 4.3.14: Hippocampus (CA1) (A,B) and motor cortex (M1) (C,D) relative gamma mid power (%) ($\gamma_{mid}$: 50-70 Hz) in WT-DMSO, WT-Panto, APP(TG)-DMSO and APP(TG)-Panto male mice.** Results are depicted considering the circadian rhythmicity (dark/light cycle). $^{*}$ $p < 0.05$; $^{**}$ $p < 0.01$; $^{***}$ $p < 0.001$.

### 4.3.4. Post-urethane and post-atropine frequencies analysis

#### Theta 1 ($\theta_1$: 4-8 Hz)

#### i) Hippocampal CA1 region

A significant increase in relative theta 1 power was observed during post-urethane (1 h) compared to post-atropine (3 h) recordings for the WT-DMSO mice (post-urethane, n = 3: 31.591 ± 6.513% vs. post-atropine, n = 3: 15.389 ± 4.525%; p = 0.0102). Likewise, a significant increase was detected during post-urethane (1 h) compared to post-atropine (3 h) recordings for the WT-Panto group (post-urethane, n = 4: 35.064 ± 2.040% vs. post-atropine, n = 4: 23.028 ± 1.245%; p = 0.0338). Moreover, an increase in relative theta 1 power was identified during post-urethane (1 h) compared to baseline (1 h) recordings for the APP(TG)-DMSO mice (baseline, n = 3: 23.510 ± 5.366% vs. post-urethane, n = 3: 38.150 ± 4.332%; p = 0.0233). Subsequently, a significant decrease in relative theta 1 power was detected during post-atropine (3 h) compared to post-urethane (1 h) recordings for the APP(TG)-DMSO mice (post-urethane, n = 3: 38.150 ± 4.332% vs. post-atropine, n = 3: 19.853 ± 6.070%; p = 0.0032).

A statistical trend in relative theta 1 power was identified during post-normal saline (1 h) compared to post-atropine (3 h) recordings for the WT-DMSO mice (post-normal saline, n = 3: 28.405 ± 1.663% vs. post-atropine, n = 3: 15.389 ± 4.525%; p = 0.0516). Additionally, a statistical trend was detected during post-urethane (1 h) compared to post-atropine (3 h) recordings for the APP(TG)-Panto (post-urethane, n = 3: 36.330 ± 6.432% vs. post-atropine, n = 3: 24.099 ± 0.828%; p = 0.074).

However, no significant differences in relative theta 1 power identified between all other study groups (Fig. 4.3.15A).

#### ii) Motor cortical M1 region

A significant increase in relative theta 1 power was observed in WT-Panto compared to APP(TG)-DMSO mice during baseline (1 h) recording (WT-Panto, n = 4: 28.810 ± 0.562% vs. APP(TG)-DMSO, n = 3: 20.113 ± 3.464%; p = 0.0309). Additionally, a significant increase was observed in WT-Panto and APP(TG)-DMSO groups compared to WT-DMSO group during post-urethane (1 h) recording (WT-DMSO, n = 3: 21.783 ± 1.571% vs. WT-Panto, n = 4: 30.206 ± 1.402%; p = 0.0384) (WT-DMSO, n = 3: 21.783 ± 1.571% vs. APP(TG)-DMSO, n = 3: 32.177 ± 2.845%; p = 0.0131). Moreover, a significant increase was detected in APP(TG)-DMSO compared to WT-DMSO mice during post-atropine (3 h) recording (WT-DMSO, n = 3: 16.132 ± 0.306% vs. APP(TG)-DMSO, n = 3: 26.287 ± 2.693%; p = 0.0159).

Furthermore, a significant increase in relative theta 1 power was observed during baseline (1 h) and post-normal saline (1 h) compared to post-atropine (3 h) recordings for the WT-DMSO mice (baseline, n = 3: 28.362 ± 1.381% vs. post-atropine, n = 3: 16.132 ± 0.306%; p = 0.0028) (post-normal saline, n = 3: 27.247 ± 1.112% vs. post-atropine, n = 3: 16.132 ± 0.306; p = 0.0073). Likewise, a significant increase was identified during baseline (1 h) and post-urethane (1 h) compared to post-atropine (3 h) recordings for the WT-Panto group (baseline, n = 4: 28.810 ± 0.562% vs. post-atropine, n = 4: 20.619 ± 3.623%; p = 0.0274) (post-urethane, n = 4: 30.206 ± 1.402% vs. post-atropine, n = 4: 20.619 ± 3.623%; p = 0.0076). Additionally, a significant increase was detected during baseline (1 h) compared to post-urethane (1 h) recordings for the APP(TG)-DMSO mice (baseline, n = 3: 20.113 ± 3.464% vs. post-urethane, n = 3: 32.177 ± 2.845%; p = 0.0032).

A statistical trend in relative theta 1 power was identified between APP(TG)-DMSO and WT-DMSO mice during baseline (1 h) recording (WT-DMSO, n = 3: 28.362 ± 1.381% vs. APP(TG)-DMSO, n = 4: 20.113 ± 3.464%; p = 0.0659). Similarly, a statistical trend was observed between APP(TG)-Panto and WT-DMSO groups during post-urethane (1 h) recording (WT-DMSO, n = 3: 21.783 ± 1.571% vs. APP(TG)-Panto, n = 3: 30.241 ± 4.369%; p = 0.0569). Furthermore, a statistical trend was also observed between APP(TG)-Panto compared to WT-DMSO mice during post-atropine (3 h) recording (WT-DMSO, n = 3: 16.132 ± 0.306% vs. APP(TG)-Panto, n = 3: 24.223 ± 1.669%; p = 0.0734). In addition, a statistical trend was detected during post-normal saline (1 h) compared to post-atropine (3 h) recordings for the WT-Panto mice (post-normal saline, n = 4: 27.373 ± 0.675% vs. post-atropine, n = 4: 20.619 ± 3.623%; p = 0.0893).

However, no significant differences in relative theta 1 power were observed between all other study groups (Fig. 4.3.15B).

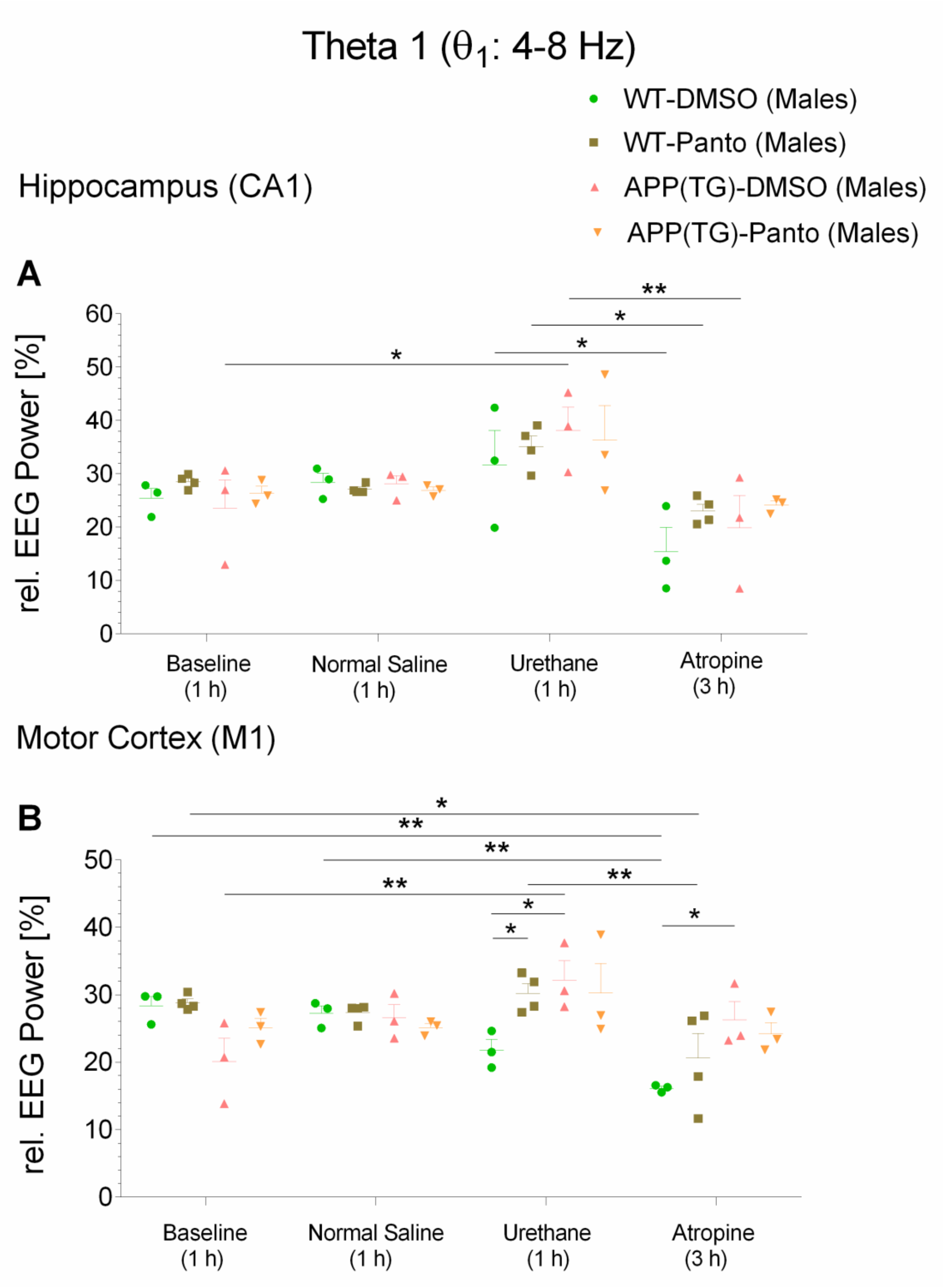

**Figure 4.3.15: Hippocampus (CA1) (A) and motor cortex (M1) (B) relative theta 1 ($\theta_1$: 4-8 Hz) power (%) in WT-DMSO, WT-Panto, APP(TG)-DMSO and APP(TG)-Panto male mice.** Results are depicted for baseline (1 h), post-normal saline (1 h), post-post-urethane (1 h) and post-atropine (3 h) recordings. $*p < 0.05$; $**p < 0.01$; $***p < 0.001$.

### Theta 2 ($\theta_2$: 4.1-12 Hz)

#### i) Hippocampal CA1 region

A significant increase in relative theta 2 power was observed in post-normal saline (1 h) compared to post-atropine (3 h) recordings for the WT-DMSO mice (post-normal saline, n = 3: 36.003 ± 2.995% vs. post-atropine, n = 3: 19.695 ± 4.682%; p = 0.0298). However, a significant decrease in relative theta 2 power was identified during post-atropine (3 h) compared to post-urethane (1 h) recordings for the APP(TG)-DMSO group (post-urethane, n = 3: 44.269 ± 4.081% vs. post-atropine, n = 3: 26.205 ± 6.268%; p = 0.0136).

A statistical trend in relative theta 2 power was detected between APP(TG)-Panto and WT-DMSO mice during post-atropine (3 h) recording (WT-DMSO, n = 3: 19.695 ± 4.682% vs. APP(TG)-Panto, n = 3: 33.144 ± 3.616%; p = 0.0947). Furthermore, a statistical trend was observed for the WT-DMSO mice during baseline (1 h) compared to post-atropine (3 h) and post-urethane (1 h) compared to post-atropine (3 h) recordings (baseline, n = 3: 34.123 ± 2.486% vs. post-atropine, n = 3: 19.695 ± 4.682%; p = 0.0649) (post-urethane, n = 3: 33.906 ± 6.617% vs. post-atropine, n = 3: 19.695 ± 4.682%; p = 0.0707). Likewise, a statistical trend was observed for the WT-Panto group during baseline (1 h) compared to post-atropine (3 h) and post-urethane (1 h) compared to post-atropine (3 h) recordings (baseline, n = 4: 43.174 ± 1.447% vs. post-atropine, n = 4: 30.865 ± 1.082%; p = 0.0707) (post-urethane, n = 4: 42.449 ± 2.439% vs. post-atropine, n = 4: 30.865 ± 1.082%; p = 0.0973).

No significant differences in relative theta 2 power were detected between all other study groups (Fig. 4.3.16A).

#### ii) Motor cortical M1 region

A significant increase in relative theta 2 power was observed during baseline (1 h) recording for the WT-DMSO compared to APP(TG)-DMSO mice and the WT-Panto group compared to APP(TG)-DMSO group (WT-DMSO, n = 3: 40.190 ± 1.819% vs. APP(TG)-DMSO, n = 3: 30.087 ± 5.158%; p = 0.0454) (WT-Panto, n = 4: 40.009 ± 1.598% vs. APP(TG)-DMSO, n = 3: 30.087 ± 5.158%; p = 0.0329). Additionally, a significant increase was identified in APP(TG)-DMSO and APP(TG)-Panto groups compared to WT-DMSO group during post-urethane (1 h) recording (WT-DMSO, n = 3: 27.477 ± 2.337% vs. APP(TG)-DMSO, n = 3: 40.077 ± 2.887%; p = 0.0084) (WT-DMSO, n = 3: 27.477 ± 2.337% vs. APP(TG)-Panto, n = 3: 39.024 ± 3.917%; p = 0.0176).

Moreover, a significant increase was detected in APP(TG)-DMSO and APP(TG)-Panto mice compared to WT-DMSO mice during post-atropine (3 h) recording (WT-DMSO, n = 3: 21.750 ±

0.611% vs. APP(TG)-DMSO, n = 3: 34.014 ± 2.754%; p = 0.0107) (WT-DMSO, n = 3: 21.750 ± 0.611% vs. APP(TG)-Panto, n = 3: 33.185 ± 4.007%; p = 0.019).

Furthermore, a significant increase in relative theta 2 power was observed during baseline (1 h) compared to post-urethane (1 h) and post-atropine (3 h) recordings for the WT-DMSO mice (baseline, n = 3: 40.190 ± 1.819% vs. post-urethane, n = 3: 27.477 ± 2.337%; p = 0.0077) (baseline, n = 3: 40.190 ± 1.819% vs. post-atropine, n = 3: 21.750 ± 0.611%; p < 0.0001). Likewise, a significant differences were identified during post-normal saline (1 h) recordings compared to post-urethane (1 h) and post-atropine (3 h) recordings for the WT-DMSO group (post-normal saline, n = 3: 38.724 ± 1.759% vs. post-urethane, n = 3: 27.477 ± 2.337%; p = 0.0215) (post-normal saline, n = 3: 38.724 ± 1.759% vs. post-atropine, n = 3: 21.750 ± 0.611%; p = 0.0003). Similarly, a significant increase was also detected during baseline (1 h) compared to post-atropine (3 h) recording for the WT-Panto mice (baseline, n = 4: 40.009 ± 1.598% vs. post-atropine, n = 4: 29.126 ± 3.107%; p = 0.0086) and also at baseline compared to post-urethane (1 h) recording for the APP(TG)-DMSO mice (baseline, n = 3: 30.087 ± 5.158% vs. post-urethane, n = 3: 40.077 ± 2.887%; p = 0.0487).

A statistical trend in relative theta 2 power was observed between WT-Panto compared to WT-DMSO mice during post-urethane (1 h) recording (WT-DMSO, n = 3: 27.477 ± 2.337% vs. WT-Panto, n = 4: 36.177 ± 1.379%; p = 0.074). Likewise, a statistical trend was detected between post-normal saline (1 h) and post-atropine (3 h) recordings for the WT-Panto group (post-normal saline, n = 4: 37.371 ± 1.440% vs. post-atropine, n = 4: 29.126 ± 3.107%; p = 0.065).

However, no significant differences in relative theta 2 power were identified between all other study groups (Fig. 4.3.16B).

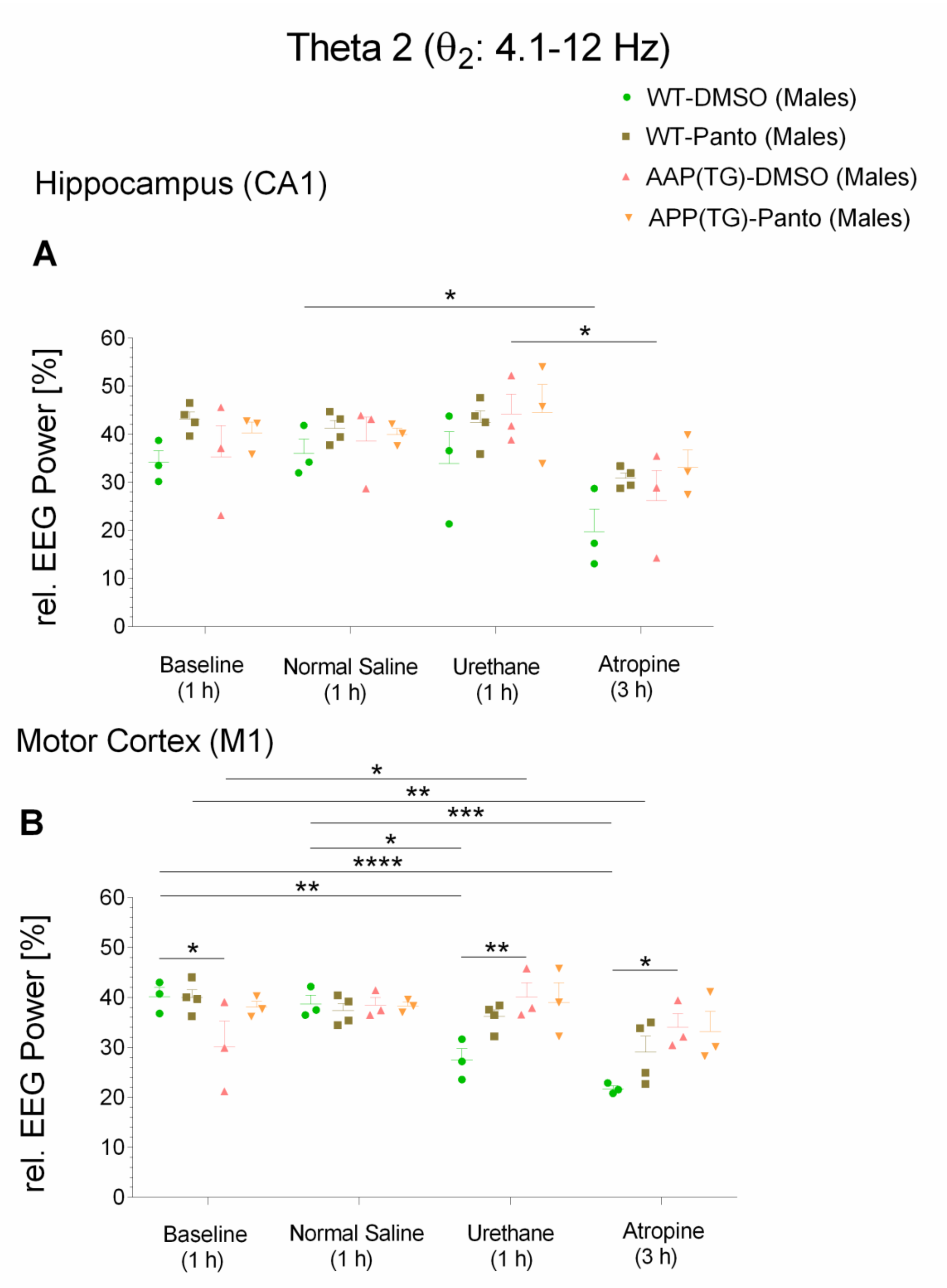

**Figure 4.3.16: Hippocampus (CA1) (A) and motor cortex (M1) (B) relative theta 2 ($\theta_2$: 4.1-12 Hz) power (%) in WT-DMSO, WT-Panto, APP(TG)-DMSO and APP(TG)-Panto male mice.** Results are depicted for baseline (1 h), post-normal saline (1 h), post-post-urethane (1 h) and post-atropine (3 h) recordings. $*p < 0.05$; $**p < 0.01$; $***p < 0.001$.

### Delta (δ: 0.5-4 Hz)

#### i) Hippocampal CA1 region

A significant increase in relative delta power was observed in WT-DMSO compared to APP(TG)-DMSO mice during post-atropine (3 h) recording (WT-DMSO, n = 3: 67.432 ± 4.310% vs. APP(TG)-DMSO, n = 3: 39.600 ± 14.742%; p = 0.0264). A statistical trend in relative delta power was detected between WT-DMSO and APP(TG)-DMSO mice during post-urethane (1 h) recording (WT-DMSO, n = 3: 54.549 ± 8.271% vs. APP(TG)-DMSO, n = 3: 31.684 ± 6.288%; p = 0.0887). Likewise, a statistical trend was observed during post-atropine (3 h) compared to baseline (1 h) recordings for the WT-Panto group (baseline, n = 4: 34.942 ± 3.650% vs. post-atropine, n = 4: 55.441 ± 1.450%; p = 0.0738).

However, no significant differences in relative delta power were detected between all other study groups (Fig. 4.3.17A).

#### ii) Motor cortical M1 region

A significant increase in relative delta power was observed in WT-DMSO compared to WT-Panto and APP(TG)-DMSO mice during post-urethane (1 h) recording (WT-DMSO, n = 3: 58.349 ± 4.012% vs. WT-Panto, n = 4: 34.944 ± 3.925%; p = 0.0259) (WT-DMSO, n = 3: 58.349 ± 4.012% vs. APP(TG)-DMSO, n = 3: 35.351 ± 3.413%; p = 0.0459). Additionally, a significant increase was detected in WT-DMSO compared to WT-Panto and APP(TG)-DMSO groups during post-atropine (3hr) recording (WT-DMSO, n = 3: 63.921 ± 4.114% vs. WT-Panto, n = 4: 41.602 ± 7.347%; p = 0.0361) (WT-DMSO, n = 3: 63.921 ± 4.114% vs. APP(TG)-DMSO, n = 3: 38.014 ± 5.281%; p = 0.0199).

Furthermore, a significant increase in relative delta power was identified during post-atropine (3 h) compared to baseline (1 h) and post-normal saline (1 h) recordings for the WT-DMSO mice (baseline, n = 3: 38.801 ± 2.920% vs. post-atropine, n = 3: 63.921 ± 4.114%; p = 0.0252) (post-normal saline, n = 3: 37.985 ± 5.993% vs. post-atropine, n = 3: 63.921 ± 4.114%; p = 0.0198).

A statistical trend in relative delta power was identified between WT-DMSO and APP(TG)-Panto mice during post-urethane (1 h) recordings (WT-DMSO, n = 3: 58.349 ± 4.012% vs. APP(TG)-Panto, n = 3: 35.683 ± 6.602%; p = 0.0503). Similarly, a statistical trend was detected during post-normal saline (1 h) and post-urethane (1 h) recording for the WT-DMSO mice (post-normal saline, n = 3: 37.985 ± 5.993% vs. post-urethane, n = 3: 58.349 ± 4.012%; p = 0.0917). However, no significant differences in relative delta power were observed between all other study groups (Fig. 4.3.17B).

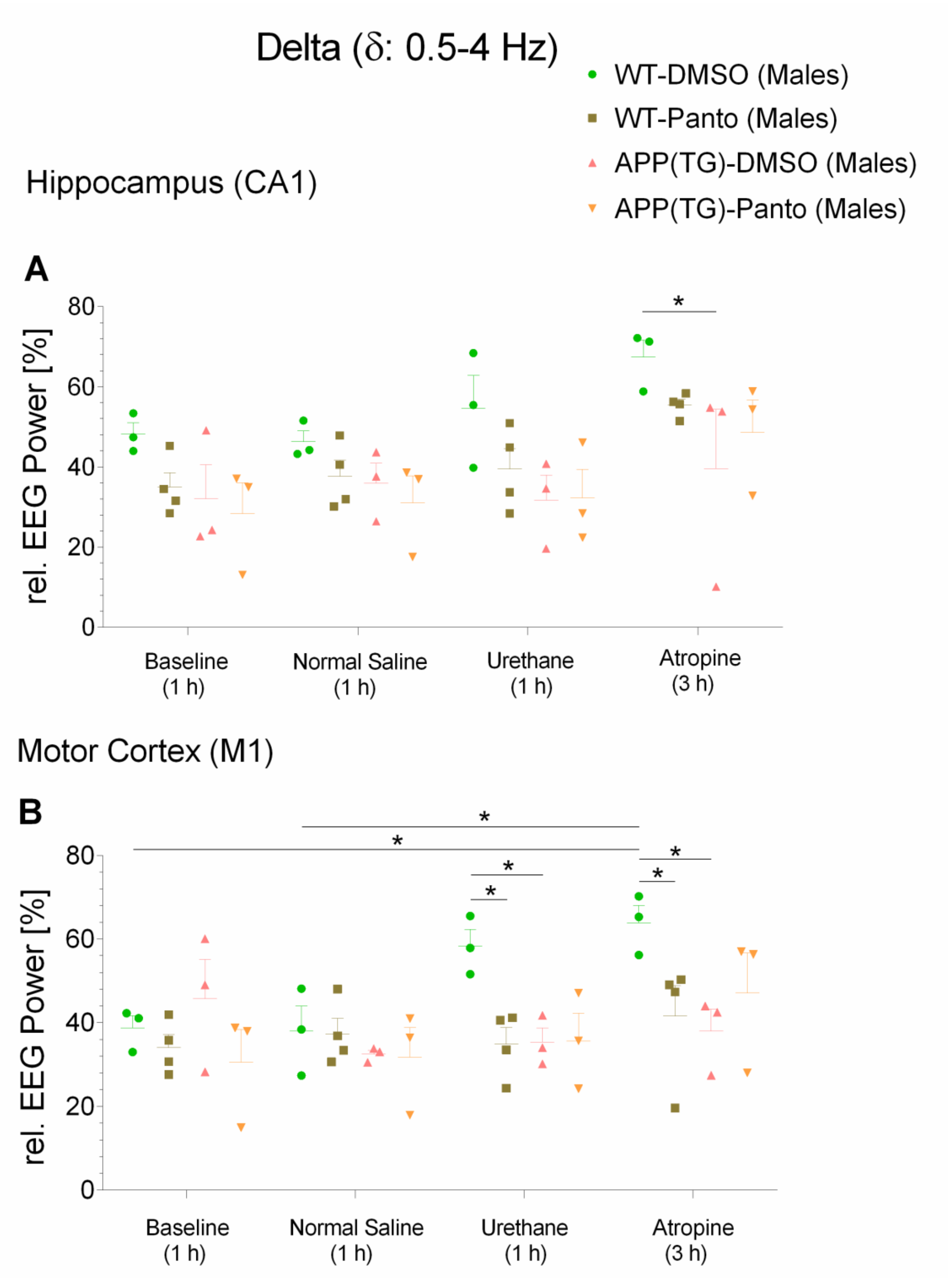

**Figure 4.3.17: Hippocampus (CA1) (A) and motor cortex (M1) (B) relative delta (δ: 0.5-4 Hz) power (%) in WT-DMSO, WT-Panto, APP(TG)-DMSO and APP(TG)-Panto male mice.** Results are depicted for baseline (1 h), post-normal saline (1 h), post-post-urethane (1 h) and post-atropine (3 h) recordings. $*p < 0.05$; $**p < 0.01$; $***p < 0.001$.

### Beta 1 ($\beta_1$: 12.1-30 Hz)

No significant differences in relative beta 1 power were detected between all study groups analyzed from hippocampal CA1 and motor cortical M1 regions (Fig. 4.3.18A,B).

### Beta 2 ($\beta_2$: 16-24 Hz)

#### i) Hippocampal CA1 region

A significant increase in relative beta 2 power was observed in APP(TG)-DMSO compared to WT-DMSO mice during baseline (1 h) recording (WT-DMSO, n = 3: 6.594 ± 0.685% vs. APP(TG)-DMSO, n = 3: 13.552 ± 5.334%; p = 0.0333). Additionally, a significant increase was detected during baseline (1 h) compared to post-normal saline (1 h), post-urethane (1 h) and post-atropine (3 h) recordings for the APP(TG)-DMSO mice (baseline, n = 3: 13.552 ± 5.334% vs. post-normal saline, n = 3: 5.544 ± 1.564%; p = 0.0113) (baseline, n = 3: 13.552 ± 5.334% vs. post-urethane, n = 3: 5.992 ± 0.767%; p = 0.0181) (baseline, n = 3: 13.552 ± 5.334% vs. post-atropine, n = 3: 3.772 ± 0.445%; p = 0.0015).

However, no significant differences in relative beta 2 power were observed between all other study groups (Fig. 4.3.19A).

#### ii) Motor cortical M1 region

A statistical trend in relative beta 2 power was detected between baseline (1 h) and post-urethane (1 h) recordings for the WT-DMSO group (baseline, n = 3: 7.482 ± 0.786% vs. post-urethane, n = 3: 3.130 ± 0.384%; p = 0.0764).

No significant differences in relative beta 2 power were observed between all other study groups (Fig. 4.3.19B).

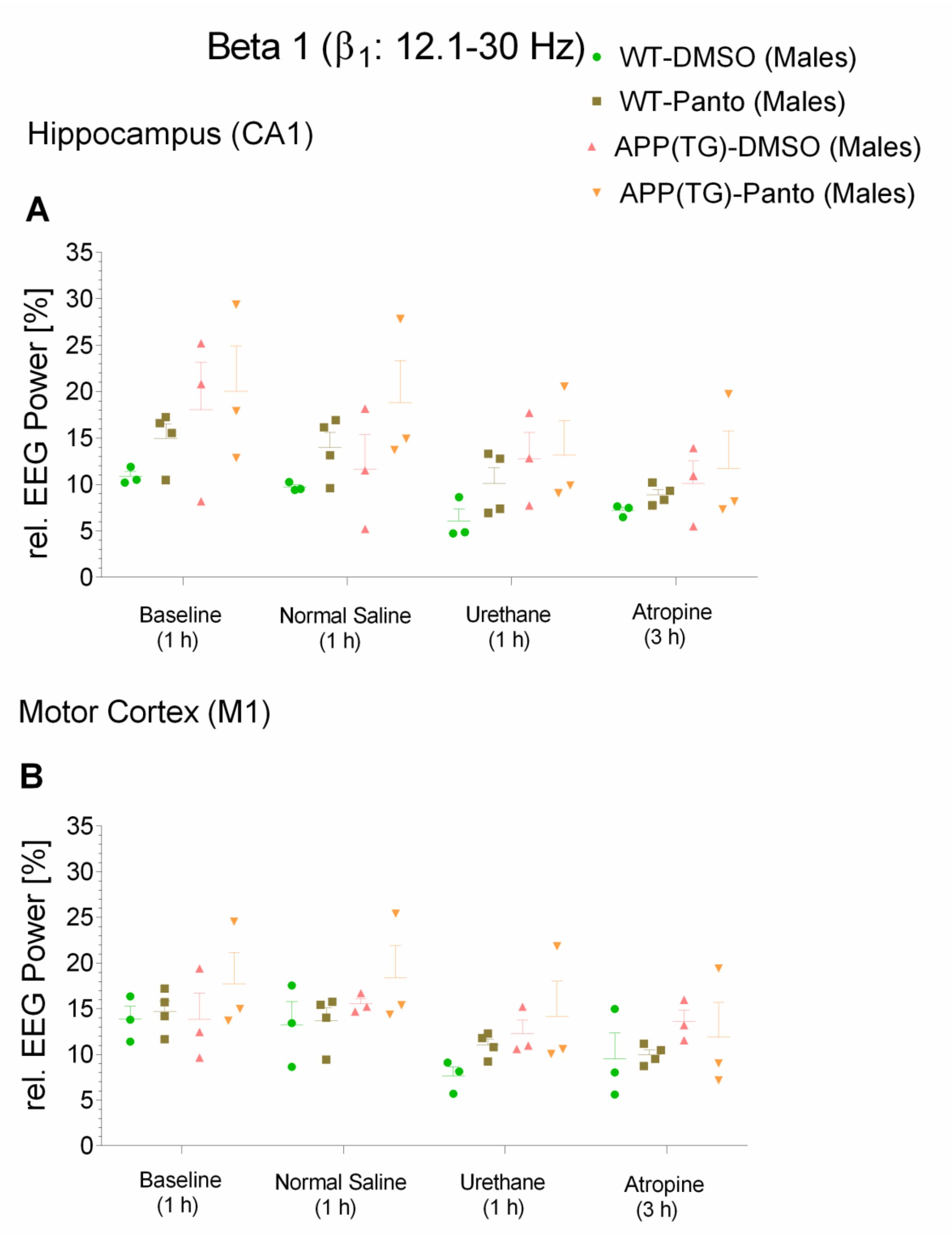

**Figure 4.3.18: Hippocampus (CA1) (A) and motor cortex (M1) (B) relative beta 1 ($\beta_1$: 12.1-30 Hz) power (%) in WT-DMSO, WT-Panto, APP(TG)-DMSO and APP(TG)-Panto male mice.** Results are depicted for baseline (1 h), post-normal saline (1 h), post-post-urethane (1 h) and post-atropine (3 h) recordings. $*p < 0.05$; $**p < 0.01$; $***p < 0.001$.

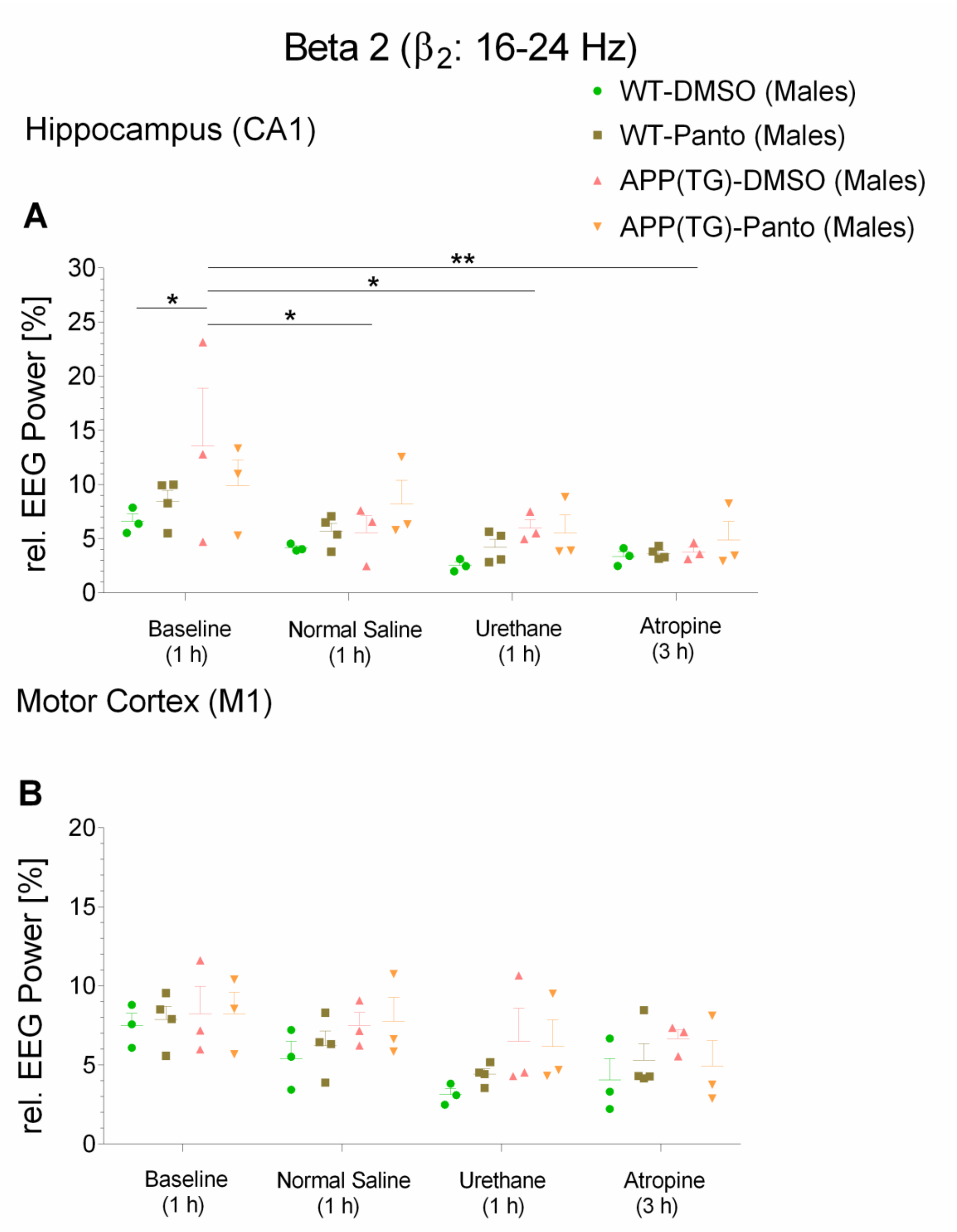

**Figure 4.3.19: Hippocampus (CA1) (A) and motor cortex (M1) (B) relative beta 2 ($\beta_2$: 16-24 Hz) power (%) in WT-DMSO, WT-Panto, APP(TG)-DMSO and APP(TG)-Panto male mice.** Results are depicted for baseline (1 h), post-normal saline (1 h), post-post-urethane (1 h) and post-atropine (3 h) recordings. $*p < 0.05$; $**p < 0.01$; $***p < 0.001$.

**Beta 3 (β3: 16-30 Hz)**

No significant differences in relative beta 3 power were identified between all study groups (Fig. 4.3.20).

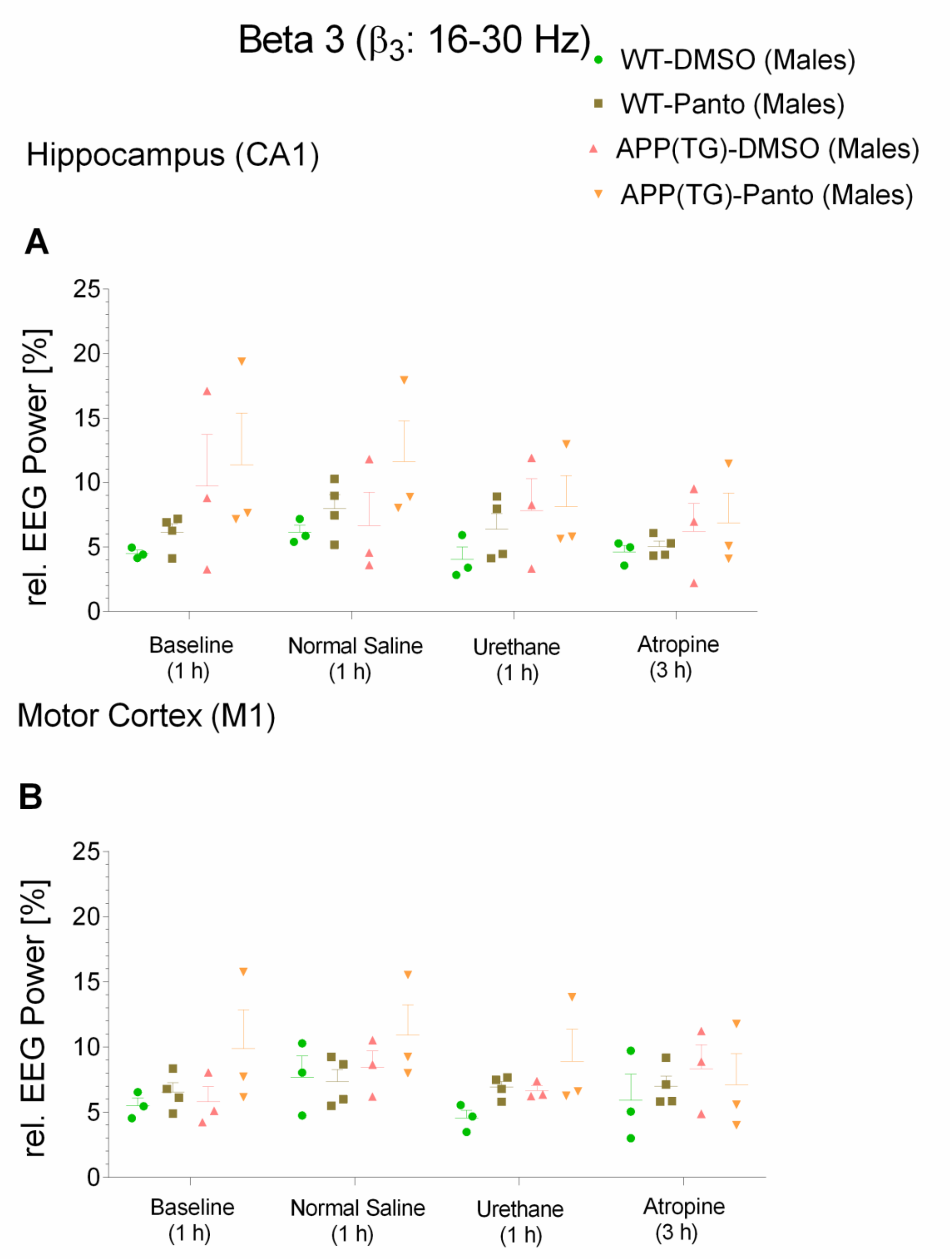

**Figure 4.3.20: Hippocampus (CA1) (A) and motor cortex (M1) (B) relative beta 3 ($\beta_3$: 16-30 Hz) power (%) in WT-DMSO, WT-Panto, APP(TG)-DMSO and APP(TG)-Panto male mice.** Results are depicted for baseline (1 h), post-normal saline (1 h), post-post-urethane (1 h) and post-atropine (3 h) recordings. $*p < 0.05$; $**p < 0.01$; $***p < 0.001$.

### Alpha (α: 8-12 Hz)

#### i) Hippocampal CA1 region

A significant increase in relative alpha power was observed in WT-Panto compared to WT-DMSO mice during baseline (1 h) recording (WT-DMSO, n = 3: 9.769 ± 1.053% vs. WT-Panto, n = 4: 15.412 ± 0.784%; p = 0.0467). Likewise, a significant increase was detected in WT-Panto compared to WT-DMSO groups during post-normal saline (1 h) recording (WT-DMSO, n = 3: 8.775 ± 1.627% vs. WT-Panto, n = 4: 14.998 ± 1.393%; p = 0.0239).

Moreover, a significant increase in relative alpha power was detected during baseline (1 h) compared to post-urethane (1 h) and post-atropine (3 h) recordings for the WT-Panto mice (baseline, n = 4: 15.412 ± 0.784% vs. post-urethane, n = 4: 8.465 ± 0.922%; p = 0.0048) (baseline, n = 4: 15.412 ± 0.784% vs. post-atropine, n = 4: 8.733 ± 0.080%; p = 0.007). Similarly, a significant increase was identified during post-normal saline (1 h) compared to post-urethane (1 h) and post-atropine (3 h) recordings for the WT-Panto mice (post-normal saline, n = 4: 14.998 ± 1.393% vs. post-urethane, n = 4: 8.465 ± 0.922%; p = 0.0085) (post-normal saline, n = 4: 14.998 ± 1.393% vs. post-atropine, n = 4: 8.733 ± 0.080%; p = 0.0123).

A statistical trend in relative alpha power was observed between baseline (1 h) and post-urethane (1 h) recordings for the WT-DMSO group (baseline, n = 3: 9.769 ± 1.053% vs. post-urethane, n = 3: 3.991 ± 0.677%; p = 0.0607). Additionally, a statistical trend was detected between baseline (1 h) compared to post-atropine (3 h) recordings for the APP(TG)-DMSO mice (baseline, n = 3: 12.536 ± 1.584% vs. post-atropine, n = 3: 7.035 ± 0.568%; p = 0.0798). Similarly, a statistical trend was identified between baseline (1 h) compared to post-urethane (1 h) recording for the APP(TG)-Panto group (baseline, n = 3: 14.643 ± 1.543% vs. post-urethane, n = 3: 9.041 ± 2.175%; p = 0.0723).

However, no significant differences in relative alpha power were detected between all other study groups (Fig. 4.3.21A).

#### ii) Motor cortical M1 region

A significant increase in relative alpha power was observed during baseline (1 h) compared to post-urethane (1 h) and post-atropine (3 h) recordings for the WT-DMSO mice (baseline, n = 3: 12.846 ± 0.727% vs. post-urethane, n = 3: 6.608 ± 0.734%; p = 0.0033) (baseline, n = 3: 12.846 ± 0.727% vs. post-atropine, n = 3: 6.240 ± 0.378%; p = 0.0018). Likewise, a significant increase was detected during post-normal saline (1 h) compared to post-urethane (1 h) and post-atropine (3 h) recordings for the WT-DMSO mice (post-normal saline, n = 3: 12.400 ± 1.098% vs. post-urethane, n = 3: 6.608 ± 0.734; p = 0.0069) (post-normal saline, n = 3: 12.400 ± 1.098% vs. post-atropine, n = 3: 6.240 ± 0.378; p = 0.0038).

Moreover, a significant increase in relative alpha power was observed during baseline (1 h) compared to post-atropine (3 h) recordings and during post-normal saline (1 h) compared to post-urethane (1 h) recordings for the WT-Panto mice(baseline, n = 4: 12.377 ± 1.220% vs. post-urethane, n = 4: 7.126 ± 0.890%; p = 0.0044) (post-normal saline, n = 4: 11.074 ± 1.168% vs. post-urethane, n = 4: 7.126 ± 0.890%; p = 0.0447).

However, a statistical trend in relative alpha power was detected between post-normal saline (1 h) compared to post-atropine (3 h) recordings for the APP(TG)-DMSO group (post-normal saline, n = 3: 12.709 ± 0.456% vs. post-atropine, n = 3: 8.637 ± 0.260%; p = 0.0858). Furthermore, a statistical trend was identified between baseline (1 h) and post-urethane (1 h) recordings for the APP(TG)-Panto mice (baseline, n = 3: 13.688 ± 0.273% vs. post-urethane, n = 3: 9.643 ± 1.745%; p = 0.0888). Similarly, a statistical trend was detected during post-normal saline (1 h) compared to post-urethane (1 h) and post-atropine (3 h) recordings for the APP(TG)-Panto mice (post-normal saline, n = 3: 13.993 ± 1.215% vs. post-urethane, n = 3: 9.643 ± 1.745%; p = 0.0594) (post-normal saline, n = 3: 13.993 ± 1.215% vs. post-atropine, n = 3: 9.880 ± 2.356%; p = 0.0814).

However, no significant differences in relative alpha power was detected between all other study groups (Fig. 4.3.21B).

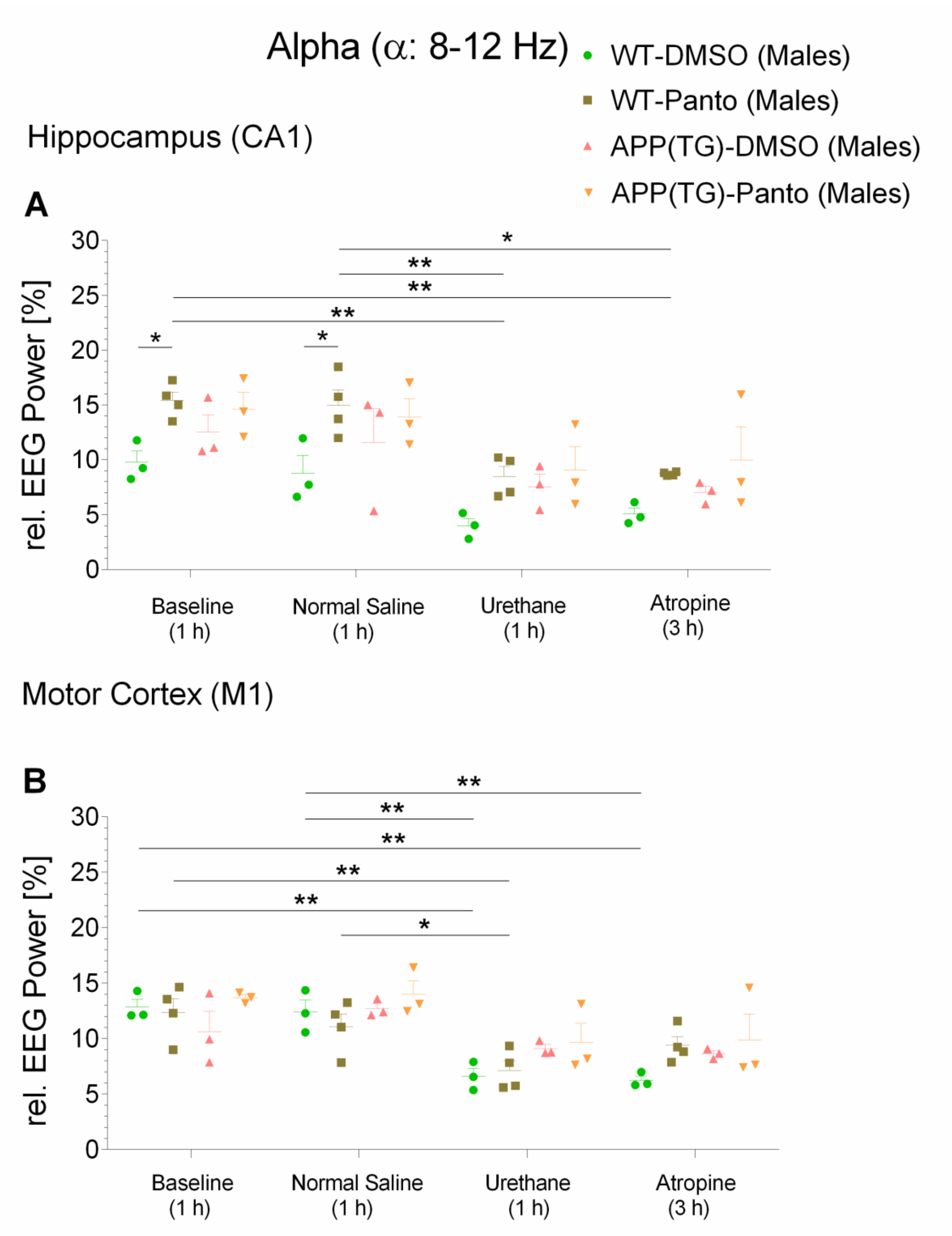

**Figure 4.3.21: Hippocampus (CA1) (A) and motor cortex (M1) (B) relative alpha (α: 8-12 Hz) power (%) in WT-DMSO, WT-Panto, APP(TG)-DMSO and APP(TG)-Panto male mice.** Results are depicted for baseline (1 h), post-normal saline (1 h), post-post-urethane (1 h) and post-atropine (3 h) recordings. $*p < 0.05$; $**p < 0.01$; $***p < 0.001$.

### Sigma (σ: 12-16 Hz)

### i) Hippocampal CA1 region

A statistical trend in relative sigma power was observed between APP(TG)-Panto and WT-DMSO mice during post-normal saline (1 h) recording (WT-DMSO, n = 3: 3.709 ± 0.310% vs. APP(TG)-Panto, n = 3: 7.416 ± 1.377%; p = 0.0561). Furthermore, a statistical trend was detected between baseline (1 h) compared to post-urethane (1 h) recordings for the WT-Panto mice (baseline, n = 4: 6.756 ± 0.568% vs. post-urethane, n = 4: 3.859 ± 0.530%; p = 0.0983).

No significant differences in relative sigma power were detected between all other analyzed groups (Fig. 4.3.22A).

### ii) Motor cortical M1 region

A significant increase in relative sigma power was observed during baseline (1 h) compared to post-atropine (3 h) recordings for the WT-Panto group (baseline, n = 4: 6.308 ± 0.899% vs. post-atropine, n = 4: 3.090 ± 0.738%; p = 0.0303). A statistical trend in relative sigma power was observed between baseline (1 h) compared to post-urethane (1 h) recordings for the WT-DMSO mice (baseline, n = 3: 6.607 ± 0.665% vs. post-urethane, n = 3: 3.208 ± 0.450%; p = 0.0541). In addition, a statistical trend was detected between post-normal saline (1 h) and post-atropine (3 h) recordings for the WT-Panto group (post-normal saline, n = 4: 5.820 ± 0.780% vs. post-atropine, n = 4: 3.090 ± 0.738%; p = 0.083).

However, no significant differences in relative sigma power were identified between all other study groups (Fig. 4.3.22B).

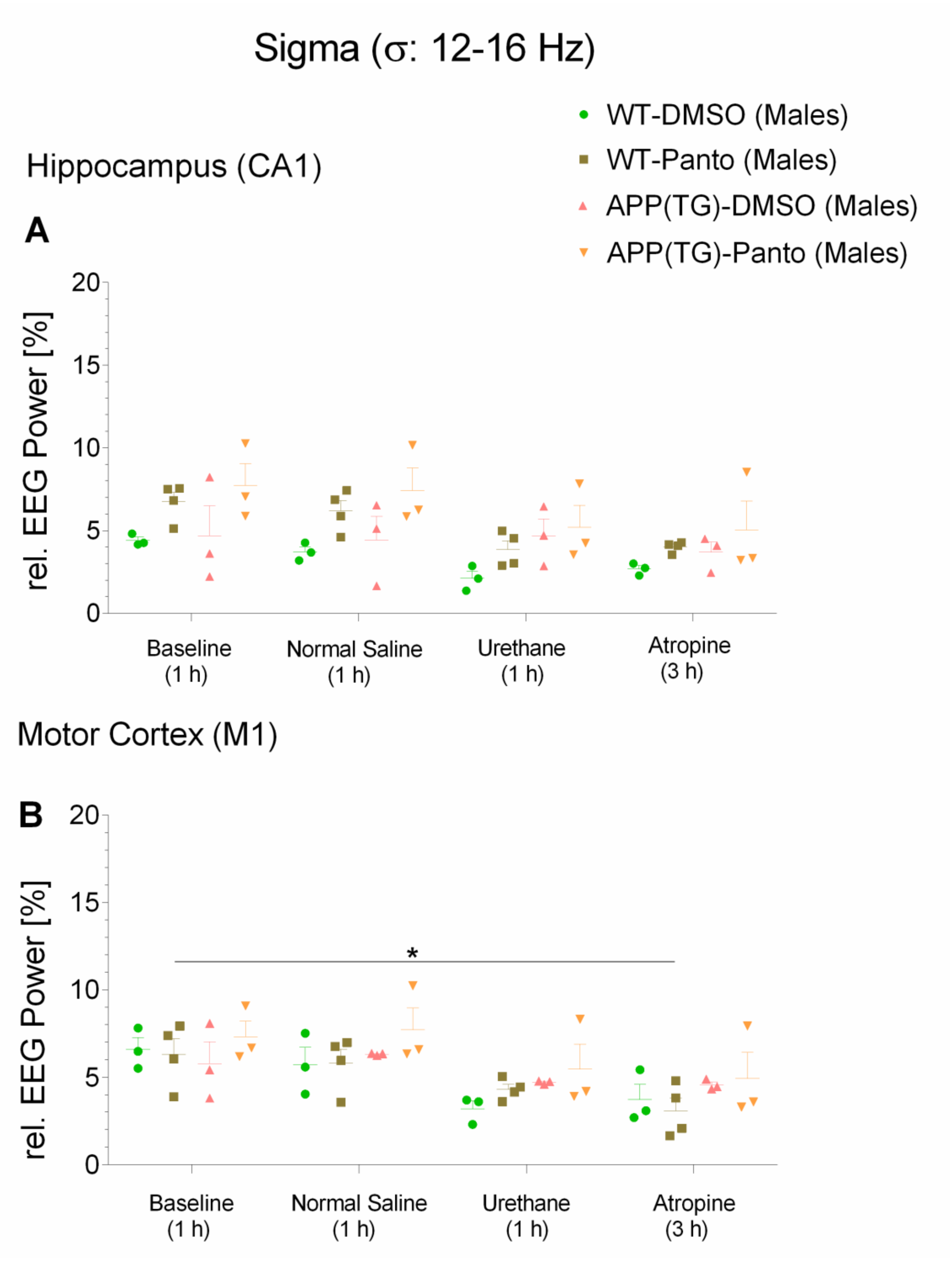

**Figure 4.3.22: Hippocampus (CA1) (A) and motor cortex (M1) (B) relative sigma (σ: 12-16 Hz) power (%) in WT-DMSO, WT-Panto, APP(TG)-DMSO and APP(TG)-Panto male mice.** Results are depicted for baseline (1 h), post-normal saline (1 h), post-post-urethane (1 h) and post-atropine (3 h) recordings. $*p < 0.05$; $**p < 0.01$; $***p < 0.001$.

### Gamma low ($\gamma_{low}$: 30-50 Hz)

#### i) Hippocampal CA1 region

A significant increase in relative gamma low power was observed in APP(TG)-DMSO compared to WT-DMSO and WT-Panto groups during post-atropine (3 h) recording (WT-DMSO, n = 3: 2.764 ± 0.840% vs. APP(TG)-DMSO, n = 3: 13.470 ± 10.702%; p = 0.0458) (WT-Panto, n = 4: 2.379 ± 0.182% vs. APP(TG)-DMSO, n = 3: 13.470 ± 10.702%; p = 0.0226). A statistical trend in relative gamma low power was detected between APP(TG)-DMSO and APP(TG)-Panto mice during post-atropine (3 h) recording (APP(TG)-DMSO, n = 3: 13.470 ± 10.702% vs. APP(TG)-Panto, n = 3: 3.353 ± 0.817%; p = 0.0644).

However, no significant differences in relative gamma low power were identified between all other study groups (Fig. 4.3.23A).

#### ii) Motor cortical M1 region

No significant differences in relative gamma low power were detected between all study groups (Fig. 4.3.23B).

### Gamma mid ($\gamma_{mid}$: 50-70 Hz)

#### i) Hippocampal CA1 region

A significant increase in relative gamma mid power was observed in APP(TG)-DMSO compared to WT-Panto mice during post-atropine (3 h) recording (WT-Panto, n = 4: 0.799 ± 0.088% vs. APP(TG)-DMSO, n = 3: 6.411 ± 5.626%; p = 0.0394).

No significant differences in relative gamma mid power were identified between all other study groups (Fig. 4.3.24A).

#### ii) Motor cortical M1 region

A statistical trend in relative gamma mid power was observed between WT-Panto and WT-DMSO mice during post-atropine (3 h) recording (WT-DMSO, n = 3: 0.819 ± 0.100% vs. WT-Panto, n = 4: 5.291 ± 3.282%; p = 0.069).

No significant differences in relative gamma mid power were detected between all other study groups (Fig. 4.3.24B).

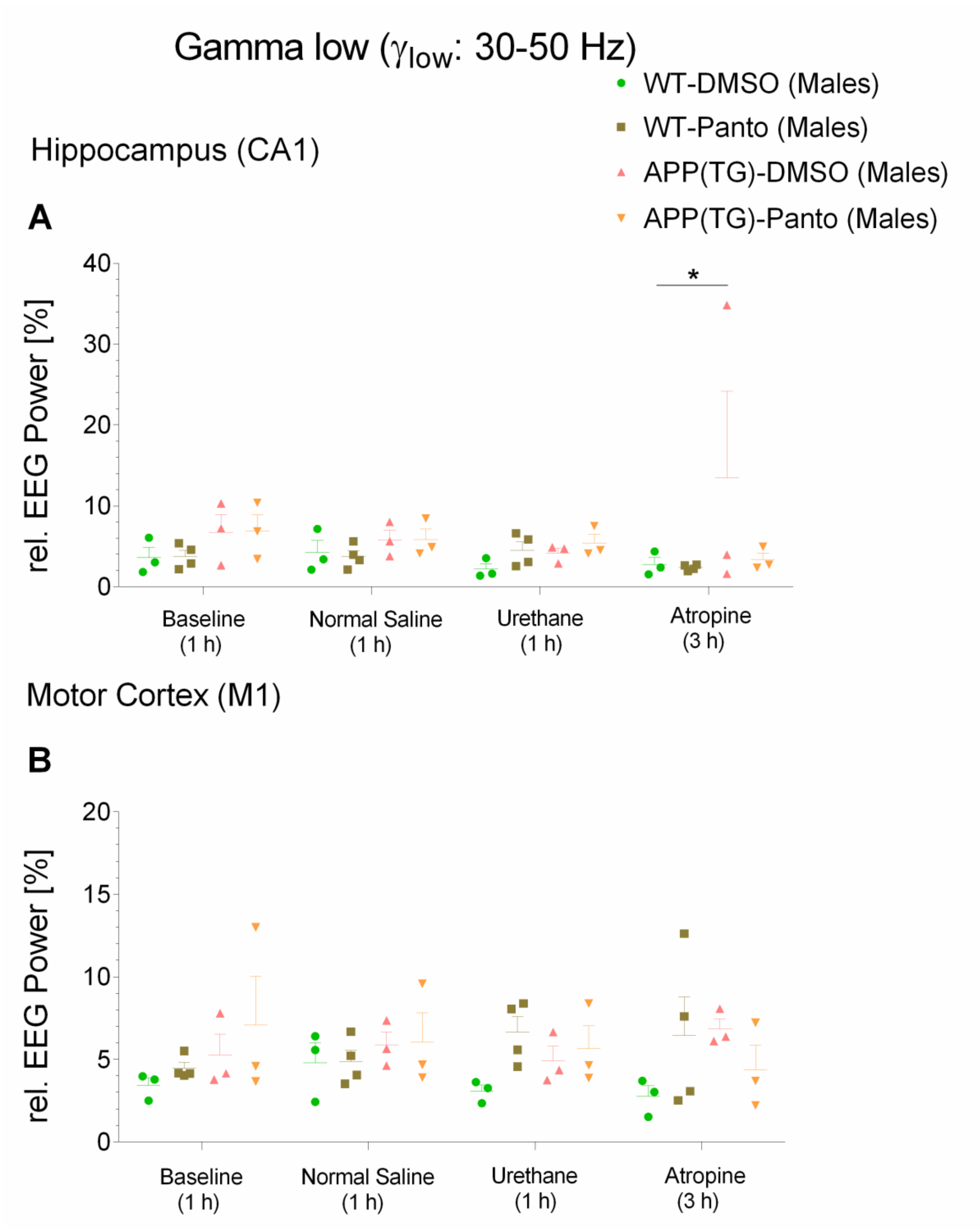

**Figure 4.3.23: Hippocampus (CA1) (A) and motor cortex (M1) (B) relative gamma low ($\gamma_{low}$: 30-50 Hz) power (%) in WT-DMSO, WT-Panto, APP(TG)-DMSO and APP(TG)-Panto male mice.** Results are depicted for baseline (1 h), post-normal saline (1 h), post-post-urethane (1 h) and post-atropine (3 h) recordings. $*p < 0.05$; $**p < 0.01$; $***p < 0.001$.

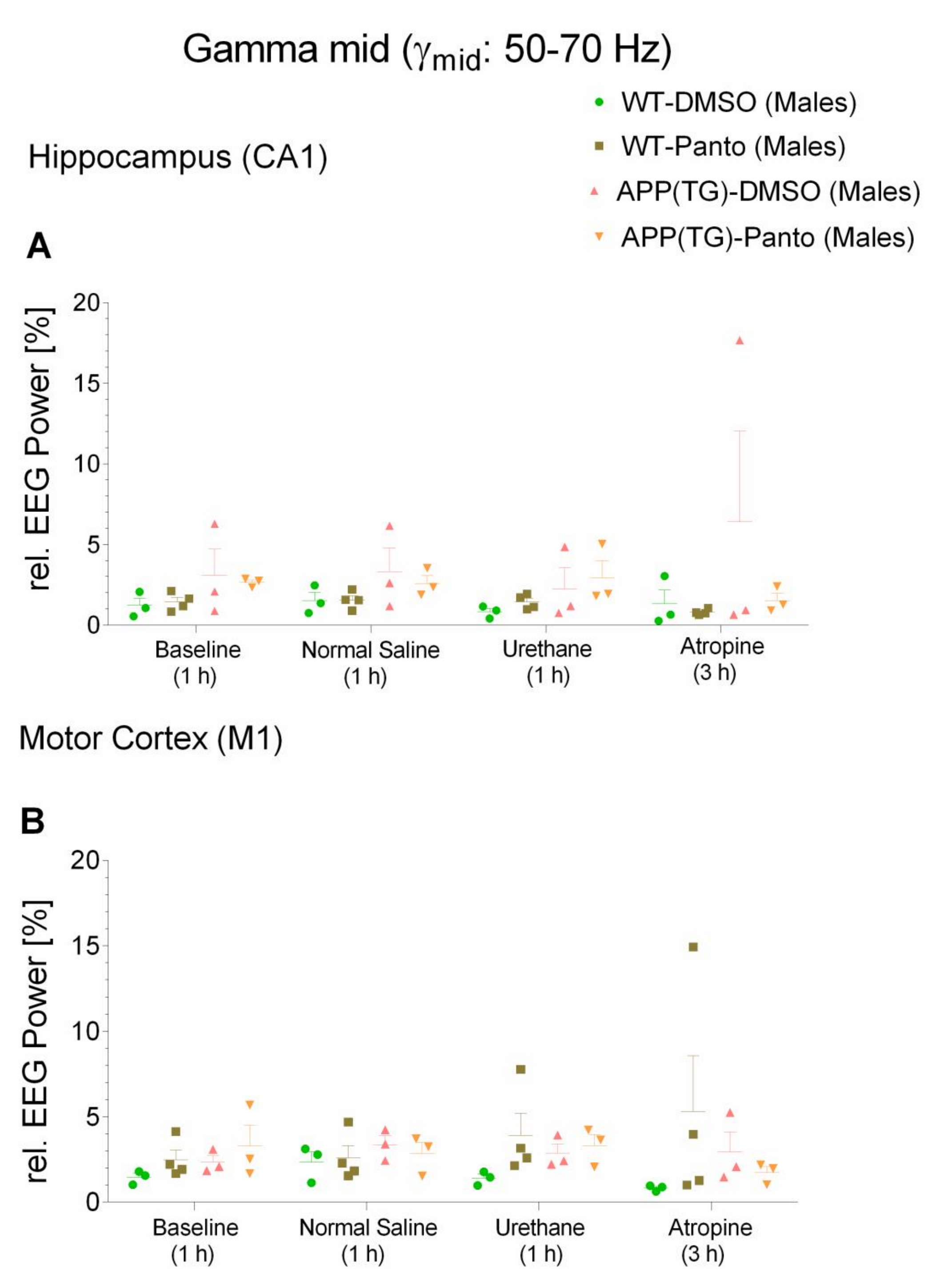

**Figure 4.3.24: Hippocampus (CA1) (A) and motor cortex (M1) (B) relative gamma mid ($\gamma_{mid}$: 50-70 Hz) power (%) in WT-DMSO, WT-Panto, APP(TG)-DMSO and APP(TG)-Panto male mice.** Results are depicted for baseline (1 h), post-normal saline (1 h), post-post-urethane (1 h) and post-atropine (3 h) recordings. $*p < 0.05$; $**p < 0.01$; $***p < 0.001$.

### 4.3.5. Electroencephalographic seizures analysis

Electroencephalographic seizures analysis was performed for wild-type controls (WT-DMSO and WT-Panto) and APPswePS1dE9 (APP(TG)-DMSO and APP(TG)-Panto) subgroups based on the EEG recordings from the hippocampal CA1 and motor cortical M1 regions of male mice.

#### Number of Spike trains

#### i) Hippocampal CA1 region

Dark cycle

A significant increase in number of spike trains was observed in APP(TG)-DMSO compared to WT-DMSO and APP(TG)-Panto mice at 19 weeks of age (WT-DMSO, n = 3: 3.167 ± 3.167 vs. APP(TG)-DMSO, n = 3: 25.167 ± 10.109; p = 0.0423) (APP(TG)-DMSO, n = 3: 25.167 ± 10.109 vs. APP(TG)-Panto, n = 3: 3.167 ± 0.928; p = 0.0423). Furthermore, a significant increase was detected at 19 weeks compared to 20 weeks of age for the APP(TG)-DMSO mice (19 weeks, n = 3: 25.167 ± 10.109 vs. 20 weeks, n = 3: 2.167 ± 1.302; p = 0.0475).

A statistical trend in number of spike trains was observed between 19 weeks and 21 weeks of age for the APP(TG)-DMSO group (19 weeks, n = 3: 25.167 ± 10.109 vs. 21 weeks, n = 3: 2.500 ± 1.803; p = 0.0525).

However, no significant differences in number of spike trains were identified between all other study groups (Fig. 4.3.25A).

Light cycle

A significant increase in number of spike trains was observed in APP(TG)-Panto compared to WT-Panto mice during 21 weeks of age (WT-Panto, n = 3: 1.500 ± 1.258 vs. APP(TG)-Panto, n = 3: 15.167 ± 9.329; p = 0.0484). A statistical trend in number of spike trains was detected between 19 weeks and 20 weeks of age for the APP(TG)-DMSO mice (19 weeks, n = 3: 13.333 ± 5.495 vs. 20 weeks, n = 3: 0.333 ± 0.333; p = 0.0973). Additionally, a statistical trend was identified between 21 weeks and 17 weeks of age for the APP(TG)-Panto group (17 weeks, n = 3: 2.000 ± 2.000 vs. 21 weeks, n = 3: 15.167 ± 9.329; p = 0.0906). Similarly, a statistical trend was observed between 21 weeks and 20 weeks of age for the APP(TG)-Panto group (20 weeks, n = 3: 1.000 ± 0.764 vs. 21 weeks, n = 3: 15.167 ± 9.329; p = 0.0579).

However, no significant differences in number of spike trains were detected between all other study groups (Fig. 4.3.25B).

### ii) Motor cortical M1 region

Dark cycle

A significant increase in number of spike trains was observed in APP(TG)-Panto compared to WT-DMSO 21 weeks of age (WT-DMSO, n = 3: 0.000 ± 0.000 vs. APP(TG)-Panto, n = 3: 23.667 ± 10.806; p = 0.0371).

However, no significant differences in number of spike trains were detected between all other study groups (Fig. 4.3.25C).

Light cycle

A significant increase in number of spike trains was observed in APP(TG)-Panto compared to WT-DMSO, WT-Panto and APP(TG)-DMSO mice at 21 weeks of age (WT-DMSO , n = 3: 0.167 ± 0.167 vs. APP(TG)-Panto, n = 3: 34.500 ± 25.799; p = 0.0226) (WT-Panto , n = 4: 3.875 ± 3.550 vs. APP(TG)-Panto, n = 3: 34.500 ± 25.799; p = 0.0321) (APP(TG)-DMSO, n = 3: 2.333 ± 1.642 vs. APP(TG)-Panto, n = 3: 34.500 ± 25.799; p = 0.0363). Likewise, a significant increase was detected at 21 weeks compared to 18 weeks of age for the APP(TG)-Panto mice (18 weeks, n = 3: 1.333 ± 0.882 vs. 21 weeks, n = 3: 34.500 ± 25.799; p = 0.0446).

A statistical trend in number of spike trains was observed between 21 weeks compared to 20 weeks of age for the APP(TG)-Panto (20 weeks, n = 3: 2.167 ± 0.882 vs. 21 weeks, n = 3: 34.500 ± 25.799; p = 0.0532).

However, no significant differences in number of spike trains were detected between all other study groups (Fig. 4.3.25D).

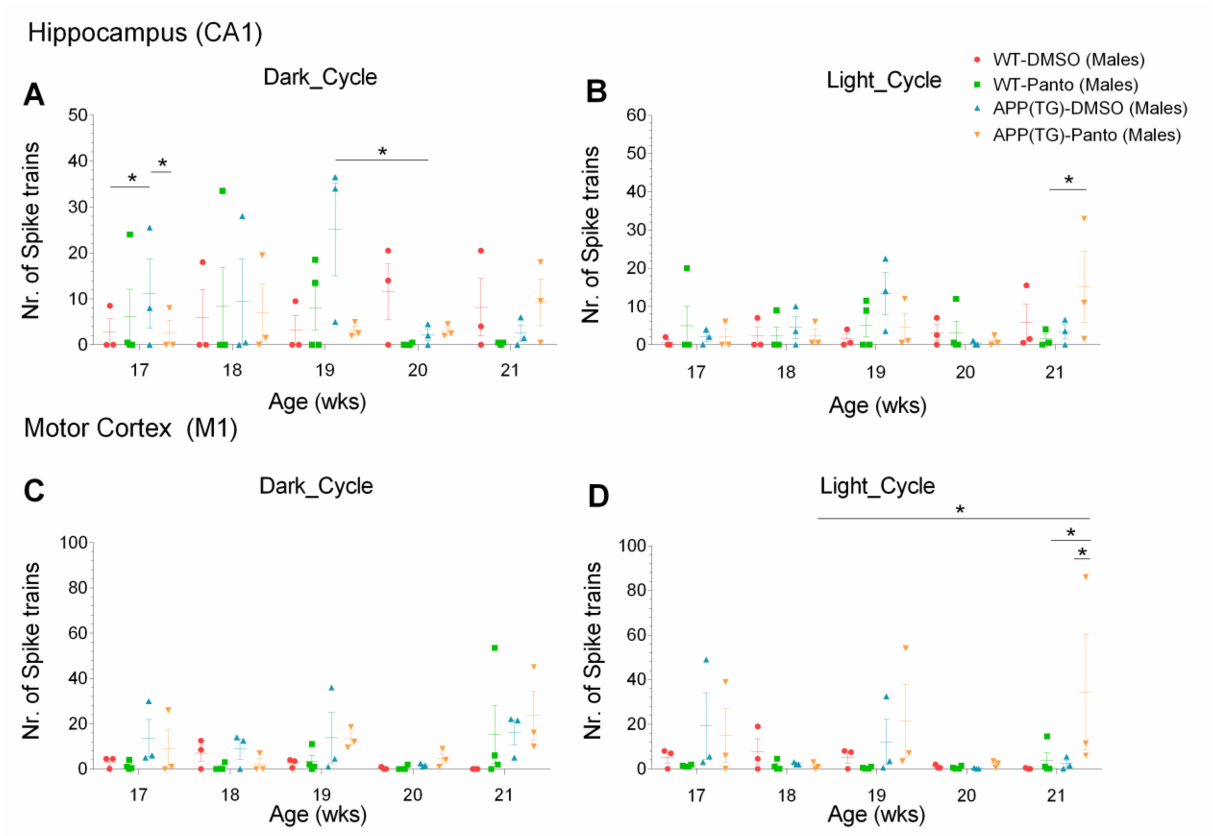

**Figure 4.3.25: Hippocampus (CA1) (A,B) and motor cortex (M1) (C,D) number of spike trains in WT-DMSO, WT-Panto, APP(TG)-DMSO and APP(TG)-Panto male mice.** Results are depicted considering the circadian rhythmicity (dark/light cycle). $^{*}$ $p < 0.05$; $^{**}$ $p < 0.01$; $^{***}$ $p < 0.001$.

### Total number of single spikes

### i) Hippocampal CA1 region

Dark cycle

A significant increase in total number of single spikes was observed in APP(TG)-DMSO compared to WT-Panto mice at 17 weeks of age (WT-Panto, n = 4: 554.750 ± 431.537 vs. APP(TG)-DMSO, n = 3: 3107.167 ± 919.196; p = 0.0402). Additionally, a significant increase was detected in APP(TG)-DMSO compared to WT-DMSO and WT-Panto mice at 19 weeks of age (WT-DMSO, n = 3: 403.167 ± 280.622 vs. APP(TG)-DMSO, n = 3: 3576.667 ± 625.012; p = 0.0127) (WT-Panto, n = 4: 716.625 ± 378.134 vs. APP(TG)-DMSO, n = 3: 3576.667 ± 625.012; p = 0.0174). However, a statistical trend in total number of single spikes was detected between APP(TG)-DMSO and WT-DMSO groups at 17 weeks of age (WT-DMSO, n = 3: 718.167 ± 356.055 vs. APP(TG)-DMSO, n = 3: 3107.167 ± 919.196; p = 0.0885).

However, no significant differences in total number of single spikes were identified between all other study groups (Fig. 4.3.26A).

Light cycle

A significant increase in total number of single spikes was observed in APP(TG)-DMSO compared to WT-DMSO mice at 19 weeks of age (WT-DMSO, n = 3: 250.333 ± 109.296 vs. APP(TG)-DMSO, n = 3: 3286.667 ± 1100.604; p = 0.0479). A statistical trend in total number of single spikes was detected between APP(TG)-DMSO and WT-Panto groups at 19 weeks of age (WT-Panto, n = 4: 545.375 ± 291.570 vs. APP(TG)-DMSO, n = 3: 3286.667 ± 1100.604; p = 0.0596). No significant differences in total number of single spikes were identified between all other study groups (Fig. 4.3.26B).

**ii) Motor cortical M1 region**

Dark cycle

A significant increase in total number of single spikes was observed in APP(TG)-DMSO group compared to WT-DMSO, WT-Panto and APP(TG)-Panto groups at 17 weeks of age (WT-DMSO, n = 3: 1042.500 ± 394.931 vs. APP(TG)-DMSO, n = 3: 3834.500 ± 264.906; p = 0.0018) (WT-Panto, n = 4: 770.250 ± 152.538 vs. APP(TG)-DMSO, n = 3: 3834.500 ± 264.906; p = 0.0002) (APP(TG)-DMSO, n = 3: 3834.500 ± 264.906 vs. APP(TG)-Panto, n = 3: 1606.333 ± 754.804; p = 0.0169). Furthermore, a significant increase was detected in APP(TG)-DMSO compared to WT-Panto mice at 18 weeks of age (WT-Panto, n = 4: 696.750 ± 319.429 vs. APP(TG)-DMSO, n = 3: 2529.333 ± 890.501; p = 0.0434).

Moreover, a significant increase in total number of single spikes was observed at 17 weeks compared to 19 weeks, 20 weeks and 21 weeks of age for the APP(TG)-DMSO mice (17 weeks, n = 3: 3834.500 ± 264.906 vs. 19 weeks, n = 3: 1328.000 ± 452.081; p = 0.0092) (17 weeks, n = 3: 3834.500 ± 264.906 vs. 20 weeks, n = 3: 1566.667 ± 493.922; p = 0.0226) (17 weeks, n = 3: 3834.500 ± 264.906 vs. 21 weeks, n = 3: 1169.500 ± 315.106; p = 0.0049).

A statistical trend in total number of single spikes was detected between APP(TG)-DMSO compared to APP(TG)-Panto mice at 18 weeks of age (APP(TG)-DMSO, n = 3: 2529.333 ± 890.501 vs. APP(TG)-Panto, n = 3: 783.167 ± 71.359; p = 0.0857). Likewise, a statistical trend was identified between WT-Panto and WT-DMSO groups at 21 weeks of age (WT-DMSO, n = 3: 403.167 ± 100.925 vs. WT-Panto, n = 4: 2029.375 ± 973.400; p = 0.0877).

However, no significant differences in total number of single spikes were identified between all other study groups (Fig. 4.3.26C).

Light cycle

A significant increase in total number of single spikes was observed in APP(TG)-DMSO compared to WT-DMSO, WT-Panto and APP(TG)-Panto mice at 17 weeks of age (WT-DMSO, n = 3: 1135.667 ± 480.889 vs. APP(TG)-DMSO, n = 3: 3640.500 ± 818.957; p = 0.0007) (WT-Panto, n = 4: 758.875 ± 134.264 vs. APP(TG)-DMSO, n = 3: 3640.500 ± 818.957; p < 0.0001) (APP(TG)-DMSO, n = 3: 3640.500 ± 818.957 vs. APP(TG)-Panto, n = 3: 1713.000 ± 755.250; p = 0.0123). Additionally, a significant increase was detected in APP(TG)-Panto compared to WT-DMSO mice at 21 weeks of age (WT-DMSO, n = 3: 259.667 ± 46.066 vs. APP(TG)-Panto, n = 3: 2264.667 ± 802.313; p = 0.0086).

Moreover, a significant increase in total number of single spikes was observed at 17 weeks compared to 18 weeks and 19 weeks of age for the APP(TG)-DMSO mice (17 weeks, n = 3: 3640.500 ± 818.957 vs. 18 weeks, n = 3: 1775.667 ± 223.053; p = 0.0253) (17 weeks, n = 3: 3640.500 ± 818.957 vs. 19 weeks, n = 3: 1373.333 ± 506.853; p = 0.0039). Likewise, a significant increase was detected at 17 weeks compare to 20 weeks and 21 weeks of age for the APP(TG)-DMSO mice (17 weeks, n = 3: 3640.500 ± 818.957 vs. 20 weeks, n = 3: 747.000 ± 420.608; p = 0.0002) (17 weeks, n = 3: 3640.500 ± 818.957 vs. 21 weeks, n = 3: 1333.000 ± 519.578; p = 0.0032).

A statistical trend in total number of single spikes was observed between APP(TG)-Panto and WT-Panto groups at 21 weeks of age (WT-Panto, n = 4: 855.875 ± 296.274 vs. APP(TG)-Panto, n = 3: 2264.667 ± 802.313; p = 0.071). Additionally, a statistical trend was detected between 21 weeks and 18 weeks of age for the APP(TG)-Panto mice (18 weeks, n = 3: 662.833 ± 103.222 vs. 21 weeks, n = 3: 2264.667 ± 802.313; p = 0.0737).

However, no significant differences in total number of single spikes were observed between all other study groups (Fig. 4.3.26D).

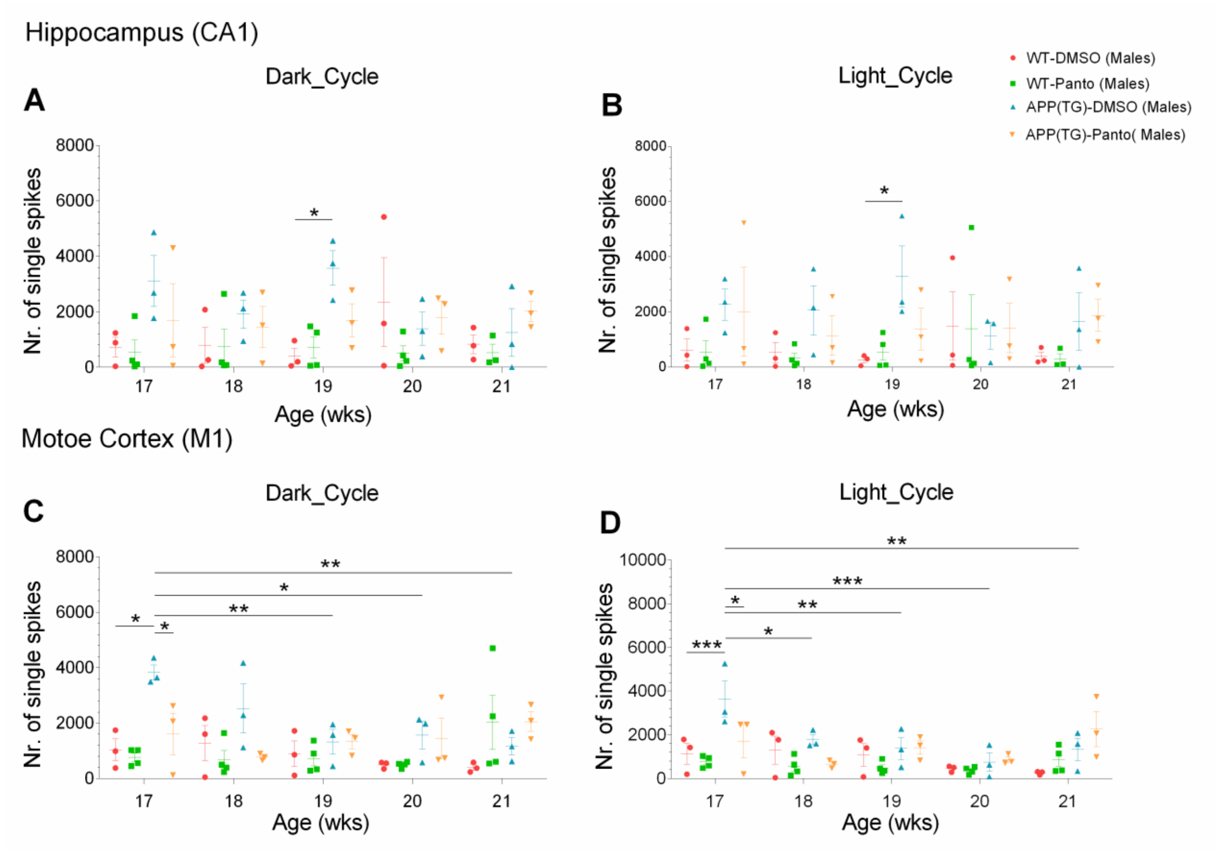

**Figure 4.3.26: Hippocampus (CA1) (A,B) and motor cortex (M1) (C,D) total number of single spikes in WT-DMSO, WT-Panto, APP(TG)-DMSO and APP(TG)-Panto male mice.** Results are depicted considering the circadian rhythmicity (dark/light cycle). $^{*}p < 0.05$; $^{**}p < 0.01$; $^{***}p < 0.001$.

**Spike trains duration (min)**

**i) Hippocampal CA1 region**

Dark cycle

A significant increase in spike trains duration (min) was observed in APP(TG)-DMSO compared to WT-DMSO and APP(TG)-Panto mice at 19 weeks of age (WT-DMSO, n = 3: 0.041 ± 0.041 vs. APP(TG)-DMSO, n = 3: 0.425 ± 0.176; p = 0.0239) (APP(TG)-DMSO, n = 3: 0.425 ± 0.176 vs. APP(TG)-Panto, n = 3: 0.033 ± 0.009; p = 0.0207). Likewise, a significant increase was detected at 19 weeks compared to 20 weeks of age for the APP(TG)-DMSO mice (19 weeks, n = 3: 0.425 ± 0.176 vs. 20 weeks, n = 3: 0.032 ± 0.021; p = 0.0311).

A statistical trend in spike trains duration (min) was identified between APP(TG)-DMSO and WT-Panto groups at 19 weeks of age (WT-Panto, n = 4: 0.111 ± 0.065 vs. APP(TG)-DMSO, n = 3: 0.425 ± 0.176; p = 0.0592). Additionally, a statistical trend was detected between 19 weeks and

21 weeks of age for the APP(TG)-DMSO group (19 weeks, n = 3: 0.425 ± 0.176 vs. 21 weeks, n = 3: 0.060 ± 0.049; p = 0.0531).

However, no significant differences in spike trains duration (min) were detected between all other study groups (Fig. 4.3.27A).

Light cycle

No significant differences in spike trains duration (min) were identified between all study groups (Fig. 4.3.27B).

**ii) Motor cortical M1 region**

Dark cycle

A significant increase in spike trains duration (min) was detected in APP(TG)-DMSO group compared to WT-DMSO, WT-Panto and APP(TG)-Panto groups at 19 weeks of age (WT-DMSO, n = 3: 0.027 ± 0.012 vs. APP(TG)-DMSO, n = 3: 0.993 ± 0.966; p = 0.0171) (WT-Panto, n = 4: 0.053 ± 0.039 vs. APP(TG)-DMSO, n = 3: 0.993 ± 0.966; p = 0.0123) (APP(TG)-DMSO, n = 3: 0.993 ± 0.966 vs. APP(TG)-Panto, n = 3: 0.152 ± 0.031; p = 0.0467). Similarly, a significant increase was observed at 19 weeks compared to 18 weeks and 20 weeks of age for the APP(TG)-DMSO mice (18 weeks, n = 3: 0.097 ± 0.049 vs. 19 weeks, n = 3: 0.993 ± 0.966; p = 0.0463) (19 weeks, n = 3: 0.993 ± 0.966 vs. 20 weeks, n = 3: 0.016 ± 0.004; p = 0.0242).

A statistical trend in spike trains duration (min) was identified between 19 weeks and 17 weeks of age for the APP(TG)-DMSO mice (17 weeks, n = 3: 0.143 ± 0.088 vs. 19 weeks, n = 3: 0.993 ± 0.966; p = 0.066).

However, no significant differences in spike trains duration (min) were observed between all other study groups (Fig. 4.3.27C).

Light cycle

A statistical trend in spike trains duration (min) was observed between APP(TG)-DMSO and WT-Panto mice at 19 weeks of age (WT-Panto, n = 4: 0.007 ± 0.004 vs. APP(TG)-DMSO, n = 3: 0.620 ± 0.596; p = 0.0759). Furthermore, a statistical trend was detected between APP(TG)-Panto compared to WT-DMSO and WT-Panto mice at 21 weeks of age (WT-DMSO, n = 3: 0.002 ± 0.002 vs. APP(TG)-Panto, n = 3: 0.632 ± 0.508; p = 0.0935) (WT-Panto, n = 4: 0.048 ± 0.044 vs. APP(TG)-Panto, n = 3: 0.632 ± 0.508; p = 0.0977).

No significant differences in spike trains duration (min) were identified between all other analyzed groups (Fig. 4.3.27D).

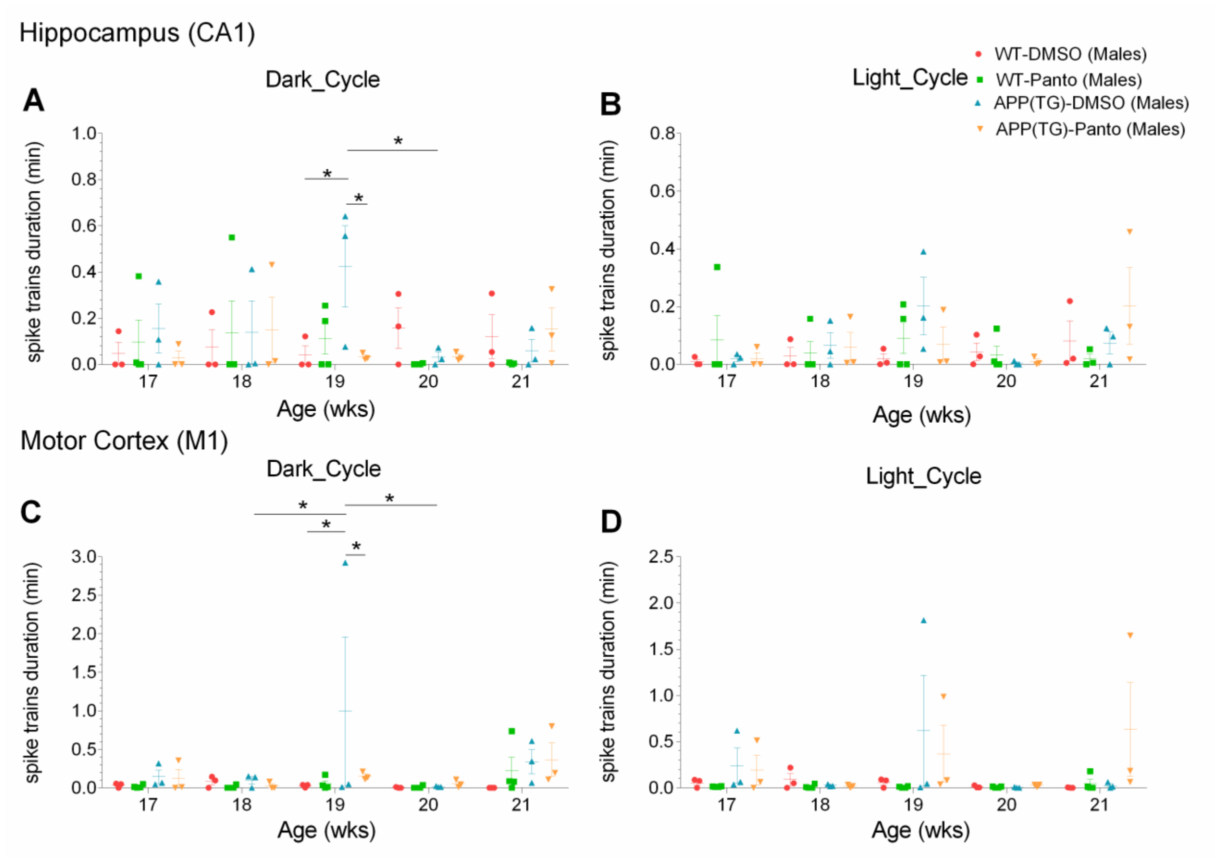

**Figure 4.3.27: Hippocampus (CA1) (A,B) and motor cortex (M1) (C,D) spike trains duration (min) in WT-DMSO, WT-Panto, APP(TG)-DMSO and APP(TG)-Panto male mice.** Results are depicted considering the circadian rhythmicity (dark/light cycle). $^{*}$ $p$ < 0.05; $^{**}$ $p$ < 0.01; $^{***}$ $p$ < 0.001.

# 5. Discussion

Neurodegenerative diseases are one of the major health concerns around the world, which are characterized by structural and functional loss of nerve cells in the peripheral and central nervous system (PNS and CNS). According to World Health Organization (WHO), neurodegenerative diseases are one of the leading threats to people health (WHO). Alzheimer's disease (AD) is one of the major forms of neurodegenerative diseases and leading cause of deaths worldwide linked with underlying conditions of dementia, memory deficit and cognitive decline mostly in ageing populations (DeTure & Dickson, 2019; N. Ma et al., 2020). Dementia is described by a number of symptoms such as decline in memory, problem solving, language and thinking skills, which effect everyday life activities (ALZ.ORG, 2020). As reported by the WHO, there are 50 million people with dementia worldwide and the prevalence is likely to increase up to 82 million in 2030 and 152 million in 2050, respectively. Importantly, about 60-70% of these cases are due to Alzheimer's disease (WHO). Electrophysiological biomarkers, most importantly the EEG fingerprints, are very important tools to detect not only the incidence of dementia but also characterize the progression of disease in later life as compared to other diagnostic tools. My present study was designed to evaluate the pathophysiological and pharmacological aspects of AD by characterization of EEG fingerprints in transgenic mouse models as follows:

## 5.1. Hippocampal EEG alterations in $Ca_v3.2$ mice and the involvement of the GABAergic system

In this study, we have investigated the role of low voltage activated (LVA) T-Type $Ca_v3.2$ ($\alpha_1H$) VGCCs in the modulation of theta oscillatory architecture regarding their involvement in motor, cognitive and behavioral activities in the hippocampus of $Ca_v3.2$ knockout mice.

It has been reported that atropine sensitive type II theta plays a significant role in the regulation of encoding and consolidation of memory engrams, the importance of which is well established in AD patients (Davies & Maloney, 1976; Whitehouse et al., 1982). Hence, hippocampal acetylcholine (ACh) levels are elevated during active memory encoding (Hasselmo & McGaughy, 2004) and numerous pharmacological studies demonstrated that ACh hinders the process of consolidation during the activation of memory encoding (Hasselmo & McGaughy, 2004; Kukolja, Thiel, & Fink, 2009; Rasch, Born, & Gais, 2006). The hippocampal memory encoding process is enhanced by activation of Schaffer collaterals (Gu & Yakel, 2011). The entorhinal cortex (EC) serves as an interface which receives sensory information from layer II and III from principal neurons from the neocortex and forwards this information to the hippocampus for memory encoding (Burwell & Amaral, 1998). The encoding trisynaptic pathway activates the EC to the dentate gyrus, the CA3 area and ultimately the CA1 region (our recording area). For memory consolidation, the direct innervation to the CA1 region from the EC via the temporoammonic pathway (EC-CA1) is also possible (Remondes & Schuman, 2004). Inversely, the hippocampal information predominantly received by principal neurons of layer V of the EC send back information to the cortex for memory consolidation (Canto, Wouterlood, & Witter, 2008). In the modulation of these processes, numerous interneuronal cell types are involved (Pelkey et al., 2017), such as oriens lacunosum molecular (OLM) interneurons of the CA1 area which control the information output by negative feedback mechanisms. The Basket / Chandelier interneuronal cells also play a crucial role in theta genesis. About ~14% of CA1, hippocampal interneurons consist of parvalbumin-expressing Basket cells, and ~4% of Chandelier cells (Pelkey et al., 2017). It is hypothesized that theta generation in the CA1 region is mediated by the relative magnitude and phase relationship of the perisomatic inhibitory and distal dendritic excitatory dipoles of hippocampal pyramidal cells (Buzsáki, 2002).

The voltage-dependent calcium influx in dendrites of hippocampal pyramidal neurons mediated by VGCCs perform a crucial role in theta generation (Buzsáki, 2002), linked with many memory processing and learning activities (Griffin, Asaka, Darling, & Berry, 2004; Seager, Johnson, Chabot, Asaka, & Berry, 2002) and movement like behavior (Bland & Oddie, 2001). The septohippocampal neural circuit receives projections from many brain regions for theta generation for the coding of sensory and motor information processing (Oddie & Bland, 1998; Vertes, Hoover, & Viana Di Prisco, 2004), and may activate the modulation of theta/alpha activity in relation to specific behavioral circumstances.

In a recent study, it has been reported that Ca$_v$3.1 VGCCs ablation leads to enhanced theta power possibly due to the tonic inhibition of GABAergic hippocampal interneurons through GABAergic septal interneurons. The latter was hypothesized to enhance theta activity by disinhibition of hippocampal pyramidal neurons (Gangadharan et al., 2016).

Clearly, Ca$_v$3.1 is expressed in the septohippocampal system. However, Ca$_v$3.2 expression dominates (Aguado et al., 2016; Talley et al., 1999). Hence, we have evaluated the role of Ca$_v$3.2 in the generation and architecture of theta/alpha activity in Ca$_v$3.2 knock out mice. Earlier studies had predicted elevated anxiety behavior and impaired memory formation in Ca$_v$3.2 knock out animals (Gangarossa et al., 2014). A decline in memory function in Ca$_v$3.2 knockout mice was illustrated by hippocampal recognition tasks such as spatial object recognition (SOR) and the novel object recognition (NOR) testing. Ca$_v$3.2 ablation in mice did not exhibit any preference for the relocated or novel object during the 24 h recall session in contrast to control animals. Particularly, impaired exploratory drives were not the cause of this modified response (Gangarossa et al., 2014). Interestingly, the motor learning skills and spatial working memory as assessed by instinctive modification in the Y-Maze, remained unchanged in $Ca_v3.2$ deficient mice. Moreover, elevated plus maze and open field behavior analysis fully endorsed the role of $Ca_v3.2$ VGCCs in anxiety-related behaviors (Gangarossa et al., 2014).

According to these findings and the evidence that $Ca_v3.2$ VGCCs is excessively expressed in the septohippocampal system (Aguado et al., 2016), we analyzed the role of $Ca_v3.2$ in theta genesis and theta architecture relevant for memory formation.

We investigated the role of $Ca_v3.2$ VGCCs in atropine sensitive type II theta oscillations and their capability to regulate theta architecture in the hippocampal CA1 region measured by implantable EEG radiotelemetry. This is the first direct functional in vivo association between $Ca_v3.2$ and theta activity in rodents. Particularly, the rise in theta/alpha relative EEG power was highly prominent at the inactive state of either the dark or the light cycle (Fig. 4.1.8B,C; Fig. 4.1.9B,C; Fig. 4.1.12B,C; Fig. 4.1.13B,C). The inactive state can be characterized (at least in part) as an alert immobile physiological phase, that expresses hippocampal type II theta activity. Hence, the altered theta activity in $Ca_v3.2$ knockout mice are likely to be linked to atropine sensitive type II theta oscillations. This is further proved by the results from the urethane injection studies (Fig. 4.1.15B,C; Fig. 4.1.16B,C). Urethane is a multi-target drug at numerous ligand and voltage-gated ion channels with agonistic effects at muscarinic and nicotinic acetylcholine receptors (AChR), gamma-aminobutyric acid type A receptors (GABA-AR) and glycine receptor (GlyR) and antagonistic effects at NMDA and AMPA receptors (Hara & Harris, 2002; Sceniak & Maciver, 2006). Urethane induces type II theta oscillations and $Ca_v3.2$ knockout mice again shows an increase in the relative theta / alpha EEG power and peak frequencies. Particularly, locomotor activity might have essential impact on theta I / theta II distribution. Therefore, it is important that $Ca_v3.2$ control animals and knockout mice show characteristic circadian pattern. Nevertheless, no significant differences were found between both genotypes demonstrating that modifications in hippocampal theta / alpha oscillations are not linked to an alteration in locomotor activity.

Anxiety related behavior in $Ca_v3.2$ knockout mice as analyzed by light and dark conflict test / context (Crawley & Goodwin, 1980) and exploratory behavior by elevated plus maze (EPM) and open field test recommended elevated anxiety in $Ca_v3.2$ deficient mice not linked with compulsive and repetitive behaviors (Gangarossa et al., 2014). Particularly, these findings are correlated with an earlier analysis by Choi et al. (2007) which reported a lack of an anxiety related phenotype in $Ca_v3.2^{-/-}$ mice in the dark and light conflict test (Choi et al., 2007). This variation could be due to the different genetic background of the $Ca_v3.2$ knockout lines (Bouwknecht & Paylor, 2002) and varying behavioral analysis used in these two studies (Bourin & Hascoet, 2003; Choi et al., 2007; Contet, Rawlins, & Bannerman, 2001; Contet, Rawlins, & Deacon, 2001; Crawley & Goodwin, 1980; Gangadharan et al., 2016). In addition, elevated anxiety does not necessarily correlate with a rise in theta power. Attenuation of type II theta activity caused by deficiency of the septal PLC$\beta_4$ isoform resulted in elevated anxiety as also reported in Ca$_v$2.3 knockout mice (Lee, Gomora, Cribbs, & Perez-Reyes, 1999; Muller et al., 2012; J. Shin et al., 2009). Overall, theta / alpha modification in Ca$_v$3.2 knockout mice does not seem to be attributable to altered anxiety levels. Furthermore, we evaluated the molecular mechanisms related to theta / alpha alterations in Ca$_v$3.2 knockout mice. VGCCs play very important role for long-term potentiation (LTP), memory formation and learning. The hippocampal and amygdala-dependent tasks are mediated by NMDA-independent Ca$^{2+}$ influx through VGCCs. Alterations in spatial memory and impaired fear conditioning were reported in HVA L-type Ca$_v$1.2 and Ca$_v$1.3 mutant mice (McKinney & Murphy, 2006; Moosmang, Lenhardt, Haider, Hofmann, & Wegener, 2005; White et al., 2008) and impaired memory function was reported upon Ca$_v$2.2 P/Q-type VGCCs deficiency (Mallmann et al., 2013). Interestingly, it has been reported that the impairment of T-type Ca$^{2+}$ channels can modify the induction and maintenance of hippocampal, cerebellum and visual cortex LTP (C. C. Chen et al., 2012; Ly et al., 2013; Yoshimura et al., 2008). Also, autism spectrum disorders (ASD) have been associated with mutations in the human Cacna1h gene (Splawski et al., 2006). Additionally, the interaction of Ca$_v$3.2 VGCCs with the neurotransmitter release machinery boosts the assumption of their impact on synaptic transmission (A. H. Tang et al., 2011; Weiss, Hameed, et al., 2012; Weiss, Zamponi, & De Waard, 2012). In a recent study, Gangadharan et al. (2016) demonstrated that Ca$_v$3.1 deficient mice exhibit an increase in type II theta activity (Gangadharan et al., 2016). This increase in theta activity was linked to a shift in the GABAergic septal interneuron-firing pattern from the burst mode to the tonic mode. T-type VGCCs are well known to generate low-threshold Ca$^{2+}$ spikes and burst activity (Cheong & Shin, 2013; C. Park et al., 2010; Steriade & Llinas, 1988). Hence, Ca$_v$3.2 deficiency leads to tonic inhibition of hippocampal GABAergic interneurons by innervation of septal GABAergic interneurons. This perisomatic disinhibition of hippocampal pyramidal neurons was assumed to increase theta activity in Ca$_v$3.1 deficient mice (Freund & Antal, 1988; Gangadharan et al., 2016; Smythe, Colom, & Bland, 1992). Due to the fact, that Ca$_v$3.2 expression exceeds that of Ca$_v$3.1 in the septohippocampal system (Aguado et al., 2016), we hypothesized that Ca$_v$3.2 ablation causes an identical sequence of septal GABAergic tonic inhibition and disinhibition of pyramidal neurons as detected in Ca$_v$3.1 deficient mice. To confirm this potential mechanism in Ca$_v$3.2 deficient mice in the septohippocampal system, we had a look at previous transcriptome analysis from the hippocampus of Ca$_v$3.2$^{+/+}$ and Ca$_v$3.2$^{-/-}$

animals (Papazoglou, Henseler, et al., 2017). A significant reduction in dynein light chain Tctex-Type 1 (Dynlt1b) was observed in $Ca_v3.2$ deficient mice as analyzed by qPCR (Fig. 4.1.18B). The translocation of GABA receptors to the subsynaptic or extrasynaptic membrane is mediated by dynein light chain as a part of GABA receptor transpotome complex (Nakamura et al., 2016; Valenzuela et al., 2014; Zapata et al., 2017).

This was first indication that the GABAergic system is indeed modified in the septohippocampal system of $Ca_v3.2$ knockout mice. Thus, we further evaluated the levels of GABA A and GABA B receptors transcripts. The transcript levels for the GABA A receptor δ subunit and GABA B1 receptor subunits were significantly decreased in $Ca_v3.2$ knockout mice and a statistical trend was observed for the GABA B2 receptor subunit (Fig. 4.1.19H,J,K). These findings fully support our GABA assumption of increased theta / alpha power in $Ca_v3.2$ deficient mice, as inhibition within the CNS mediated by GABA A receptors take place by sustained tonic inhibition and fast synaptic transmission (Capogna & Pearce, 2011). GABA A receptor subunit-δ located extra synaptically in thalamic neurons and dentate gyrus granule cells mediate tonic current relevant for neuronal and interneuronal stimulation in response to ambient GABA concentrations (Belelli & Lambert, 2005; Farrant & Nusser, 2005; Mody & Pearce, 2004). Alternatively, GABA B1 subunit receptors can be identified within dendritic spines that mediate slow postsynaptic inhibition (Perez-Garci, Gassmann, Bettler, & Larkum, 2006; Vigot et al., 2006).

We also found a significant trend for 5-hydroxytryptamine receptor 2C (5Ht2c) upregulation (Fig. 4.1.18C). This 5HT2c upregulation might contribute to the detected theta / alpha phenotype (Busceti et al., 2015; Imbrici, Tucker, D'Adamo, & Pessia, 2000; Papp et al., 2019). It has been reported by Hajos et al. (2003) that theta activity is tonically regulated in the septohippocampal system by 5HT2c receptors as observed in anesthetized rat (Hajos, Hoffmann, & Weaver, 2003). Postsynaptic 5HT2c receptors are known to mediate tonic inhibition and 5HT2c receptors agonists such as 1-(3-cholophenyl)piperazine dihydrochloride (m-CCP) or [S]-2-(chloro-5-fluoro-indol-1-yl)-1-methyl-ethylamine fumarate (Ro 60-0175) cause a dose dependent inhibition of firing activity in the MS/DBB neurons and reduction of theta activity in MS/DBB and hippocampal neurons (Hajos et al., 2003). Along with impaired theta activity in the MS/DBB, the desynchronized hippocampal EEG changes to lower frequencies in the power density plots. 5HT2c receptors upregulation in $Ca_v3.2$ knockout mice could represent a compensatory mechanism to counterbalance the septal GABAergic tonic inhibition, hippocampal disinhibition and increase in type II theta activity. Significantly, we have no other indications from our own microarray and qPCR analysis that there are compensatory transcriptional alterations of the other T-Type $Ca^{2+}$

channels such as Ca$_v$3.1 and Ca$_v$3.3 in the hippocampus (Fig. 4.1.18F; Fig. 4.1.19G). Thus, changes observed seem to be entirely due to Ca$_v$3.2 ablation itself.

In summary, our qPCR findings propose that extrasynaptic and postsynaptic GABA receptors are reduced due to tonic inhibition of hippocampal interneurons and a decline in plasma membrane density is likely to be due to an impaired dynein / GABA receptor containing transpotome complex (Fig. 5.1A,B).

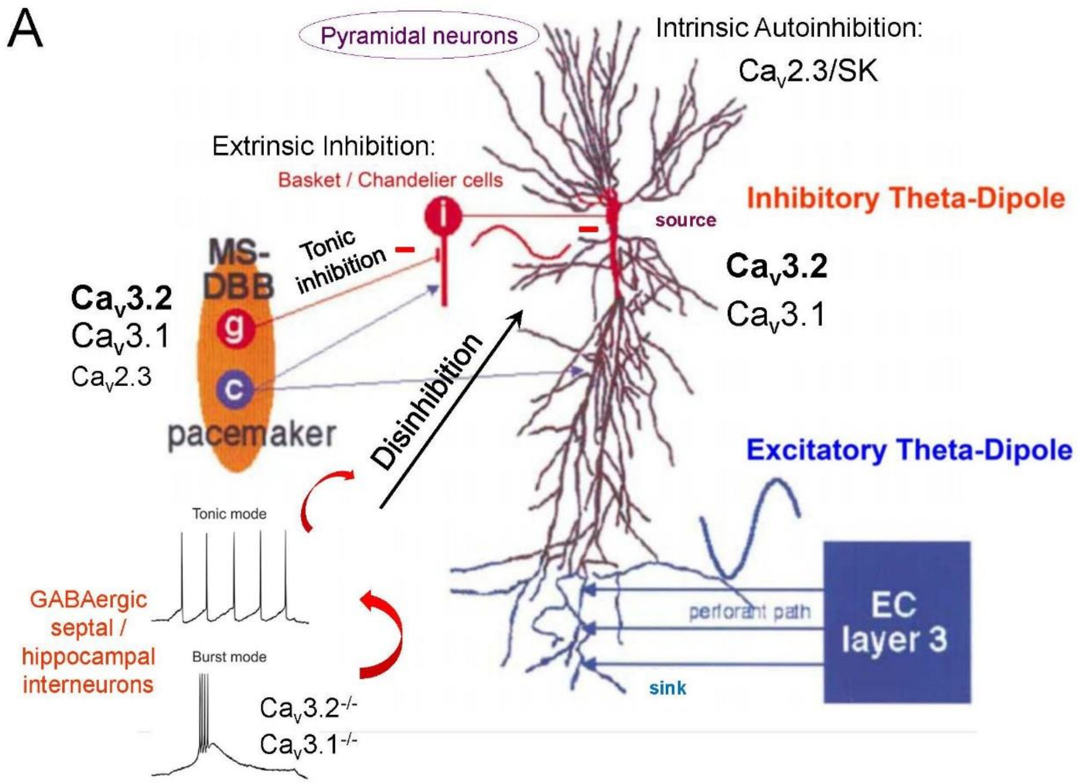

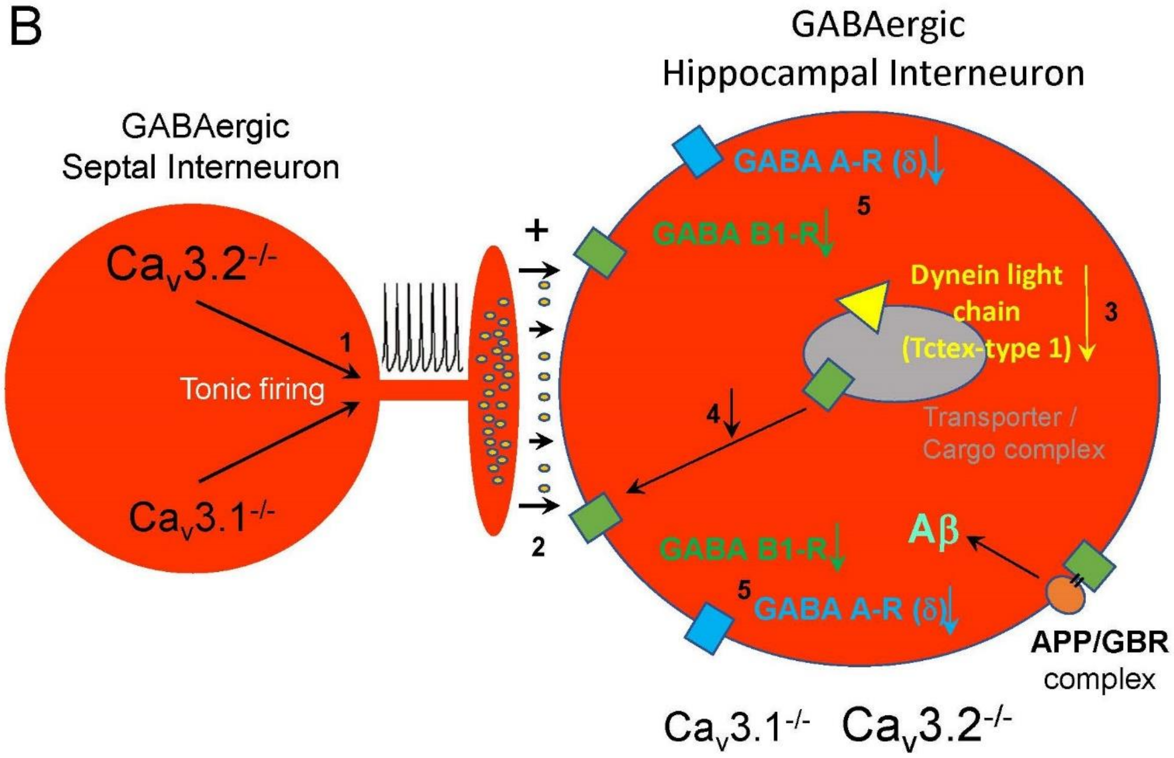

**Figure 5.1: T-type VGCCs and the GABAergic transmission in hippocampal thetagenesis.** (A) Septal GABAergic interneurons express both $Ca_v3.1$ and $Ca_v3.2$ VGCCs and project on hippocampal interneurons. Ablation of both T-type $Ca^{2+}$ channel entities significantly impairs burst activity and favors the tonic mode of action in septal interneurons. The later exert tonic inhibition of hippocampal GABAergic interneurons, resulting in disinhibition of hippocampal pyramidal neurons. Consequently, hippocampal type 2 theta oscillations are increased in $Ca_v3.1^{-/-}$ and $Ca_v3.2^{-/-}$ (modified from (Buzsáki, 2002) (B) Increased GABA release from septal interneurons upon tonic inhibition (1) could result in increased GABA release into the synaptic cleft (2) and a decline in GABA receptor density in hippocampal interneurons. This hypothesis is supported by a decrease in Dynlt1b transcripts (3). Dynein containing cellular transportomes were reported to mediate GABA receptor transfer and integration into the sub and post-synaptic membrane (4). In addition, we found a reduction in GABA A receptor delta subunit and GABA B1 receptor subunit transcript (5). Delta subunit containing GABA A receptors are localized extrasynaptically and are known to mediate tonic inhibition. As APP forms complexes with GABA B receptor, it might be speculated that APP/GBR complexes are destabilized in $Ca_v3.2$ deficient mice as well.

## 5.2. Pantoprazole effects in APPswePS1dE9 mice

### 5.2.1. Pantoprazole effects in APPswePS1dE9 mice aged 12-16 weeks

In this study, we have analyzed the relative activity units; relative EEG oscillatory pattern by an FFT based approach and seizures from the hippocampus (CA1) and motor cortex (M1) regions of the brain. The evaluation of these above-mentioned parameters was performed in both male and female wild type controls and APPswePS1dE9 transgenic (TG) mice subgroups.

In males, there was no significant difference in relative activity between controls and APPswePS1dE9 mice during both light and dark phases recorded at 12, 14 and 16 weeks of age from cortex and hippocampus (Fig. 4.2.1) while in female mice, increased relative activity in pantoprazole treated controls (WT-Panto) was found at 16 weeks of age compared to 14 weeks. The latter might be due to one of potential outlier (Fig. 4.2.2). Numerous studies have reported no significant difference in activity behavior among transgenic mouse AD models as compared to controls in this younger age (Lalonde, Dumont, Paly, London, & Strazielle, 2004; Lok et al., 2013; Pugh & Raman, 2006).

Moreover, in males, FFT based frequency analysis revealed an increase in theta (4-8 Hz) power observed in pantoprazole treated controls (WT-Panto) mice as compared to untreated controls (WT-DMSO) animals during the dark cycle at age of 12 weeks from hippocampus and at 16 weeks of age from cortex (Fig. 4.2.3A,C). Likewise, an increase in theta (4.1-12 Hz) power also detected in pantoprazole treated controls (WT-Panto) mice as compared to untreated controls (WT-DMSO) animals during the dark cycle at age of 12 and 14 weeks from hippocampus and at 16 weeks of age from cortex (Fig. 4.2.4A,C). Which might proposed that the increased theta in pantoprazole treated healthy controls could be correlated with enhanced cognitive performance because theta is an important marker in cognition and memory formation (Buzsáki, 2005), spatial and non-spatial cognitive processing (A. Goyal et al., 2020; Korotkova et al., 2018). These observations linked with the findings of previous studies that reported an increase in cognition after use of pantoprazole (Goldstein et al., 2017) and also decrease risk of dementia after use of PPIs (Booker et al., 2016). Theta oscillations are highly organized waves, involved in various neurological and behavioral functions such as learning and memory consolidation, awakening state, REM sleep and attention (Muller et al., 2012; Vertes, 2005). The nucleus of medial septum and diagonal band of broca MS/vDBB are assumed to be the pacemakers for the hippocampal theta generation (Broncel, Bocian, Kłos-Wojtczak, & Konopacki, 2018; Buzsáki, Leung, & Vanderwolf, 1983). Disruption of the septohippocampal system in AD might be the reason for hippocampal dysrhythmia, especially the impairment of theta oscillatory patterns (Babiloni et al., 2007; Babiloni et al., 2009; Cummins, Broughton, & Finnigan, 2008; Papazoglou, Soos, et al., 2016), as reported earlier that a decrease in theta power associated with cognitive deficit in AD (Scott et al., 2012). In my study, a significant increase in hippocampal theta power (4-8 Hz) was found at 12 weeks of age compared to 14 and 16 weeks old healthy control mice of both groups (WT-DMSO and WT-Panto). While the overall increase in theta (4-8 Hz) activity found in both healthy control groups (WT-DMSO and WT-Panto) compared to AD APPswePS1dE9 mice groups (APP (TG)-DMSO and APP (TG)-Panto) (Fig. 4.2.3). The reduction in theta power found in APPswePS1dE9 mice in my study might be correlated with the findings of previous studies that reported a decrease in theta activity recorded under urethane-induced anesthesia and evoked by brainstem stimulation in APPswePS1dE9 mice at 4 and 8 month of age (Scott et al., 2012). Similarly, Stoiljkovic et al. (2016) also reported a decrease in brain stem stimulation-evoked hippocampal theta activity in Aβ overloaded 5xFAD mice at 8 month of age (Stoiljkovic, Kelley, Nagy, Hurst, & Hajós, 2016). Stoiljkovic et al. (2018) further explored that the donepezil administration enhanced the brainstem stimulation-induced hippocampal theta power in 6 months old adults and 12 months old aged TgF344_AD rats (Stoiljkovic, Kelley, Horvath, & Hajós, 2018). There was also a significant increase in hippocampal and cortical theta (4-8 Hz) activity observed during dark cycle in pantoprazole treated control mice (WT-Panto) as compared to pantoprazole treated APPswePS1dE9 mice (Fig. 4.2.3A,C), which might be due to a decline in theta power found in AD as reported in previous studies (Scott et al., 2012; Stoiljkovic et al., 2018; Stoiljkovic et al., 2016). No significant difference in theta oscillatory power was detected between untreated (APP(TG)-DMSO) and pantoprazole treated (APP(TG)-Panto) mice during both dark and light phases from the hippocampus and motor cortex (Fig. 4.2.3; Fig. 4.2.4), indicating no inhibitory or beneficial effects of pantoprazole in theta related cognitive decline in AD as previously reported by Goldstein et al. (2017) (Goldstein et al., 2017). However, various previous studies have reported different findings about the use of PPIs and risk of dementia (Ortiz-Guerrero, Amador-Muñoz, Calderón-Ospina, López-Fuentes, & Nava Mesa, 2018). Previous studies have reported the long-term use of PPIs as a risk factor for dementia especially in elderly people (Gomm et al., 2016; Haenisch et al., 2015; Kumar et al., 2020; S. Y. Tai et al., 2017; X. Zhang, Clarke, & Rhynas, 2019). On the other hand, studies also reported the neuroprotective effect and decreased risk of dementia after use of PPIs. (Booker et al., 2016; Hashioka et al., 2009, 2011). Hashioka et al. (2009) and Hashioka et al. (2011) reported that the PPIs significantly attenuate the interferon-gamma (IFN-γ) activated neurotoxicity of human astrocytes by inhibition of the signal transducer and activator of transcription (STAT) 3 signaling pathway. Antineurotoxic properties of PPIs are useful option for the treatment of AD and other neuroinflammatory disorders linked with activated astrocytes (Hashioka et al., 2009, 2011).

Furthermore, we have also identified an increases cortical beta activity of different beta ranges (β: 12.1-30 Hz, 16-24 Hz, 16-30 Hz) in both untreated and treated APPswePS1dE9 (APP(TG)-DMSO) and (APP(TG)-Panto) mice as compared to healthy control mice (WT-DMSO and WT-Panto) at 12 and 14 weeks of age (Fig. 4.2.6; Fig. 4.2.7; Fig. 4.2.8). Increased cortical beta activity in transgenic AD mice could be linked with the findings of Schmidt et al., (2019) which demonstrated the correlation between increased beta power and discontinuation of retrieval of long-term memory (Schmidt et al., 2019), and also linked with hindrance of encoding and decoding of working memory as observed by Lundqvist et al. (2016, 2018) (Lundqvist, Herman, Warden, Brincat, & Miller, 2018; Lundqvist et al., 2016b). Proskovec et al. (2018) also revealed inverse association between cortical beta oscillatory activity and processing of spatial working memory, observed in behavioral analysis (Proskovec, Heinrichs-Graham, Wiesman, McDermott, & Wilson, 2018). Further, Hanslmayr et al. (2014) also observed impairment of memory encoding after beta activity stimulation during behavioral analysis (Hanslmayr & Staudigl, 2014). Alternatively, no significant difference observed in relative cortical beta power between pantoprazole treated and untreated APPswePS1dE9 (APP(TG)-DMSO and APP(TG)-Panto) indicated that no negative or positive pantoprazole effect found on beta related memory regulation in AD mouse models which further support our findings.

Likewise, we have observed significantly increased relative gamma low power (30-50 Hz) in pantoprazole treated APPswePS1dE9 (APP(TG)-Panto) compared to pantoprazole treated controls (WT-Panto) mice at 12 weeks of age at dark cycle from hippocampus (Fig. 4.2.11A). Moreover, increased relative gamma power also found in pantoprazole treated APPswePS1dE9 (APP(TG)-Panto) compared to pantoprazole treated controls (WT-Panto) mice at 12 and 14 weeks of age during dark cycle from cortex and at 12 weeks of age from cortex during light cycle (Fig. 4.2.11C,D). In addition, cortical gamma mid activity (50-70 Hz) was significantly enhanced in pantoprazole treated APPswePS1dE9 (APP(TG)-Panto) compared to controls (WT-Panto) at 12 weeks of age, and in untreated APPswePS1dE9 (APP(TG)-DMSO) compared to controls (WT-DMSO) at 14 weeks of age during dark cycle (Fig. 4.2.12C). Previous studies by Deursen et al. (2008) revealed similar findings of enhanced gamma power in AD patients as compared to mild cognitive impaired individuals and healthy controls (van Deursen, Vuurman, Verhey, van Kranen-Mastenbroek, & Riedel, 2008). Further, similar findings of previous studies also reported the enhanced gamma oscillatory activity in AD patients compared to healthy control subjects (J. Wang, Gu, Masters, & Wang, 2017). Gamma waves are involved in various cognitive process in the brain such as attention, perception ability and working memory (Jia, Smith, & Kohn, 2011; Nottage & Horder, 2015; Uhlhaas & Singer, 2006). They are thought to be generated by

GABAergic interneuronal circuitries (Buzsaki, Anastassiou, & Koch, 2012) that are innervated by stimulatory NMDA glutamatergic and inhibitory cholinergic networks (Picciotto, Higley, & Mineur, 2012). Dysregulation or disruption of this network may lead to abnormal discharge of gamma activities (J. Wang et al., 2017). It has been reported in various AD mouse models that the dysregulation of GABAergic interneuronal networks is associated with the pathophysiology of AD (Hazra et al., 2013; K. Ma & McLaurin, 2014; Verret et al., 2012). As reduced cholinergic activity and enhanced activation of NDMA glutamergic innervation are linked with dementia and a decrease in cognition and memory functions (J. Wang et al., 2017). Cisse et al. (2011) described that the NDMA glutamatergic neuronal communications are disrupted by Aβ accumulation, which is the hallmark of AD (Cissé et al., 2011). It is concluded from previous studies that the enhanced gamma activity found in AD mice in my study might be due to hyperstimulation of NDMA glutamatergic innervation and reduced cholinergic system activity mediated by dysregulation of GABAergic interneuronal network in AD (J. Wang et al., 2017).

In female mice subgroups, no significant changes were observed in theta activity (4-8 Hz and 4.1-12 Hz) between healthy controls and APPswePS1dE9 AD mice recorded from all 12, 14 and 16 weeks of age from both cortex and hippocampus (Fig. 4.2.13; Fig. 4.2.14). The overall decrease in theta activity in APPswePS1dE9 AD mice compared to healthy control males and no difference in theta activity was observed in APPswePS1dE9 mice compared to healthy controls females at the same age groups in my study. These observations might be associated with findings, which reported the amyloid plaques detection in hippocampus and cortex of three months old male mice that demonstrated the early formation of Aβ plaques in males as compared to females of same age (Ordóñez-Gutiérrez, Antón, & Wandosell, 2015). In addition, it has been revealed by in vitro and in vivo analysis that Aβ can diminish the theta oscillation in septohippocampal system (Chung, Park, Jang, Kohl, & Kwag, 2020; Colom et al., 2010; Gutiérrez-Lerma, Ordaz, & Peña-Ortega, 2013; Leão, Colom, Borgius, Kiehn, & Fisahn, 2012; K. Park et al., 2020; Peña-Ortega & Bernal-Pedraza, 2012).

On the other hand, a significant increase in beta activity (12.1-30 Hz, 16-24 Hz, 16-30 Hz) was observed in APPswePS1dE9 AD mice compared to healthy controls recorded at age of 12, 14 and 16 weeks during light cycle from cortex (Fig. 4.2.16D; Fig. 4.2.17D; Fig. 4.2.18D) and also similar changes were recorded in beta activity (16-24 Hz, 16-30 Hz) at 14 weeks of age during dark cycle from cortex (Fig. 4.2.17C; Fig. 4.2.18C). Likewise, an increase in beta activity was associated with memory problems observed in previous findings (Hanslmayr & Staudigl, 2014; Lundqvist et al., 2018; Lundqvist et al., 2016a, 2016b; Proskovec et al., 2018; Schmidt et al., 2019). An increase in gamma oscillation (30-50 Hz) was also identified in pantoprazole treated APPswePS1dE9 mice compared to pantoprazole treated female controls recorded at 14 weeks of age during the light and dark phases from cortex (Fig. 4.2.21C,D). Similar findings were observed by Deursen et al. (2008) and Wang et al. (2017) (van Deursen et al., 2008; J. Wang et al., 2017).

Additionally, we have also performed gender specific seizures analysis in AD mice. Various studies have reported the association of AD with epileptic seizures in elderly humans (Amatniek et al., 2006; Lozsadi & Larner, 2006; Papazoglou, Soos, et al., 2016). Epileptic seizures prevalence enhanced in AD patients compared to normal individuals of the same age (Baker, Libretto, Henley, & Zeman, 2019; Sen, Capelli, & Husain, 2018). Early presence of cognitive decline reported in mild cognitive impaired and AD patients with epilepsy compared to MCI and AD patient without epilepsy (Vossel et al., 2013). Earlier experimental studies in transgenic AD mouse models also revealed a similar correlation of hyperexcitability of neurons, epileptic seizures discharges and AD progression (Gurevicius et al., 2013; Minkeviciene et al., 2009; Palop et al., 2007; Papazoglou, Soos, et al., 2016; Siwek et al., 2015). Although the exact mechanisms of ictal discharge generation in APPswePS1dE9 AD mice are not fully understood, however, it has been reported in numerous AD mouse models that high levels of Aβ can generate aberrant neuronal discharges and epileptic seizures (Palop et al., 2007). Moreover, neuronal hyperactivity was observed in the hippocampus and cortical slices induced by exogenous $A\beta_{1\text{-}42}$ (Minkeviciene et al., 2009; Tamagnini et al., 2015). Lei et al. (2016) reported that disruption of hippocampal synaptic plasticity and LTP, and enhancement of neuronal hyperactivity generated by soluble Aβ oligomers mediated modification of glutamate neurotransmission and dysregulation of GABAergic/glutamatergic homeostasis in AD mouse models (Lei et al., 2016). Various other factors were also reported to be involved in mechanisms of epileptic discharge in AD such as neuroinflammation (Giorgi, Saccaro, Busceti, Biagioni, & Fornai, 2020; Giorgi et al., 2019), neurodegeneration of the locus coeruleus (Giorgi et al., 2017; Theofilas et al., 2017) and the dendrites (Šišková et al., 2014). Gurevicius et al. (2013) reported that seizure episodes peak occurred at the time of amyloid plaque formation in hippocampus and cortex of APPswePS1dE9 mice (Gurevicius et al., 2013). Numerous studies have evaluated the neuronal activity in the electrocorticogram in APP transgenic mice (Garcia-Alloza et al., 2006; Minkeviciene et al., 2009; Palop et al., 2007; Wisor & Kilduff, 2005; Y. W. Zhang, Thompson, Zhang, & Xu, 2011). However, we analyzed a number of seizures parameters in my study such as the number of spike trains, spike trains duration (min) and number of single spikes. We performed this analysis from both males and females mice subgroups recorded from hippocampus (CA1) and motor cortex (M1). In my study, i have found significant increase in the number of spike trains and spike trains duration (min) in APPswePS1dE9 mice (APP(TG)-DMSO) as compared to healthy controls (WT-DMSO) males at the age of 14 weeks recorded from cortex during both the dark and light cycles (Fig. 4.2.23C,D; Fig. 4.2.25C,D). In addition, similar changes observed in the number of single spikes recorded at the age of 14 weeks from the cortex during the light cycle (Fig. 4.2.24D). Significant increase in seizures parameters in APPswePS1dE9 mice were detected in my study and correlated with previous findings mentioned earlier. Further studies by Nicastro et al. (2016) reported the role of Aβ in the generation of aberrant neuronal discharges in a review of epidemiological studies analysis (Nicastro, Assal, & Seeck, 2016). Sima et al. (2014) observed an association between an increase of Aβ precursor protein expression in hippocampal and temporal cortex tissues of chronic epileptic patients (Sima, Xu, Li, Zhong, & You, 2014). Zarea et al. (2016) detected a relationship between duplication/mutation in APP and PSEN1 in autosomal dominal early onset of AD (ADEOAD) with enhanced seizures risk (Zarea et al., 2016). It has been demonstrated in various findings from AD mouse models that the cortical neuronal hyperexcitability and seizures susceptibility is linked with the Aβ accumulation in AD (Born, 2015; Horváth, Szűcs, Barcs, Noebels, & Kamondi, 2016). Epilepsy also promotes the Aβ synthesize and could be responsible for cognitive decline and behavioral issues in humans and animal models (Chin & Scharfman, 2013). In addition, epileptic interictal neuronal firing was reported to be responsible for the disruption of cognition and memory (Kleen et al., 2013; Ung et al., 2017). Furthermore, Vogt et al. (2011) demonstrated that the overexpression of amyloid precursor protein (APP) intracellular domain (AICD) and Fe65 binding element of ACID in AD could promote the disruption of neural circuits and trigger seizures (Vogt et al., 2011). It has been reported that Aβ plaques dysregulate various voltage-gated ion channels (Plant et al., 2006; Thibault, Pancani, Landfield, & Norris, 2012) such as upregulation of the voltage dependent sodium channels ($Na_v1.6$) mediated nerves hyperactivity by Aβ ($Aβ_{1-42}$) in Tg2576 AD mice (Ciccone et al., 2019) and also in APP/PS1 mice (X. Wang et al., 2016). In addition, hyperactive cortical nerve cells clusters observed close to Aβ deposition in APP/PS1 mice activates seizures (Busche et al., 2008). Further, Hijazi et al. (2020) observed the disruption of parvalbumin interneuronal network, synaptic communication and hyper-excitation of pyramidal cells by Aβ that leads to progression of AD (Hijazi et al., 2020).

Additionally, we have also identified increased total number of spike trains and number of single spikes in APPswePS1dE9 untreated (APP(TG)-DMSO) mice compared to APPswePS1dE9 pantoprazole treated (APP(TG)-Panto) mice at 14 week of age during light cycle from cortex (Fig. 4.2.23D; Fig. 4.2.24D). This reduction in seizures parameters in pantoprazole treated (APP(TG)-Panto) mice could be correlated with the findings by Taskiran et al. (2020) that reported the memory preservation and a delay in onset of pentylenetetrazole induced seizures by pantoprazole treatment in rats (Taskiran et al., 2020). In another study, Saez et al. (2016) has not identified any rise in seizures risk associated with PPIs use in patients (Sáez et al., 2016).

Moreover, in female mice of my study, a significant increase in total number of spike trains and spike trains duration were identified in untreated APPswePS1dE9 (APP(TG)-DMSO) mice compared to untreated controls (WT-DMSO) at 16 weeks of age during dark cycle and 14 weeks of age during the light cycle recorded from the cortex (Fig. 4.2.26C,D; Fig. 4.2.28C,D). This correlated with the findings of Reyes-Marin and Nunez et al. (2017) which revealed in a study of 4-9 month old APP/PS1 AD mice that enhanced Aβ accumulation in the brain could be the reason for abnormal neuronal seizure like discharges in mice and also enhanced seizures activity in AD patients as well (Reyes-Marin & Nuñez, 2017). It was reported that Aβ starts accumulating in cerebral cortex at the age of 3 months in mice linked with early AD symptoms that leads to sensory motor cognitive decline as Aβ plaque formation in cerebral cortex progresses (Reyes-Marin & Nuñez, 2017; Z. Wang et al., 2012). Garcia-Marin et al. (2009) and Ramos-Miguel et al. (2015) showed that the decline in GABAergic perisomatic nerve endings in cortical pyramidal neurons appeared close to Aβ plaque formation as observed in APP/PS1 mice and AD patients that leads to the disruption of GABAergic activity (Garcia-Marin et al., 2009; Ramos-Miguel et al., 2015). This GABAergic dysfunctioning of cortical neurons might be the reason of hyperexcitability of cortical neurons and activates seizures (Reyes-Marin & Nuñez, 2017). Similar findings appeared in my study. Furthermore, we have also observed a significant increase in total number of spike trains and spike trains duration at 16 weeks of age compared to early 12 weeks of age in untreated APPswePS1dE9 (APP(TG)-DMSO) mice recorded during the dark cycle from cortex (Fig. 4.2.26C; Fig. 4.2.28C). This could be associated with previous findings that describe an increased number of seizure like episodes linked with number of Aβ plaques in experimental animals (Reyes-Marin & Nuñez, 2017). Additionally, in my study, increase in total number of spike trains and spike trains duration in APPswePS1dE9 untreated (APP(TG)-DMSO) mice compared to APPswePS1dE9 pantoprazole treated (APP(TG)-Panto) mice was observed at 14 weeks of age recorded during the light cycle from the cortex (Fig. 4.2.26D; Fig. 4.2.28D). This reduction in seizures parameters in pantoprazole treated (APP(TG)-Panto) mice might be associated with the findings of memory preservation and a delay in onset of pentylenetetrazole induced seizures by pantoprazole treatment in rats (Taskiran et al., 2020). In another study, Saez et al. (2016) has not identified any increase in seizures risk associated with PPIs use in patients (Sáez et al., 2016).

Additionally, we have also performed the LC-MS/MS analysis to quantify pantoprazole concentration in plasma and liver tissues of all mice groups (age 12-16 weeks). We have observed significant pantoprazole concentration in plasma and liver tissues of treated male mice (Fig.

4.2.30A,C). Interestingly, in female treated control mice, we have not detected significant pantoprazole concentration (Fig. 4.2.30B,D) which might be due to insufficient release of pantoprazole from osmotic pumps but some other experimental and physiochemical factors could be involved. In addition, a high metabolic tendency can be one reason for the absence of pantoprazole in female control mice. However, in future studies, a comprehensive evaluation of pharmacokinetic and pharmacodynamics parameters of pantoprazole in age and gender specific AD patients and mouse models required to investigate its capability to cross the blood brain barrier, efficacy and safety profile. Moreover, we have also performed initial qualitative analysis of pantoprazole metabolites with a short semi-quantitative estimation of the area ratios, to evaluate the metabolic tendency of pantoprazole, and collect first data for possible future upcoming studies. We have detected pantoprazolesulfane and pantoprazolesulfone as major metabolites (Fig. 4.2.31; Fig. 4.2.32). However, there are limitations associated with pantoprazole metabolite analysis in my study. For the detailed quantitative analysis of pantoprazole metabolite profile, reference standards of different pantoprazole metabolites are needed to run for the quantification of respective metabolite.

### 5.2.2. Pantoprazole effects in mice APPswePS1dE9 aged 17-21 weeks

In the second part of my study, there was also no significant difference detected in relative activity units (counts) and temperature ($^{o}$C) in both healthy controls (WT-DMSO and WT-Panto) and APPswePS1dE9 (APP(TG)-DMSO and APP(TG)-Panto) male mice, recorded at all 17, 18, 19, 20 and 21 weeks of age during both the dark and light phases from the hippocampus and motor cortex regions.

However, in post-urethane/atropine analysis, an increase in relative activity units found in APPswePS1dE9 (APP(TG)-Panto) mice compared to healthy controls (WT-Panto) was recorded during 1 h baseline, 1 h post-normal saline and 3 h post atropine from both hippocampus and cortex (Fig. 4.3.2). Moreover, a significant increase in temperature ($^{o}$C) found in treated APPswePS1dE9 (APP(TG)-Panto) mice compared to treated healthy controls (WT-Panto) recorded during 1 h baseline and 1 h post-urethane from both hippocampus and cortex (Fig. 4.3.4). Furthermore, by FFT base frequency analysis in my study, a significant rise in theta (4-8 Hz) oscillatory relative power was found in untreated healthy controls (WT-DMSO) as compared to APPswePS1dE9 (APP(TG)-DMSO) male mice at 21 weeks of age recorded during the dark cycle from hippocampus (CA1) (Fig. 4.3.5A). Hippocampal theta activity is involved in cognition and memory formation (Buzsáki, 2005), spatial and non-spatial cognitive processing (Goyal, Lee, Luna, & Aruin, 2020; Korotkova et al., 2018) and various behavioral functions (Müller et al., 2017;

Muller et al., 2012; Vertes, 2005). The medial septum and diagonal band of Broca MS/vDBB are thought to be the pacemakers for the hippocampal theta generation (Broncel et al., 2018; Buzsáki et al., 1983). Disruption of the septohippocampal system in AD could be the reason for hippocampal dysrhythmia, especially the impairment of theta oscillatory patterns (Babiloni et al., 2007; Babiloni et al., 2009; Cummins et al., 2008; Papazoglou, Soos, et al., 2016). It has been reported earlier that cognitive deficit in AD was associated with reduced theta activity (Cummins et al., 2008; Scott et al., 2012; Scott, Kiss, Kawabe, & Hajós, 2016). Aβ can regulate and alter the glutamatergic, GABAergic and cholinergic neuronal network in the septohippocampal system (Colom et al., 2010; Fang et al., 2012; Gutiérrez-Lerma et al., 2013; Peña-Ortega & Bernal-Pedraza, 2012). It has been revealed by in vitro and in vivo analysis that Aβ can diminish the theta oscillation in septohippocampal system (Chung et al., 2020; Colom et al., 2010; Gutiérrez-Lerma et al., 2013; Leão et al., 2012; K. Park et al., 2020; Peña-Ortega & Bernal-Pedraza, 2012).

Based on dualistic theory there are two type of theta oscillation, atropine insensitive (type I) and atropine sensitive (type II) theta oscillation. Atropine insensitive (type I) oscillations are linked with voluntary behavior, movement and awakening, unaffected by muscarinic blockers i.e. atropine, and thought to be linked with metabotropic glutamate receptor 1, but also NDMA and AMPA receptors (Buzsáki, 2002; Chuang et al., 2001; Gillies et al., 2002; Mikulovic et al., 2018). Atropine sensitive (type II) theta oscillations are produced during alert immobility, urethane induced anesthesia and abolished by atropine (Broncel et al., 2018; Buzsáki, 1986, 2002; Buzsáki et al., 2003; Gu et al., 2020; Kramis et al., 1975; Mikulovic et al., 2018; Vanderwolf et al., 1988). In my study, a significant rise in hippocampal theta activity was observed in APPswePS1dE9 (APP(TG)-DMSO) mice after urethane administration as compared to baseline recordings (Fig. 4.3.15A), followed by reduction of theta activity found after atropine injection (Fig. 4.3.15A; Fig. 4.3.16A). Overall enhanced theta activity detected after urethane administration and reduced activity found after atropine injection in both controls and APPswePS1dE9 mice recorded from hippocampus (Fig. 4.3.15A). Our findings of increased post-urethane theta followed by reduced post-atropine theta activity correlates with the hypothesis of atropine sensitive (type II) theta genesis (Buzsáki, 1986, 2002; Buzsáki et al., 2003; Kramis et al., 1975; Vanderwolf et al., 1988). Thetagenesis is reported to be generated by the activation of muscarinic receptors (M1/M3/M5) by further stimulation of G-protein coupled receptors (GPCRs; $G\alpha_{q/11}$) and signaling cascades through phospholipase $\beta_{1/4}$ (PLC $\beta_{1/4}$), diacylglycerol (DG), inositol triphosphate (InsP3), $Ca^{2+}$ and phosphor kinase C (PKC) (Muller et al., 2012; J. Shin et al., 2009). The theta oscillation generated by cholinergic stimulation can be fully diminish by blockage of hippocampal PLCβ1 and septal PLCβ4 (J. Shin et al., 2009; J. Shin et al., 2005).

Furthermore, I have detected consistent findings in gamma oscillatory activity as younger study group (12-16 weeks age). A significant increase in gamma (50-70 Hz) activity in untreated APPswePS1dE9 (APP(TG)-DMSO) mice compared to untreated controls (WT-DMSO) was observed at 20 weeks of age recorded during the light cycle from the cortex (Fig. 4.3.13D). Deursen et al. (2008) and Wang et al. (2017) reported similar findings that an increased gamma activity in AD patients compared to mild cognitive impaired individual and healthy controls (van Deursen et al., 2008; J. Wang et al., 2017).

We have not observed any significant difference in theta and gamma activity between untreated APPswePS1dE9 (APP(TG)-DMSO) and pantoprazole treated APPswePS1dE9 (APP(TG)-Panto) mice recorded at 17, 18, 19, 20 and 21 weeks of age during both dark and light cycles from the hippocampus and the cortex (Fig. 4.3.5; Fig. 4.3.6; Fig. 4.3.13; Fig; 4.3.14). Similarly consistent findings were detected from younger APPswePS1dE9 (age 12-16 weeks) mice groups of my study which indicated no inhibitory or beneficial effect of pantoprazole on cognition in AD mice.

Additionally, we have also performed a detailed analysis of a number of seizures parameters, such as total number of spike trains, total number of single spikes and spike trains duration (min) by using a non-restraining radiotelemetry approach. While, Minkeviciene et al. (2009) analyzed EEG in APPswePS1dE9 mice by restraining tethered approach. Numerous previous studies analyzed electrocorticogram in APPswePS1dE9 AD mice (Garcia-Alloza et al., 2006; Minkeviciene et al., 2009; Palop et al., 2007; Wisor & Kilduff, 2005; Y. W. Zhang et al., 2011). Numerous studies have reported the correlation of AD with seizures in elderly (Amatniek et al., 2006; Beagle et al., 2017; Lozsadi & Larner, 2006; Papazoglou, Soos, et al., 2016; Sarkis et al., 2016) and revealed an increased epileptic seizures prevalence in AD patients compared to normal individuals of the same age (Baker et al., 2019; Giorgi et al., 2020; Horváth et al., 2016; Sen et al., 2018). In addition, early presence of cognitive decline was reported in MCI and AD patients with epilepsy as compared to MCI and AD patients without epilepsy (Vossel et al., 2013). Previous experimental studies showed an association between hyperexcitability of neurons, epileptic discharges and AD progression (Gurevicius et al., 2013; Minkeviciene et al., 2009; Palop et al., 2007; Papazoglou, Soos, et al., 2016; Siwek et al., 2015). Whereas the exact mechanism of ictal discharge in APPswePS1dE9 AD mice is unknown, it has been reported in various studies of AD mouse models that increased levels of Aβ can activate aberrant neuronal discharge and epileptic seizures (Palop et al., 2007). Besides, hyperexcitability in neurons was observed in cortical and hippocampal slices of APPswePS1dE9 AD mice after exposure to exogenous $A\beta_{1-42}$ (Minkeviciene et al., 2009; Tamagnini et al., 2015). Lei et al. (2016) reported that disruption of hippocampal synaptic plasticity, long-term potentiation (LTP) and enhancement of neuronal hyperactivity generated by soluble Aβ oligomers mediated modification of glutamate neurotransmission and dysregulation of GABAergic/glutamatergic homeostasis in AD mouse models (Lei et al., 2016). Numerous other factors are reported to play a role in mechanism of epileptic ictal discharge in AD such as neuroinflammation (Giorgi et al., 2020; Giorgi et al., 2019), neurodegeneration of the dendrites (Šišková et al., 2014) and locus coeruleus (Giorgi et al., 2017; Theofilas et al., 2017). Gurvicius et al. (2013) revealed the peak level of seizure episodes occurred at the age of Aβ formation in the cortex and hippocampus of APPswePS1dE9 mice (Gurevicius et al., 2013). In my study, a significant increase in total number of spike trains observed in untreated APPswePS1dE9 (APP(TG)-DMSO) mice as compared to controls (WT-DMSO) at 17 weeks of age recorded during the dark cycle from the hippocampus (Fig. 4.3.25A). In addition, an increase in total number of spike trains identified in treated APPswePS1dE9 (APP(TG)-Panto) mice compared to controls (WT-Panto) at 21 weeks of age during the light cycle from the hippocampus and cortex (Fig. 4.3.25B,D). Furthermore, enhanced total number of single spikes observed in untreated APPswePS1dE9 (APP(TG)-DMSO) mice as compared to controls (WT-DMSO) at 19 weeks of age recorded during dark and light cycles from hippocampus and 17 weeks of age recorded during dark and light cycles from cortex (Fig. 4.3.26). Moreover, a significant increase in spike trains duration (min) observed in untreated APPswePS1dE9 (APP(TG)-DMSO) mice compared to controls (WT-DMSO) at 19 weeks of age during dark cycle from hippocampus and cortex (Fig. 4.3.27A,C). Significant increase in the above seizure parameters observed in APPswePS1dE9 mice of my study correlated with findings described before which reported the association of neuronal excitability and seizures with AD mouse models and patients.

Additionally, we detected a significant increase in the total number of spike trains in APPswePS1dE9 untreated (APP(TG)-DMSO) mice compared to APPswePS1dE9 pantoprazole treated (APP (TG)-Panto) at 17 weeks of age during the dark cycle from hippocampus and light and dark cycles from cortex (Fig. 4.3.25A,C,D). Furthermore, an increase in the spike trains duration (min) observed in APPswePS1dE9 untreated (APP(TG)-DMSO) mice compared to APPswePS1dE9 pantoprazole treated (APP(TG)-Panto) at 19 weeks of age during the dark cycle from the hippocampus and cortex (Fig. 4.3.27A,C). This reduction in seizures parameters in APPswePS1dE9 pantoprazole treated (APP(TG)-Panto) mice is consistent with our findings from younger APPswePS1dE9 mice (aged 12-16 weeks) as described earlier and associated with the findings from Taskiran et al. (2020).

# 6. Conclusions and future perspective

## 6.1. Hippocampal EEG alterations in $Ca_v3.2$ mice and the involvement of the GABAergic system.

My study is the first one to demonstrate that the ablation of $Ca_v3.2$ VGCCs results in enhanced hippocampal atropine sensitive type II theta activity. I also found that tonic firing of septal GABAergic interneurons and subsequent tonic inhibition of hippocampal interneurons and disinhibition of pyramidal cells leads to compensatory changes in the GABAergic system. These findings suggest a downregulation of dynein containing GABA receptor transporter/trafficking complex and GABA A and B receptors complexes themselves. Dinamarca et al. (2019) reported that GABA B receptors (GBR) forms a complex with amyloid precursor protein (APP) (Dinamarca et al., 2019). This GBR/APP complex is assumed to stabilize APP at the surface membrane of pyramidal neurons and to reduce proteolysis of APP to form amyloid beta (Aβ). Thus, APP membrane stability might be impaired in $Ca_v3.2$ deficient mice due to reduced GBR expression and GABA receptor trafficking. In future studies, it will be necessary to explore the possible functional interdependence between T-type VGCCs, the GABAergic system, APP, and its relevance in the aetiopathogenesis of Alzheimer’s disease (AD).

## 6.2. Analysis of the alteration of central rhythmicity in 3-6 months old APPswePS1dE9 Alzheimer mice following chronic administration of pantoprazole.

My analysis indicated the age and gender specific alterations in theta, gamma and beta oscillatory activity in APPswePS1dE9 mice. Reduced theta related cognitive performance appeared early in male APPswePS1dE9 mice compared to females and might propose early onset of AD related pathophysiological changes in males. An increased theta activity in pantoprazole treated controls might be associated with enhanced theta related cognitive ability in healthy male controls. No positive or negative effect of chronic pantoprazole administration appeared in theta and gamma relative power in APPswePS1dE9 mice. These findings suggest a neutral role of pantoprazole in AD progression. However, future clinical studies are required to investigate the potential beneficial or adverse potential of long-term use of pantoprazole in MCI and AD patients. Additionally, increased hippocampal and cortical seizure parameters in APPswePS1dE9 mice compared to healthy controls of both genders exhibited the association of aberrant discharge and dysrhythmia in AD pathology. A pantoprazole-mediated decline in seizure activity in APPswePS1dE9 mice of both genders might demonstrate its positive role in AD associated epileptic discharges. Future studies need to investigate the correlation of pantoprazole and AD related to epileptogenesis in detail. Age and gender EEG oscillatory activity specific alterations in APPswePS1dE9 mice suggest a functional and diagnostic role of EEG. In the future, EEG could be recognized as diagnostic biomarker for AD. In addition, a broad gender and age targeted pharmacokinetics, pharmacodynamics and pharmacogenetics approaches will be necessary to analyze the efficacy and safety profile of pantoprazole/PPIs in normal healthy controls, mild cognitive impairment (MCI) and AD patients on individualized basis.

# 7. References

Aguado, C., Garcia-Madrona, S., Gil-Minguez, M., & Lujan, R. (2016). Ontogenic Changes and Differential Localization of T-type Ca(2+) Channel Subunits Cav3.1 and Cav3.2 in Mouse Hippocampus and Cerebellum. *Front Neuroanat, 10*, 83. doi:10.3389/fnana.2016.00083

Aisen, P., Touchon, J., Amariglio, R., Andrieu, S., Bateman, R., Breitner, J., . . . Vellas, B. (2017). EU/US/CTAD Task Force: Lessons Learned from Recent and Current Alzheimer's Prevention Trials. *J Prev Alzheimers Dis, 4*(2), 116-124. doi:10.14283/jpad.2017.13

Akter, S., Hassan, M. R., Shahriar, M., Akter, N., Abbas, M. G., & Bhuiyan, M. A. (2015). Cognitive impact after short-term exposure to different proton pump inhibitors: assessment using CANTAB software. *Alzheimers Res Ther, 7*, 79. doi:10.1186/s13195-015-0164-8

Albert, M. S., DeKosky, S. T., Dickson, D., Dubois, B., Feldman, H. H., Fox, N. C., . . . Phelps, C. H. (2011). The diagnosis of mild cognitive impairment due to Alzheimer's disease: recommendations from the National Institute on Aging-Alzheimer's Association workgroups on diagnostic guidelines for Alzheimer's disease. *Alzheimers Dement, 7*(3), 270-279. doi:10.1016/j.jalz.2011.03.008

Almansoub, H., Tang, H., Wu, Y., Wang, D. Q., Mahaman, Y. A. R., Wei, N., . . . Liu, D. (2019). Tau Abnormalities and the Potential Therapy in Alzheimer's Disease. *J Alzheimers Dis, 67*(1), 13-33. doi:10.3233/jad-180868

Altmann, A., Tian, L., Henderson, V. W., & Greicius, M. D. (2014). Sex modifies the APOE-related risk of developing Alzheimer disease. *Ann Neurol, 75*(4), 563-573. doi:10.1002/ana.24135

Alturki, F. A., AlSharabi, K., Abdurraqeeb, A. M., & Aljalal, M. (2020). EEG Signal Analysis for Diagnosing Neurological Disorders Using Discrete Wavelet Transform and Intelligent Techniques. *Sensors (Basel), 20*(9). doi:10.3390/s20092505

ALZ.ORG. (2020). *American Alzheimer's disease association - 2020 Alzheimer's disease facts and figures* (1552-5260). Retrieved from

Alzheimer's and Dementia in Germany. (2020). Retrieved from https://www.alz.org/de/dementia-alzheimers-germany.asp

Alzheimer, A., Stelzmann, R. A., Schnitzlein, H. N., & Murtagh, F. R. (1995). An English translation of Alzheimer's 1907 paper, "Uber eine eigenartige Erkankung der Hirnrinde". *Clin Anat, 8*(6), 429-431. doi:10.1002/ca.980080612

Amatniek, J. C., Hauser, W. A., DelCastillo-Castaneda, C., Jacobs, D. M., Marder, K., Bell, K., . . . Stern, Y. (2006). Incidence and predictors of seizures in patients with Alzheimer's disease. *Epilepsia, 47*(5), 867-872. doi:10.1111/j.1528-1167.2006.00554.x

Anderson, M. P., Mochizuki, T., Xie, J., Fischler, W., Manger, J. P., Talley, E. M., . . . Tonegawa, S. (2005). Thalamic Cav3.1 T-type Ca2+ channel plays a crucial role in stabilizing sleep. *Proc Natl Acad Sci U S A, 102*(5), 1743-1748. doi:10.1073/pnas.0409644102

Atri, A. (2019). Current and Future Treatments in Alzheimer's Disease. *Semin Neurol, 39*(2), 227-240. doi:10.1055/s-0039-1678581

Babiloni, C., Cassetta, E., Binetti, G., Tombini, M., Del Percio, C., Ferreri, F., . . . Rossini, P. M. (2007). Resting EEG sources correlate with attentional span in mild cognitive impairment and Alzheimer's disease. *Eur J Neurosci, 25*(12), 3742-3757. doi:10.1111/j.1460-9568.2007.05601.x

Babiloni, C., Pievani, M., Vecchio, F., Geroldi, C., Eusebi, F., Fracassi, C., . . . Frisoni, G. B. (2009). White-matter lesions along the cholinergic tracts are related to cortical sources of EEG rhythms in amnesic mild cognitive impairment. *Hum Brain Mapp, 30*(5), 1431-1443. doi:10.1002/hbm.20612

Badiola, N., Alcalde, V., Pujol, A., Münter, L. M., Multhaup, G., Lleó, A., . . . Aloy, P. (2013). The proton-pump inhibitor lansoprazole enhances amyloid beta production. *PLoS One, 8*(3), e58837. doi:10.1371/journal.pone.0058837

Bahar-Fuchs, A., Martyr, A., Goh, A. M., Sabates, J., & Clare, L. (2019). Cognitive training for people with mild to moderate dementia. *Cochrane Database Syst Rev, 3*(3), Cd013069. doi:10.1002/14651858.CD013069.pub2

Baker, J., Libretto, T., Henley, W., & Zeman, A. (2019). A Longitudinal Study of Epileptic Seizures in Alzheimer's Disease. *Front Neurol, 10*, 1266. doi:10.3389/fneur.2019.01266

Ball, S. L., & Gregg, R. G. (2002). Using mutant mice to study the role of voltage-gated calcium channels in the retina. *Adv Exp Med Biol, 514*, 439-450. doi:10.1007/978-1-4615-0121-3_26

Ballard, C., Mobley, W., Hardy, J., Williams, G., & Corbett, A. (2016). Dementia in Down's syndrome. *Lancet Neurol, 15*(6), 622-636. doi:10.1016/s1474-4422(16)00063-6

Barnes, L. L., Wilson, R. S., Bienias, J. L., Schneider, J. A., Evans, D. A., & Bennett, D. A. (2005). Sex differences in the clinical manifestations of Alzheimer disease pathology. *Arch Gen Psychiatry, 62*(6), 685-691. doi:10.1001/archpsyc.62.6.685

Beagle, A. J., Darwish, S. M., Ranasinghe, K. G., La, A. L., Karageorgiou, E., & Vossel, K. A. (2017). Relative Incidence of Seizures and Myoclonus in Alzheimer's Disease, Dementia with Lewy Bodies, and Frontotemporal Dementia. *J Alzheimers Dis, 60*(1), 211-223. doi:10.3233/jad-170031

Becker, A. J., Pitsch, J., Sochivko, D., Opitz, T., Staniek, M., Chen, C. C., . . . Beck, H. (2008). Transcriptional upregulation of Cav3.2 mediates epileptogenesis in the pilocarpine model of epilepsy. *J Neurosci, 28*(49), 13341-13353. doi:10.1523/JNEUROSCI.1421-08.2008

Belelli, D., & Lambert, J. J. (2005). Neurosteroids: endogenous regulators of the GABA(A) receptor. *Nat Rev Neurosci, 6*(7), 565-575. doi:10.1038/nrn1703

Benwell, C. S. Y., Davila-Pérez, P., Fried, P. J., Jones, R. N., Travison, T. G., Santarnecchi, E., . . . Shafi, M. M. (2020). EEG spectral power abnormalities and their relationship with cognitive dysfunction in patients with Alzheimer's disease and type 2 diabetes. *Neurobiol Aging, 85*, 83-95. doi:10.1016/j.neurobiolaging.2019.10.004

Bernshteyn, M. A., & Masood, U. (2020). Pantoprazole. In *StatPearls*. Treasure Island (FL): StatPearls Publishing Copyright © 2020, StatPearls Publishing LLC.

Bettler, B., Kaupmann, K., Mosbacher, J., & Gassmann, M. (2004). Molecular structure and physiological functions of GABA(B) receptors. *Physiol Rev, 84*(3), 835-867. doi:10.1152/physrev.00036.2003

Bland, B. H., & Oddie, S. D. (2001). Theta band oscillation and synchrony in the hippocampal formation and associated structures: the case for its role in sensorimotor integration. *Behav Brain Res, 127*(1-2), 119-136.

Blennow, K., de Leon, M. J., & Zetterberg, H. (2006). Alzheimer's disease. *Lancet, 368*(9533), 387-403. doi:10.1016/s0140-6736(06)69113-7

Blokh, D., Stambler, I., Lubart, E., & Mizrahi, E. H. (2017). The application of information theory for the estimation of old-age multimorbidity. *Geroscience, 39*(5-6), 551-556. doi:10.1007/s11357-017-9996-4

Bloodgood, B. L., & Sabatini, B. L. (2007). Nonlinear regulation of unitary synaptic signals by CaV(2.3) voltage-sensitive calcium channels located in dendritic spines. *Neuron, 53*(2), 249-260. doi:10.1016/j.neuron.2006.12.017

Bondareff, W., Mountjoy, C. Q., & Roth, M. (1982). Loss of neurons of origin of the adrenergic projection to cerebral cortex (nucleus locus ceruleus) in senile dementia. *Neurology, 32*(2), 164-168. doi:10.1212/wnl.32.2.164

Booker, A., Jacob, L. E., Rapp, M., Bohlken, J., & Kostev, K. (2016). Risk factors for dementia diagnosis in German primary care practices. *Int Psychogeriatr, 28*(7), 1059-1065. doi:10.1017/s1041610215002082

Borhegyi, Z., Varga, V., Szilagyi, N., Fabo, D., & Freund, T. F. (2004). Phase segregation of medial septal GABAergic neurons during hippocampal theta activity. *J Neurosci, 24*(39), 8470-8479. doi:10.1523/JNEUROSCI.1413-04.2004

Born, H. A. (2015). Seizures in Alzheimer's disease. *Neuroscience, 286*, 251-263. doi:10.1016/j.neuroscience.2014.11.051

Bosch, M. A., Hou, J., Fang, Y., Kelly, M. J., & Rønnekleiv, O. K. (2009). 17Beta-estradiol regulation of the mRNA expression of T-type calcium channel subunits: role of estrogen receptor alpha and estrogen receptor beta. *J Comp Neurol, 512*(3), 347-358. doi:10.1002/cne.21901

Bourin, M., & Hascoet, M. (2003). The mouse light/dark box test. *Eur J Pharmacol, 463*(1-3), 55-65. doi:10.1016/s0014-2999(03)01274-3

Bouwknecht, J. A., & Paylor, R. (2002). Behavioral and physiological mouse assays for anxiety: a survey in nine mouse strains. *Behav Brain Res, 136*(2), 489-501. doi:10.1016/s0166-4328(02)00200-0

Bowery, N. G., Bettler, B., Froestl, W., Gallagher, J. P., Marshall, F., Raiteri, M., . . . Enna, S. J. (2002). International Union of Pharmacology. XXXIII. Mammalian gamma-aminobutyric acid(B) receptors: structure and function. *Pharmacol Rev, 54*(2), 247-264. doi:10.1124/pr.54.2.247

Bowery, N. G., & Enna, S. J. (2000). gamma-aminobutyric acid(B) receptors: first of the functional metabotropic heterodimers. *J Pharmacol Exp Ther, 292*(1), 2-7.

Braak, H., & Del Tredici, K. (2020). From the Entorhinal Region via the Prosubiculum to the Dentate Fascia: Alzheimer Disease-Related Neurofibrillary Changes in the Temporal Allocortex. *J Neuropathol Exp Neurol, 79*(2), 163-175. doi:10.1093/jnen/nlz123

Broncel, A., Bocian, R., Kłos-Wojtczak, P., & Konopacki, J. (2018). Medial septal cholinergic mediation of hippocampal theta rhythm induced by vagal nerve stimulation. *PLoS One, 13*(11), e0206532. doi:10.1371/journal.pone.0206532

Brothers, H. M., Gosztyla, M. L., & Robinson, S. R. (2018). The Physiological Roles of Amyloid-β Peptide Hint at New Ways to Treat Alzheimer's Disease. *Front Aging Neurosci, 10*, 118. doi:10.3389/fnagi.2018.00118

Brown, D. A. (2010). Muscarinic acetylcholine receptors (mAChRs) in the nervous system: some functions and mechanisms. *J Mol Neurosci, 41*(3), 340-346. doi:10.1007/s12031-010-9377-2

Burwell, R. D., & Amaral, D. G. (1998). Cortical afferents of the perirhinal, postrhinal, and entorhinal cortices of the rat. *J Comp Neurol, 398*(2), 179-205. doi:10.1002/(sici)1096-9861(19980824)398:2<179::aid-cne3>3.0.co;2-y

Busceti, C. L., Di Pietro, P., Riozzi, B., Traficante, A., Biagioni, F., Nistico, R., . . . Bruno, V. (2015). 5-HT(2C) serotonin receptor blockade prevents tau protein hyperphosphorylation and corrects the defect in hippocampal synaptic plasticity caused by a combination of environmental stressors in mice. *Pharmacol Res, 99*, 258-268. doi:10.1016/j.phrs.2015.06.017

Busche, M. A., Eichhoff, G., Adelsberger, H., Abramowski, D., Wiederhold, K. H., Haass, C., . . . Garaschuk, O. (2008). Clusters of hyperactive neurons near amyloid plaques in a mouse model of Alzheimer's disease. *Science, 321*(5896), 1686-1689. doi:10.1126/science.1162844

Buzsáki, G. (1986). Hippocampal sharp waves: their origin and significance. *Brain Res, 398*(2), 242-252. doi:10.1016/0006-8993(86)91483-6

Buzsáki, G. (2002). Theta oscillations in the hippocampus. *Neuron, 33*(3), 325-340. doi:10.1016/s0896-6273(02)00586-x

Buzsáki, G. (2005). Theta rhythm of navigation: link between path integration and landmark navigation, episodic and semantic memory. *Hippocampus, 15*(7), 827-840. doi:10.1002/hipo.20113

Buzsaki, G., Anastassiou, C. A., & Koch, C. (2012). The origin of extracellular fields and currents--EEG, ECoG, LFP and spikes. *Nat Rev Neurosci, 13*(6), 407-420. doi:10.1038/nrn3241

Buzsáki, G., Buhl, D. L., Harris, K. D., Csicsvari, J., Czéh, B., & Morozov, A. (2003). Hippocampal network patterns of activity in the mouse. *Neuroscience, 116*(1), 201-211. doi:10.1016/s0306-4522(02)00669-3

Buzsáki, G., Leung, L. W., & Vanderwolf, C. H. (1983). Cellular bases of hippocampal EEG in the behaving rat. *Brain Res, 287*(2), 139-171. doi:10.1016/0165-0173(83)90037-1

Caillet-Boudin, M. L., Buée, L., Sergeant, N., & Lefebvre, B. (2015). Regulation of human MAPT gene expression. *Mol Neurodegener, 10*, 28. doi:10.1186/s13024-015-0025-8

Canto, C. B., Wouterlood, F. G., & Witter, M. P. (2008). What does the anatomical organization of the entorhinal cortex tell us? *Neural Plast, 2008*, 381243. doi:10.1155/2008/381243

Capogna, M., & Pearce, R. A. (2011). GABA A,slow: causes and consequences. *Trends Neurosci, 34*(2), 101-112. doi:10.1016/j.tins.2010.10.005

Cassani, R., Estarellas, M., San-Martin, R., Fraga, F. J., & Falk, T. H. (2018). Systematic Review on Resting-State EEG for Alzheimer's Disease Diagnosis and Progression Assessment. *Dis Markers, 2018*, 5174815. doi:10.1155/2018/5174815

Catterall, W. A. (2011). Voltage-gated calcium channels. *Cold Spring Harb Perspect Biol, 3*(8), a003947. doi:10.1101/cshperspect.a003947

Catterall, W. A., Leal, K., & Nanou, E. (2013). Calcium channels and short-term synaptic plasticity. *J Biol Chem, 288*(15), 10742-10749. doi:10.1074/jbc.R112.411645

Cheer, S. M., Prakash, A., Faulds, D., & Lamb, H. M. (2003). Pantoprazole: an update of its pharmacological properties and therapeutic use in the management of acid-related disorders. *Drugs, 63*(1), 101-133. doi:10.2165/00003495-200363010-00006

Chemin, J., Monteil, A., Perez-Reyes, E., Bourinet, E., Nargeot, J., & Lory, P. (2002). Specific contribution of human T-type calcium channel isotypes (alpha(1G), alpha(1H) and alpha(1I)) to neuronal excitability. *J Physiol, 540*(Pt 1), 3-14. doi:10.1113/jphysiol.2001.013269

Chen, C. C., Lamping, K. G., Nuno, D. W., Barresi, R., Prouty, S. J., Lavoie, J. L., . . . Campbell, K. P. (2003). Abnormal coronary function in mice deficient in alpha1H T-type Ca2+ channels. *Science, 302*(5649), 1416-1418. doi:10.1126/science.1089268

Chen, C. C., Shen, J. W., Chung, N. C., Min, M. Y., Cheng, S. J., & Liu, I. Y. (2012). Retrieval of context-associated memory is dependent on the Ca(v)3.2 T-type calcium channel. *PLoS One, 7*(1), e29384. doi:10.1371/journal.pone.0029384

Chen, Z. W., & Olsen, R. W. (2007). GABAA receptor associated proteins: a key factor regulating GABAA receptor function. *J Neurochem, 100*(2), 279-294. doi:10.1111/j.1471-4159.2006.04206.x

Cheng, Y., Liu, J., Tan, X., Dai, Y., Xie, C., Li, X., . . . Li, J. (2020). Direct Comparison of the Efficacy and Safety of Vonoprazan Versus Proton-Pump Inhibitors for Gastroesophageal Reflux Disease: A Systematic Review and Meta-Analysis. *Dig Dis Sci*. doi:10.1007/s10620-020-06141-5

Cheong, E., & Shin, H. S. (2013). T-type Ca2+ channels in normal and abnormal brain functions. *Physiol Rev, 93*(3), 961-992. doi:10.1152/physrev.00010.2012

Chin-Chan, M., Navarro-Yepes, J., & Quintanilla-Vega, B. (2015). Environmental pollutants as risk factors for neurodegenerative disorders: Alzheimer and Parkinson diseases. *Front Cell Neurosci, 9*, 124. doi:10.3389/fncel.2015.00124

Chin, J., Palop, J. J., Yu, G. Q., Kojima, N., Masliah, E., & Mucke, L. (2004). Fyn kinase modulates synaptotoxicity, but not aberrant sprouting, in human amyloid precursor protein transgenic mice. *J Neurosci, 24*(19), 4692-4697. doi:10.1523/jneurosci.0277-04.2004

Chin, J., & Scharfman, H. E. (2013). Shared cognitive and behavioral impairments in epilepsy and Alzheimer's disease and potential underlying mechanisms. *Epilepsy Behav, 26*(3), 343-351. doi:10.1016/j.yebeh.2012.11.040

Choi, S., Na, H. S., Kim, J., Lee, J., Lee, S., Kim, D., . . . Shin, H. S. (2007). Attenuated pain responses in mice lacking Ca(V)3.2 T-type channels. *Genes Brain Behav, 6*(5), 425-431. doi:10.1111/j.1601-183X.2006.00268.x

Chuang, S. C., Bianchi, R., Kim, D., Shin, H. S., & Wong, R. K. (2001). Group I metabotropic glutamate receptors elicit epileptiform discharges in the hippocampus through PLCbeta1 signaling. *J Neurosci, 21*(16), 6387-6394.

Chung, H., Park, K., Jang, H. J., Kohl, M. M., & Kwag, J. (2020). Dissociation of somatostatin and parvalbumin interneurons circuit dysfunctions underlying hippocampal theta and gamma oscillations impaired by amyloid β oligomers in vivo. *Brain Struct Funct, 225*(3), 935-954. doi:10.1007/s00429-020-02044-3

Ciccone, R., Franco, C., Piccialli, I., Boscia, F., Casamassa, A., de Rosa, V., . . . Pannaccione, A. (2019). Amyloid β-Induced Upregulation of Na(v)1.6 Underlies Neuronal Hyperactivity in Tg2576 Alzheimer's Disease Mouse Model. *Sci Rep, 9*(1), 13592. doi:10.1038/s41598-019-50018-1

Cissé, M., Halabisky, B., Harris, J., Devidze, N., Dubal, D. B., Sun, B., . . . Mucke, L. (2011). Reversing EphB2 depletion rescues cognitive functions in Alzheimer model. *Nature, 469*(7328), 47-52. doi:10.1038/nature09635

Cohen, M. X., & Gulbinaite, R. (2014). Five methodological challenges in cognitive electrophysiology. *Neuroimage, 85 Pt 2*, 702-710. doi:10.1016/j.neuroimage.2013.08.010

Colloby, S. J., Cromarty, R. A., Peraza, L. R., Johnsen, K., Jóhannesson, G., Bonanni, L., . . . Taylor, J. P. (2016). Multimodal EEG-MRI in the differential diagnosis of Alzheimer's disease and dementia with Lewy bodies. *J Psychiatr Res, 78*, 48-55. doi:10.1016/j.jpsychires.2016.03.010

Colom, L. V., Castañeda, M. T., Bañuelos, C., Puras, G., García-Hernández, A., Hernandez, S., . . . Lehker, C. (2010). Medial septal beta-amyloid 1-40 injections alter septo-hippocampal anatomy and function. *Neurobiol Aging, 31*(1), 46-57. doi:10.1016/j.neurobiolaging.2008.05.006

Contet, C., Rawlins, J. N., & Bannerman, D. M. (2001). Faster is not surer--a comparison of C57BL/6J and 129S2/Sv mouse strains in the watermaze. *Behav Brain Res, 125*(1-2), 261-267. doi:10.1016/s0166-4328(01)00295-9

Contet, C., Rawlins, J. N., & Deacon, R. M. (2001). A comparison of 129S2/SvHsd and C57BL/6JOlaHsd mice on a test battery assessing sensorimotor, affective and cognitive behaviours: implications for the study of genetically modified mice. *Behav Brain Res, 124*(1), 33-46. doi:10.1016/s0166-4328(01)00231-5

Corder, E. H., Ghebremedhin, E., Taylor, M. G., Thal, D. R., Ohm, T. G., & Braak, H. (2004). The biphasic relationship between regional brain senile plaque and neurofibrillary tangle distributions: modification by age, sex, and APOE polymorphism. *Ann N Y Acad Sci, 1019*, 24-28. doi:10.1196/annals.1297.005

Crawley, J., & Goodwin, F. K. (1980). Preliminary report of a simple animal behavior model for the anxiolytic effects of benzodiazepines. *Pharmacol Biochem Behav, 13*(2), 167-170. doi:10.1016/0091-3057(80)90067-2

Cummings, J. L., Tong, G., & Ballard, C. (2019). Treatment Combinations for Alzheimer's Disease: Current and Future Pharmacotherapy Options. *J Alzheimers Dis, 67*(3), 779-794. doi:10.3233/jad-180766

Cummins, T. D., Broughton, M., & Finnigan, S. (2008). Theta oscillations are affected by amnestic mild cognitive impairment and cognitive load. *Int J Psychophysiol, 70*(1), 75-81. doi:10.1016/j.ijpsycho.2008.06.002

Dabrowski, A., Štabuc, B., & Lazebnik, L. (2018). Meta-analysis of the efficacy and safety of pantoprazole in the treatment and symptom relief of patients with gastroesophageal reflux disease - PAN-STAR. *Prz Gastroenterol, 13*(1), 6-15. doi:10.5114/pg.2018.74556

Davies, P., & Maloney, A. J. (1976). Selective loss of central cholinergic neurons in Alzheimer's disease. *Lancet, 2*(8000), 1403. doi:10.1016/s0140-6736(76)91936-x

Dementia. (2020). *National Institute on Aging.* Retrieved from https://www.nia.nih.gov/health/how-alzheimers-disease-diagnosed).

Dementia Pathology. (2019). Retrieved from https://www.medscape.com/answers/2003174-197212/which-histologic-findings-are-characteristic-of-alzheimer-disease

DeTure, M. A., & Dickson, D. W. (2019). The neuropathological diagnosis of Alzheimer's disease. *Mol Neurodegener, 14*(1), 32. doi:10.1186/s13024-019-0333-5

Dinamarca, M. C., Raveh, A., Schneider, A., Fritzius, T., Früh, S., Rem, P. D., . . . Bettler, B. (2019). Complex formation of APP with GABA(B) receptors links axonal trafficking to amyloidogenic processing. *Nat Commun, 10*(1), 1331. doi:10.1038/s41467-019-09164-3

Ehrenberg, A. J., Khatun, A., Coomans, E., Betts, M. J., Capraro, F., Thijssen, E. H., . . . Paterson, R. W. (2020). Relevance of biomarkers across different neurodegenerative diseases. *Alzheimers Res Ther, 12*(1), 56. doi:10.1186/s13195-020-00601-w

El-Hayek, Y. H., Wiley, R. E., Khoury, C. P., Daya, R. P., Ballard, C., Evans, A. R., . . . Atri, A. (2019). Tip of the Iceberg: Assessing the Global Socioeconomic Costs of Alzheimer's Disease and Related Dementias and Strategic Implications for Stakeholders. *J Alzheimers Dis, 70*(2), 323-341. doi:10.3233/jad-190426

Emson, P. C. (2007). GABA(B) receptors: structure and function. *Prog Brain Res, 160*, 43-57. doi:10.1016/S0079-6123(06)60004-6

Fang, L., Duan, J., Ran, D., Fan, Z., Yan, Y., Huang, N., . . . Zhu, Y. (2012). Amyloid-β depresses excitatory cholinergic synaptic transmission in Drosophila. *Neurosci Bull, 28*(5), 585-594. doi:10.1007/s12264-012-1267-x

Farina, F. R., Emek-Savaş, D. D., Rueda-Delgado, L., Boyle, R., Kiiski, H., Yener, G., & Whelan, R. (2020). A comparison of resting state EEG and structural MRI for classifying Alzheimer's disease and mild cognitive impairment. *Neuroimage, 215*, 116795. doi:10.1016/j.neuroimage.2020.116795

Farina, N., Rusted, J., & Tabet, N. (2014). The effect of exercise interventions on cognitive outcome in Alzheimer's disease: a systematic review. *Int Psychogeriatr, 26*(1), 9-18. doi:10.1017/s1041610213001385

Farrant, M., & Nusser, Z. (2005). Variations on an inhibitory theme: phasic and tonic activation of GABA(A) receptors. *Nat Rev Neurosci, 6*(3), 215-229. doi:10.1038/nrn1625

Fitton, A., & Wiseman, L. (1996). Pantoprazole. A review of its pharmacological properties and therapeutic use in acid-related disorders. *Drugs, 51*(3), 460-482. doi:10.2165/00003495-199651030-00012

Fox, J. G. (2007). *The mouse in biomedical research* (2 ed.).

Freund, T. F., & Antal, M. (1988). GABA-containing neurons in the septum control inhibitory interneurons in the hippocampus. *Nature, 336*(6195), 170-173. doi:10.1038/336170a0

Fu, H., Hardy, J., & Duff, K. E. (2018). Selective vulnerability in neurodegenerative diseases. *Nat Neurosci, 21*(10), 1350-1358. doi:10.1038/s41593-018-0221-2

Fukushima, R. L. M., do Carmo, E. G., Pedroso, R. D. V., Micali, P. N., Donadelli, P. S., Fuzaro, G. J., . . . Costa, J. L. R. (2016). Effects of cognitive stimulation on neuropsychiatric symptoms in elderly with Alzheimer's disease: A systematic review. *Dement Neuropsychol, 10*(3), 178-184. doi:10.1590/s1980-5764-2016dn1003003

Games, D., Adams, D., Alessandrini, R., Barbour, R., Berthelette, P., Blackwell, C., . . . et al. (1995). Alzheimer-type neuropathology in transgenic mice overexpressing V717F beta-amyloid precursor protein. *Nature, 373*(6514), 523-527. doi:10.1038/373523a0

Gangadharan, G., Shin, J., Kim, S. W., Kim, A., Paydar, A., Kim, D. S., . . . Shin, H. S. (2016). Medial septal GABAergic projection neurons promote object exploration behavior and type 2 theta rhythm. *Proc Natl Acad Sci U S A, 113*(23), 6550-6555. doi:10.1073/pnas.1605019113

Gangarossa, G., Laffray, S., Bourinet, E., & Valjent, E. (2014). T-type calcium channel Cav3.2 deficient mice show elevated anxiety, impaired memory and reduced sensitivity to psychostimulants. *Front Behav Neurosci, 8*, 92. doi:10.3389/fnbeh.2014.00092

Garcia-Alloza, M., Tsang, S. W., Gil-Bea, F. J., Francis, P. T., Lai, M. K., Marcos, B., . . . Ramirez, M. J. (2006). Involvement of the GABAergic system in depressive symptoms of Alzheimer's disease. *Neurobiol Aging, 27*(8), 1110-1117. doi:10.1016/j.neurobiolaging.2005.06.003

Garcia-Marin, V., Blazquez-Llorca, L., Rodriguez, J. R., Boluda, S., Muntane, G., Ferrer, I., & Defelipe, J. (2009). Diminished perisomatic GABAergic terminals on cortical neurons adjacent to amyloid plaques. *Front Neuroanat, 3*, 28. doi:10.3389/neuro.05.028.2009

Garn, H., Coronel, C., Waser, M., Caravias, G., & Ransmayr, G. (2017). Differential diagnosis between patients with probable Alzheimer's disease, Parkinson's disease dementia, or dementia with Lewy bodies and frontotemporal dementia, behavioral variant, using quantitative electroencephalographic features. *J Neural Transm (Vienna), 124*(5), 569-581. doi:10.1007/s00702-017-1699-6

Giessel, A. J., & Sabatini, B. L. (2010). M1 muscarinic receptors boost synaptic potentials and calcium influx in dendritic spines by inhibiting postsynaptic SK channels. *Neuron, 68*(5), 936-947. doi:10.1016/j.neuron.2010.09.004

Gillies, M. J., Traub, R. D., LeBeau, F. E., Davies, C. H., Gloveli, T., Buhl, E. H., & Whittington, M. A. (2002). A model of atropine-resistant theta oscillations in rat hippocampal area CA1. *J Physiol, 543*(Pt 3), 779-793. doi:10.1113/jphysiol.2002.024588

Giorgi, F. S., Ryskalin, L., Ruffoli, R., Biagioni, F., Limanaqi, F., Ferrucci, M., . . . Fornai, F. (2017). The Neuroanatomy of the Reticular Nucleus Locus Coeruleus in Alzheimer's Disease. *Front Neuroanat, 11*, 80. doi:10.3389/fnana.2017.00080

Giorgi, F. S., Saccaro, L. F., Busceti, C. L., Biagioni, F., & Fornai, F. (2020). Epilepsy and Alzheimer's Disease: Potential mechanisms for an association. *Brain Res Bull, 160*, 107-120. doi:10.1016/j.brainresbull.2020.04.009

Giorgi, F. S., Saccaro, L. F., Galgani, A., Busceti, C. L., Biagioni, F., Frati, A., & Fornai, F. (2019). The role of Locus Coeruleus in neuroinflammation occurring in Alzheimer's disease. *Brain Res Bull, 153*, 47-58. doi:10.1016/j.brainresbull.2019.08.007

Goldstein, F. C., Steenland, K., Zhao, L., Wharton, W., Levey, A. I., & Hajjar, I. (2017). Proton Pump Inhibitors and Risk of Mild Cognitive Impairment and Dementia. *J Am Geriatr Soc, 65*(9), 1969-1974. doi:10.1111/jgs.14956

Gomm, W., von Holt, K., Thomé, F., Broich, K., Maier, W., Fink, A., . . . Haenisch, B. (2016). Association of Proton Pump Inhibitors With Risk of Dementia: A Pharmacoepidemiological Claims Data Analysis. *JAMA Neurol, 73*(4), 410-416. doi:10.1001/jamaneurol.2015.4791

Götz, J., Streffer, J. R., David, D., Schild, A., Hoerndli, F., Pennanen, L., . . . Chen, F. (2004). Transgenic animal models of Alzheimer's disease and related disorders: histopathology, behavior and therapy. *Mol Psychiatry, 9*(7), 664-683. doi:10.1038/sj.mp.4001508

Goutagny, R., Manseau, F., Jackson, J., Danik, M., & Williams, S. (2008). In vitro activation of the medial septum-diagonal band complex generates atropine-sensitive and atropine-resistant hippocampal theta rhythm: an investigation using a complete septohippocampal preparation. *Hippocampus, 18*(6), 531-535. doi:10.1002/hipo.20418

Goyal, A., Miller, J., Qasim, S. E., Watrous, A. J., Zhang, H., Stein, J. M., . . . Jacobs, J. (2020). Functionally distinct high and low theta oscillations in the human hippocampus. *Nat Commun, 11*(1), 2469. doi:10.1038/s41467-020-15670-6

Goyal, N., Lee, Y., Luna, G., & Aruin, A. S. (2020). Individual and combined effects of a cognitive task, light finger touch, and vision on standing balance in older adults with mild cognitive impairment. *Aging Clin Exp Res, 32*(5), 797-807. doi:10.1007/s40520-019-01262-y

Graham, W. V., Bonito-Oliva, A., & Sakmar, T. P. (2017). Update on Alzheimer's Disease Therapy and Prevention Strategies. *Annu Rev Med, 68,* 413-430. doi:10.1146/annurev-med-042915-103753

Green, K. N., Billings, L. M., Roozendaal, B., McGaugh, J. L., & LaFerla, F. M. (2006). Glucocorticoids Increase Amyloid-β and Tau Pathology in a Mouse Model of Alzheimer's Disease. *The Journal of Neuroscience, 26*(35), 9047-9056. doi:10.1523/jneurosci.2797-06.2006

Griffin, A. L., Asaka, Y., Darling, R. D., & Berry, S. D. (2004). Theta-contingent trial presentation accelerates learning rate and enhances hippocampal plasticity during trace eyeblink conditioning. *Behav Neurosci, 118*(2), 403-411. doi:10.1037/0735-7044.118.2.403

Groot, C., Hooghiemstra, A. M., Raijmakers, P. G., van Berckel, B. N., Scheltens, P., Scherder, E. J., . . . Ossenkoppele, R. (2016). The effect of physical activity on cognitive function in patients with dementia: A meta-analysis of randomized control trials. *Ageing Res Rev, 25,* 13-23. doi:10.1016/j.arr.2015.11.005

Grossberg, G. T., Christensen, D. D., Griffith, P. A., Kerwin, D. R., Hunt, G., & Hall, E. J. (2010). The art of sharing the diagnosis and management of Alzheimer's disease with patients and caregivers: recommendations of an expert consensus panel. *Prim Care Companion J Clin Psychiatry, 12*(1), PCC.09cs00833. doi:10.4088/PCC.09cs00833oli

Gu, Z., Smith, K. G., Alexander, G. M., Guerreiro, I., Dudek, S. M., Gutkin, B., . . . Yakel, J. L. (2020). Hippocampal Interneuronal α7 nAChRs Modulate Theta Oscillations in Freely Moving Mice. *Cell Rep, 31*(10), 107740. doi:10.1016/j.celrep.2020.107740

Gu, Z., & Yakel, J. L. (2011). Timing-dependent septal cholinergic induction of dynamic hippocampal synaptic plasticity. *Neuron, 71*(1), 155-165. doi:10.1016/j.neuron.2011.04.026

Gurevicius, K., Lipponen, A., & Tanila, H. (2013). Increased cortical and thalamic excitability in freely moving APPswe/PS1dE9 mice modeling epileptic activity associated with Alzheimer's disease. *Cereb Cortex, 23*(5), 1148-1158. doi:10.1093/cercor/bhs105

Gutiérrez-Lerma, A. I., Ordaz, B., & Peña-Ortega, F. (2013). Amyloid Beta peptides differentially affect hippocampal theta rhythms in vitro. *Int J Pept, 2013,* 328140. doi:10.1155/2013/328140

Haenisch, B., von Holt, K., Wiese, B., Prokein, J., Lange, C., Ernst, A., . . . Scherer, M. (2015). Risk of dementia in elderly patients with the use of proton pump inhibitors. *Eur Arch Psychiatry Clin Neurosci, 265*(5), 419-428. doi:10.1007/s00406-014-0554-0

Hafiz, R. A., Wong, C., Paynter, S., David, M., & Peeters, G. (2018). The Risk of Community-Acquired Enteric Infection in Proton Pump Inhibitor Therapy: Systematic Review and Meta-analysis. *Ann Pharmacother, 52*(7), 613-622. doi:10.1177/1060028018760569

Hajos, M., Hoffmann, W. E., & Weaver, R. J. (2003). Regulation of septo-hippocampal activity by 5-hydroxytryptamine(2C) receptors. *J Pharmacol Exp Ther, 306*(2), 605-615. doi:10.1124/jpet.103.051169

Hangya, B., Borhegyi, Z., Szilágyi, N., Freund, T. F., & Varga, V. (2009). GABAergic neurons of the medial septum lead the hippocampal network during theta activity. *J Neurosci, 29*(25), 8094-8102. doi:10.1523/jneurosci.5665-08.2009

Hanslmayr, S., & Staudigl, T. (2014). How brain oscillations form memories--a processing based perspective on oscillatory subsequent memory effects. *Neuroimage, 85 Pt 2*, 648-655. doi:10.1016/j.neuroimage.2013.05.121

Hara, K., & Harris, R. A. (2002). The anesthetic mechanism of urethane: the effects on neurotransmitter-gated ion channels. *Anesth Analg, 94*(2), 313-318, table of contents. doi:10.1097/00000539-200202000-00015

Hartmann, M., Huber, R., Bliesath, H., Steinijans, V. W., Koch, H. J., Wurst, W., & Kunz, K. (1996). Lack of interaction between pantoprazole and digoxin at therapeutic doses in man. *Int J Clin Pharmacol Ther, 34*(1 Suppl), S67-71.

Hashioka, S., Klegeris, A., & McGeer, P. L. (2009). Proton pump inhibitors exert anti-inflammatory effects and decrease human microglial and monocytic THP-1 cell neurotoxicity. *Exp Neurol, 217*(1), 177-183. doi:10.1016/j.expneurol.2009.02.002

Hashioka, S., Klegeris, A., & McGeer, P. L. (2011). Proton pump inhibitors reduce interferon-γ-induced neurotoxicity and STAT3 phosphorylation of human astrocytes. *Glia, 59*(5), 833-840. doi:10.1002/glia.21157

Hasselmo, M. E., & McGaughy, J. (2004). High acetylcholine levels set circuit dynamics for attention and encoding and low acetylcholine levels set dynamics for consolidation. *Prog Brain Res, 145*, 207-231. doi:10.1016/S0079-6123(03)45015-2

Hazra, A., Gu, F., Aulakh, A., Berridge, C., Eriksen, J. L., & Ziburkus, J. (2013). Inhibitory neuron and hippocampal circuit dysfunction in an aged mouse model of Alzheimer's disease. *PLoS One, 8*(5), e64318. doi:10.1371/journal.pone.0064318

Heemels, M. T. (2016). Neurodegenerative diseases. *Nature, 539*(7628), 179. doi:10.1038/539179a

Hegerl, U., & Möller, H. J. (1997). Electroencephalography as a diagnostic instrument in Alzheimer's disease: reviews and perspectives. *Int Psychogeriatr, 9 Suppl 1*, 237-246; discussion 247-252. doi:10.1017/s1041610297004948

Helgadottir, H., & Bjornsson, E. S. (2019). Problems Associated with Deprescribing of Proton Pump Inhibitors. *Int J Mol Sci, 20*(21). doi:10.3390/ijms20215469

Hellemans, J., Mortier, G., De Paepe, A., Speleman, F., & Vandesompele, J. (2007). qBase relative quantification framework and software for management and automated analysis of real-time quantitative PCR data. *Genome Biol, 8*(2), R19. doi:10.1186/gb-2007-8-2-r19

Hijazi, S., Heistek, T. S., van der Loo, R., Mansvelder, H. D., Smit, A. B., & van Kesteren, R. E. (2020). Hyperexcitable Parvalbumin Interneurons Render Hippocampal Circuitry Vulnerable to Amyloid Beta. *iScience, 23*(7), 101271. doi:10.1016/j.isci.2020.101271

Hillen, H. (2019). The Beta Amyloid Dysfunction (BAD) Hypothesis for Alzheimer's Disease. *Front Neurosci, 13*, 1154. doi:10.3389/fnins.2019.01154

Holtzman, D. M., Herz, J., & Bu, G. (2012). Apolipoprotein E and apolipoprotein E receptors: normal biology and roles in Alzheimer disease. *Cold Spring Harb Perspect Med, 2*(3), a006312. doi:10.1101/cshperspect.a006312

Horváth, A., Szűcs, A., Barcs, G., Noebels, J. L., & Kamondi, A. (2016). Epileptic Seizures in Alzheimer Disease: A Review. *Alzheimer Dis Assoc Disord, 30*(2), 186-192. doi:10.1097/wad.0000000000000134

Hou, Y., Dan, X., Babbar, M., Wei, Y., Hasselbalch, S. G., Croteau, D. L., & Bohr, V. A. (2019). Ageing as a risk factor for neurodegenerative disease. *Nat Rev Neurol, 15*(10), 565-581. doi:10.1038/s41582-019-0244-7

Howard, R., McShane, R., Lindesay, J., Ritchie, C., Baldwin, A., Barber, R., . . . Phillips, P. P. (2015). Nursing home placement in the Donepezil and Memantine in Moderate to Severe Alzheimer's Disease (DOMINO-AD) trial: secondary and post-hoc analyses. *Lancet Neurol, 14*(12), 1171-1181. doi:10.1016/s1474-4422(15)00258-6

Hsiao, K. (1994). A proposed strategic research program for Alzheimer's disease. *Neurobiol Aging, 15 Suppl 2*, S113-115. doi:10.1016/0197-4580(94)90186-4

Huang, L. K., Chao, S. P., & Hu, C. J. (2020). Clinical trials of new drugs for Alzheimer disease. *J Biomed Sci, 27*(1), 18. doi:10.1186/s12929-019-0609-7

Huber, R., Kohl, B., Sachs, G., Senn-Bilfinger, J., Simon, W. A., & Sturm, E. (1995). Review article: the continuing development of proton pump inhibitors with particular reference to pantoprazole. *Aliment Pharmacol Ther, 9*(4), 363-378. doi:10.1111/j.1365-2036.1995.tb00394.x

Hyman, B. T., Van Hoesen, G. W., Damasio, A. R., & Barnes, C. L. (1984). Alzheimer's disease: cell-specific pathology isolates the hippocampal formation. *Science, 225*(4667), 1168-1170. doi:10.1126/science.6474172

Imbrici, P., Tucker, S. J., D'Adamo, M. C., & Pessia, M. (2000). Role of receptor protein tyrosine phosphatase alpha (RPTPalpha) and tyrosine phosphorylation in the serotonergic inhibition of voltage-dependent potassium channels. *Pflugers Arch, 441*(2-3), 257-262. doi:10.1007/s004240000406

Iwamoto, N., Thangnipon, W., Crawford, C., & Emson, P. C. (1991). Localization of calpain immunoreactivity in senile plaques and in neurones undergoing neurofibrillary degeneration in Alzheimer's disease. *Brain Res, 561*(1), 177-180. doi:10.1016/0006-8993(91)90766-o

Jacob, T. C., Moss, S. J., & Jurd, R. (2008). GABA(A) receptor trafficking and its role in the dynamic modulation of neuronal inhibition. *Nat Rev Neurosci, 9*(5), 331-343. doi:10.1038/nrn2370

Jacus, M. O., Uebele, V. N., Renger, J. J., & Todorovic, S. M. (2012). Presynaptic Cav3.2 channels regulate excitatory neurotransmission in nociceptive dorsal horn neurons. *J Neurosci, 32*(27), 9374-9382. doi:10.1523/jneurosci.0068-12.2012

Jankowsky, J. L., Fadale, D. J., Anderson, J., Xu, G. M., Gonzales, V., Jenkins, N. A., . . . Borchelt, D. R. (2004). Mutant presenilins specifically elevate the levels of the 42 residue beta-amyloid peptide in vivo: evidence for augmentation of a 42-specific gamma secretase. *Hum Mol Genet, 13*(2), 159-170. doi:10.1093/hmg/ddh019

Jansen, I. E., Savage, J. E., Watanabe, K., Bryois, J., Williams, D. M., Steinberg, S., . . . Posthuma, D. (2019). Genome-wide meta-analysis identifies new loci and functional pathways influencing Alzheimer's disease risk. *Nat Genet, 51*(3), 404-413. doi:10.1038/s41588-018-0311-9

Jia, X., Smith, M. A., & Kohn, A. (2011). Stimulus selectivity and spatial coherence of gamma components of the local field potential. *J Neurosci, 31*(25), 9390-9403. doi:10.1523/jneurosci.0645-11.2011

Johnson, K. A., Minoshima, S., Bohnen, N. I., Donohoe, K. J., Foster, N. L., Herscovitch, P., . . . Hartley, D. M. (2013). Update on appropriate use criteria for amyloid PET imaging: dementia experts, mild cognitive impairment, and education. Amyloid Imaging Task Force of the Alzheimer’s Association and Society for Nuclear Medicine and Molecular Imaging. *Alzheimers Dement, 9*(4), e106-109. doi:10.1016/j.jalz.2013.06.001

Jonkman, E. J. (1997). The role of the electroencephalogram in the diagnosis of dementia of the Alzheimer type: an attempt at technology assessment. *Neurophysiol Clin, 27*(3), 211-219. doi:10.1016/s0987-7053(97)83777-x

Jurcak, V., Tsuzuki, D., & Dan, I. (2007). 10/20, 10/10, and 10/5 systems revisited: their validity as relative head-surface-based positioning systems. *Neuroimage, 34*(4), 1600-1611. doi:10.1016/j.neuroimage.2006.09.024

Jyoti, A., Plano, A., Riedel, G., & Platt, B. (2010). EEG, activity, and sleep architecture in a transgenic AβPPswe/PSEN1A246E Alzheimer's disease mouse. *J Alzheimers Dis, 22*(3), 873-887. doi:10.3233/jad-2010-100879

Kang, J., Lemaire, H. G., Unterbeck, A., Salbaum, J. M., Masters, C. L., Grzeschik, K. H., . . . Müller-Hill, B. (1987). The precursor of Alzheimer's disease amyloid A4 protein resembles a cell-surface receptor. *Nature, 325*(6106), 733-736. doi:10.1038/325733a0

Karch, C. M., Hernández, D., Wang, J. C., Marsh, J., Hewitt, A. W., Hsu, S., . . . Goate, A. M. (2018). Human fibroblast and stem cell resource from the Dominantly Inherited Alzheimer Network. *Alzheimers Res Ther, 10*(1), 69. doi:10.1186/s13195-018-0400-0

Kim, D., Song, I., Keum, S., Lee, T., Jeong, M. J., Kim, S. S., . . . Shin, H. S. (2001). Lack of the burst firing of thalamocortical relay neurons and resistance to absence seizures in mice lacking alpha(1G) T-type Ca(2+) channels. *Neuron, 31*(1), 35-45. doi:10.1016/s0896-6273(01)00343-9

Kleen, J. K., Scott, R. C., Holmes, G. L., Roberts, D. W., Rundle, M. M., Testorf, M., . . . Jobst, B. C. (2013). Hippocampal interictal epileptiform activity disrupts cognition in humans. *Neurology, 81*(1), 18-24. doi:10.1212/WNL.0b013e318297ee50

Korotkova, T., Ponomarenko, A., Monaghan, C. K., Poulter, S. L., Cacucci, F., Wills, T., . . . Lever, C. (2018). Reconciling the different faces of hippocampal theta: The role of theta oscillations in cognitive, emotional and innate behaviors. *Neurosci Biobehav Rev, 85*, 65-80. doi:10.1016/j.neubiorev.2017.09.004

Korpi, E. R., Grunder, G., & Luddens, H. (2002). Drug interactions at GABA(A) receptors. *Prog Neurobiol, 67*(2), 113-159. doi:10.1016/s0301-0082(02)00013-8

Kramer, K., & Kinter, L. B. (2003). Evaluation and applications of radiotelemetry in small laboratory animals. *Physiol Genomics, 13*(3), 197-205. doi:10.1152/physiolgenomics.00164.2002

Kramis, R., Vanderwolf, C. H., & Bland, B. H. (1975). Two types of hippocampal rhythmical slow activity in both the rabbit and the rat: relations to behavior and effects of atropine, diethyl ether, urethane, and pentobarbital. *Exp Neurol, 49*(1 Pt 1), 58-85. doi:10.1016/0014-4886(75)90195-8

Kraus, B. J., Brandon, M. P., Robinson, R. J., 2nd, Connerney, M. A., Hasselmo, M. E., & Eichenbaum, H. (2015). During Running in Place, Grid Cells Integrate Elapsed Time and Distance Run. *Neuron, 88*(3), 578-589. doi:10.1016/j.neuron.2015.09.031

Kromer, W. (1995). Similarities and differences in the properties of substituted benzimidazoles: a comparison between pantoprazole and related compounds. *Digestion, 56*(6), 443-454. doi:10.1159/000201275

Kukolja, J., Thiel, C. M., & Fink, G. R. (2009). Cholinergic stimulation enhances neural activity associated with encoding but reduces neural activity associated with retrieval in humans. *J Neurosci, 29*(25), 8119-8128. doi:10.1523/JNEUROSCI.0203-09.2009

Kumar, R., Kumar, A., Nordberg, A., Långström, B., & Darreh-Shori, T. (2020). Proton pump inhibitors act with unprecedented potencies as inhibitors of the acetylcholine biosynthesizing enzyme-A plausible missing link for their association with incidence of dementia. *Alzheimers Dement, 16*(7), 1031-1042. doi:10.1002/alz.12113

Kuzmiski, J. B., Barr, W., Zamponi, G. W., & MacVicar, B. A. (2005). Topiramate inhibits the initiation of plateau potentials in CA1 neurons by depressing R-type calcium channels. *Epilepsia, 46*(4), 481-489. doi:10.1111/j.0013-9580.2005.35304.x

Lalonde, R., Dumont, M., Paly, E., London, J., & Strazielle, C. (2004). Characterization of hemizygous SOD1/wild-type transgenic mice with the SHIRPA primary screen and tests of sensorimotor function and anxiety. *Brain Res Bull, 64*(3), 251-258. doi:10.1016/j.brainresbull.2004.07.011

Lane, C. A., Hardy, J., & Schott, J. M. (2018). Alzheimer's disease. *Eur J Neurol, 25*(1), 59-70. doi:10.1111/ene.13439

Leão, R. N., Colom, L. V., Borgius, L., Kiehn, O., & Fisahn, A. (2012). Medial septal dysfunction by Aβ-induced KCNQ channel-block in glutamatergic neurons. *Neurobiol Aging, 33*(9), 2046-2061. doi:10.1016/j.neurobiolaging.2011.07.013

Lee, J. H., Gomora, J. C., Cribbs, L. L., & Perez-Reyes, E. (1999). Nickel block of three cloned T-type calcium channels: low concentrations selectively block alpha1H. *Biophys J, 77*(6), 3034-3042. doi:10.1016/S0006-3495(99)77134-1

Lei, M., Xu, H., Li, Z., Wang, Z., O'Malley, T. T., Zhang, D., . . . Li, S. (2016). Soluble Aβ oligomers impair hippocampal LTP by disrupting glutamatergic/GABAergic balance. *Neurobiol Dis, 85*, 111-121. doi:10.1016/j.nbd.2015.10.019

Leissring, M. A., Farris, W., Chang, A. Y., Walsh, D. M., Wu, X., Sun, X., . . . Selkoe, D. J. (2003). Enhanced proteolysis of beta-amyloid in APP transgenic mice prevents plaque formation, secondary pathology, and premature death. *Neuron, 40*(6), 1087-1093. doi:10.1016/s0896-6273(03)00787-6

Leresche, N., & Lambert, R. C. (2017). T-type calcium channels in synaptic plasticity. *Channels (Austin), 11*(2), 121-139. doi:10.1080/19336950.2016.1238992

Li, T., Xie, Y., & Al-Aly, Z. (2018). The association of proton pump inhibitors and chronic kidney disease: cause or confounding? *Curr Opin Nephrol Hypertens, 27*(3), 182-187. doi:10.1097/mnh.0000000000000406

Lindberg, P., Brändström, A., Wallmark, B., Mattsson, H., Rikner, L., & Hoffmann, K. J. (1990). Omeprazole: the first proton pump inhibitor. *Med Res Rev, 10*(1), 1-54. doi:10.1002/med.2610100102

Lok, K., Zhao, H., Shen, H., Wang, Z., Gao, X., Zhao, W., & Yin, M. (2013). Characterization of the APP/PS1 mouse model of Alzheimer's disease in senescence accelerated background. *Neurosci Lett, 557 Pt B*, 84-89. doi:10.1016/j.neulet.2013.10.051

Lory, P., Nicole, S., & Monteil, A. (2020). Neuronal Cav3 channelopathies: recent progress and perspectives. *Pflugers Arch, 472*(7), 831-844. doi:10.1007/s00424-020-02429-7

Loy, C. T., Schofield, P. R., Turner, A. M., & Kwok, J. B. (2014). Genetics of dementia. *Lancet, 383*(9919), 828-840. doi:10.1016/s0140-6736(13)60630-3

Lozsadi, D. A., & Larner, A. J. (2006). Prevalence and causes of seizures at the time of diagnosis of probable Alzheimer's disease. *Dement Geriatr Cogn Disord, 22*(2), 121-124. doi:10.1159/000093664

Lubenov, E. V., & Siapas, A. G. (2009). Hippocampal theta oscillations are travelling waves. *Nature, 459*(7246), 534-539. doi:10.1038/nature08010

Lundqvist, M., Herman, P., Warden, M. R., Brincat, S. L., & Miller, E. K. (2018). Gamma and beta bursts during working memory readout suggest roles in its volitional control. *Nat Commun, 9*(1), 394. doi:10.1038/s41467-017-02791-8

Lundqvist, M., Rose, J., Herman, P., Brincat, S. L., Buschman, T. J., & Miller, E. K. (2016a). *Neuron, 90*(1), 152-164. doi:10.1016/j.neuron.2016.02.028

Lundqvist, M., Rose, J., Herman, P., Brincat, S. L., Buschman, T. J., & Miller, E. K. (2016b). Gamma and Beta Bursts Underlie Working Memory. *Neuron, 90*(1), 152-164. doi:10.1016/j.neuron.2016.02.028

Lundt, A., Wormuth, C., Siwek, M. E., Muller, R., Ehninger, D., Henseler, C., . . . Weiergraber, M. (2016). EEG Radiotelemetry in Small Laboratory Rodents: A Powerful State-of-the Art Approach in Neuropsychiatric, Neurodegenerative, and Epilepsy Research. *Neural Plast, 2016*, 8213878. doi:10.1155/2016/8213878

Lundt, A., Wormuth, C., Siwek, M. E., Müller, R., Ehninger, D., Henseler, C., . . . Weiergräber, M. (2016). EEG Radiotelemetry in Small Laboratory Rodents: A Powerful State-of-the Art Approach in Neuropsychiatric, Neurodegenerative, and Epilepsy Research. *Neural Plast, 2016*, 8213878. doi:10.1155/2016/8213878

Luscher, B., Fuchs, T., & Kilpatrick, C. L. (2011). GABAA receptor trafficking-mediated plasticity of inhibitory synapses. *Neuron, 70*(3), 385-409. doi:10.1016/j.neuron.2011.03.024

Ly, R., Bouvier, G., Schonewille, M., Arabo, A., Rondi-Reig, L., Lena, C., . . . Feltz, A. (2013). T-type channel blockade impairs long-term potentiation at the parallel fiber-Purkinje cell synapse and cerebellar learning. *Proc Natl Acad Sci U S A, 110*(50), 20302-20307. doi:10.1073/pnas.1311686110

Ma, K., & McLaurin, J. (2014). α-Melanocyte stimulating hormone prevents GABAergic neuronal loss and improves cognitive function in Alzheimer's disease. *J Neurosci, 34*(20), 6736-6745. doi:10.1523/jneurosci.5075-13.2014

Ma, N., Tie, C., Yu, B., Zhang, W., & Wan, J. (2020). Identifying lncRNA-miRNA-mRNA networks to investigate Alzheimer's disease pathogenesis and therapy strategy. *Aging (Albany NY), 12*(3), 2897-2920. doi:10.18632/aging.102785

Ma, S., Olucha-Bordonau, F. E., Hossain, M. A., Lin, F., Kuei, C., Liu, C., . . . Gundlach, A. L. (2009). Modulation of hippocampal theta oscillations and spatial memory by relaxin-3 neurons of the nucleus incertus. *Learn Mem, 16*(11), 730-742. doi:10.1101/lm.1438109

MacDonald, C. J., Carrow, S., Place, R., & Eichenbaum, H. (2013). Distinct hippocampal time cell sequences represent odor memories in immobilized rats. *J Neurosci, 33*(36), 14607-14616. doi:10.1523/jneurosci.1537-13.2013

Magee, J. C., & Carruth, M. (1999). Dendritic voltage-gated ion channels regulate the action potential firing mode of hippocampal CA1 pyramidal neurons. *J Neurophysiol, 82*(4), 1895-1901. doi:10.1152/jn.1999.82.4.1895

Magee, J. C., & Johnston, D. (1995). Synaptic activation of voltage-gated channels in the dendrites of hippocampal pyramidal neurons. *Science, 268*(5208), 301-304. doi:10.1126/science.7716525

Makunts, T., Alpatty, S., Lee, K. C., Atayee, R. S., & Abagyan, R. (2019). Proton-pump inhibitor use is associated with a broad spectrum of neurological adverse events including impaired hearing, vision, and memory. *Sci Rep, 9*(1), 17280. doi:10.1038/s41598-019-53622-3

Mallmann, R. T., Elgueta, C., Sleman, F., Castonguay, J., Wilmes, T., van den Maagdenberg, A., & Klugbauer, N. (2013). Ablation of Ca(V)2.1 voltage-gated Ca(2)(+) channels in mouse forebrain generates multiple cognitive impairments. *PLoS One, 8*(10), e78598. doi:10.1371/journal.pone.0078598

Mann, D. M., & Hardy, J. (2013). Amyloid or tau: the chicken or the egg? *Acta Neuropathol, 126*(4), 609-613. doi:10.1007/s00401-013-1162-1

Mathews, S., Reid, A., Tian, C., & Cai, Q. (2010). An update on the use of pantoprazole as a treatment for gastroesophageal reflux disease. *Clin Exp Gastroenterol, 3,* 11-16. doi:10.2147/ceg.s6355

Matsunaga, S., Kishi, T., & Iwata, N. (2015). Memantine monotherapy for Alzheimer's disease: a systematic review and meta-analysis. *PLoS One, 10*(4), e0123289. doi:10.1371/journal.pone.0123289

Mattson, M. P., & Magnus, T. (2006). Ageing and neuronal vulnerability. *Nat Rev Neurosci, 7*(4), 278-294. doi:10.1038/nrn1886

Mazure, C. M., & Swendsen, J. (2016). Sex differences in Alzheimer's disease and other dementias. *Lancet Neurol, 15*(5), 451-452. doi:10.1016/s1474-4422(16)00067-3

McCafferty, D. J., Gallon, S., & Nord, A. (2015). Challenges of measuring body temperatures of free-ranging birds and mammals. *Animal Biotelemetry, 3*(1), 33. doi:10.1186/s40317-015-0075-2

McGowan, E., Pickford, F., Kim, J., Onstead, L., Eriksen, J., Yu, C., . . . Golde, T. (2005). Abeta42 is essential for parenchymal and vascular amyloid deposition in mice. *Neuron, 47*(2), 191-199. doi:10.1016/j.neuron.2005.06.030

McKhann, G. M., Knopman, D. S., Chertkow, H., Hyman, B. T., Jack, C. R., Jr., Kawas, C. H., . . . Phelps, C. H. (2011). The diagnosis of dementia due to Alzheimer's disease: recommendations from the National Institute on Aging-Alzheimer's Association workgroups on diagnostic guidelines for Alzheimer's disease. *Alzheimers Dement, 7*(3), 263-269. doi:10.1016/j.jalz.2011.03.005

McKinney, B. C., & Murphy, G. G. (2006). The L-Type voltage-gated calcium channel Cav1.3 mediates consolidation, but not extinction, of contextually conditioned fear in mice. *Learn Mem, 13*(5), 584-589. doi:10.1101/lm.279006

Mendu, S. K., Bhandage, A., Jin, Z., & Birnir, B. (2012). Different subtypes of GABA-A receptors are expressed in human, mouse and rat T lymphocytes. *PLoS One, 7*(8), e42959. doi:10.1371/journal.pone.0042959

Meyer, U. A. (1996). Interaction of proton pump inhibitors with cytochromes P450: consequences for drug interactions. *Yale J Biol Med, 69*(3), 203-209.

Mikulovic, S., Restrepo, C. E., Siwani, S., Bauer, P., Pupe, S., Tort, A. B. L., . . . Leão, R. N. (2018). Ventral hippocampal OLM cells control type 2 theta oscillations and response to predator odor. *Nat Commun, 9*(1), 3638. doi:10.1038/s41467-018-05907-w

Minkeviciene, R., Rheims, S., Dobszay, M. B., Zilberter, M., Hartikainen, J., Fülöp, L., . . . Tanila, H. (2009). Amyloid beta-induced neuronal hyperexcitability triggers progressive epilepsy. *J Neurosci, 29*(11), 3453-3462. doi:10.1523/jneurosci.5215-08.2009

Mody, I., & Pearce, R. A. (2004). Diversity of inhibitory neurotransmission through GABA(A) receptors. *Trends Neurosci, 27*(9), 569-575. doi:10.1016/j.tins.2004.07.002

Modyanov, N. N., Petrukhin, K. E., Sverdlov, V. E., Grishin, A. V., Orlova, M. Y., Kostina, M. B., . . . Sverdlov, E. D. (1991). The family of human Na,K-ATPase genes. ATP1AL1 gene is transcriptionally competent and probably encodes the related ion transport ATPase. *FEBS Lett, 278*(1), 91-94. doi:10.1016/0014-5793(91)80091-g

Molineux, M. L., McRory, J. E., McKay, B. E., Hamid, J., Mehaffey, W. H., Rehak, R., . . . Turner, R. W. (2006). Specific T-type calcium channel isoforms are associated with distinct burst phenotypes in deep cerebellar nuclear neurons. *Proc Natl Acad Sci U S A, 103*(14), 5555-5560. doi:10.1073/pnas.0601261103

Moons, C. P., Hermans, K., Remie, R., Duchateau, L., & Odberg, F. O. (2007). Intraperitoneal versus subcutaneous telemetry devices in young Mongolian gerbils (Meriones unguiculatus). *Lab Anim, 41*(2), 262-269. doi:10.1258/002367707780378177

Moosmang, S., Lenhardt, P., Haider, N., Hofmann, F., & Wegener, J. W. (2005). Mouse models to study L-type calcium channel function. *Pharmacol Ther, 106*(3), 347-355. doi:10.1016/j.pharmthera.2004.12.003

Moretti, D. V., Babiloni, C., Binetti, G., Cassetta, E., Dal Forno, G., Ferreric, F., . . . Rossini, P. M. (2004). Individual analysis of EEG frequency and band power in mild Alzheimer's disease. *Clin Neurophysiol, 115*(2), 299-308. doi:10.1016/s1388-2457(03)00345-6

Morrison, J. H., & Hof, P. R. (2002). Selective vulnerability of corticocortical and hippocampal circuits in aging and Alzheimer's disease. *Prog Brain Res, 136,* 467-486. doi:10.1016/s0079-6123(02)36039-4

Morschel, C. F., Mafra, D., & Eduardo, J. C. C. (2018). The relationship between proton pump inhibitors and renal disease. *J Bras Nefrol, 40*(3), 301-306. doi:10.1590/2175-8239-jbn-2018-0021

Morse, H. C. (2007). Chapter 1 - Building a Better Mouse: One Hundred Years of Genetics and Biology. In J. G. Fox, M. T. Davisson, F. W. Quimby, S. W. Barthold, C. E. Newcomer, & A. L. Smith (Eds.), *The Mouse in Biomedical Research (Second Edition)* (pp. 1-11). Burlington: Academic Press.

Mroczko, B., Groblewska, M., & Litman-Zawadzka, A. (2019). The Role of Protein Misfolding and Tau Oligomers (TauOs) in Alzheimer's Disease (AD). *Int J Mol Sci, 20*(19). doi:10.3390/ijms20194661

Müller, R., Papazoglou, A., Soos, J., Lundt, A., Wormuth, C., Henseler, C., . . . Weiergräber, M. (2017). Automatic Detection of Highly Organized Theta Oscillations in the Murine EEG. *J Vis Exp*(121). doi:10.3791/55089

Muller, R., Struck, H., Ho, M. S., Brockhaus-Dumke, A., Klosterkotter, J., Broich, K., . . . Weiergraber, M. (2012). Atropine-sensitive hippocampal theta oscillations are mediated by Cav2.3 R-type Ca(2)(+) channels. *Neuroscience, 205*, 125-139. doi:10.1016/j.neuroscience.2011.12.032

Muratore, C. R., Zhou, C., Liao, M., Fernandez, M. A., Taylor, W. M., Lagomarsino, V. N., . . . Young-Pearse, T. L. (2017). Cell-type Dependent Alzheimer's Disease Phenotypes: Probing the Biology of Selective Neuronal Vulnerability. *Stem Cell Reports, 9*(6), 1868-1884. doi:10.1016/j.stemcr.2017.10.015

Myers, A., & McGonigle, P. (2019). Overview of Transgenic Mouse Models for Alzheimer's Disease. *Curr Protoc Neurosci, 89*(1), e81. doi:10.1002/cpns.81

Nakamura, T., Arima-Yoshida, F., Sakaue, F., Nasu-Nishimura, Y., Takeda, Y., Matsuura, K., . . . Akiyama, T. (2016). PX-RICS-deficient mice mimic autism spectrum disorder in Jacobsen syndrome through impaired GABAA receptor trafficking. *Nat Commun, 7*, 10861. doi:10.1038/ncomms10861

Nanou, E., & Catterall, W. A. (2018). Calcium Channels, Synaptic Plasticity, and Neuropsychiatric Disease. *Neuron, 98*(3), 466-481. doi:10.1016/j.neuron.2018.03.017

Nelson, P. T., Head, E., Schmitt, F. A., Davis, P. R., Neltner, J. H., Jicha, G. A., . . . Scheff, S. W. (2011). Alzheimer's disease is not "brain aging": neuropathological, genetic, and epidemiological human studies. *Acta Neuropathol, 121*(5), 571-587. doi:10.1007/s00401-011-0826-y

Neto, E., Allen, E. A., Aurlien, H., Nordby, H., & Eichele, T. (2015). EEG Spectral Features Discriminate between Alzheimer's and Vascular Dementia. *Front Neurol, 6*, 25. doi:10.3389/fneur.2015.00025

Neto, E., Biessmann, F., Aurlien, H., Nordby, H., & Eichele, T. (2016). Regularized Linear Discriminant Analysis of EEG Features in Dementia Patients. *Front Aging Neurosci, 8*, 273. doi:10.3389/fnagi.2016.00273

Nicastro, N., Assal, F., & Seeck, M. (2016). From here to epilepsy: the risk of seizure in patients with Alzheimer's disease. *Epileptic Disord, 18*(1), 1-12. doi:10.1684/epd.2016.0808

Nottage, J. F., & Horder, J. (2015). State-of-the-Art Analysis of High-Frequency (Gamma Range) Electroencephalography in Humans. *Neuropsychobiology, 72*(3-4), 219-228. doi:10.1159/000382023

Novotny, M., Klimova, B., & Valis, M. (2018). PPI Long Term Use: Risk of Neurological Adverse Events? *Front Neurol, 9*, 1142. doi:10.3389/fneur.2018.01142

Nunez, P. L., & Srinivasan, R. (2014). Neocortical dynamics due to axon propagation delays in cortico-cortical fibers: EEG traveling and standing waves with implications for top-down influences on local networks and white matter disease. *Brain Res, 1542*, 138-166. doi:10.1016/j.brainres.2013.10.036

Oddie, S. D., & Bland, B. H. (1998). Hippocampal formation theta activity and movement selection. *Neurosci Biobehav Rev, 22*(2), 221-231.

Olsen, R. W., & Sieghart, W. (2008). International Union of Pharmacology. LXX. Subtypes of gamma-aminobutyric acid(A) receptors: classification on the basis of subunit composition, pharmacology, and function. Update. *Pharmacol Rev, 60*(3), 243-260. doi:10.1124/pr.108.00505

Olsen, R. W., & Sieghart, W. (2009). GABA A receptors: subtypes provide diversity of function and pharmacology. *Neuropharmacology, 56*(1), 141-148. doi:10.1016/j.neuropharm.2008.07.045

Olsson, B., Lautner, R., Andreasson, U., Öhrfelt, A., Portelius, E., Bjerke, M., . . . Zetterberg, H. (2016). CSF and blood biomarkers for the diagnosis of Alzheimer's disease: a systematic review and meta-analysis. *Lancet Neurol, 15*(7), 673-684. doi:10.1016/s1474-4422(16)00070-3

Ordóñez-Gutiérrez, L., Antón, M., & Wandosell, F. (2015). Peripheral amyloid levels present gender differences associated with aging in AβPP/PS1 mice. *J Alzheimers Dis, 44*(4), 1063-1068. doi:10.3233/jad-141158

Ortiz-Guerrero, G., Amador-Muñoz, D., Calderón-Ospina, C. A., López-Fuentes, D., & Nava Mesa, M. O. (2018). Proton Pump Inhibitors and Dementia: Physiopathological Mechanisms and Clinical Consequences. *Neural Plast, 2018*, 5257285. doi:10.1155/2018/5257285

Paesler, K., Xie, K., Hettich, M. M., Siwek, M. E., Ryan, D. P., Schröder, S., . . . Ehninger, D. (2015). Limited effects of an eIF2αS51A allele on neurological impairments in the 5xFAD mouse model of Alzheimer's disease. *Neural Plast, 2015*, 825157. doi:10.1155/2015/825157

Palop, J. J., Chin, J., Roberson, E. D., Wang, J., Thwin, M. T., Bien-Ly, N., . . . Mucke, L. (2007). Aberrant excitatory neuronal activity and compensatory remodeling of inhibitory hippocampal circuits in mouse models of Alzheimer's disease. *Neuron, 55*(5), 697-711. doi:10.1016/j.neuron.2007.07.025

Papazoglou, A., Henseler, C., Lundt, A., Wormuth, C., Soos, J., Broich, K., . . . Weiergraber, M. (2017). Gender specific hippocampal whole genome transcriptome data from mice lacking the Cav2.3 R-type or Cav3.2 T-type voltage-gated calcium channel. *Data Brief, 12*, 81-86. doi:10.1016/j.dib.2017.03.031

Papazoglou, A., Lundt, A., Wormuth, C., Ehninger, D., Henseler, C., Soos, J., . . . Weiergraber, M. (2016). Non-restraining EEG Radiotelemetry: Epidural and Deep Intracerebral Stereotaxic EEG Electrode Placement. *J Vis Exp*(112). doi:10.3791/54216

Papazoglou, A., Soos, J., Lundt, A., Wormuth, C., Ginde, V. R., Müller, R., . . . Weiergräber, M. (2016). Gender-Specific Hippocampal Dysrhythmia and Aberrant Hippocampal and Cortical Excitability in the APPswePS1dE9 Model of Alzheimer's Disease. *Neural Plast, 2016*, 7167358. doi:10.1155/2016/7167358

Papazoglou, A., Soos, J., Lundt, A., Wormuth, C., Ginde, V. R., Muller, R., . . . Weiergraber, M. (2017). Motor Cortex Theta and Gamma Architecture in Young Adult APPswePS1dE9 Alzheimer Mice. *PLoS One, 12*(1), e0169654. doi:10.1371/journal.pone.0169654

Papp, N., Koncz, S., Kostyalik, D., Kitka, T., Petschner, P., Vas, S., & Bagdy, G. (2019). Acute 5-HT2C Receptor Antagonist SB-242084 Treatment Affects EEG Gamma Band Activity Similarly to Chronic Escitalopram. *Front Pharmacol, 10*, 1636. doi:10.3389/fphar.2019.01636

Park, C., Kim, J. H., Yoon, B. E., Choi, E. J., Lee, C. J., & Shin, H. S. (2010). T-type channels control the opioidergic descending analgesia at the low threshold-spiking GABAergic neurons in the periaqueductal gray. *Proc Natl Acad Sci U S A, 107*(33), 14857-14862. doi:10.1073/pnas.1009532107

Park, K., Lee, J., Jang, H. J., Richards, B. A., Kohl, M. M., & Kwag, J. (2020). Optogenetic activation of parvalbumin and somatostatin interneurons selectively restores theta-nested gamma oscillations and oscillation-induced spike timing-dependent long-term potentiation impaired by amyloid β oligomers. *BMC Biol, 18*(1), 7. doi:10.1186/s12915-019-0732-7

Paxinos, G. W., Charles. (1998). *The Rat Brain in Stereotaxic Coordinates* (4 ed.).

Pelkey, K. A., Chittajallu, R., Craig, M. T., Tricoire, L., Wester, J. C., & McBain, C. J. (2017). Hippocampal GABAergic Inhibitory Interneurons. *Physiol Rev, 97*(4), 1619-1747. doi:10.1152/physrev.00007.2017

Peña-Ortega, F., & Bernal-Pedraza, R. (2012). Amyloid Beta Peptide slows down sensory-induced hippocampal oscillations. *Int J Pept, 2012,* 236289. doi:10.1155/2012/236289

Peng, C., Trojanowski, J. Q., & Lee, V. M. (2020). Protein transmission in neurodegenerative disease. *Nat Rev Neurol, 16*(4), 199-212. doi:10.1038/s41582-020-0333-7

Penke, B., Bogár, F., Paragi, G., Gera, J., & Fülöp, L. (2019). Key Peptides and Proteins in Alzheimer's Disease. *Curr Protein Pept Sci, 20*(6), 577-599. doi:10.2174/1389203720666190103123434

Penke, B., Szűcs, M., & Bogár, F. (2020). Oligomerization and Conformational Change Turn Monomeric β-Amyloid and Tau Proteins Toxic: Their Role in Alzheimer's Pathogenesis. *Molecules, 25*(7). doi:10.3390/molecules25071659

Perez-Garci, E., Gassmann, M., Bettler, B., & Larkum, M. E. (2006). The GABAB1b isoform mediates long-lasting inhibition of dendritic Ca2+ spikes in layer 5 somatosensory pyramidal neurons. *Neuron, 50*(4), 603-616. doi:10.1016/j.neuron.2006.04.019

Perez-Reyes, E. (1998). Molecular characterization of a novel family of low voltage-activated, T-type, calcium channels. *J Bioenerg Biomembr, 30*(4), 313-318. doi:10.1023/a:1021981420839

Perlman, R. L. (2016). Mouse models of human disease: An evolutionary perspective. *Evol Med Public Health, 2016*(1), 170-176. doi:10.1093/emph/eow014

Petersen, R. C. (2018). How early can we diagnose Alzheimer disease (and is it sufficient)? The 2017 Wartenberg lecture. *Neurology, 91*(9), 395-402. doi:10.1212/wnl.0000000000006088

Picciotto, M. R., Higley, M. J., & Mineur, Y. S. (2012). Acetylcholine as a neuromodulator: cholinergic signaling shapes nervous system function and behavior. *Neuron, 76*(1), 116-129. doi:10.1016/j.neuron.2012.08.036

Pin, J. P., Kniazeff, J., Binet, V., Liu, J., Maurel, D., Galvez, T., . . . Rondard, P. (2004). Activation mechanism of the heterodimeric GABA(B) receptor. *Biochem Pharmacol, 68*(8), 1565-1572. doi:10.1016/j.bcp.2004.06.035

Pin, J. P., Neubig, R., Bouvier, M., Devi, L., Filizola, M., Javitch, J. A., . . . Spedding, M. (2007). International Union of Basic and Clinical Pharmacology. LXVII. Recommendations for the recognition and nomenclature of G protein-coupled receptor heteromultimers. *Pharmacol Rev, 59*(1), 5-13. doi:10.1124/pr.59.1.5

Pineda, A. M., Ramos, F. M., Betting, L. E., & Campanharo, A. (2020). Quantile graphs for EEG-based diagnosis of Alzheimer's disease. *PLoS One, 15*(6), e0231169. doi:10.1371/journal.pone.0231169

Plant, L. D., Webster, N. J., Boyle, J. P., Ramsden, M., Freir, D. B., Peers, C., & Pearson, H. A. (2006). Amyloid beta peptide as a physiological modulator of neuronal 'A'-type K+ current. *Neurobiol Aging, 27*(11), 1673-1683. doi:10.1016/j.neurobiolaging.2005.09.038

Plassman, B. L., Langa, K. M., McCammon, R. J., Fisher, G. G., Potter, G. G., Burke, J. R., . . . Wallace, R. B. (2011). Incidence of dementia and cognitive impairment, not dementia in the United States. *Ann Neurol, 70*(3), 418-426. doi:10.1002/ana.22362

Poole, P. (2001). Pantoprazole. *Am J Health Syst Pharm, 58*(11), 999-1008. doi:10.1093/ajhp/58.11.999

Powell, K. L., Cain, S. M., Snutch, T. P., & O'Brien, T. J. (2014). Low threshold T-type calcium channels as targets for novel epilepsy treatments. *Br J Clin Pharmacol, 77*(5), 729-739. doi:10.1111/bcp.12205

Proskovec, A. L., Heinrichs-Graham, E., Wiesman, A. I., McDermott, T. J., & Wilson, T. W. (2018). Oscillatory dynamics in the dorsal and ventral attention networks during the reorienting of attention. *Hum Brain Mapp, 39*(5), 2177-2190. doi:10.1002/hbm.23997

Pugh, J. R., & Raman, I. M. (2006). Potentiation of mossy fiber EPSCs in the cerebellar nuclei by NMDA receptor activation followed by postinhibitory rebound current. *Neuron, 51*(1), 113-123. doi:10.1016/j.neuron.2006.05.021

Rajan, K. B., Wilson, R. S., Barnes, L. L., Aggarwal, N. T., Weuve, J., & Evans, D. A. (2017). A Cognitive Turning Point in Development of Clinical Alzheimer's Disease Dementia and Mild Cognitive Impairment: A Biracial Population Study. *J Gerontol A Biol Sci Med Sci, 72*(3), 424-430. doi:10.1093/gerona/glw246

Ramos-Miguel, A., Hercher, C., Beasley, C. L., Barr, A. M., Bayer, T. A., Falkai, P., . . . Honer, W. G. (2015). Loss of Munc18-1 long splice variant in GABAergic terminals is associated with cognitive decline and increased risk of dementia in a community sample. *Mol Neurodegener, 10*, 65. doi:10.1186/s13024-015-0061-4

Rasch, B. H., Born, J., & Gais, S. (2006). Combined blockade of cholinergic receptors shifts the brain from stimulus encoding to memory consolidation. *J Cogn Neurosci, 18*(5), 793-802. doi:10.1162/jocn.2006.18.5.793

Remondes, M., & Schuman, E. M. (2004). Role for a cortical input to hippocampal area CA1 in the consolidation of a long-term memory. *Nature, 431*(7009), 699-703. doi:10.1038/nature02965

Reyes-Marin, K. E., & Nuñez, A. (2017). Seizure susceptibility in the APP/PS1 mouse model of Alzheimer's disease and relationship with amyloid β plaques. *Brain Res, 1677*, 93-100. doi:10.1016/j.brainres.2017.09.026

Rosenthal, N., & Brown, S. (2007). The mouse ascending: perspectives for human-disease models. *Nat Cell Biol, 9*(9), 993-999. doi:10.1038/ncb437

Rountree, S. D., Atri, A., Lopez, O. L., & Doody, R. S. (2013). Effectiveness of antidementia drugs in delaying Alzheimer's disease progression. *Alzheimers Dement, 9*(3), 338-345. doi:10.1016/j.jalz.2012.01.002

Sachs, G., Chang, H. H., Rabon, E., Schackman, R., Lewin, M., & Saccomani, G. (1976). A nonelectrogenic H+ pump in plasma membranes of hog stomach. *J Biol Chem, 251*(23), 7690-7698.

Sachs, G., Shin, J. M., & Howden, C. W. (2006). Review article: the clinical pharmacology of proton pump inhibitors. *Aliment Pharmacol Ther, 23 Suppl 2*, 2-8. doi:10.1111/j.1365-2036.2006.02943.x

Sáez, M. E., González-Pérez, A., Gaist, D., Johansson, S., Nagy, P., & García Rodríguez, L. A. (2016). Risk of seizure associated with use of acid-suppressive drugs: An observational cohort study. *Epilepsy Behav, 62*, 72-80. doi:10.1016/j.yebeh.2016.06.039

Salminen, A., Kaarniranta, K., Kauppinen, A., Ojala, J., Haapasalo, A., Soininen, H., & Hiltunen, M. (2013). Impaired autophagy and APP processing in Alzheimer's disease: The potential role of Beclin 1 interactome. *Prog Neurobiol, 106-107*, 33-54. doi:10.1016/j.pneurobio.2013.06.002

Sarkis, R. A., Alam, J., Pavlova, M. K., Dworetzky, B. A., Pennell, P. B., Stickgold, R., & Bubrick, E. J. (2016). Sleep-dependent memory consolidation in the epilepsy monitoring unit: A pilot study. *Clin Neurophysiol, 127*(8), 2785-2790. doi:10.1016/j.clinph.2016.05.275

Sarter, M., & Bruno, J. P. (2002). Mild cognitive impairment and the cholinergic hypothesis: a very different take on recent data. *Ann Neurol, 52*(3), 384-385. doi:10.1002/ana.10308

Sceniak, M. P., & Maciver, M. B. (2006). Cellular actions of urethane on rat visual cortical neurons in vitro. *J Neurophysiol, 95*(6), 3865-3874. doi:10.1152/jn.01196.2005

Schampel, A., & Kuerten, S. (2017). Danger: High Voltage-The Role of Voltage-Gated Calcium Channels in Central Nervous System Pathology. *Cells, 6*(4). doi:10.3390/cells6040043

Schmidt, R., Herrojo Ruiz, M., Kilavik, B. E., Lundqvist, M., Starr, P. A., & Aron, A. R. (2019). Beta Oscillations in Working Memory, Executive Control of Movement and Thought, and Sensorimotor Function. *J Neurosci, 39*(42), 8231-8238. doi:10.1523/jneurosci.1163-19.2019

Scott, L., Feng, J., Kiss, T., Needle, E., Atchison, K., Kawabe, T. T., . . . Hajós, M. (2012). Age-dependent disruption in hippocampal θ oscillation in amyloid-β overproducing transgenic mice. *Neurobiol Aging, 33*(7), 1481.e1413-1423. doi:10.1016/j.neurobiolaging.2011.12.010

Scott, L., Kiss, T., Kawabe, T. T., & Hajós, M. (2016). Neuronal network activity in the hippocampus of tau transgenic (Tg4510) mice. *Neurobiol Aging, 37*, 66-73. doi:10.1016/j.neurobiolaging.2015.10.002

Seager, M. A., Johnson, L. D., Chabot, E. S., Asaka, Y., & Berry, S. D. (2002). Oscillatory brain states and learning: Impact of hippocampal theta-contingent training. *Proc Natl Acad Sci U S A, 99*(3), 1616-1620. doi:10.1073/pnas.032662099

Seeck, M., Koessler, L., Bast, T., Leijten, F., Michel, C., Baumgartner, C., . . . Beniczky, S. (2017). The standardized EEG electrode array of the IFCN. *Clin Neurophysiol, 128*(10), 2070-2077. doi:10.1016/j.clinph.2017.06.254

Sen, A., Capelli, V., & Husain, M. (2018). Cognition and dementia in older patients with epilepsy. *Brain, 141*(6), 1592-1608. doi:10.1093/brain/awy022

Shaw, L. M., Arias, J., Blennow, K., Galasko, D., Molinuevo, J. L., Salloway, S., . . . Fifer, S. (2018). Appropriate use criteria for lumbar puncture and cerebrospinal fluid testing in the diagnosis of Alzheimer's disease. *Alzheimers Dement, 14*(11), 1505-1521. doi:10.1016/j.jalz.2018.07.220

Shemer, I., Holmgren, C., Min, R., Fülöp, L., Zilberter, M., Sousa, K. M., . . . Harkany, T. (2006). Non-fibrillar beta-amyloid abates spike-timing-dependent synaptic potentiation at excitatory synapses in layer 2/3 of the neocortex by targeting postsynaptic AMPA receptors. *Eur J Neurosci, 23*(8), 2035-2047. doi:10.1111/j.1460-9568.2006.04733.x

Shin, J., Gireesh, G., Kim, S. W., Kim, D. S., Lee, S., Kim, Y. S., . . . Shin, H. S. (2009). Phospholipase C beta 4 in the medial septum controls cholinergic theta oscillations and anxiety behaviors. *J Neurosci, 29*(49), 15375-15385. doi:10.1523/jneurosci.3126-09.2009

Shin, J., Kim, D., Bianchi, R., Wong, R. K., & Shin, H. S. (2005). Genetic dissection of theta rhythm heterogeneity in mice. *Proc Natl Acad Sci U S A, 102*(50), 18165-18170. doi:10.1073/pnas.0505498102

Shin, J. M., & Kim, N. (2013). Pharmacokinetics and pharmacodynamics of the proton pump inhibitors. *J Neurogastroenterol Motil, 19*(1), 25-35. doi:10.5056/jnm.2013.19.1.25

Shin, J. M., & Sachs, G. (2008). Pharmacology of proton pump inhibitors. *Curr Gastroenterol Rep, 10*(6), 528-534. doi:10.1007/s11894-008-0098-4

Shiraev, T. P., & Bullen, A. (2018). Proton Pump Inhibitors and Cardiovascular Events: A Systematic Review. *Heart Lung Circ, 27*(4), 443-450. doi:10.1016/j.hlc.2017.10.020

Sieghart, W. (2006). Structure, pharmacology, and function of GABAA receptor subtypes. *Adv Pharmacol, 54*, 231-263. doi:10.1016/s1054-3589(06)54010-4

Sigel, E., & Steinmann, M. E. (2012). Structure, function, and modulation of GABA(A) receptors. *J Biol Chem, 287*(48), 40224-40231. doi:10.1074/jbc.R112.386664

Sima, X., Xu, J., Li, J., Zhong, W., & You, C. (2014). Expression of β-amyloid precursor protein in refractory epilepsy. *Mol Med Rep, 9*(4), 1242-1248. doi:10.3892/mmr.2014.1977

Simon, A. P., Poindessous-Jazat, F., Dutar, P., Epelbaum, J., & Bassant, M. H. (2006). Firing properties of anatomically identified neurons in the medial septum of anesthetized and unanesthetized restrained rats. *J Neurosci, 26*(35), 9038-9046. doi:10.1523/JNEUROSCI.1401-06.2006

Šišková, Z., Justus, D., Kaneko, H., Friedrichs, D., Henneberg, N., Beutel, T., . . . Remy, S. (2014). Dendritic structural degeneration is functionally linked to cellular hyperexcitability in a mouse model of Alzheimer's disease. *Neuron, 84*(5), 1023-1033. doi:10.1016/j.neuron.2014.10.024

Siwek, M. E., Müller, R., Henseler, C., Trog, A., Lundt, A., Wormuth, C., . . . Papazoglou, A. (2015). Altered theta oscillations and aberrant cortical excitatory activity in the 5XFAD model of Alzheimer's disease. *Neural Plast, 2015*, 781731. doi:10.1155/2015/781731

Smythe, J. W., Colom, L. V., & Bland, B. H. (1992). The extrinsic modulation of hippocampal theta depends on the coactivation of cholinergic and GABA-ergic medial septal inputs. *Neurosci Biobehav Rev, 16*(3), 289-308. doi:10.1016/s0149-7634(05)80203-9

Sperling, R. A., Jack, C. R., Jr., Black, S. E., Frosch, M. P., Greenberg, S. M., Hyman, B. T., . . . Schindler, R. J. (2011). Amyloid-related imaging abnormalities in amyloid-modifying therapeutic trials: recommendations from the Alzheimer's Association Research Roundtable Workgroup. *Alzheimers Dement, 7*(4), 367-385. doi:10.1016/j.jalz.2011.05.2351

Splawski, I., Yoo, D. S., Stotz, S. C., Cherry, A., Clapham, D. E., & Keating, M. T. (2006). CACNA1H mutations in autism spectrum disorders. *J Biol Chem, 281*(31), 22085-22091. doi:10.1074/jbc.M603316200

Steriade, M., & Llinas, R. R. (1988). The functional states of the thalamus and the associated neuronal interplay. *Physiol Rev, 68*(3), 649-742. doi:10.1152/physrev.1988.68.3.649

Stoiljkovic, M., Kelley, C., Horvath, T. L., & Hajós, M. (2018). Neurophysiological signals as predictive translational biomarkers for Alzheimer's disease treatment: effects of donepezil on neuronal network oscillations in TgF344-AD rats. *Alzheimers Res Ther, 10*(1), 105. doi:10.1186/s13195-018-0433-4

Stoiljkovic, M., Kelley, C., Nagy, D., Hurst, R., & Hajós, M. (2016). Activation of α7 nicotinic acetylcholine receptors facilitates long-term potentiation at the hippocampal-prefrontal cortex synapses in vivo. *Eur Neuropsychopharmacol, 26*(12), 2018-2023. doi:10.1016/j.euroneuro.2016.11.003

Stranahan, A. M., & Mattson, M. P. (2010). Selective vulnerability of neurons in layer II of the entorhinal cortex during aging and Alzheimer's disease. *Neural Plast, 2010*, 108190. doi:10.1155/2010/108190

Strand, D. S., Kim, D., & Peura, D. A. (2017). 25 Years of Proton Pump Inhibitors: A Comprehensive Review. *Gut Liver, 11*(1), 27-37. doi:10.5009/gnl15502

Tabares, L., & Betz, B. (2010). Multiple functions of the vesicular proton pump in nerve terminals. *Neuron, 68*(6), 1020-1022. doi:10.1016/j.neuron.2010.12.012

Tai, C., Kuzmiski, J. B., & MacVicar, B. A. (2006). Muscarinic enhancement of R-type calcium currents in hippocampal CA1 pyramidal neurons. *J Neurosci, 26*(23), 6249-6258. doi:10.1523/JNEUROSCI.1009-06.2006

Tai, S. Y., Chien, C. Y., Wu, D. C., Lin, K. D., Ho, B. L., Chang, Y. H., & Chang, Y. P. (2017). Risk of dementia from proton pump inhibitor use in Asian population: A nationwide cohort study in Taiwan. *PLoS One, 12*(2), e0171006. doi:10.1371/journal.pone.0171006

Takano, Y., & Hanada, Y. (2009). The driving system for hippocampal theta in the brainstem: an examination by single neuron recording in urethane-anesthetized rats. *Neurosci Lett, 455*(1), 65-69. doi:10.1016/j.neulet.2009.03.028

Talley, E. M., Cribbs, L. L., Lee, J. H., Daud, A., Perez-Reyes, E., & Bayliss, D. A. (1999). Differential distribution of three members of a gene family encoding low voltage-activated (T-type) calcium channels. *J Neurosci, 19*(6), 1895-1911. doi:10.1523/jneurosci.19-06-01895.1999

Tamagnini, F., Novelia, J., Kerrigan, T. L., Brown, J. T., Tsaneva-Atanasova, K., & Randall, A. D. (2015). Altered intrinsic excitability of hippocampal CA1 pyramidal neurons in aged PDAPP mice. *Front Cell Neurosci, 9*, 372. doi:10.3389/fncel.2015.00372

Tang, A. H., Karson, M. A., Nagode, D. A., McIntosh, J. M., Uebele, V. N., Renger, J. J., . . . Alger, B. E. (2011). Nerve terminal nicotinic acetylcholine receptors initiate quantal GABA release from perisomatic interneurons by activating axonal T-type (Cav3) Ca(2)(+) channels and Ca(2)(+) release from stores. *J Neurosci, 31*(38), 13546-13561. doi:10.1523/JNEUROSCI.2781-11.2011

Tang, M. X., Stern, Y., Marder, K., Bell, K., Gurland, B., Lantigua, R., . . . Mayeux, R. (1998). The APOE-epsilon4 allele and the risk of Alzheimer disease among African Americans, whites, and Hispanics. *Jama, 279*(10), 751-755. doi:10.1001/jama.279.10.751

Taskiran, A. S., Ergul, M., Gunes, H., Ozturk, A., Sahin, B., & Ozdemir, E. (2020). The Effects of Proton Pump Inhibitors (Pantoprazole) on Pentylenetetrazole-Induced Epileptic Seizures in Rats and Neurotoxicity in the SH-SY5Y Human Neuroblastoma Cell Line. *Cell Mol Neurobiol*. doi:10.1007/s10571-020-00956-6

Theofilas, P., Ehrenberg, A. J., Dunlop, S., Di Lorenzo Alho, A. T., Nguy, A., Leite, R. E. P., . . . Grinberg, L. T. (2017). Locus coeruleus volume and cell population changes during Alzheimer's disease progression: A stereological study in human postmortem brains with potential implication for early-stage biomarker discovery. *Alzheimers Dement, 13*(3), 236-246. doi:10.1016/j.jalz.2016.06.2362

Thibault, O., Pancani, T., Landfield, P. W., & Norris, C. M. (2012). Reduction in neuronal L-type calcium channel activity in a double knock-in mouse model of Alzheimer's disease. *Biochim Biophys Acta, 1822*(4), 546-549. doi:10.1016/j.bbadis.2012.01.004

Thuesen, A. D., Andersen, K., Lyngsø, K. S., Burton, M., Brasch-Andersen, C., Vanhoutte, P. M., & Hansen, P. B. L. (2018). Deletion of T-type calcium channels Ca(v)3.1 or Ca(v)3.2 attenuates endothelial dysfunction in aging mice. *Pflugers Arch, 470*(2), 355-365. doi:10.1007/s00424-017-2068-x

Tsolaki, A., Kazis, D., Kompatsiaris, I., Kosmidou, V., & Tsolaki, M. (2014). Electroencephalogram and Alzheimer's disease: clinical and research approaches. *Int J Alzheimers Dis, 2014*, 349249. doi:10.1155/2014/349249

Tsubota, M., Okawa, Y., Irie, Y., Maeda, M., Ozaki, T., Sekiguchi, F., . . . Kawabata, A. (2018). Involvement of the cystathionine-γ-lyase/Ca(v)3.2 pathway in substance P-induced bladder pain in the mouse, a model for nonulcerative bladder pain syndrome. *Neuropharmacology, 133*, 254-263. doi:10.1016/j.neuropharm.2018.01.037

Uhlhaas, P. J., & Singer, W. (2006). Neural synchrony in brain disorders: relevance for cognitive dysfunctions and pathophysiology. *Neuron, 52*(1), 155-168. doi:10.1016/j.neuron.2006.09.020

Ulrich, D., & Bettler, B. (2007). GABA(B) receptors: synaptic functions and mechanisms of diversity. *Curr Opin Neurobiol, 17*(3), 298-303. doi:10.1016/j.conb.2007.04.001

Ung, H., Cazares, C., Nanivadekar, A., Kini, L., Wagenaar, J., Becker, D., . . . Davis, K. A. (2017). Interictal epileptiform activity outside the seizure onset zone impacts cognition. *Brain, 140*(8), 2157-2168. doi:10.1093/brain/awx143

Valenzuela, J. I., Jaureguiberry-Bravo, M., Salas, D. A., Ramirez, O. A., Cornejo, V. H., Lu, H. E., . . . Couve, A. (2014). Transport along the dendritic endoplasmic reticulum mediates the trafficking of GABAB receptors. *J Cell Sci, 127*(Pt 15), 3382-3395. doi:10.1242/jcs.151092

van Deursen, J. A., Vuurman, E. F., Verhey, F. R., van Kranen-Mastenbroek, V. H., & Riedel, W. J. (2008). Increased EEG gamma band activity in Alzheimer's disease and mild cognitive impairment. *J Neural Transm (Vienna), 115*(9), 1301-1311. doi:10.1007/s00702-008-0083-y

Van Rensburg, C. J., Honiball, P. J., Van Zyl, J. H., Grundling, H. D., Eloff, F. P., Spies, S. K., . . . Louw, J. A. (1999). Safety and efficacy of pantoprazole 40 mg daily as relapse prophylaxis in patients with healed reflux oesophagitis-a 2-year follow-up. *Aliment Pharmacol Ther, 13*(8), 1023-1028. doi:10.1046/j.1365-2036.1999.00573.x

Vanderwolf, C. H., Buzsaki, G., Cain, D. P., Cooley, R. K., & Robertson, B. (1988). Neocortical and hippocampal electrical activity following decapitation in the rat. *Brain Res, 451*(1-2), 340-344. doi:10.1016/0006-8993(88)90780-9

Varga, V., Hangya, B., Kranitz, K., Ludanyi, A., Zemankovics, R., Katona, I., . . . Borhegyi, Z. (2008). The presence of pacemaker HCN channels identifies theta rhythmic GABAergic neurons in the medial septum. *J Physiol, 586*(16), 3893-3915. doi:10.1113/jphysiol.2008.155242

Vegeto, E., Villa, A., Della Torre, S., Crippa, V., Rusmini, P., Cristofani, R., . . . Poletti, A. (2020). The Role of Sex and Sex Hormones in Neurodegenerative Diseases. *Endocr Rev, 41*(2), 273-319. doi:10.1210/endrev/bnz005

Vermunt, L., Sikkes, S. A. M., van den Hout, A., Handels, R., Bos, I., van der Flier, W. M., . . . Visser, P. J. (2019). Duration of preclinical, prodromal, and dementia stages of Alzheimer's disease in relation to age, sex, and APOE genotype. *Alzheimers Dement, 15*(7), 888-898. doi:10.1016/j.jalz.2019.04.001

Verret, L., Mann, E. O., Hang, G. B., Barth, A. M., Cobos, I., Ho, K., . . . Palop, J. J. (2012). Inhibitory interneuron deficit links altered network activity and cognitive dysfunction in Alzheimer model. *Cell, 149*(3), 708-721. doi:10.1016/j.cell.2012.02.046

Vertes, R. P. (2005). Hippocampal theta rhythm: a tag for short-term memory. *Hippocampus, 15*(7), 923-935. doi:10.1002/hipo.20118

Vertes, R. P., Hoover, W. B., & Viana Di Prisco, G. (2004). Theta rhythm of the hippocampus: subcortical control and functional significance. *Behav Cogn Neurosci Rev, 3*(3), 173-200. doi:10.1177/1534582304273594

Vickrey, B. G., Mittman, B. S., Connor, K. I., Pearson, M. L., Della Penna, R. D., Ganiats, T. G., . . . Lee, M. (2006). The effect of a disease management intervention on quality and outcomes of dementia care: a randomized, controlled trial. *Ann Intern Med, 145*(10), 713-726. doi:10.7326/0003-4819-145-10-200611210-00004

Vigot, R., Barbieri, S., Brauner-Osborne, H., Turecek, R., Shigemoto, R., Zhang, Y. P., . . . Bettler, B. (2006). Differential compartmentalization and distinct functions of GABAB receptor variants. *Neuron, 50*(4), 589-601. doi:10.1016/j.neuron.2006.04.014

Vithlani, M., Terunuma, M., & Moss, S. J. (2011). The dynamic modulation of GABA(A) receptor trafficking and its role in regulating the plasticity of inhibitory synapses. *Physiol Rev, 91*(3), 1009-1022. doi:10.1152/physrev.00015.2010

Vogt, D. L., Thomas, D., Galvan, V., Bredesen, D. E., Lamb, B. T., & Pimplikar, S. W. (2011). Abnormal neuronal networks and seizure susceptibility in mice overexpressing the APP intracellular domain. *Neurobiol Aging, 32*(9), 1725-1729. doi:10.1016/j.neurobiolaging.2009.09.002

Voisin, T., Bourinet, E., & Lory, P. (2016). Genetic alteration of the metal/redox modulation of Cav3.2 T-type calcium channel reveals its role in neuronal excitability. *J Physiol, 594*(13), 3561-3574. doi:10.1113/jp271925

Vossel, K. A., Beagle, A. J., Rabinovici, G. D., Shu, H., Lee, S. E., Naasan, G., . . . Mucke, L. (2013). Seizures and epileptiform activity in the early stages of Alzheimer disease. *JAMA Neurol, 70*(9), 1158-1166. doi:10.1001/jamaneurol.2013.136

Wallmark, B., Larsson, H., & Humble, L. (1985). The relationship between gastric acid secretion and gastric H+,K+-ATPase activity. *J Biol Chem, 260*(25), 13681-13684.

Wang, D., & Hiesinger, P. R. (2013). The vesicular ATPase: a missing link between acidification and exocytosis. *J Cell Biol, 203*(2), 171-173. doi:10.1083/jcb.201309130

Wang, J., Gu, B. J., Masters, C. L., & Wang, Y. J. (2017). A systemic view of Alzheimer disease - insights from amyloid-β metabolism beyond the brain. *Nat Rev Neurol, 13*(10), 612-623. doi:10.1038/nrneurol.2017.111

Wang, R., & Lewin, G. R. (2011). The Cav3.2 T-type calcium channel regulates temporal coding in mouse mechanoreceptors. *J Physiol, 589*(Pt 9), 2229-2243. doi:10.1113/jphysiol.2010.203463

Wang, X., Zhang, X. G., Zhou, T. T., Li, N., Jang, C. Y., Xiao, Z. C., . . . Li, S. (2016). Elevated Neuronal Excitability Due to Modulation of the Voltage-Gated Sodium Channel Nav1.6 by Aβ1-42. *Front Neurosci, 10*, 94. doi:10.3389/fnins.2016.00094

Wang, Z., Nie, B., Li, D., Zhao, Z., Han, Y., Song, H., . . . Li, K. (2012). Effect of acupuncture in mild cognitive impairment and Alzheimer disease: a functional MRI study. *PLoS One, 7*(8), e42730. doi:10.1371/journal.pone.0042730

Ward, A., Tardiff, S., Dye, C., & Arrighi, H. M. (2013). Rate of conversion from prodromal Alzheimer's disease to Alzheimer's dementia: a systematic review of the literature. *Dement Geriatr Cogn Dis Extra, 3*(1), 320-332. doi:10.1159/000354370

Watt, J. A., Goodarzi, Z., Veroniki, A. A., Nincic, V., Khan, P. A., Ghassemi, M., . . . Straus, S. E. (2019). Comparative Efficacy of Interventions for Aggressive and Agitated Behaviors in Dementia: A Systematic Review and Network Meta-analysis. *Ann Intern Med, 171*(9), 633-642. doi:10.7326/m19-0993

Weiergraber, M., Henry, M., Hescheler, J., Smyth, N., & Schneider, T. (2005). Electrocorticographic and deep intracerebral EEG recording in mice using a telemetry system. *Brain Res Brain Res Protoc, 14*(3), 154-164. doi:10.1016/j.brainresprot.2004.12.006

Weiergraber, M., Henry, M., Sudkamp, M., de Vivie, E. R., Hescheler, J., & Schneider, T. (2005). Ablation of Ca(v)2.3 / E-type voltage-gated calcium channel results in cardiac arrhythmia and altered autonomic control within the murine cardiovascular system. *Basic Res Cardiol, 100*(1), 1-13. doi:10.1007/s00395-004-0488-1

Weiergraber, M., Papazoglou, A., Broich, K., & Muller, R. (2016). Sampling rate, signal bandwidth and related pitfalls in EEG analysis. *J Neurosci Methods, 268*, 53-55. doi:10.1016/j.jneumeth.2016.05.010

Weiss, N., Hameed, S., Fernandez-Fernandez, J. M., Fablet, K., Karmazinova, M., Poillot, C., . . . De Waard, M. (2012). A Ca(v)3.2/syntaxin-1A signaling complex controls T-type channel activity and low-threshold exocytosis. *J Biol Chem, 287*(4), 2810-2818. doi:10.1074/jbc.M111.290882

Weiss, N., Zamponi, G. W., & De Waard, M. (2012). How do T-type calcium channels control low-threshold exocytosis? *Commun Integr Biol, 5*(4), 377-380. doi:10.4161/cib.19997

Weller, J., & Budson, A. (2018). Current understanding of Alzheimer's disease diagnosis and treatment. *F1000Res, 7*. doi:10.12688/f1000research.14506.1

White, J. A., McKinney, B. C., John, M. C., Powers, P. A., Kamp, T. J., & Murphy, G. G. (2008). Conditional forebrain deletion of the L-type calcium channel Ca V 1.2 disrupts remote spatial memories in mice. *Learn Mem, 15*(1), 1-5. doi:10.1101/lm.773208

Whitehouse, P. J., Price, D. L., Struble, R. G., Clark, A. W., Coyle, J. T., & Delon, M. R. (1982). Alzheimer's disease and senile dementia: loss of neurons in the basal forebrain. *Science, 215*(4537), 1237-1239. doi:10.1126/science.7058341

WHO. *World Health Organization - Dementia*. Retrieved from https://www.who.int/health-topics/dementia#tab=tab_1

WHO. *World Health Organization - Guidelines Approved by the Guidelines Review Committee*. Retrieved from Geneva:

Wildburger, N. C., Esparza, T. J., LeDuc, R. D., Fellers, R. T., Thomas, P. M., Cairns, N. J., . . . Brody, D. L. (2017). Diversity of Amyloid-beta Proteoforms in the Alzheimer's Disease Brain. *Sci Rep, 7*(1), 9520. doi:10.1038/s41598-017-10422-x

Wisor, J. P., & Kilduff, T. S. (2005). Molecular genetic advances in sleep research and their relevance to sleep medicine. *Sleep, 28*(3), 357-367.

World Health, O. (2019). *World Health Organization model list of essential medicines: 21st list 2019*. Retrieved from Geneva: https://apps.who.int/iris/handle/10665/325771

Xiong, Z., Hongmei, Z., Lu, S., & Yu, L. (2011). Curcumin mediates presenilin-1 activity to reduce β-amyloid production in a model of Alzheimer's Disease. *Pharmacol Rep, 63*(5), 1101-1108. doi:10.1016/s1734-1140(11)70629-6

Yasuda, R., Sabatini, B. L., & Svoboda, K. (2003). Plasticity of calcium channels in dendritic spines. *Nat Neurosci, 6*(9), 948-955. doi:10.1038/nn1112

Yiannopoulou, K. G., & Papageorgiou, S. G. (2013). Current and future treatments for Alzheimer's disease. *Ther Adv Neurol Disord, 6*(1), 19-33. doi:10.1177/1756285612461679

Yiannopoulou, K. G., & Papageorgiou, S. G. (2020). Current and Future Treatments in Alzheimer Disease: An Update. *J Cent Nerv Syst Dis, 12*, 1179573520907397. doi:10.1177/1179573520907397

Yoshimura, Y., Inaba, M., Yamada, K., Kurotani, T., Begum, T., Reza, F., . . . Komatsu, Y. (2008). Involvement of T-type Ca2+ channels in the potentiation of synaptic and visual responses during the critical period in rat visual cortex. *Eur J Neurosci, 28*(4), 730-743. doi:10.1111/j.1460-9568.2008.06384.x

Yu, H., Zhu, L., Cai, L., Wang, J., Liu, C., Shi, N., & Liu, J. (2020). Variation of functional brain connectivity in epileptic seizures: an EEG analysis with cross-frequency phase synchronization. *Cogn Neurodyn, 14*(1), 35-49. doi:10.1007/s11571-019-09551-y

Yu, H., Zhu, L., Cai, L., Wang, J., Liu, J., Wang, R., & Zhang, Z. (2020). Identification of Alzheimer's EEG With a WVG Network-Based Fuzzy Learning Approach. *Front Neurosci, 14*, 641. doi:10.3389/fnins.2020.00641

Zamponi, G. W., Lory, P., & Perez-Reyes, E. (2010). Role of voltage-gated calcium channels in epilepsy. *Pflugers Arch, 460*(2), 395-403. doi:10.1007/s00424-009-0772-x

Zapata, J., Moretto, E., Hannan, S., Murru, L., Longatti, A., Mazza, D., . . . Passafaro, M. (2017). Epilepsy and intellectual disability linked protein Shrm4 interaction with GABABRs shapes inhibitory neurotransmission. *Nat Commun, 8*, 14536. doi:10.1038/ncomms14536

Zarea, A., Charbonnier, C., Rovelet-Lecrux, A., Nicolas, G., Rousseau, S., Borden, A., . . . Wallon, D. (2016). Seizures in dominantly inherited Alzheimer disease. *Neurology, 87*(9), 912-919. doi:10.1212/wnl.0000000000003048

Zhang, X., Clarke, C. L., & Rhynas, S. J. (2019). What is the meaning of filial piety for people with dementia and their family caregivers in China under the current social transitions? An interpretative phenomenological analysis. *Dementia (London), 18*(7-8), 2620-2634. doi:10.1177/1471301217753775

Zhang, Y., Jiang, X., Snutch, T. P., & Tao, J. (2013). Modulation of low-voltage-activated T-type $Ca^{2+}$ channels. *Biochim Biophys Acta, 1828*(7), 1550-1559. doi:10.1016/j.bbamem.2012.08.032

Zhang, Y., Liang, M., Sun, C., Song, E. J., Cheng, C., Shi, T., . . . Sun, Y. (2020). Proton pump inhibitors use and dementia risk: a meta-analysis of cohort studies. *Eur J Clin Pharmacol, 76*(2), 139-147. doi:10.1007/s00228-019-02753-7

Zhang, Y. W., Thompson, R., Zhang, H., & Xu, H. (2011). APP processing in Alzheimer's disease. *Mol Brain, 4*, 3. doi:10.1186/1756-6606-4-3

Zhou, Y., Sun, Y., Ma, Q. H., & Liu, Y. (2018). Alzheimer's disease: amyloid-based pathogenesis and potential therapies. *Cell Stress, 2*(7), 150-161. doi:10.15698/cst2018.07.143

Zimdahl Kahlin, A. (2020). *Pharmacogenetic studies of thiopurine methyltransferase genotype-phenotype concordance and effect of methotrexate on thiopurine metabolism*.